THE UNIVERSITY
of EDINBURGH

Cardiovascular 11β-HSD1: its role in myocardial physiology and pathophysiology

Christopher Iain White

Philosophiæ Doctor (Ph.D.)

University of Edinburgh

2016

Declaration

I hereby declare that all the work described in this thesis was performed entirely by myself, except where stated in the acknowledgements or appropriate methods sections. The work contains no material that has been accepted for the award of any other degree or diploma in any university or tertiary institution, and to the best of my knowledge contains no material published or written by any other person, except where stated in the text.

Christopher Iain White

Acknowledgements

Firstly I would like to thank my supervisors Gillian Gray and Karen Chapman for their enthusiastic support, scientific guidance and unfailing encouragement throughout my Ph.D. studies.

I am hugely indebted to Gill Brooker for all her surgical expertise, limitless patience, and fantastic sense of humour during all those hours of surgery. I'd also like to thank Adrian Thomson for performing the echocardiography, Maurits Jansen and Ross Lennen for conducting the MRI, the staff at the Queen's Medical Research Institute Histology Department, and all the technicians in the BRF for their help with animal-related matters.

I would also like to thank all the people I've worked closely with in laboratory E3.17 and across the centre for all their help and advice during my studies. A special mention must also go to everyone else in office E3.24 for their entertaining banter and good humour when answering my many questions over the past few years.

Finally I'd like to thank the British Heart Foundation for funding my Ph.D.

Abstract

Glucocorticoid production by the adrenal gland is regulated by hypothalamic-pituitary-adrenal (HPA) axis activity. Within cells, glucocorticoid levels are modulated by 11β-hydroxysteroid dehydrogenase (11β-HSD), which interconverts active and intrinsically inert glucocorticoids. Glucocorticoids have widespread physiological effects and, in the cardiovascular system, they play a crucial role in heart development and maturation, blood pressure control, and myocardial calcium cycling. Mice which are unable to regenerate the physiological glucocorticoid, corticosterone, from 11-dehydrocorticosterone due to deletion of the type 1 11β-HSD isozyme (11β-HSD1) have previously been shown to have smaller, lighter hearts but unaltered systolic function. Moreover, a single nucleotide polymorphism (SNP) in the *Hsd11b1* gene has been associated with reduced left ventricular mass in humans, suggesting a role for 11β-HSD1 in regulating cardiac size. After myocardial infarction (MI), 11β-HSD1 deficient mice have an augmented inflammatory response, increased numbers of pro-reparative alternatively-activated macrophages in the heart, enhanced peri-infarct angiogenesis and improved cardiac function compared to C57BL/6 controls. However, the role of 'cardiovascular' 11β-HSD1 in the development of these phenotypes, both basally and after MI, is unknown. It was hypothesised that 'cardiovascular' 11β-HSD1 deficiency would result in smaller hearts, and that this selective deletion would lead to altered calcium handling protein expression and diastolic abnormalities. Furthermore, it was hypothesised that 'cardiovascular' 11β-HSD1 deletion would reproduce the beneficial post-MI phenotype previously seen in global 11β-HSD1 deficient mice.

The first aim was to characterise the cardiac phenotype of mice with global deletion of 11β-HSD1 (DelI mice), and mice in which deletion is restricted to cardiomyocytes and vascular smooth muscle cells (SMAC mice). SMAC mice have 'floxed' 11β-HSD1 alleles and a Cre recombinase transgene inserted into the *Sm22α* gene. *Sm22α* is expressed in vascular smooth muscle cells, and transiently in cardiomyocytes during development. Thus, Cre expression in these cells results in deletion of exon three of the *Hsd11b1* gene and gives rise to a non-functional protein. Controls for DelI mice were C57BL/6 mice, and controls for SMAC mice were their Cre^- littermates. DelI, but not SMAC, mice have smaller, lighter hearts, which may be explained by their shorter cardiomyocytes measured following isolation using a Langendorff preparation. Cardiomyocyte cross-sectional area is unchanged. *In vivo* measurement of cardiac function using ultrasound imaging showed systolic function is comparable between DelI mice and SMAC mice and their respective controls. However, there is mild diastolic dysfunction in both DelI and SMAC mice, characterised by reduced E wave deceleration and an increased mitral valve deceleration time. This phenotype occurred following pharmacological inhibition of 11β-HSD1, by administration of UE2316, a selective 11β-HSD1 inhibitor, to adult C57BL6/SJL mice. While ventricular collagen content is unaltered in DelI, SMAC and UE2316-treated mice compared to their respective controls, expression of sarcoplasmic reticulum Ca^{2+} ATPase (SERCA) is reduced, suggesting that altered calcium handling, rather than changes in stiffness, may underlie this phenotype.

The second aim was to determine whether the beneficial acute outcomes seen previously in 11β-HSD1 deficient mice after MI could be reproduced by selective cardiovascular deletion of the enzyme. Seven days after MI, compared to Cre^-

littermate controls, SMAC mice have similar peri-infarct angiogenesis, total macrophage and alternatively-activated macrophage infiltration into the heart, infarct size, ventricular dilatation and systolic function. This suggests 11β-HSD1 deletion in another cell type, or types, is responsible for the phenotype seen in global 11β-HSD1 deficient mice.

The final aim was to assess the impact of global 11β-HSD1 deficiency and 'cardiovascular' 11β-HSD1 deletion on the development of heart failure, using magnetic resonance imaging to determine structure and function. Eight weeks after MI, mice globally deficient in 11β-HSD1 have attenuated expression of ANP and β-MHC, RNA markers of heart failure, and show attenuated pulmonary oedema, reduced chamber dilatation, preserved systolic function and smaller infarcts compared to control. None of these parameters are altered in SMAC mice relative to control.

In conclusion, the data presented in this thesis shows that cardiovascular 11β-HSD1 influences physiological cardiac function, potentially through regulation of calcium handling. 11β-HSD1 in other cells influences cardiomyocyte length, resulting in smaller hearts in its absence. Despite this, global 11β-HSD1 deficiency prevents heart failure development after MI, suggesting that pharmacological inhibition of 11β-HSD1 may be of benefit in treating this condition. Cardiovascular 11β-HSD1 does not, however, account for the changes in infarct healing or remodelling associated with this beneficial outcome, therefore these effects must be related to 11β-HSD1 deficiency elsewhere, such as fibroblasts or myeloid cells.

Presentations

Oral

‘11β-HSD1 deficiency alters heart chamber size but not contractility’, Cardiovascular Progress in Research Seminar Series, Edinburgh, UK, November 2011.

‘Local cardiovascular glucocorticoid regeneration by 11β-HSD1 is essential for normal post-natal cardiac growth and function in the mouse’, Scottish Cardiovascular Forum, Dundee, UK, February 2012. Awarded first prize for best oral communication.

‘Valve assessment using Doppler ultrasound – correlation with gene expression and valve phenotype’, 4th Pre-clinical Ultrasound Imaging Day, Edinburgh, UK, November 2012.

‘Cardiovascular 11β-HSD1: investigation of its role in myocardial physiology and pathophysiology’, Cardiovascular Progress in Research Seminar Series, Edinburgh, UK, June 2013.

Poster

‘Normal post-natal cardiac growth in the mouse requires 11β-HSD1: is local cardiovascular expression key?’, Centre for Cardiovascular Science Symposium, Edinburgh, UK, May 2012.

‘Cardiovascular phenotyping in mice with targeted 11β-hydroxysteroid dehydrogenase type 1 deletion’, The British Society for Cardiovascular Research Autumn Meeting, Belfast, UK, September 2012.

‘Cardiovascular phenotyping in mice with targeted 11β-hydroxysteroid dehydrogenase type 1 deletion’, Scottish Cardiovascular Forum, Strathclyde, UK, February 2013.

‘Lack of myocardial intracellular glucocorticoid regeneration results in reduced SERCA expression and mild diastolic dysfunction’, Centre for Cardiovascular Science Symposium, Edinburgh, UK, June 2013.

‘Lack of myocardial intracellular glucocorticoid regeneration results in reduced SERCA expression and mild diastolic dysfunction’, International Society for Heart Research XXI World Congress, San Diego, USA, June 2013.

‘Does cardiovascular specific 11β-HSD1 deletion reproduce the beneficial effects of global 11β-HSD1 deficiency in the healing myocardial infarct?’, European Society for Cardiology Congress, Amsterdam, The Netherlands, August 2013.

Papers

White CI, Jansen MA, McGregor K, Mylonas KJ, Richardson RV, Thomson A, Moran CM, Seckl JR, Walker BR, Chapman KE, Gray GA (2016) Cardiomyocyte and vascular smooth muscle-independent 11β-hydroxysteroid dehydrogenase 1 amplifies infarct expansion, hypertrophy, and the development of heart failure after myocardial infarction in male mice. *Endocrinology*, **157** (1), pp. 346-357.

Gray GA, **White CI**, Thomson A, Kozak A, Moran CM & Jansen MA (2013) Imaging the healing murine myocardial infarct in vivo: ultrasound, magnetic resonance imaging and fluorescence molecular tomography. *Journal of Experimental Physiology*, **98** (3), pp. 606-613.

Kipari T, Hadoke PWF, Iqbal J, Man TY, Miller E, Coutinho AE, Zhang Z, Sullivan KM, Mitic T, Livingstone DEW, Schrecker C, Samuel K, **White CI**, Bouhlel MA, Chinetti-Gbaguidi G, Staels B, Andrew R, Walker BR, Savill JS, Chapman KE & Seckl JR (2013) 11β-hydroxysteroid dehydrogenase type 1 deficiency in bone marrow-derived cells reduces atherosclerosis. *The FASEB Journal*, **27** (4), pp. 1519-1531.

Abbreviations

Abbreviation	Term
11β-HSD	11β-hydroxysteroid dehydrogenase
α-MHC	α-myosin heavy chain
α-SMA	α-smooth muscle actin
β-MHC	β-myosin heavy chain
ACE	Angiotensin converting enzyme
ACTH	Adrenocorticotropic hormone
Ang-1	Angiopoietin-1
Ang-2	Angiopoietin-2
ANOVA	Analysis of variance
ANP	Atrial natriuretic peptide
ApoE	Apolipoprotein E
APS	Ammonium persulphate
AV	Atrio-ventricular
BCA	Bicinchoninic acid
BCL-2	B-cell lymphoma-2
BNP	B-type natriuretic peptide
BP	Blood pressure
BSA	Bovine serum albumin
CaMKII	Ca^{2+}/calmodulin-dependent protein kinase II
$CaV_{1.2}$	Voltage dependent L-type calcium channel α1C subunit
CBG	Corticosteroid-binding globulin

CD31	Cluster of differentiation 31
cDNA	Complementary deoxyribonucleic acid
cGMP	Cyclin guanosine monophosphate
CICR	Calcium-induced calcium release
CK	Creatine kinase
CK-MB	Creatine phosphokinase-MB
CO	Cardiac output
Col1α2	Collagen type 1 α 2
Col3α1	Collagen type 3 α 1
COPD	Chronic obstructive pulmonary disease
Cp	Crossing point
CRF	Corticotropin-releasing factor
CRP	C-reactive protein
CT-1	Cardiotrophin-1
cTnI	Cardiac troponin-I
CXCR2	Chemokine (C-X-C motif) receptor 2
Cy3	Cyanine-3
DAB	3,3'-diaminobenzidine
DAMP	Damage-associated molecular pattern
DAPI	4'6-diamidino-2-phenylindole
dH_2O	Deionised water
DNA	Deoxyribonucleic acid
dNTP	Deoxyribonucleotide triphosphate
EC	Endothelial cell
ECG	Electrocardiography

ECM	Extracellular matrix
EDTA	Ethylenediaminetetraacetic acid
EF	Ejection fraction
EKV	ECG-gated kilohertz visualisation
ELAM-1	Endothelial-leukocyte adhesion molecule-1
eNOS	Endothelial nitric oxide synthase
EPHESUS	Eplerenone Post Acute Myocardial Infarction Heart Failure Efficacy and Survival Study
ER	Endoplasmic reticulum
EtOH	Ethanol
FGF	Fibroblast growth factor
FITC	Fluorescein isothiocyanate
FKBP5	FK506 binding protein 5
FS	Fractional shortening
G-CSF	Granulocyte colony-stimulating factor
GC-A	Guanylyl cyclase-A
GILZ	Glucocorticoid-induced leucine zipper
GR	Glucocorticoid receptor
GRE	Glucocorticoid response element
H_2O_2	Hydrogen peroxide
H6PDH	Hexose-6-phosphate dehydrogenase
HAoEC	Human aortic endothelial cell
HIF-1	Hypoxia-inducible factor-1
HPA	Hypothalamic-pituitary-adrenal
HRP	Horseradish peroxidise

Hsp70	Heat shock protein 70
Hsp90	Heat shock protein 90
HUVEC	Human umbilical vein endothelial cell
IκB	Inhibitor of κB
ICAD/DEF45	Inhibitor of caspase-activated deoxyribonuclease/DNA fragmentation factor-45
ICAM-1	Intercellular adhesion molecule-1
IGF-1	Insulin-like growth factor-1
IL	Interleukin
iNOS	Inducible nitric oxide synthase
KO	Knock-out
L-NAME	L-N^G-nitroarginine methyl ester
LAD	Left anterior descending
LDH	Lactate dehydrogenase
LIF	Leukaemia inhibitory factor
LPS	Lipopolysaccharide
LVEDA	Left ventricular end diastolic area
LVESA	Left ventricular end systolic area
LVEDV	Left ventricular end diastolic volume
LVESV	Left ventricular end systolic volume
Ly6C	Lymphocyte antigen 6C
M-CSF	Macrophage colony-stimulating factor
MCP-1	Monocyte chemoattractant protein-1
MI	Myocardial infarction
MIP-2	Macrophage inflammatory protein-2

MMP	Matrix metalloproteinase
MOMP	Mitochondrial outer membrane permeability
MR	Mineralocorticoid receptor
MRI	Magnetic resonance imaging
mRNA	Messenger ribonucleic acid
MV DT	Mitral valve deceleration time
NADPH	Nicotinamide adenine dinucleotide phosphate
NaOH	Sodium hydroxide
NCX	Sodium-calcium exchanger
NFκB	Nuclear factor-κB
NGF	Nerve growth factor
NO	Nitric oxide
PBS	Phosphate-buffered saline
PCR	Polymerase chain reaction
PDGFB	Platelet derived growth factor B
PECAM-1	Platelet endothelial cell adhesion molecule-1
PGC1α	Peroxisome proliferator-activated receptor-γ coactivator 1-α
PKA	Protein kinase A
PLN	Phospholamban
POMC	Pro-opiomelanocortin
PPAR-γ	Peroxisome proliferator-activator receptor-γ
qRT-PCR	Quantitative real time polymerase chain reaction
RALES	Randomised Aldactone Evaluation Study
RF	Radio frequency
RIPA	Radioimmunoprecipitation assay

RNA	Ribonucleic acid
ROS	Reactive oxygen species
RT	Reverse transcriptase
RU486	Mifepristone
RyR	Ryanodine receptor
SAME	Syndrome of Apparent Mineralocorticoid Excess
SDS	Sodium dodecyl sulphate
SDS-PAGE	Sodium dodecyl sulphate-polyacrilamide gel electrophoresis
SERCA	Sarcoplasmic reticulum Ca^{2+} ATPase
SGK	Serum glucocorticoid regulated kinase
SKA	Skeletal muscle α-actin
SkM	Skeletal muscle
SNP	Single nucleotide polymorphism
SR	Sarcoplasmic reticulum
STAT3	Signal transducer and activator of transcription 3
SV	Stroke volume
TBE	Tris-borate-ethylenediaminetetraacetic acid
TBP	TATA-binding protein
TBS	Tris-buffered saline
TBST	Tris-buffered saline/Tween 20
TE	Echo time
TE buffer	Tris-ethylenediaminetetraacetic acid buffer
TEMED	Tetramethylethylenediamine
TF	Transcription factor
TGFβ	Transforming growth factor β

TLR	Toll-like receptor
TNFα	Tumour necrosis factor α
TR	Repetition time
UPL	Universal Probe Library
VCAM-1	Vascular cell adhesion protein-1
VEGF	Vascular endothelial growth factor
VEGFR2	Vascular endothelial growth factor receptor 2
VSMC	Vascular smooth muscle cell
WGA	Wheat germ agglutinin

Contents

List of Figures

List of Tables

Chapter 1

Introduction

Cardiovascular disease remains the primary cause of mortality worldwide, accounting for one third of all deaths. In the United Kingdom, cardiovascular disease is responsible for around 180, 000 deaths annually with the majority due to cerebrovascular disease, coronary heart disease, and heart failure (Scarborough, *et al*., 2010; Townsend, *et al*., 2012). Myocardial infarction (MI) is the leading cause of heart failure, a condition characterised by loss of cardiac function to such an extent that myocardial performance cannot meet the demands of the body. Drug treatments which aim to reduce the load on the heart and manage this condition include angiotensin converting enzyme (ACE) inhibitors, β-adrenoceptor antagonsists (β blockers), loop diuretics, statins and nitrates. While these can improve quality of life they have had limited success in prolonging life. Sixty percent of heart failure patients die within five years of diagnosis (Tribouilloy, *et al*., 2008). Because of this poor prognosis, further research into MI, the principal cause of heart failure, is key to facilitating the development of new therapeutic agents and the identification of novel targets.

Previous work in our laboratory has suggested that targeting local glucocorticoid synthesis may provide a novel method of preventing the development of heart failure after MI. The focus of this thesis is to understand the physiological role of glucocorticoid metabolism in cardiovascular tissue, and whether manipulation of glucocorticoid metabolism in the cardiovascular system prevents the progression of heart failure after infarction.

1.1 Glucocorticoids

1.1.1 Glucocorticoid synthesis and secretion

Glucocorticoids are a class of steroid hormones produced in, and secreted by the zona fasciculata of the adrenal gland (Buckingham, 2006). Endogenous circulating glucocorticoid levels are regulated by the hypothalamic-pituitary-adrenal (HPA) axis (see Figure 1.1). In response to physical or psychological stressful stimuli, such as pain, trauma, infection, or elevated temperature, corticotropin-releasing factor (CRF) and arginine vasopressin (AVP) are released from the paraventricular nucleus in the hypothalamus (Jacobson, 2005). This causes cleavage of pro-opiomelanocortin (POMC) in the anterior pituitary gland resulting in production of adrenocorticotropic hormone (ACTH) (Aguilera, *et al*., 2001; Jacobson, 2005; Buckingham, 2006). ACTH is released into the systemic circulation and acts in the adrenal gland to stimulate glucocorticoid synthesis (Axelrod & Reisine, 1984). In addition, ACTH also induces production of mineralocorticoids and androgen precursors. Glucocorticoids exert a negative feedback effect over their own synthesis, whereby they inhibit production of CRF and ACTH (Gagner & Drouin, 1985; Ma, *et al*., 2001; Jacobson, 2005; Buckingham, 2006).

The primary active glucocorticoid in humans is cortisol, whereas in rodents it is corticosterone (Lin & Achermann, 2004). This is due to rodents lacking the 17α-hydroxylase enzyme (Lin & Achermann, 2004). Glucocortcoids display a diurnal circadian rhythm, with levels in humans peaking early in the morning and declining to a nadir in the evening (Lupien, *et al*., 1998; Jacobson, 2005). This is reversed in nocturnal animals such as rodents (Windle, *et al*., 1998).

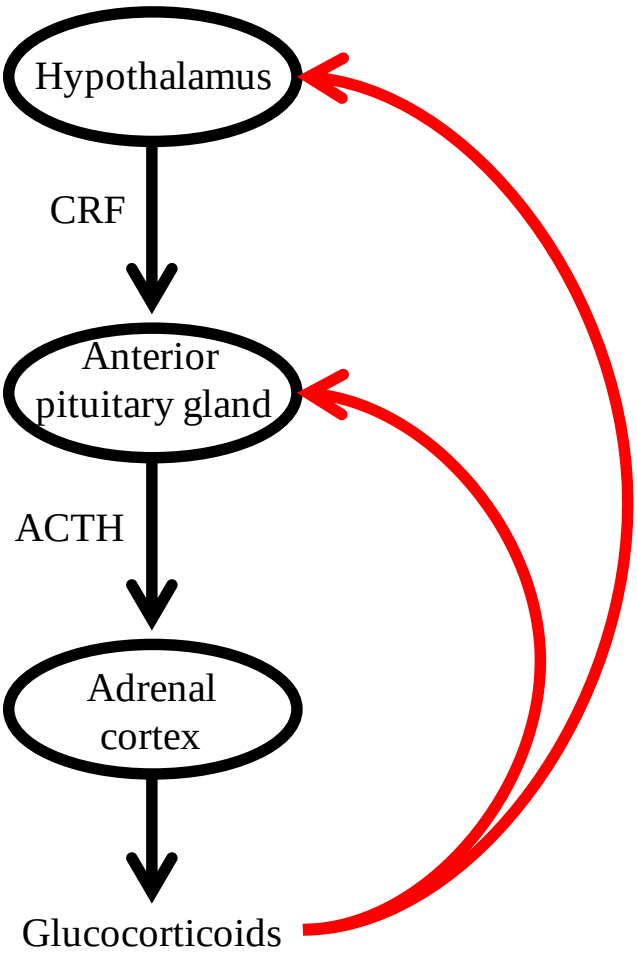

Figure 1.1 The hypothalamic-pituitary-adrenal axis
In response to physical or psychological stressful stimuli, corticotropin-releasing factor (CRF) is released from the paraventricular nucleus in the hypothalamus. This acts in the anterior pituitary gland to produce adrenocorticotropic hormone (ACTH). ACTH is released into the systemic circulation and acts in the adrenal gland to stimulate glucocorticoid synthesis. Glucocorticoids exert a negative feedback effect over their own synthesis, whereby they inhibit production of CRF and ACTH (designated by red arrows).

Once in the circulation, approximately 95% of cortisol is sequestered by plasma proteins, namely corticosteroid-binding globulin (CBG) and albumin (Dunn, *et al*., 1981; Lewis, *et al*., 2005). This generally renders them inactive and prevents them from entering cells and binding to cytosolic glucocorticoid receptors (GR) and mineralocorticoid receptors (MR). Glucocorticoids which do cross the cell membrane and enter the cytosol are subject to pre-receptor metabolism by the two isozymes of the enzyme 11β-hydroxysteroid dehydrogenase (11β-HSD).

1.1.2 11β-HSDs

Glucocorticoids exist in both 'active' and 'inactive' forms, and are interconverted between these two states by 11β-HSD type 1 (11β-HSD1) and 11β-HSD type 2 (11β-HSD2) (Tomlinson & Stewart, 2005) (see Figure 1.2). 11β-HSD1 regenerates glucocorticoids, converting inactive cortisone (11-dehydrocorticosterone in rodents) to its active form, cortisol (corticosterone in rodents). 11β-HSD2 catalyses the reverse reaction, essentially inactivating glucocorticoids in the cytosol and preventing them from binding to GR or MR.

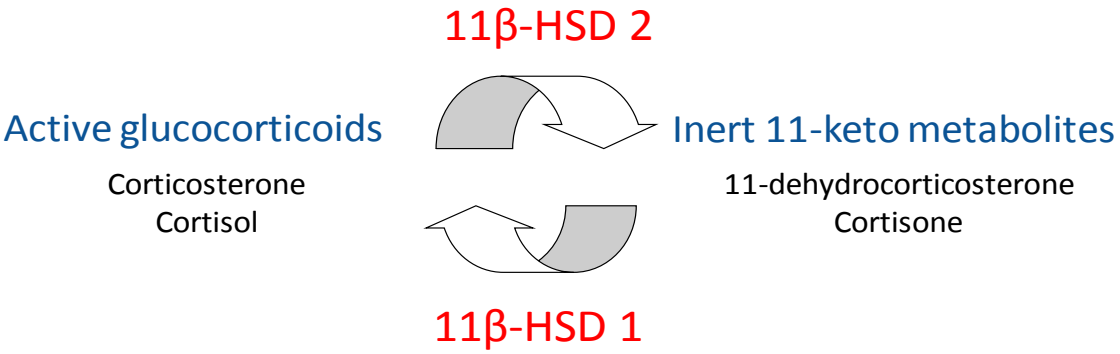

Figure 1.2 The intracellular action of the 11β-HSD isozymes
11β-HSD1 regenerates glucocorticoids, converting inactive cortisone (11-dehydrocorticosterone in rodents) to its active form, cortisol (corticosterone in rodents). 11β-HSD2 catalyses the reverse reaction, inactivating cortisol/corticosterone to cortisone/11-dehydrocorticosterone.

1.1.2.1 11β-HSD1

11β-HSD1 is a bidirectional enzyme with the ability to function as both a reductase enzyme and a dehydrogenase enzyme. In cell homogenates it has been shown to elicit both actions, and in primary cell cultures of human omental adipose stromal cells it has been shown to act as a dehydrogenase (Bujalska, *et al*., 2005), however only reductase activity has been reported in intact cells (Gao, *et al*., 1997; Seckl, 2004). This reductase action appears to be regulated by the enzyme hexose-6-phosphate dehydrogenase (H6PDH) which catalyses the conversion of glucose-6-phosphate to 6-phosphogluconolactonate resulting in the concomitant reduction of nicotinamide adenine disphosphonucleotide (NADPH) from its oxidised form $NADP^+$ (Bujalska, *et al*., 2005; Morton, 2010). NADPH is a crucial cofactor required by 11β-HSD1 in order for it to function as a reductase, as experiments using H6PDH knock-out (KO) mice, which lack NADPH, result in 11β-HSD1 acting as a dehydrogenase (Lavery, *et al*., 2006). Furthermore, humans with mutations which inactivate H6PDH have 'apparent cortisone reductase deficiency', and mutations in the 11β-HSD1 gene (*Hsd11b1*) itself give rise to 'cortisone reductase deficiency' (Tomlinson & Stewart, 2005; Lavery, *et al*., 2006; Lawson, *et al*., 2011). Inactivating mutations in H6PDH can lead to increased activation of the HPA axis, as a compensatory mechanism for reduced cortisol signalling, which also results in increased production of androgens (Tomlinson & Stewart, 2005). Inhibition of androgen synthesis in this setting can be achieved by treatment with the synthetic glucocorticoid dexamethasone (Tomlinson & Stewart, 2005).

Both 11β-HSD1 and H6PDH are localised at the lumen of the endoplasmic reticulum (ER). The N terminus of the 11β-HSD1 protein is attached to the ER membrane and

the C terminus resides in the ER lumen (Ozols, 1998; Odermatt, *et al*., 1999). 11β-HSD1 is widely expressed in various tissues and distribution has been found to be similar in rodents and humans, with highest expression in the liver (Moisan, *et al*., 1990). 11β-HSD1 has also been found in lung, skeletal muscle, brain, adipose, gonads and the gastrointestinal tract (Walker & Seckl, 2003; Tomlinson & Stewart, 2005). 11β-HSD1 has also been detected in inflammatory cells, with expression induced in monocytes after stimulation with proinflammatory cytokines such as interleukin (IL)-4 or IL-13 (Thieringer, *et al*., 2001). It is also induced in macrophages after differentiation from monocytes, and expression has been shown to be further increased *in vitro* after treatment with lipopolysaccharide (LPS) (Thieringer, *et al*., 2001). *In vivo*, 11β-HSD1 is present in neutrophils during inflammation as well as in mast cells (Kardon, *et al*., 2008; Coutinho, 2009). In the cardiovascular system, 11β-HSD1 is found in cardiomyocytes, vascular smooth muscle cells, fibroblasts and the vascular wall (Hadoke, *et al*., 2001; Christy, *et al*., 2003; Klusonova, *et al*., 2009; McSweeney, 2010). During development it has been shown to be present in lung and liver, as well as in neonatal heart (Sheppard & Autelitano, 2002; Speirs, *et al*., 2004).

The *in vivo* role of 11β-HSD1 has largely been investigated using the 11β-HSD1 deficient mouse (Kotelevtsev, *et al*., 1997). Originally, this mouse was described as a knock-out mouse, however it has since been found to be hypomorphic for 11β-HSD1, and is now referred to as 'deficient' for 11β-HSD1 (see Section 2.1.2 for full details). Nevertheless, in most tissues, including the liver, 11β-HSD1 deficient mice are unable to regenerate 11-dehydrocorticosterone to corticosterone intracellularly, confirming that 11β-HSD1 is the only 11β-reductase enzyme present in rodents

(Kotelevtsev, *et al*., 1997). On the C57BL/6 background, 11β-HSD1 deficient mice show increased insulin sensitivity in both liver and adipose tissue and show resistance to diet-induced central obesity when fed a high fat diet (Kotelevtsev, *et al*., 1997; Morton, *et al*., 2001; Morton, *et al*., 2004). Age-related cognitive decline is also attenuated in these mice (Yau, *et al*., 2001; Yau, *et al*., 2007). In addition, mice with genetic overexpression of 11β-HSD1 in adipose have increased adipose levels of corticosterone and increased fat mass, whereas overexpression of 11β-HSD1 in liver leads to insulin resistance, dyslipidaemia, and fatty deposits in this tissue (Masuzaki, *et al*., 2001; Paterson, *et al*., 2005).

1.1.2.1.1 11β-HSD1 and the vasculature

In the cardiovascular system, the role of 11β-HSD1 has also been investigated using the 11β-HSD1 deficient mouse. The expression of 11β-HSD1 in VSMCs indicates that it may play a role in vasoconstriction, but *ex vivo* aortic ring myography preparations from 11β-HSD1 deficient mice revealed vessel contraction after norepinephrine treatment was similar to control (Hadoke, *et al*., 2001).

Apolipoprotein E (ApoE) KO mice are atherosclerosis-prone (Meir & Leitersdorf, 2004; Kolovou, *et al*., 2008). 'Double KO' mice created by crossing ApoE KO mice with 11β-HSD1 deficient mice, have reduced atherosclerosis and decreased macrophage recruitment into atherosclerotic plaques (Kipari, *et al*., 2013). This may be due to the decreased expression of vascular cell adhesion protein (VCAM)-1 seen in these 'double KO' mice (Kipari, *et al*., 2013). Further investigation has revealed a role for 11β-HSD1 in myeloid cells in this setting (Kipari, *et al*., 2013). Irradiated

ApoE KO mice which received 11β-HSD1 deficient bone marrow also exhibited an atheroprotective phenotype, suggesting 11β-HSD1 in myeloid cells is key (Kipari, *et al*., 2013).

11β-HSD1 has been shown to play a key role in angiogenesis and vascular remodelling (Small, *et al*., 2005; Hadoke, *et al*., 2006; McSweeney, *et al*., 2010). Glucocorticoids are known to inhibit angiogenesis and neointimal proliferation (Van Put, *et al*., 1995). In agreement with this, 11β-HSD1 deficiency has been shown to result in enhanced angiogenesis in aortic ring preparations *in vitro* and in implanted subcutaneous sponges *in vivo* (Small, *et al*., 2005). Furthermore, 11β-HSD1 deficiency results in increased angiogenesis *in vivo* in the peri-infarct region of the heart 7d after myocardial infarction (MI) (Small, *et al*., 2005; McSweeney, *et al*., 2010). However, it is unclear whether this increase in angiogenesis is due to direct effects of 11β-HSD1 deficiency in the vasculature, or secondary to changes in pro-angiogenic signalling elsewhere. For example, in the healing myocardial infarct, expression of IL-8, a potent pro-angiogenic cytokine, is increased (Matsukawa, *et al*., 1999; McSweeney, *et al*., 2010; Balamayooran, *et al*., 2011). The inflammatory response is also altered in these mice, with increased neutrophils seen in the heart 48h after MI which may be a result of increased monocyte chemoattractant protein (MCP)-1 expression (McSweeney, *et al*., 2010). Moreover, increased numbers of pro-reparative, pro-angiogenic, alternatively-activated macrophages are also seen in these hearts 7d post-MI (McSweeney, *et al*., 2010).

1.1.2.1.2 11β-HSD1 and the myocardium

11β-HSD1 has also been shown to regulate heart size, with a single nucleotide polymorphism in the *Hsd11b1* gene, which encodes the 11β-HSD1 protein, associating with reduced left ventricular mass in a human population study (Rahman, *et al*., 2011). 11β-HSD1 deficient mice also exhibit a reduced heart size and weight at 12w of age, but systolic function appears to be maintained (McSweeney, 2010). The influence of glucocorticoids on heart structure and function is discussed in Section 1.1.4.

1.1.2.2 11β-HSD2

11β-HSD2 is a $NADP^+$-dependent enzyme which functions solely as a dehydrogenase, and oxidises active glucocorticoids to their inert 11-keto metabolites (Albiston, *et al*., 1994). Like 11β-HSD1, 11β-HSD2 is similarly localised to the ER, however the catalytic domain faces the cytosol rather than the ER lumen (Odermatt, *et al*., 1999). 11β-HSD2 functions to confer specificity for MR by preventing glucocorticoids from illicitly activating these receptors, and allowing occupation by the mineralocorticoid, aldosterone. Aldosterone is not a substrate for 11β-HSD2 (Funder, 1997). The concentration of circulating glucocorticoids is approximately 100 fold higher than that of aldosterone (Krozowski & Funder, 1983; Chapman, *et al*., 2013). MR have a relatively higher affinity for aldosterone, corticosterone and cortisol (K_D = 0.5-2nM) whereas GR have a lower binding affinity for glucocorticoids (K_D = 10-20nM) and show virtually no binding of aldosterone

(Krozowski & Funder, 1983; Hollenberg, *et al*., 1985; Arriza, *et al*., 1987; Sheppard & Funder, 1987; Buckingham, 2006; Nishi & Kawata, 2007).

11β-HSD2 is present in the collecting ducts and medulla of the kidneys, where it protects MR from glucocorticoid activation (Edwards, *et al*., 1988; Brown, *et al*., 1996). This is crucial because glucocorticoid-mediated MR activation in this tissue leads to increased water and sodium retention and potassium excretion, resulting in hypertension (Morton & Seckl, 2008). 11β-HSD2 is also found in the colon, adrenal cortex, salivary glands and placenta (Edwards, *et al*., 1988; Brown, *et al*., 1996; Walker & Stewart, 2003). There is some debate as to whether 11β-HSD2 is present in the vasculature, since 11β-HSD2 KO mice exhibit altered vascular function suggesting a functional role for 11β-HSD2 in this tissue (Hadoke, *et al*., 2001; Christy, *et al*., 2003). For example, aortic preparations from these mice exhibit enhanced contraction after norepinephrine treatment, and impaired vessel relaxation. Importantly, there is no evidence for 11β-HSD2 in cardiomyocytes (Christy, *et al*., 2003), but it is expressed, albeit at relatively modest levels, in the vascular endothelium (Brem, *et al*., 1998). Therefore in the heart, GR and MR are both primarily activated by cortisol/corticosterone (Esteban, *et al*., 1991; Funder, 1997).

Approximately 50% of 11β-HSD2 KO mice die within 48h of birth, with survivors displaying renal hypertrophy, hypokalaemia and hypertension, in addition to the impaired vascular function described above (Kotelevtsev, *et al*., 1999). Human mutations in the 11β-HSD2 gene (*Hsd11b2*) can lead to the Syndrome of Apparent Mineralocorticoid Excess (SAME), characterised by high blood pressure (Draper & Stewart, 2005).

1.1.2.3 11β-HSD1 inhibitors

Glucocorticoids were first reported to possess anti-inflammatory properties in the 1940s and have been used to treat a wide variety of inflammatory diseases ever since, including asthma and rheumatoid arthritis (Hench & Slocumb, 1949). However, in humans with chronically elevated plasma glucocorticoid levels (Cushing's Syndrome), elevated cortisol gives rise to the characteristic hypertension and central obesity observed in these patients (De Bosscher, *et al*., 2003; Souverein, *et al*., 2004). Leptin-resistant obese Zucker rats exhibit glucocorticoid-dependent obesity and elevated 11β-HSD1 expression in adipose tissue (Livingstone, *et al*., 2000). Furthermore, pharmacological doses of glucocorticoids administered to combat inflammatory diseases can have severe adverse side effects, such as type 2 diabetes mellitus and cardiovascular disease.

As previously described, 11β-HSD1 deficient mice show increased insulin sensitivity and resistance to diet-induced central obesity when fed a high fat diet (Kotelevtsev, *et al*., 1997; Morton, *et al*., 2001; Morton, *et al*., 2004), attenuated age-related cognitive decline (Yau, *et al*., 2001; Yau, *et al*., 2007), as well as reduced atherosclerosis on the ApoE KO background (Kipari, *et al*., 2013). As such, inhibition of 11β-HSD1 has been investigated as a possible therapeutic target.

Selective 11β-HSD1 inhibitors have been developed by several pharmaceutical companies such as Merck, Biovitrum and Amgen. In animals models of obesity they have been shown to lower body weight, fasting glucose levels, and plasma cholesterol and triglycerides (Hermanowski-Vosatka, *et al*., 2005). 11β-HSD1 inhibitors have also been shown to improve glucose tolerance and insulin sensitivity in a model of diabetes mellitus (Hermanowski-Vosatka, *et al*., 2005). In

atherosclerosis-prone ApoE KO mice, administration of an 11β-HSD1 inhibitor attenuates plaque development (Hermanowski-Vosatka, *et al*., 2005). More recently, a selective 11β-HSD1 inhibitor developed in our centre has demonstrated efficacy in experimental models of aging and cognitive impairment (Sooy, *et al*., 2010; Yau, *et al*., 2011). Further development of pharmacological 11β-HSD1 inhibitors therefore remains a promising area of pharmaceutical research with widespread clinical applications.

1.1.3 Glucocorticoid signalling

Glucocorticoid action is largely mediated by binding to two intracellular nuclear receptors, GR and MR. GR are ubiquitously expressed in almost all tissues and are chiefly responsible for the physiological effects of glucocorticoids. MR, on the other hand, have a more specific expression pattern and are co-localised with 11β-HSD2 to prevent inappropriate activation by glucocorticoids. MR are found in mineralocorticoid target tissues such as the distal tubule of the kidney, the colon, the brain and the salivary glands as well as the heart and vasculature (reviewed in Chapman, *et al*., 2013).

When GR are not occupied by glucocorticoids they are sequestered in the cytosol by a 300kDa chaperone complex which consists of Hsp70 and Hsp90 as well as stabilising proteins including p23, CyP-40, FKBP51 and FKBP52 (Pratt, *et al*., 2004; Newton & Holden, 2007). When glucocorticoids bind to GR this complex dissociates and allows GR to dimerise and translocate to the nucleus where they regulate gene transcription (Bledsoe, *et al*., 2004; Grad & Picard, 2007). Activated GR bind to

glucocorticoid response elements (GRE) in the DNA which lie upstream of the promoter regions of target genes (Smoak & Cidlowski, 2004). GREs consist of two hexameric half sites which each bind one activated GR (Barnes, 1998). These half sites are imperfect palindromic sequences (5'-GGTACAxxxTGTTCT-3') which are separated by three nucleotides (denoted 'x') (Barnes, 1998). It is primarily through this mechanism that GR promote gene expression, however a non-genomic role for GR transcriptional regulation has been described, with GR monomers binding to other transcription factors (TF), such as signal transducer and activator of transcription 3 (STAT3), which promotes expression of IL-10 (Beck, *et al*., 2009). GR-mediated repression of gene expression has also been reported, although the mechanism behind this is not completely understood. However, it has been proposed that GR binding to AP-1 or nuclear factor-κB (NFκB) may prevent these pro-inflammatory TFs from interacting with DNA binding sites and initiating pro-inflammatory gene transcription (McKay & Cidlowski, 1999; Liberman, *et al*., 2007).

1.1.4 Glucocorticoids and the cardiovascular system

Despite the therapeutic anti-inflammatory properties of glucocorticoids providing effective treatment against several inflammatory diseases, prolonged glucocorticoid administration can lead to adverse cardiovascular side effects, including diabetes mellitus, central obesity and hypertension. In the cardiovascular system, GR and MR are expressed in VSMCs, endothelial cells (EC), cardiomyocytes and fibroblasts, although MR expression in cardiomyocytes is relatively low compared to that of GR

(Walker, *et al*., 1991; Ullian, 1999; Yang & Zhang, 2004; Hadoke, *et al*., 2006; Takeda, *et al*., 2007; Lother, *et al*., 2011).

1.1.4.1 Blood pressure, vascular function and cardiac size

Physiologically, glucocorticoids regulate blood pressure by acting in the kidney, the heart and the vasculature (Connell, *et al*., 1987; Fraser, *et al*., 1999; Masuzaki, *et al*., 2003; Van Raalte, *et al*., 2013). The importance of glucocorticoids in blood pressure control is highlighted by the human conditions Cushing's Syndrome and Addison's Disease, whereby glucocorticoid excess (Cushing's Syndrome) leads to hypertension and, correspondingly, glucocorticoid deficiency (Addison's Disease) leads to hypotension (De Bosscher, *et al*., 2003; Chrousos, 2004; Souverein, *et al*., 2004).

Blood pressure and circulating cortisol are both known to increase with age, and both have been shown to enhance the development of cardiac hypertrophy (Landahl, *et al*., 1986; Van Cauter, *et al*., 1996; Walker, 2007a; De, *et al*., 2011; Drazner, 2011). Furthermore, epidemiological studies have shown a clear link between circulating cortisol and cardiovascular disease. For example, increased HPA axis activity associates with insulin resistance in men (Phillips, *et al*., 1998), and in a cohort of patients with type 2 diabetes mellitus, elevated circulating cortisol was associated with the prevalence of ischaemic heart disease (Reynolds, *et al*., 2010a)

In the kidney GR- and MR-mediated glucocorticoid action results in water and sodium retention which increases blood volume and, therefore, blood pressure (Morton & Seckl, 2008). 11β-HSD2 is highly expressed in the kidney and may serve to regulate glucocorticoid action through MR, since 11β-HSD2 deficiency results in

hypertension (Kotelevtsev, *et al*., 1999; Draper & Stewart, 2005). Within the kidney itself, glucocorticoids can induce vasodilatation of afferent and efferent arterioles by promoting expression of nitric oxide (NO), a potent vasodilator (De Matteo & May, 1997; Whitworth, *et al*., 2000).

In the systemic circulation, glucocorticoids increase vascular tone and peripheral resistance, and facilitate vasoconstriction in a GR-mediated manner (Walker & Williams, 1992). Glucocorticoids reduce expression of the calcium-activated potassium channel in VSMCs (Brem, 2001). This channel extrudes potassium from the cell which aides cellular relaxation (Brem, 2001). Glucocorticoids also stimulate the renin-angiotensin-aldosterone system (RAAS) by upregulating production of angiotensinogen and angiotensin-converting enzyme (ACE) (Sato, *et al*., 1994). This leads to increased angiotensin-mediated vasoconstriction (Sato, *et al*., 1994). Additionally, glucocorticoids inhibit several vasodilators, namely prostacyclin (Walker & Williams, 1992) and prostaglandin I2 (Falardeau & Martineau, 1989), as well as endothelial nitric oxide synthase (eNOS) and inducible nitric oxide synthase (iNOS), which reduces NO bioavailability (Mitchell & Webb, 2002). Glucocorticoids also enhance the effect of vasoconstrictors, including endothelin, and catecholamines such as noradrenaline (Ullian, 1999; Hadoke, *et al*., 2006; Goodwin, *et al*., 2011).

Blood pressure and blood volume both affect preload, a term used to describe the pressure exerted on the left ventricle at the end of diastole. A reduced blood volume decreases the end diastolic filling pressure and results in a smaller left ventricular end diastolic volume (De Simone, 2003). This is because the pressure experienced by the cardiomyocytes in the left ventricular wall is reduced and so cardiomyocyte diastolic

length is reduced (Hanft, *et al*., 2008). As such, hypotensive Addison's Disease patients exhibit reduced heart size (Fallo, *et al*., 1999; Oakley, *et al*., 2013), whereas hypertensive Cushing's Syndrome patients exhibit cardiac hypertrophy and dilated cardiomyopathy (Petramala, *et al*., 2007; Hey, *et al*., 2013; Kim, *et al*., 2014).

The effect of glucocorticoids on heart size has recently come to light, with 11β-HSD1 deficient mice exhibiting reduced heart size and weight (McSweeney, 2010). However, the mechanism for this remains unknown. Moreover, a single nucleotide polymorphism in the *Hsd11b1* gene, which encodes the 11β-HSD1 protein, has been associated with reduced left ventricular mass in a human population study (Rahman, *et al*., 2011). Studies using the GR KO mouse have shown a crucial role for glucocorticoids in heart maturation. GR KO mice die at birth due to underdeveloped lungs (Cole, *et al*., 1995), however a number of these mice die prenatally, prior to lung function being required. It is suggested that this is due to diastolic dysfunction, disorganised myofibrils within cardiomyocytes, and impaired calcium-induced calcium release (Rog-Zielinska, *et al*., 2013).

1.1.4.2 Glucocorticoids and angiogenesis

The anti-angiogenic properties of glucocorticoids have been established for a number of years (Folkman, *et al*., 1983) and, more recently, 11β-HSD1 deficiency has been shown to enhance angiogenesis in subcutaneous sponge implants (Small, *et al*., 2005), suggesting that endogenous, as well as exogenous, glucocorticoids play a role in angiogenesis. Furthermore, in 11β-HSD1 deficient mice, implantation of sponges impregnated with cortisol abolished this increase in angiogenesis (Small, *et al*.,

2005). However, implantation of sponges impregnated with the cortisol precursor cortisone did not attenuate this increased angiogenesis, confirming a key role for 11β-HSD1 in this phenotype (Small, *et al*., 2005). This anti-angiogenic effect of glucocorticoids seems to be GR-mediated, as administration of RU486, a GR antagonist, also enhances angiogenesis (Small, *et al*., 2005). This is in agreement with *in vitro* experiments which showed that angiogenesis is attenuated in cultured VSMCs and ECs treated with dexamethasone, but not aldosterone, suggesting this anti-angiogenic influence is GR-mediated (Longenecker, *et al*., 1982; Longenecker, *et al*., 1984).

Hypoxia in adipose tissue is seen in obesity (Hosogai, *et al*., 2007). Deficiency of 11β-HSD1 in this tissue attenuates hypoxia and results in increased angiogenesis, possibly due to upregulation of hypoxia-inducible factor-1α (HIF-1α) and reduced fibrosis in this tissue (Michailidou, *et al*., 2012). HIF-1α is a transcription factor which, under normoxic conditions, is cytosolically sequestered by ubiquitination and subsequent proteosomal degradation (Ke & Costa, 2006). However, at low oxygen tension HIF-1α translocates to the nucleus where it transcribes genes involved in metabolism, erythropoiesis and angiogenesis, such as vascular endothelial growth factor (VEGF), transforming growth factor β (TGFβ), angiopoetin-1 (Ang-1), angiopoetin-1 (Ang-2) and platelet derived growth factor B (PDGFB) (Kelly, et al., 2003). VEGF binds to the VEGF receptor 2 (VEGFR2), a tyrosine kinase receptor, on endothelial cells to initiate a signalling cascade which results in production of eNOS (Kroll & Waltenberger, 1998). This enzyme catalyses the conversion of L-arginine to NO which increases vascular permeability and has been shown to mediate VEGF-mediated angiogenesis; administration of eNOS inhibitors attenuates

angiogenesis *in vitro* and *in vivo* (Palmer, *et al*., 1988; Ziche, *et al*., 1997; Fukumara, *et al*., 2001). VEGF signalling also stimulates fibroblast growth factor (FGF), which is involved in proliferation and survival of ECs and VSMCs (Sunderkotter, *et al*., 1994).

The role of HIF-1α and VEGF in inhibition of angiogenesis by glucocorticoids has been shown by experiments in which osteoblasts and osteocytes transgenically express 11β-HSD2 (Weinstein, *et al*., 2010). 11β-HSD2 expression in these cells attenuates the decline in bone strength and mass usually seen in aging by enhancing angiogenesis, possibly by diminishing the inhibition of HIF-1α and VEGF (Weinstein, *et al*., 2010). In humans, Cushing's Syndrome patients have elevated glucocorticoid levels and display impaired wound healing, potentially through reduced VEGF signalling (Gordon, *et al*., 1994; Stojadinovic, *et al*., 2007).

1.1.5 Cardiac function

Calcium handling is an important regulator of cardiomyocyte contraction and relaxation. Contraction is regulated by a process called excitation-contraction coupling, which is a term used to describe the conversion of an electrical stimulus, such as an action potential, into a cellular response. As an action potential propagates along a cardiomyocyte and depolarises the cell membrane, calcium flows into the cell from the extracellular space predominantly through L-type calcium channels, which are primarily located on the t-tubules (Sham, *et al*., 1995; Cannell & Soeller, 1997), although the sodium calcium exchanger (NCX) also contributes to calcium entry (Weisser-Thomas, *et al*., 2003) (see Figure 1.3). Upon entering the cell,

calcium binds to ryanodine receptors (RyR) which are present on the surface of the sarcoplasmic reticulum (SR) (Fabiato & Fabiato, 1972; Sham, *et al*., 1995; Cannell & Soeller, 1997). This activates ryanodine receptors and allows further calcium to enter the cytosol from the SR (Fabiato & Fabiato, 1972; Sham, *et al*., 1995; Cannell & Soeller, 1997). These small releases of calcium from one RyR, or from a cluster of RyRs, comprise the basic events of excitation-contraction coupling and are called calcium sparks (Cheng, *et al*., 1993). The summation of several thousand calcium sparks gives rise to the calcium transient, which ultimately increases the concentration of intracellular calcium (Lopez-Lopez, *et al*., 1995). This process is called calcium-induced calcium release (CICR), which is one of the key mechanisms involved in excitation-contraction coupling in cardiac muscle. The rise in intracellular calcium concentration causes calcium to bind to troponin C, which is part of the myofilament complex (Haikala, *et al*., 1995; Spyracopoulos, *et al*., 1997). Upon calcium binding, troponin C undergoes a conformational change which ultimately allows the myosin heads access to the actin filament, resulting in cellular contraction (Spyracopoulos, *et al*., 1997).

Following contraction, calcium is removed from the cytosol via a number of mechanisms. Calcium is either taken back up into the SR through the action of the sarcoplasmic reticulum Ca^{2+} ATPase (SERCA), or extruded from the cell by NCX (Reeves & Hale, 1984; Periasamy & Kalyanasundaram, 2007). The sarcolemmal Ca^{2+} ATPase also contributes to calcium extrusion from the cell but only accounts for approximately 2-3% of calcium removal (Bassani, *et al*., 1992). Efficient removal of calcium from the cytosol facilitates rapid cardiomyocyte, and thus ventricular, relaxation.

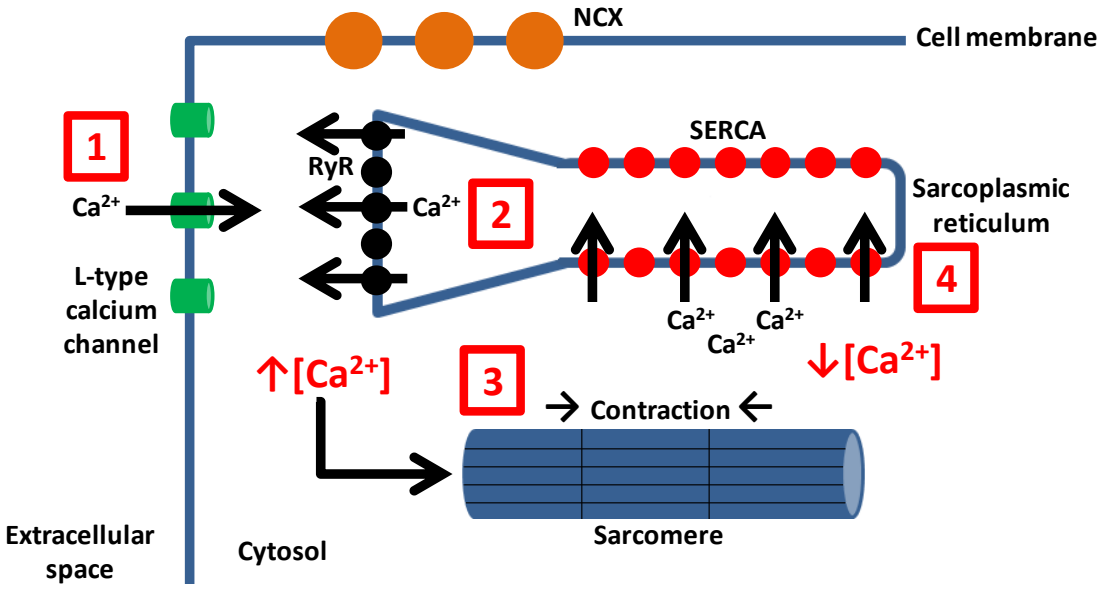

Figure 1.3 The mechanism of excitation-contraction coupling in cardiomyocytes
(1) An action potential is sensed by the L-type calcium channel, which opens and allows extracellular calcium to enter the cell. (2) This calcium binds to RyR on the surface of the SR, causing high levels of calcium to be released from the SR into the cytosol which raises the intracellular calcium concentration. (3) Calcium then binds to the troponin complex on the sarcomeres causing contraction. (4) Calcium is then removed from the cytosol either by re-uptake into the SR by SERCA, or by extrusion from the cell by NCX.

In rodents, re-uptake of calcium back into the SR by SERCA is the dominant mechanism, accounting for over 90% of calcium removal from the cytosol (Bers, 2001). This is in contrast with humans, where SERCA is only responsible for removing approximately two thirds of calcium from the cytosol (Haghighi, et al., 2003). SERCA is also important for appropriate systolic function, as mice heterozygous for the gene encoding SERCA, *Atp2a2*, show a reduction in contractile capacity (Schultz, *et al*., 2004). SERCA KO mice show reduced contractility possibly due to reduced SR calcium stores and therefore reduced calcium release during excitation-contraction coupling (Ji, et al., 2000). Furthermore, overexpression of SERCA results in an enhanced rate of contractility, due to a doubling of the calcium transient amplitude, as well as relaxation (Baker, *et al*., 1998; Vetter, *et al*., 2002).

SERCA activity is regulated by phospholamban (PLN) (MacLennan, *et al*., 2003). When PLN is phosphorylated, it is unable to interact with SERCA and so SERCA can transport calcium into the SR (MacLennan, *et al*., 2003). When PLN is not phosphorylated, it inhibits SERCA activity (MacLennan, *et al*., 2003). PLN phosphorylation at Serine 16 (Ser16) and Threonine 17 (Thr17), by protein kinase A (PKA) and Ca^{2+}/calmodulin dependent protein kinase II (CamKII), respectively, is key to relieving inhibition of SERCA (McIvor, *et al*., 1988; Picht, *et al*., 2007). NCX is the primary mechanism by which calcium is extruded from the cell and is inhibited by phospholemman (Cheung, *et al*., 2007). This inhibition is lifted by PKA-mediated phosphorylation of phospholemman (Cheung, *et al*., 2007).

There is clear interplay between these two mechanisms of calcium removal from the cytosol, as they can be thought of as ‘competing’ for the same pool of intracellular

calcium. For example, in the SERCA KO mouse, there is a 2.5 fold increase in calcium extrusion by NCX, which is possibly to compensate for the lack of calcium reuptake into the SR (Li, *et al*., 2011). In heart failure, several clinical studies have reported reduced SERCA mRNA levels and protein expression (Mercadier, *et al*., 1990; Takahashi, *et al*., 1992) and a subsequent increase in NCX mRNA and protein expression (Studer, *et al*., 1994; Flesch, *et al*., 1996). Global NCX KO is embryonic lethal (Cho, *et al*., 2000), but cardiomyocyte-specific NCX KO mice survive through to adulthood (Henderson, *et al*., 2004). These mice appear to compensate for lack of NCX by increasing activity of the sarcolemmal calcium pump (Henderson, *et al*., 2004). L-type calcium channel current is reduced by approximately 50% and so these mice avoid intracellular calcium overload by limiting calcium entry into the cell (Henderson, *et al*., 2004).

1.1.5.1 Glucocorticoids and cardiac function

The role of glucocorticoids on cardiac function has also been investigated, primarily through the use of genetically modified animals. GR overexpression studies have shown the importance of glucocorticoids in maintaining cardiac homeostasis with tissue-specific myocardial overexpression of GR contributing to bradycardia, atrio-ventricular block, and altered calcium cycling (Sainte-Marie, *et al*., 2007). For example, isolated ventricular cardiomyocytes from these mice have increased calcium transients and increased SR calcium load (Sainte-Marie, *et al*., 2007). Glucocorticoids have been shown to play a role in SERCA expression developmentally, in adulthood, and after an ischaemic insult. In late gestation an increase in SERCA mRNA is normally seen, however this is attenuated in GR KO

mice suggesting immature excitation-contraction coupling, as well as calcium-induced calcium release, in these mice (Rog-Zielinska, *et al*., 2013). In a setting of myocardial ischaemia in piglets, methylprednisolone treatment after cardio-pulmonary graft prevents loss of SERCA protein and maintains the calcium transient in cardiomyocytes (Pearl, *et al*., 2011). Furthermore, hexose-6-phosphate dehydrogenase (H6PDH) KO mice have reduced SERCA protein expression in skeletal muscle (Lavery, *et al*., 2008)

Glucocorticoids have been known for a long time to be implicated in contractile function, as adrenalectomy in rats decreased papillary muscle contractile force (Lefer, 1968). This phenotype can be reversed by dexamethasone administration (Lefer, 1968). Experimental investigation of MR has also provided insights into the role of these receptors in cardiac function. MR cardiac deletion and cardiac overexpression studies have found that both these genetic manipulations lead to premature death (Beggah, *et al*., 2002; Ouvrard-Pascaud, *et al*., 2005). Furthermore, surviving mice with cardiac overexpression of MR have arrhythmias (Ouvrard-Pascaud, *et al*., 2005). Cardiac overexpression of 11β-HSD2 has been shown to enhance cardiac fibrosis and lead to hypertrophy and heart failure (Qin, *et al*., 2003). With regard to intracellular glucocorticoid amplification, 11β-HSD1 deficiency does not seem to impact upon systolic function (McSweeney, 2010), however diastolic function in this setting remains unknown. Considering all the above literature, this shows glucocorticoids clearly play a key role in regulating cardiac function.

1.1.6 Glucocorticoids and inflammation

Historically, glucocorticoids have been viewed as anti-inflammatory, however their role is best described as immunomodulatory (Sapolsky, *et al*., 2000). Glucocorticoids inhibit production of the pro-inflammatory cytokines and chemokines IL-1β, IL-6, IL-8, tumour necrosis factor α (TNFα) and MCP-1, as well as increasing expression of anti-inflammatory molecules such as IL-4 and IL-10 (Barnes, 1998; Tuckermann, *et al*., 2007). Due to a lack of GREs in the promoter regions of some of these genes, and due to the relatively short timescale in which these glucocorticoid-mediated effects are seen (minutes rather than hours), it is thought these actions are achieved via non-genomic mechanisms. For example, macrophage phagocytosis is inhibited *in vitro* within 30min of corticosterone administration, and neutrophil degranulation is suppressed *in vitro* within 5min of 6α-methylprednisolone administration (Liu, *et al*., 2005; Long, et al., 2005). Furthermore, mice with a mutation in the GR DNA binding domain, which prevents activated GR from dimerising and binding to GREs, still exhibit anti-inflammatory properties by suppressing the action of NFκB and AP-1 (Reichardt, *et al*., 1998). Activated GR also stimulate production of inhibitor of κB (IκB) (Barnes, 1998). IκB is a regulatory subunit which sequesters NFκB in the cytosol and prevents it from translocating to the nucleus.

Recently, glucocorticoids have also been shown to possess pro-inflammatory actions. Following LPS exposure, administration of glucocorticoids has been shown to suppress production of the pro-inflammatory mediators TNFα, IL-1β and IL-6 in rodents *in vivo*, whereas administration of glucocorticoids prior to LPS treatment enhances the expression of these molecules (Frank, *et al*., 2010). Endogenous glucocorticoids have also been demonstrated to mobilise neutrophils from the bone

marrow in a GR-dependent manner (Cavalcanti, *et al*., 2007). Administration of granulocyte colony-stimulating factor (G-CSF) has been shown to increase circulating neutrophil numbers, an effect which is potentiated by administration of the exogenous glucocorticoid, dexamethasone (Liles, *et al*., 1997).

Intracellular glucocorticoid regeneration by 11β-HSD1 has implicated a further role for glucocorticoids in modulating the inflammatory response. For example, 11β-HSD1 mRNA levels are known to increase once monocytes differentiate into macrophages (Thieringer, *et al*., 2001) and 11β-HSD1 activity in macrophages is potentiated in a model of sterile peritonitis (Gilmour, *et al*., 2006). Furthermore, administration of an 11β-HSD1 inhibitor following LPS treatment attenuates pro-inflammatory cytokine production (Ishii, *et al*., 2007).

The role of 11β-HSD1 in modulating the inflammatory response and regulating angiogenesis has therefore led to speculation that 11β-HSD1 may be a suitable target for beneficially modifying the post-MI response.

1.2 Myocardial infarction

Myocardial infarction results from an occlusion in one of the coronary arteries which perfuse the myocardium. This occlusion is usually due to the rupture of an atherosclerotic plaque and subsequent thrombus formation. In the past ten years, there has been a three fold rise in percutaneous coronary interventions, a procedure used to unblock stenosed coronary arteries (Townsend, *et al*., 2012). As such, investigation into preventing and treating MI, as well as attenuating the post-MI progression to heart failure remains a key area of medical research.

1.2.1 Cardiomyocyte necrosis

Tissue distal to the point of occlusion in the the coronary artery becomes ischaemic leading to necrotic and apoptotic cell death (Mani, 2008), which triggers an inflammatory response and ultimately results in formation of a collagen scar, as the myocardium is unable to efficiently regenerate in order to replace the damaged tissue. Intracellular hallmarks of necrosis include calcium accumulation, increased levels of reactive oxygen species (ROS), such as superoxide and peroxynitrite, and mitochondrial dysfunction, resulting in reduced anaerobic respiration (Niehaus Jr, 1978; Mani, 2008). In a normal physiological environment, ROS are essential for cell signalling and are regulated by antioxidants (Thannickal & Fanburg, 2000). However, high levels of ROS, such as those seen after MI, can escape this regulatory mechanism and lead to cell injury; they reduce cardiomyocyte cell membrane integrity by peroxidising membrane lipids and therefore contribute to the spilling of cytosolic contents into the extracellular matrix (ECM) (Thollon, *et al*., 1995; Von

Harsdorf, *et al*., 1999). Spillage of mitochondrial proteins, such as cardiolipin, from necrotic cardiomyocytes triggers the sequential serine protease reactions of the complement cascade (Rossen, *et al*., 1994).

Necrosis of cardiomyocytes is a powerful inflammatory stimulus which activates toll-like receptors (TLRs) and the complement cascade through the release of damage-associated molecular patterns (DAMPs) from cardiomyocytes (De Haan, *et al*., 2013). ROS, TNFα, and DNA and RNA spilled into the ECM by necrotic cardiomyocytes activates TLRs, specifically TLR2, and other pathways leading to the dissociation of NFκB from its regulatory subunit IκB, allowing NFκB to translocate to the nucleus (Kin, *et al*., 2006). Once in the nucleus, it initiates the transcription of genes involved in the inflammatory response, as well as cell proliferation and survival (Kin, *et al*., 2006). These include IL-1β, IL-6, IL-8, MCP-1 and macrophage inflammatory protein-2 (MIP-2) (Li, *et al*., 2001; Zhou, *et al*., 2003), which are involved in neutrophil and macrophage recruitment to the site of injury. The importance of TLR2 has been shown using the TLR2 KO mouse, which exhibits reduced fibrosis and preserved ejection fraction after MI (Shishido, *et al*., 2003).

1.2.2 Cardiomyocyte apoptosis

Cardiomyocyte apoptosis occurs in areas of low oxygen tension, primarily around the infarct border, and is characterised by shrinkage of the cell, chromatin condensation and DNA fragmentation (Shih, *et al*., 2011). Hypoxia can activate the B-cell lymphoma-2 (BCL-2) family which increases the mitochondrial outer

membrane permeability (MOMP) (Youle & Strasser, 2008). This results in cytochrome-C entering the cytosol and activating caspases, namely caspase-9 and caspase-3 (Youle & Strasser, 2008). These caspases stimulate nuclear lamins and nuclear inhibitor of caspase-activated deoxyribonuclease/DNA fragmentation factor-45 (ICAD/DEF45) leading to DNA fragmentation (Henkart, 1996; Sakahira, *et al*., 1998). Alternatively, activation of death receptors by TNFα or Fas ligand can activate bax which in turn modifies MOMP and results in caspase activation (Chao, *et al*., 2002). Compared to necrosis, apoptosis does not elicit an inflammatory response, and apoptotic cells can even promote expression of anti-inflammatory molecules, such as TGFβ, from macrophages (Huynh, *et al*., 2002).

Several studies, going back to the 1970s, have investigated the therapeutic capacity of administering glucocorticoids after MI (Libby, *et al*., 1973; Hoffstein, *et al*., 1976). In a canine model, glucocorticoids given immediately after infarction were found to be initially protective, by reducing ischaemic cell death, and therefore limiting infarct size (Libby, *et al*., 1973), possibly by preserving the integrity of lysosomal membranes and thus preventing the spillage of lysozymes into the cytosol (Hoffstein, *et al*., 1976). This led to studies in humans which showed that administration of glucocorticoids within 48h of infarction reduced mortality and infarct size (Barzilai, *et al*., 1972; Morrison, *et al*., 1976). However, chronic glucocorticoid treatment increases infarct size and the prevalence of arrhythmias (Roberts, *et al*., 1976), as well as increasing the likelihood of left ventricular rupture (Hammerman, *et al*., 1983). In a rat model of MI, long term corticosteroid administration has been shown to increase infarct size (Scheuer & Mifflin, 1997)

1.2.3 Neutrophil recruitment

Induction of proinflammatory cytokines and chemokines by necrosis after MI, such as IL-6, IL-8 and TNFα leads, firstly, to neutrophil infiltration and then shortly thereafter to macrophage infiltration (Li, *et al*., 2001; Zhou, *et al*., 2003). Neutrophils appear early after MI, with levels peaking at 24-48 hours after infarction, and are responsible for removing necrotic cells, which are mainly cardiomyocytes, from the site of injury (Nahrendorf, *et al*., 2007). Neutrophils are very important to the post-MI inflammatory response, since they play a key role in clearing cell debris from the site of injury. Furthermore, they secrete IL-4 which contributes to regulation of the pro-reparative phase of infarct healing (Brandt, *et al*., 2000). In normal conditions, they remain in the systemic circulation, but migrate towards the heart after MI in response to pro-inflammatory stimuli and interact with the vessel wall (Frangogiannis, *et al*., 2002). Upregulation of adhesion molecules on ECs, such as P-selectin, intercellular adhesion molecule-1 (ICAM-1), and platelet endothelial cell adhesion molecule-1 (PECAM-1, also called CD31) allows neutrophils to adhere to and then roll along the vessel wall (Briaud, *et al*., 2001; Thompson, *et al*., 2001). β2-integrins and L-selectin on the cell surface of neutrophils facilitates tethering to ECs and subsequent transmigration into tissues (Frangogiannis, *et al*., 2002).

IL-6 and IL-8 are key pro-inflammatory molecules involved in neutrophil recruitment to the site of injury (Frangogiannis, *et al*., 2002). After splanchnic artery occlusion shock, IL-6 KO mice have reduced P-selectin and ICAM-1 expression in the ileum and attenuated neutrophil infiltration into the reperfused intestine (Cuzzocrea, *et al*., 1999). IL-8 deficiency, or antagonism of its receptor CXCR2, has been shown to impair neutrophil infiltration into the heart after MI and into the

synovial vasculature in another inflammatory model; monarticular antigen-induced arthritis (Kukielka, *et al*., 1995; Coelho, *et al*., 2008).

As has been described in Section 1.1.6, endogenous glucocorticoids play a role in mobilising neutrophils from the bone marrow in a GR-dependent manner (Cavalcanti, *et al*., 2007). Furthermore, the increase in circulating neutrophils in response to G-CSF treatment is potentiated by administration of the exogenous glucocorticoid, dexamethasone (Liles, *et al*., 1997). ACTH administration has also been shown to augment neutrophil liberation from the bone marrow (Roth, *et al*., 1982), which may provide a mechanism for the well-established increase in recruited neutrophils seen in the heart after MI (Frangogiannis, 2008), since circulating cortisol is also known to increase after infarction (Nito, *et al*., 2004). Although glucocorticoids have been shown to prolong neutrophil survival *in vitro* (Ruiz, *et al*., 2002), they do not inhibit neutrophil apoptosis in hypoxic conditions (Marwick, *et al*., 2013), which are similar to those found in the heart after MI. Moreover, primary cultured endothelial cells from adrenalectomised rats, which are glucocorticoid deficient, have increased expression of ICAM-1, VCAM-1 and L-selectin (Cavalcanti, *et al*., 2007). These genes are involved in cellular adhesion, and neutrophil tethering and extravasation (Cavalcanti, *et al*., 2007). In agreement with these findings are experiments which show dexamethasone treatment inhibits the increase in expression of endothelial-leukocyte adhesion molecule-1 (ELAM-1) and ICAM-1 on LPS-stimulated human umbilical vein endothelial cells (HUVECs) (Cronstein, *et al*., 1992). Dexamethasone treatment has also been shown to reduce expression of L-selectin and β2 integrins on circulating neutrophils and lymphocytes

(Burton, *et al*., 1995; Jilma, *et al*., 1997; Briaud, *et al*., 2001). These genes are required for neutrophil adhesion and transmigration into tissues.

1.2.4 Macrophage infiltration

In the bone marrow, $CD34^+$ macrophage and dendritic cell progenitor cells give rise to monocytes, which circulate in the blood and enter tissues in response to pro-inflammatory stimuli (Van Furth & Cohn, 1968; Auffray, *et al*., 2009; Geissmann, *et al*., 2010). After MI, they are one of the first cell types to enter the heart where they differentiate into macrophages (Jung, *et al*., 2013). In mice, as in humans, there are two distinct monocyte subsets, which are characterised by their relative expression of lymphocyte antigen 6C (Ly6C) (Geissmann, *et al*., 2003). $Ly6C^{hi}$ monocytes are potent proinflammatory mediators, whereas $Ly6C^{lo}$ monocytes play a key role in the resolution of inflammation and are thus regarded as anti-inflammatory (Geissmann, *et al*., 2003; Nahrendorf, *et al*., 2007). Macrophage differentiation from monocytes is stimulated by macrophage colony-stimulating factor (M-CSF) (Frangogiannis, *et al*., 2002), and macrophages have been shown to be crucial for appropriate healing of the myocardium after MI, since macrophage depletion using anti-macrophage serum impairs wound healing (Cohen, *et al*., 1987). Furthermore, inhibition of macrophage function by administration of clodronate-containing liposomes results in impaired angiogenesis in the infarct border *in vivo*, as well as reduced vessel sprouting in an *ex vivo* aortic ring preparation (Gelati, *et al*., 2008; Van Amerongen, *et al*., 2008). This phenotype may be rescued following treatment with bone marrow-derived macrophages which highlights the important role of macrophages in the induction of angiogenesis (Gelati, *et al*., 2008). Moreover, injection of macrophages into the heart

in an experimental model of MI leads to preserved systolic function and attenuated left ventricular remodelling (Leor, *et al*., 2006).

In the first 3 to 4 days after MI, $Ly6C^{hi}$ monocytes are the dominant subset in the myocardium, where they are attracted to the site of injury by MCP-1 and differentiate into 'classically-activated' macrophages, also called M1 macrophages (Kakio, *et al*., 2000; Nahrendorf, *et al*., 2007). These cells digest infarcted tissue, and remove apoptotic neutrophils and necrotic cardiomyocytes. Furthermore, these cells produce the pro-inflammatory mediators IL-1, IL-6 and IL-23, thus augmenting the inflammatory response (Sunderkotter, *et al*., 1994). M1 macrophages are also involved in regulating ECM remodelling by expressing matrix metalloproteinases (MMP), such as MMP-9 (Schmidt, *et al*., 2006). MCP-1 has been shown to be a key promoter of $Ly6C^{hi}$ monocyte recruitment to sites of injury, for example in atherosclerosis and rheumatoid arthritis (Nelken, *et al*., 1991; Koch, *et al*., 1992). MCP-1 is known to enhance angiogenesis and maintain systolic function after MI (Morimoto, *et al*., 2006), possibly via its effect on macrophages. This is because disruption of the MCP-1 gene results in abnormal macrophage polarisation and delayed macrophage infiltration into the heart after MI (Dewald, *et al*., 2005). This is hypothesised to be due to the decreased expression of IL-1β, IL-10, TNFα and TGFβ, which are cytokines necessary for differentiation into the pro-reparative alternatively-activated state (Dewald, *et al*., 2005).

From day four after MI, more 'alternatively-activated' $Ym1^{+}$ macrophages are seen in the heart, where they play a crucial role in scar resolution and infarct healing (Nahrendorf, *et al*., 2007; McSweeney, *et al*., 2010). Induction of this M2 phenotype is primarily mediated by IL-4 and IL-13 (Gordon, 2003). These cells secrete the anti-

inflammatory cytokines IL-10 and TGFβ (Nahrendorf, *et al*., 2007; Lambert, *et al*., 2008; Van Amerongen, *et al*., 2008) and are involved in induction of post-MI angiogenesis, particularly in the peri-infarct region, by releasing basic FGF, insulin-like growth factor-1 (IGF-1) and VEGF (Berse, *et al*., 1992; Henke, *et al*., 1993; Nahrendorf, *et al*., 2007; Dobrucki, *et al*., 2010). Depletion of macrophages via administration of diphtheria toxin to mice expressing the diphtheria toxin receptor under the control of the CD11b promoter leads to impaired wound healing (Mirza, *et al*., 2009). Reduced granulation tissue formation and scar deposition, as well as increased haemorrhage and apoptosis of neovascular ECs, were seen in these mice in response to excisional skin wounding thus showing an essential role for macrophages in wound repair (Lucas, *et al*., 2010).

The pro-angiogenic factor, IL-8, is secreted by macrophages and endothelial cells, and its action is mediated by it binding to its receptor, CXCR2 (Koch, *et al*., 1992; Heidemann, *et al*., 2003; Li, *et al*., 2003). IGF-1 is also secreted by macrophages (Dobrucki, *et al*., 2010), and has been shown to upregulate IL-8 expression and enhance angiogenesis after isoproterenol-induced MI in rats (Haleagrahara, *et al*., 2011). M2 macrophages are also involved in ECM remodelling and scar resolution by activating myofibroblasts, which serves to initiate collagen, laminin, and fibronectin deposition (Weber & Brilla, 1991).

The effects of glucocorticoids on modulating the inflammatory response has been extensively investigated (reviewed in Walker, 2007a; Chapman, *et al*., 2009; Cooper & Stewart, 2009; Hadoke, *et al*., 2009). Evidence from clinical trials has shown the importance of the post-MI inflammatory response, and the modulatory effect of glucocorticoids, with administration of methylprednisolone in MI patients resulting

in increased mortality due to left ventricular rupture (Hammerman, *et al*., 1983). MR blockade has been shown to result in a modified inflammatory response, with an increase in alternatively-activated macrophages, and enhanced neovascularisation in a rat model of MI (Fraccarollo, *et al*., 2008). Moreover, MR deletion in myeloid cells leads to enhanced M2 polarisation, with concomitant protection against hypertrophy and fibrosis in response to L-N^G-nitroarginine methyl ester (L-NAME) and angiotensin II treatment (Usher, *et al*., 2010).

The role of 11β-HSD1 in modifying inflammation after infarction has also been investigated. Mice globally deficient in 11β-HSD1 have an augmented inflammatory response, associated with increased representation of pro-reparative alternatively-activated macrophages 7d post-MI (McSweeney, *et al*., 2010).

1.2.5 Post-MI angiogenesis

Angiogenesis, the formation and growth of new vessels from existing capillaries, is a complex process and can be induced by several mechanisms including hypoxia (Wang, *et al*., 2006), nitric oxide (Papapetropoulos, *et al*., 1997; Matsunaga, *et al*., 2000), chemokines such as IL-8 (Li, *et al*., 2003; McSweeney, *et al*., 2010) and pro-angiogenic growth factors such as nerve growth factor (NGF) (Meloni, *et al*., 2010), FGF (Giordano, *et al*., 1996), IGF-1 (Dobrucki, *et al*., 2010) and VEGF (Pearlman, *et al*., 1995; Ziche, *et al*., 1997; Schwarz, *et al*., 2000). These signals activate quiescent endothelial cells, which causes an increase in vascular permeability and allows endothelial cell migration and proliferation. Following endothelial sprouting, the primitive vessel system is pruned and organised into an efficient network

(Bergers & Song, 2005). Upon pericyte coating, these vessels mature and provide a long term blood supply to the surrounding tissue (Bergers & Song, 2005).

The induction of HIF-1α expression in ischaemic conditions leads to the upregulation of several pro-angiogenic factors, such as VEGF, TGFβ, Ang-1, Ang-2 and PDGFB (Kelly, *et al*., 2003). VEGF-induced angiogenesis is stimulated by eNOS-mediated NO production (Ziche, *et al*., 1997), and experimental data has shown VEGF gene therapy increases neovascularisation and improves ejection fraction in rat (Hao, *et al*., 2007) and rabbit (Bull, *et al*., 2003) models of MI. Moreover, genetic manipulation of HIF-1α has confirmed the key role of this protein in mediating angiogenesis. Deletion results in impaired vascular development, whereas over-expression leads to increased angiogenesis and reduced infarct size after MI (Kido, *et al*., 2005; Shohet & Garcia, 2007).

Stimulation of angiogenesis through the use of growth factors has had limited success, (Losordo, *et al*., 1998; Simons, 2005; Ellis, *et al*., 2006), as this leads to the formation of a disorganised network of leaky vasculature (Korpisalo, *et al*., 2008). Gene therapy studies aimed at enhancing post-MI angiogenesis have included using VEGF. VEGF gene therapy in this setting is probably the most extensively investigated of all growth factors, and therapy using the VEGF-165 isoform has been shown to enhance angiogenesis, leading to improved ejection fraction and increased myocardial viability (Zhang, *et al*., 2002; Ferrarini, *et al*., 2006; Rissanen & Yla-Herttuala, 2007). However, unregulated expression or chronic overexpression of VEGF has been shown to accelerate atherosclerosis and lead to the formation of intramural vascular tumours (Lee, *et al*., 2000; Celletti, *et al*., 2001). Furthermore, clinical trials, such as the EUROINJECT and NORTHERN trials, were unable to

demonstrate a clear benefit of VEGF therapy (Kastrup, *et al*., 2005; Stewart, *et al*., 2009). As such, the identification of an alternative means of promoting angiogenesis after MI is required.

The role of cardiac fibroblasts in regulating angiogenesis is now also well recognised, with several fibroblast-derived proteins, such as collagen I, procollagen C endopeptidase enhancer, osteonectin, TGF β-induced protein ig-h3 and IGF-binding protein 7, having been shown to be critical for lumen formation and EC sprouting (Newman, *et al*., 2011).

The anti-angiogenic properties of glucocorticoids have been established for a number of years (Folkman, *et al*., 1983). Administration of physiological levels of either dexamethasone or cortisol to cultured HUVECs and human aortic endothelial cells (HAoECs) results in inhibition of endothelial cell sprouting and therefore decreased formation of tube-like structures *in vitro* (Logie, *et al*., 2010). This effect is GR-mediated since the phenotype is reversed by addition of RU486, a GR antagonist (Logie, *et al*., 2010). Furthermore, *in vivo* experiments have shown exogenous glucocorticoid administration suppresses angiogenesis in murine bone, a phenotype which is attenuated by overexpression of 11β-HSD2 (Weinstein, *et al*., 2010). The anti-angiogenic properties of glucocorticoids in this setting appear to be due to their inhibition of HIF1α and VEGF expression in murine osteoblasts and osteocytes (Weinstein, *et al*., 2010). In a pathophysiological setting of cancer, administration of glucocorticoids to renal cell carcinoma cells inhibit VEGF mRNA production and protein expression *in vitro* (Iwai, *et al*., 2004). Moreover, mice with a DU145 cell line (prostate cancer cell line) xenograft show reduced VEGF and IL-8 expression in response to dexamethasone treatment *in vivo* (Yano, *et al*., 2006).

After infarction, 11β-HSD1 deficient mice have also been shown to have increased angiogenesis in the peri-infarct region which is associated with maintained ejection fraction (Small, *et al*., 2005; McSweeney, *et al*., 2010). In the long term, maintenance of peri-infarct angiogenesis is crucial to prevent infarct expansion (Liu, *et al*., 2007). For example, in humans, capillary density in infarcted hearts correlates with reduced infarct size (Prech, *et al*., 2006).

1.2.6 Scar formation

Following the inflammatory phase after infarction, necrotic cardiomyocytes are replaced with non-contractile, fibrotic tissue resulting in the formation of a collagen-rich scar (Frangogiannis, *et al*., 2002), which is necessary to maintain the structural integrity of the left ventricular wall, and to prevent cardiac rupture (Porter & Turner, 2009). Deposition of collagen type I and type III, and other molecules necessary for appropriate ECM remodelling, such as fibronectin and proteoglycans, is primarily performed by myofibroblasts; cells which have differentiated from cardiac fibroblasts and assume phenotypic characteristics similar to smooth muscle cells (Gabbiani, 1998). Expression of pro-inflammatory and pro-fibrotic cytokines, such as IL-1β, IL-6, TNFα and TGFβ are all increased in patients following infarction (Nian, *et al*., 2004).

IL-6, along with TNFα, has been shown to enhance fibroblast proliferation (Siwik, *et al*., 2000; Hellkvist, *et al*., 2002), with TGFβ known to stimulate fibroblast differentiation into myofibroblasts (Hao, *et al*., 2008). IL-1β and IL-6 have been shown to degrade the ECM, primarily through expression of MMPs, such as MMP-2,

MMP-9, and MMP-13 (Siwik, *et al*., 2000). TGFβ also plays a crucial role in stimulating collagen, fibronectin and proteoglycan deposition from myofibroblasts (Eghbali, *et al*., 1991; Heimer, *et al*., 1995; Villarreal, *et al*., 1996). Atrial natriuretic peptide (ANP), which is released from cardiomyocytes in heart failure, performs a contrasting role; it inhibits fibroblast proliferation, differentiation into myofibroblasts, and collagen synthesis (Li, *et al*., 2008).

Fibrillar collagen type I is the most abundant type of collagen present in the heart, accounting for approximately 80% of total myocardial collagen, with collagen type III comprising approximately 11% (De Souza, 2002). Collagen accumulation is associated with reduced compliance and can lead to cardiac pathology (Pauschinger, *et al*., 1999), such as diastolic dysfunction (Kass, *et al*., 2004; Moreo *et al*., 2009). Collagen type I is stiffer than the more elastic collagen type III, and in infarct scars an increase in the relative proportion of collagen type I to collagen type III in seen (Pauschinger, *et al*., 1999). This increase in relative expression, as well as collagen cross-linking, may contribute to maintaining the structural integrity of the ventricle after MI (Pauschinger, *et al*., 1999; Dean, *et al*., 2005). Enhancing collagen deposition, by injecting collagen into the heart immediately following MI in rats, has been shown to reduce infarct expansion and preserve cardiac function up to six weeks after occlusion (Dai, *et al*., 2005). Administration of physiological levels of glucocorticoids have recently been shown to inhibit cardiac fibroblast proliferation *in vitro* (He, *et al*., 2011). These effects were abrogated by the addition of the GR antagonist RU486 showing these effects were GR-mediated (He, *et al*., 2011). In an inflammatory setting, 11β-HSD1 deficient mice display increased collagen in the lung following bleomycin treatment (Yang, *et al*., 2009) and an attenuated response

to the age-induced reduction in skin collagen density (Tiganescu, *et al*., 2013). Moreover, 11β-HSD1 deficiency on the ApoE KO background leads to increased fibrosis in atherosclerotic plaques following administration of a cholesterol rich diet (Kipari, *et al*., 2013). However, 11β-HSD1 deficient mice fed a high fat diet have reduced collagen deposition in adipose tissue, which is hypothesised to be due to the increased angiogenesis seen in this tissue (Michailidou, *et al*., 2012).

1.2.7 Hypertrophy, remodelling and heart failure

Cardiac remodeling can occur as a result of several diseases or pathological conditions, such as MI, chronic hypertension, aortic stenosis, myocarditis and idiopathic dilated cardiomyopathy (Cohn, *et al*., 2000). The extent of remodelling which occurs after MI is largely dependent on initial infarct size, and infarct size has been shown to negatively correlate with morbidity and mortality (Yang, *et al*., 2002a; Numaguchi, *et al*., 2006). For example, high levels of ROS released from necrotic cells immediately after infarction have been shown to contribute to the pathogenesis of heart failure (Dhalla, *et al*., 1996), and have been shown to play a role in TLR-mediated vascular dysfunction and arrhythmias (Shishido, *et al*., 2003). After initial collagen deposition, subsequent expansion and thinning of the scar leads to reduced cardiac function and left ventricular dilatation (Pfeffer & Braunwald, 1990). Whilst hypertrophy may be initially compensatory, it can lead to adverse outcomes in the long term and dilatation can become progressively decompensatory (Sabbah & Goldstein, 1993).

Reduction in cardiac performance, increased wall stress and expression of TNFα, TGFβ and endothelin result in cardiomyocytes reverting back to a foetal phenotype, whereby they express ANP and β-myosin heavy chain (β-MHC), which are typical characteristics of cardiac hypertrophy (Buttrick, *et al*., 1991; Takahashi, *et al*., 1992; Stanley, *et al*., 2004; Lu, *et al*., 2010; Vaz Perez, *et al*., 2010).

ANP has been shown to be vital for survival within the first seven days following occlusion, and that its action via the guanylyl cyclase-A (GC-A) receptor attenuates fibrotic and hypertrophic responses (Nakanishi, *et al*., 2005). Myocardial and plasma ANP levels have been shown to increase after MI, and increasing levels correlate with the extent of left ventricular dysfunction (Lu, *et al*., 2010; Vaz Perez, *et al*., 2010).

β-MHC is upregulated in heart failure (Buttrick, *et al*., 1991; Takahashi, *et al*., 1992). Cardiac muscle myosin is a hexameric protein which consists of two heavy chain subunits, two light chain subunits and two regulatory subunits. The heavy chains exist as two isoforms, α and β. In the myocardium of small mammals, such as mice, expression of the α isoform predominates (Lompre, *et al*., 1979) whereas this is reversed in humans, with the β isoform accounting for over 90% of the MHC subunits (Gorza, *et al*., 1984). The role of α-MHC in regulating cardiac contractility has been shown by genetic manipulation in an experimental model of familial hypertrophic cardiomyopathy, with disruption of this gene resulting in cardiac dysfunction (Geisterfer-Lowrance, *et al*., 1996). The ratio of α-MHC:β-MHC has been shown to directly correlate with cardiac function in both animals and humans (Miyata, *et al*., 2000; Abraham, *et al*., 2002; Herron & McDonald, 2002) and can thus be used to help determine the extent of heart failure in a model of infarction.

As detailed in Section 1.2.4, 11β-HSD1 deficient mice show a beneficial phenotype 7d post-MI, and this outcome is still apparent 4w post-MI. In these mice, the enhanced peri-infarct angiogenesis, increased scar thickness and improved ejection fraction are sustained through to 4w after MI, suggesting attenuated development of heart failure (McSweeney, *et al*., 2010). Genetic disruption of the MR gene specifically in murine cardiomyocytes results in attenuated adverse remodelling and left ventricular dysfunction after MI (Fraccarollo, *et al*., 2011). Moreover, clinical trials, such as RALES and EPHESUS, have demonstrated the beneficial effect of early MR inhibition after infarction in humans (Pitt, *et al*., 1999; Pitt, *et al*., 2003). In these studies, eplerenone treatment and spironolactone treatment was shown to reduced morbidity and mortality in acute MI patients, and in patients with severe heart failure (Pitt, *et al*., 1999; Pitt, *et al*., 2003). Considering the above literature, it is clear that glucocorticoids, and 11β-HSD1, play a key role in the post-MI setting and in the development of heart failure.

1.3 Aims and hypotheses

Previous work has shown that global 11β-HSD1 deficiency leads to smaller hearts (McSweeney, *et al*., 2010), however the mechanism for this remains unknown. Systolic function appears to be maintained but diastolic function and calcium regulation have not been studied. In addition, global 11β-HSD1 deficient mice exhibit a beneficial phenotype after MI, with an augmented inflammatory response, associated with increased representation of pro-reparative alternatively-activated macrophages, enhanced peri-infarct angiogenesis and improved cardiac function (McSweeney, *et al*., 2010). However, whether this is due to 'cardiovascular' 11β-HSD1 is unknown. Therefore the work in this thesis addressed the hypotheses that:

1. Deletion of 11β-HSD1 in cardiomyocytes and VSMCs (SMAC mice) would result in smaller, lighter hearts, but would not influence systolic function.
2. Deletion of 11β-HSD1 in cardiomyocytes and VSMCs would reproduce the beneficial post-MI phenotype previously seen in global 11β-HSD1 deficient mice.

The first aim was to characterise the cardiac phenotype of mice globally deficient in 11β-HSD1 (DelI mice), and mice in which deletion was restricted to cardiomyocytes and vascular smooth muscle cells (SMAC mice).

The second aim was to determine whether the beneficial acute outcomes seen previously in 11β-HSD1 deficient mice 7d after MI could be reproduced by selective cardiovascular deletion of the enzyme.

The final aim was to assess the impact of global 11β-HSD1 deficiency and cardiovascular-specific 11β-HSD1 deletion on the development of heart failure, 8w after MI.

Chapter 2

Materials and Methods

2.1 Animals and breeding

2.1.1 Mouse colonies

Experiments were approved by the University of Edinburgh ethics committee and the Home Office (PPL 60/4247, Dr. Gillian Gray) and carried out in strict accordance with the Animals (Scientific Procedures) Act (UK) 1986. I performed all techniques except where stated.

2.1.2 Mouse lines with 11β-HSD1 deficiency

2.1.2.1 Global 11β-HSD1 deletion

Male global 11β-HSD1 knock-out (KO) mice were generated from *Hsd11b1* 'floxed' mice (*Hsd11b1*$^{fl/fl}$) in which loxP sites flank exon 3 of the *Hsd11b1* gene. These mice were created by homologous recombination in C57Bl/6 stem cells. Homozygous 'floxed' mice (*Hsd11b1*$^{fl/fl}$) were crossed with mice in which the Cre recombinase enzyme was under control of the hypoxanthine-guanine phosphoribosyltransferase promoter. Cre recombination allowed removal of exon three, which encodes the binding site for the cofactor NADPH, and also resulted in a frameshift mutation thus creating a non-sense transcript.

Mice were backcrossed with C57BL/6 mice for 7 generations generating heterozygous (+/-) mice. Heterozygous mice were then intercrossed to give homozygous KO, and this global KO mouse strain is referred to as 'DelI' hereafter. All of the above work was performed by Karen Chapman and Janet Man (University

of Edinburgh). Pairs of DelI mice were then set up for breeding, and in-house male C57BL/6 mice were used as controls.

2.1.2.2 Global deficiency of 11β-HSD1

Male 11β-HSD1 deficient mice, which are hypomorphic for 11β-HSD1, were generated in house by Yuri Kotelevtsev (Kotelevtsev, *et al*., 1997). 11β-HSD1 is transcribed from three promoters, with lung mainly using the P1 promoter and most other tissues, such as liver, brain and adipose tissue, using the P2 promoter, which lies downstream (Bruley, *et al*., 2006). The *Hsd11b1* gene is disrupted in these mice by insertion of a neomycin cassette which interferes with, and therefore reduces, expression of 11β-HSD1 driven from the P2 promoter. However, there appears to be less interference with the more distant P1 promoter. The initial observations after MI by Small *et al* (2005) and McSweeney *et al* (2010) were made using these mice and they were again used for investigating the development of heart failure in this thesis (Chapter 5). DelI mice were initially used but all mice (n=16) died between d3 and d5 after surgery from cardiac rupture. 11β-HSD1 deficient mice were genotyped by Janet Man and in-house male C57BL/6 mice were used as controls.

2.1.2.3 'Cardiovascular' deletion of 11β-HSD1

Male tissue specific knock-out (*Hsd11b1*$^{fl/fl}$*Sm22α-Cre*$^{+}$) mice were obtained from the primary colony maintained by Janet Man upon request, having already been genotyped. Pairs of male *Hsd11b1*$^{fl/fl}$*Sm22α-Cre*$^{+}$ mice were bred with 'floxed' female mice (*Hsd11b1*$^{fl/fl}$) to give *Hsd11b1*$^{fl/fl}$*Sm22α-Cre*$^{+}$ mice and

Hsd11b1$^{fl/fl}$*Sm22α-Cre*$^{-}$ controls. This tissue specific KO mouse strain is referred to as 'SMAC' hereafter, with Cre^{+} mice being SMAC and Cre^{-} littermates referred to as 'control'.

2.1.3 Genotyping

Genotyping of DelI and SMAC animals was performed on ear notch tissue using PCR. DNA was extracted using a DNeasy Blood and Tissue Kit (Qiagen). Ear tissue was placed into a 1.5ml Eppendorf tube, and 180µl Buffer ATL and 20µl proteinase K solution was added. Tubes were vortexed and incubated at 56^{o}C for 3h, ensuring the tissue was completely lysed. 200µl Buffer AL was added to each sample before vortexing again. 200µl 100% ethanol was added to each sample, the tubes were vortexed again, and the mixture was transferred to a DNeasy Mini spin column which was placed in a 2ml collection tube. The spin column was centrifuged at 8,000 G for 1min, the flow-through was discarded and 500µl Buffer AW1 was added. Each spin column was centrifuged again at 8,000 G for 1min. The flow-through was again discarded and 500µl Buffer AW2 was added to each sample. The spin columns were centrifuged again at 12,000 G for 3min to dry the DNeasy membrane. The collection tube was discarded and the spin column placed in a 1.5ml Eppendorf. 200µl Buffer AE was added to each sample, incubated at room temperature for 1min and centrifuged at 8,000 G for 1min to elute the DNA.

To check the DelI breeding pairs were producing only DelI animals, three custom primers (Invitrogen, designed by Janet Man) were used to identify wild type, heterozygous and knock-out animals:

Flox F: 5'-CTTGCATGTGTTTGGTGTTGG-3'

Flox R: 5'-AATGTTTCCAAATGCATTGTGGG-3'

Del F: 5'-GTGATGTCAGATCTACAGAAGG-3'

Two PCR reactions were performed (Figure 2.1). A Del PCR, consisting of DelF and FloxR primers, was used to determine whether exon 3 had been deleted (Figure 2.1a). In the Del PCR, DelI mice produce a 363bp product, whereas control mice produce a 1066bp product. A Flox PCR, consisting of FloxF and FloxR primers, was used to determine if the floxed allele was present (Figure 2.1b). In the Flox PCR, DelI mice generate no product whereas control mice produce a 255bp product. Wild-type animals produce a 998bp product in the Del PCR and a 221bp product in the Flox PCR. This is similar to the products seen for control mice, except each band is shorter due to the lack of 34bp loxP sites.

To identify SMAC and Cre- control animals, two custom primers (Invitrogen, designed by Janet Man) were used to detect the presence of Cre recombinase (Guy, *et al*., 2001):

Cre F: 5'-GACCGTACACCAAAATTTGCCTG-3'

Cre R: 5'-TTACGTATATCCTGGCAGCGATC-3'

SMAC animals were identified by the presence of a 465bp Cre product, and control animals by its absence (Figure 2.3).

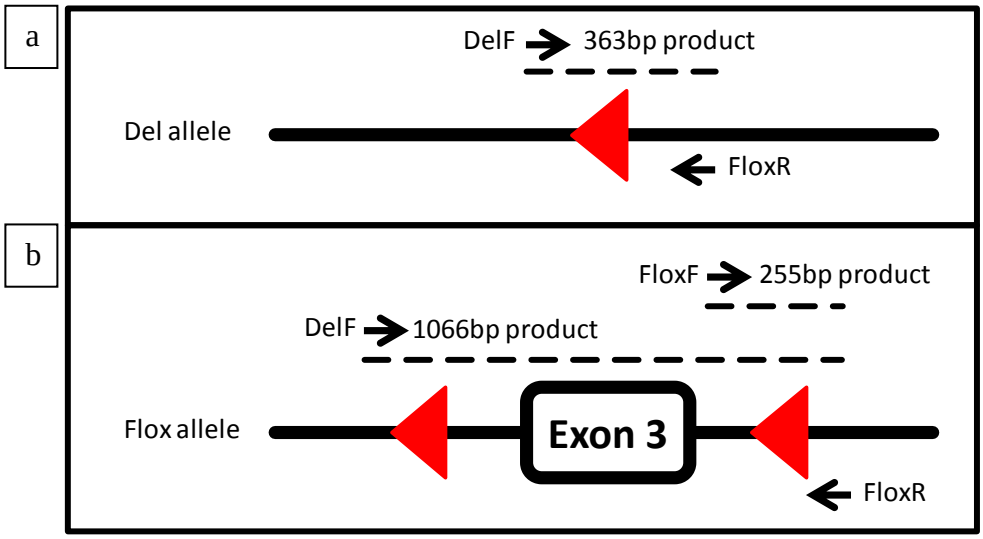

Figure 2.1 DelI genotyping

DelI animals have two copies of the Del allele shown in (a), in which exon three has been completely excised using the Cre-lox system. Control animals have two copies of the floxed allele shown in (b), whereby exon three is present but is flanked by two lox-P sites (red triangles). PCR products are shown as dashed lines.

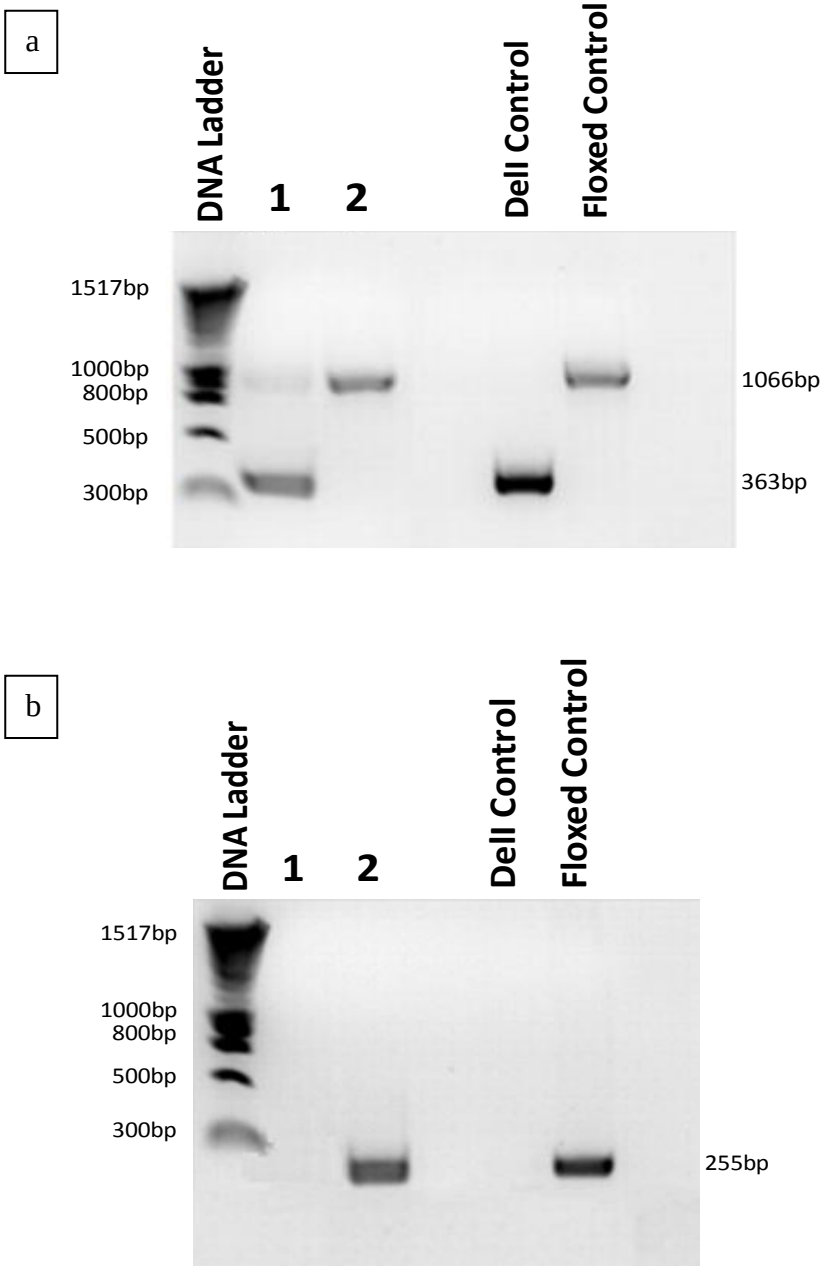

Figure 2.2 PCR gels for selection of DelI and control mice

Identification of a DelI animal (1 in the gels above) was confirmed by the presence of a 363bp product from the Del PCR (a), and no product on the Flox PCR (b). A control animal (2 in the gels above) was identified by the presence of a 1066bp product from the Del PCR, and a 255bp product from the Flox PCR. DNA from known DelI and control animals were used for controls. This was to aid the identification of animals of as-yet-unknown genotype and to determine if there was any cross-contamination in the assay.

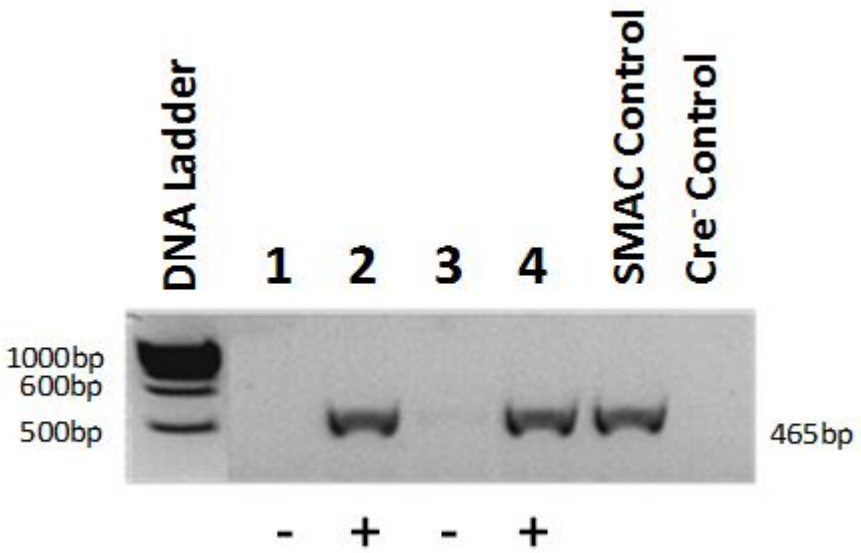

Figure 2.3 PCR gels for selection of SMAC and control mice
SMAC mice were identified by the presence of a 465bp Cre product (animals 2 and 4) and control animals were identified by its absence (animals 1 and 3). DNA from known SMAC and Cre^- mice were used as controls.

Each reaction mix consisted of 1.3 µl extracted DNA, 2 µl 2.5 µM dNTPs (Promega), 1 µl 10 pmol/µl forward primer (Flox F or Del F for DelI, Cre F for SMAC), 1 µl 10 pmol/µl reverse primer (Flox R for DelI, Cre R for SMAC), 0.2 µl Taq DNA Polymerase (Invitrogen), 2.25 µl $MgCl_2$, 2.5 µl buffer and 14.75 µl deionised water (dH_2O). PCR was initiated with a 95 ^oC denaturing step for 10 min followed by 35 cycles of 30 s at 95 ^oC to denature the DNA, 30 s at 60 ^oC to allow primer annealing and 1 min 30 s at 72 ^oC to allow primer extension. The reaction mixtures were then heated to 72 ^oC for a further 10 min to allow further extension before being held at 4 ^oC to stop the reaction. 5 µl loading dye was added to each PCR product and 10 µl of each product was run on a 1.5 % agarose gel with a 1 kb DNA ladder (New England Biolabs), a blank (where 1.3 µl Tris-EDTA (TE) buffer was substituted into the reaction mixture instead of DNA), a known wild-type sample and a known knock-out sample (obtained from Janet Man). For the DelI animals, this was performed twice; one reaction mix contained Flox F and Flox R primers, and the second contained Del F and Flox R primers. GelRed (Biotium) was used to visualise the gels in a Transilluminator Box to allow identification of wild-type, heterozygous and knock-out animals. DelI genotyping was performed with help from Kieran McGregor.

Controls for the floxed mice were not used, and investigation into whether cardiac function is altered by insertion of the Cre recombinase was not performed and are limitations of the study. This should be investigated in future experiments.

2.2 In vivo techniques

2.2.1 Tail plethysmography

Blood pressure (BP) was measured by tail cuff plethysmography (Shesely, *et al*., 1996) in mice at 12 weeks of age. Calibration of the device was performed by Christopher Kenyon. Tail cuff measurement involves the mouse being placed in a restrainer and a pulse sensor attached to the tail. The cuff is gradually inflated until the pulse stops, indicating the pressure is above systolic BP. The point at which the pulse stops is recorded as systolic BP. In order to obtain as accurate a measure of systolic BP as possible, mice were preconditioned to the technique for 4 d and BP measurement was recorded on the fifth day. Preconditioning was performed as follows: mice were placed in a heat box at 38 ^{o}C for 5 min then restrained in the restraining tube for 6-8 min, at the same time of day, for 4 d. Whilst restrained, the tail cuff was placed on the mouse's tail and inflated to 60 mmHg for 5 min. Preconditioning was deemed to have been achieved when systolic BP recordings were similar on consecutive days and the mice walked into the restraining chamber of their own accord, showing no visible signs of stress. On the day of recording the mice were weighed, placed in the heat box and restrained before four separate measurements of systolic BP were taken. Replicates were averaged and accepted providing standard deviation of the values was <3mmHg. The mean of these four measurements was then used.

2.2.2 Echocardiography

Echocardiography was performed using a Vevo 770 High Resolution Ultrasound Scanner (Visualsonics). Two dimensional echocardiography is based on the measurement of the reflection of ultrasound waves, emitted from the end of a probe. These waves reflect back on to the probe differently at different tissue boundaries due to the change in tissue density. Thus, images based on tissue density can be acquired and analysed. Mice were weighed and anaesthesia was induced with 2 % isoflurane. The chest was shaved and the mouse was placed in a supine position on a heated table to maintain body temperature at 37 ^{o}C. Temperature was continuously monitored by a rectal thermometer. The electrocardiogram was monitored by taping the limbs of the mouse down onto contact points on the table, which ensured scanning was performed with the heart rate in a range of 500-550 bpm. The ultrasound transducer, operating at a frequency of 45 MHz, was placed parasternally in order to obtain 2D images of the heart. Long axis views of the heart in ECG-Gated Kilohertz Visualisation (EKV) mode (Figure 2.4a) and M-mode (Figure 2.4b) were acquired. Mitral valve pulsed-wave Doppler ultrasound (Figure 2.4c) was performed to measure blood flow across the mitral valve. B-mode images were also acquired in the long axis and the short axis should further analysis be required at a later stage. All scanning was performed by Adrian Thomson, Edinburgh Preclinical Imaging.

Vevo Image Analysis Software (Visualsonics) was used to measure several parameters. From the EKV images, cardiac output (CO), stroke volume (SV), ejection fraction (EF), left ventricular end diastolic area (LVEDA) and left ventricular end systolic area (LVESA) were calculated. Fractional shortening (FS) was calculated from M-mode. From the mitral valve pulsed-wave Doppler

ultrasound, peak E wave velocity, peak A wave velocity, E/A wave ratio, E wave deceleration, and E wave deceleration time were measured. Table 2.1 lists the formulae used to calculate parameters derived from the raw measurements.

Parameter	Mode	Formula
SV	EKV	$LV\ vol;d - LV\ vol;s$
CO	EKV	$HR\ x\ SV$
EF	EKV	$\left(\frac{SV}{LV\ Vol;d}\right) x\ 100$
FS	M	$\left(\frac{LVID;d - LVID;s}{LVID;d}\right) x\ 100$

Table 2.1 Ultrasound parameter formulae

Stroke volume (SV) was calculated by subtracting the end systolic left ventricular volume (LV vol;s) from the end diastolic left ventricular volume (LV vol;d). Cardiac output (CO) was calculated by multiplying heart rate (HR) by stroke volume (SV). Ejection fraction (EF) was calculated by dividing SV LV vol;d and multiplying by 100. Fractional shortening (FS) was calculated by subtracting the end systolic left ventricular inner diameter (LVID;s) from the end diastolic left ventricular inner diameter (LVID;d) and dividing that by LVID;d then multiplying by 100.

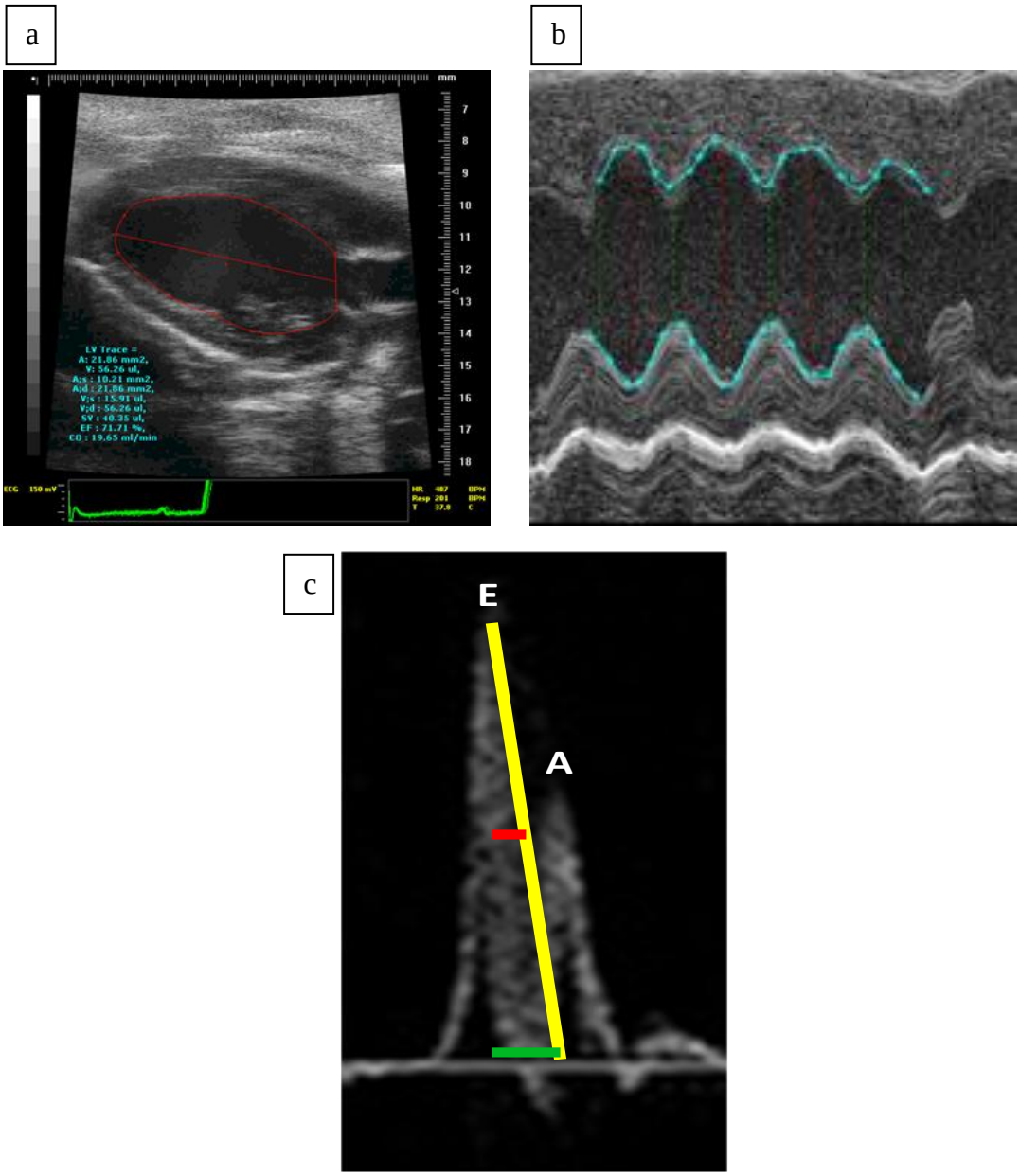

Figure 2.4 Echocardiography traces

An example EKV-mode image showing the LV endocardial trace (a), an example M-mode image showing the LV inner diameters during systole and diastole (b) and an example Doppler image (c) showing the E and A waves and measurements of E wave deceleration (yellow line), mitral valve deceleration time (MV DT, green line) and pressure half time (red line).

2.2.3 Coronary artery ligation surgery

Coronary artery ligation surgery was performed using the method described in McSweeney *et al* (2010) but with modifications to the anaesthetic procedure, which are described by Takagawa *et al* (2007). This surgery aims to mimic experimentally what happens during MI, namely the occlusion of a coronary artery. By ligating the left anterior descending coronary artery in this surgery, tissue which is supplied by this artery will become ischaemic and allow for experimental investigation of infarction.

Male mice, aged 10-12 weeks, were anaesthetised using 2 % isoflurane and maintained on 2 % isoflurane with oxygen throughout the surgery at a flow rate of 1 L/min. They were intubated via the mouth for mechanical ventilation (120 strokes/min, 200 µl stroke volume, HSE-Harvard MiniVent Ventilator) using a 20 gauge IV cannula. Lacri-lube eye ointment (Allergan) was applied to the eyes to prevent dessication. Buprenorphine (0.05 mg/kg) was administered subcutaneously before an incision was made at the left upper thorax. The superficial pectoralis muscles were blunt-dissected and the chest was opened at the fourth intercostal space. This was held open using retractors (Mini-Goldstein, Fine Science Tools) and the pericardium was removed from the heart.

The left anterior descending (LAD) coronary artery was ligated using a 6-0 prolene suture (Ethicon) just below the left atrium. Sham surgeries were performed by passing the suture underneath the LAD coronary artery, but omitting the ligation. The retractors were removed and the chest was closed using a 5-0 mersilk suture (Ethicon) ensuring no air remained in the chest cavity, thus avoiding pneumothorax.

The skin was closed using 9 mm autoclips (Harvard Apparatus). 1.5 ml 0.9 % sterile saline was administered subcutaneously to aid recovery and isoflurane was stopped. Mice were returned to their cages which were left on a 37 ^{o}C heat pad overnight. 1.5 ml 0.9 % saline and 0.05 mg/kg buprenorphine were administered subcutaneously 24 h after surgery, and tail blood was taken as described in Section 2.2.4 in order to measure plasma cardiac troponin-I levels (Section 2.6.5).

2.2.4 Tail blood collection

Tail blood was collected 24 h after surgery in order to determine plasma cardiac troponin-I levels (Gassenmaier, *et al*., 2012). Approximately 2 mm of tail was removed using surgical scissors and the cut tail was dipped in sodium citrate buffer to prevent clotting. Then, approximately 45 µl tail blood was gently milked into the lid of a 0.5 ml Eppendorf tube which contained 15 µl sodium citrate buffer. Once the blood had been collected (approximately 1 min) the end of the tail was dried using a sterile paper towel until bleeding ceased. The mouse was then placed back in its cage.

The blood sample was temporarily stored at 4 ^{o}C (approximately 10 min) before being centrifuged (3,000 G for 5 min) and the supernatant collected and stored at -80^{o} C until required for the cardiac troponin-I assay (Section 2.6.5).

2.2.5 CINE magnetic resonance imaging

Eight weeks after coronary artery ligation surgery, cardiac structure, function and infarct size were measured using CINE magnetic resonance imaging (MRI) (Marshall, *et al*., 2013). The basis of MRI revolves around the manipulation of protons. Present throughout every tissue, protons are subject to magnetic fields and will either align in parallel or anti-parallel with a magnetic field. During MRI image acquisition, a magnetic field is applied to the mouse followed by radiofrequency (RF) pulses which aim to disturb these protons by the transfer of energy. The time taken to 'relax' back to their original state is dependent upon the molecule they are present in. As such, different tissues will 'relax' at different rates allowing images to be constructed based on their relative relaxation times.

Mice were anaesthetised using isoflurane and maintained on 1.5 % isoflurane with oxygen throughout the procedure. Respiration rate was maintained at 50-60 breaths/min using a pressure pad. Needle electrodes (Small Animal Instruments Inc.) placed subdermally either side of the heart allowed monitoring of the heart rate from ECG traces. Temperature was also monitored via a rectal thermometer and maintained at 37 ^{o}C using an adjustable hot air blower.

Animals were placed, in a supine position, inside a 7T MRI scanner (Agilent Technologies) with a 39 mm quadrature coil. ECG-gating and respiratory-gating were used to synchronise images. The short axis of the heart was identified by performing several 'scout' scans, and short axis cardiac images were acquired using a gradient echo 'CINE' sequence (TR/TE = 7.3/2.7 ms with a flip angle of 15^{o}) with gradient and RF spoiling. Nine consecutive 1mm thick slices from 12-13 time frames were acquired, which encompassed the entire heart from base to apex. The field of

view was 30mm with a 192 x 192 matrix and 4 averages were used. All scanning was performed by Maurits Jansen and Ross Lennen.

ImageJ software (National Institutes of Health) was used to measure a number of parameters such as left ventricular end diastolic volume (LVEDV), left ventricular end systolic volume (LVESV), and ejection fraction (EF). Infarct length was measured by segmenting each short axis image into 20 sections. Any section which was thinned and akinetic or dyskinetic over the cardiac cycle was designated as infarcted tissue. Grey scale contrast also allowed visual confirmation of infarcted tissue. Infarct length was quantified by adding together the endo and epicardial circumference of infarcted tissue and dividing this by the sum of the total endo and epicardial circumferences, as described by Nahrendorf *et al* (2000).

2.3 Ex vivo techniques

2.3.1 Perfusion fixation

Perfusion fixation allows the morphology of blood vessel to be preserved as best as possible. This is because the vessels are being perfused with fixative via cannulation, rather than a tissue simply being submerged in fixative once it has been excised. This technique is of particular use when studying changes in vasculature structure and morphology.

Mice culled by retrograde perfusion fixation were anaesthetised (1 mg/kg medetomidine and 75 mg/kg ketamine administered intraperitoneally) and an incision was made in the abdomen before the abdominal aorta was cannulated below the branch of the hepatic vein. An arterial blood sample (approximately 500 μl) was drawn up into a syringe containing 15 μl sodium citrate buffer before organs were perfused with heparinised phosphate-buffered saline (PBS, 2 min) and 10 % formalin in PBS (5 min) at physiological pressure (100 mmHg). Following perfusion with 10 % formalin in PBS, the inferior vena cava was cut to release the perfusate. Perfusion was stopped according to time (a minimum of 5 min) and by using visual cues; blanching of the liver and clear fluid running from the inferior vena cava indicated satisfactory perfusion. Heart, spleen, aorta and liver were then harvested, placed in 10 % formalin in PBS for 24 h and transferred to 70 % EtOH before processing and paraffin embedding for immunohistological analysis. The processing and paraffin embedding was carried out by the Histology Department (Queen's Medical Research Institute, University of Edinburgh).

2.3.2 Blood volume

Calculation of blood volume is performed by injecting a known quantity of dye into the mouse and allowing it to circulate. Once dispersed evenly, a blood sample can be drawn and the concentration of the dye measured. By scaling up this concentration, and by knowing the quantity of dye initially injected, blood volume can be determined. Male DelI and control mice, aged 12 weeks, were anaesthetised (1 mg/kg medetomidine and 75 mg/kg ketamine administered intraperitoneally) and the jugular vein was cannulated with a 27 gauge needle. 1 µl/g of body weight Evans Blue stock solution (0.5 µg/ml Evans Blue in sterile 0.9 % saline) was injected into the jugular vein and left to circulate for 10 min. The abdominal aorta was cannulated during this time using a 27 gauge needle and, after 10 min had elapsed, an arterial blood sample (approx 500 µl) was drawn up into a heparinised blood collection tube. Cannulation was performed by Gill Brooker. Blood from the collection tube was drawn up into a capillary tube and haematocrit was measured by centrifuging the capillary tube (8,000 G for 5min) and determining the packed cell volume. The remaining blood in the collection tube was centrifuged at 3,000 G for 5min. 95 µl of the supernatant, which consisted of plasma and Evans Blue solution, and 95 µl of each Evans Blue standard (0, 0.05, 0.1, 0.2 and 0.5 µg/ml) were loaded onto a clear 96 well plate in duplicate. Absorbance was read at 620 nm and blood volume was calculated using the following formulae (Greenleaf, *et al*., 1979; Zhang, *et al*., 2005):

$$Plasma\ volume = \frac{Injected\ Evans\ Blue\ (\mu g)}{plasma\ concentration\ (\mu g/ml)}$$

$$Blood\ volume = Plasma\ volume\ x\ \frac{100}{100 - (Hct\ x\ 0.96\ x\ 0.91)}$$

2.3.3 Myocardial interstitial fluid volume

Interstitial fluid volume can be determined by simply calculating the difference in heart weight immediately after excision, and once it has been thoroughly desiccated. Male DelI and C57BL/6 control mice, aged 12 weeks, were culled by cervical dislocation. Hearts were removed immediately below the thymus and massaged in ice cold 0.9 % saline to remove any residual blood in the atria and ventricles. The hearts were weighed (wet weight) and wrapped in tin foil before being placed in a desiccator containing silica. The hearts were weighed daily for 7 d which allowed for complete desiccation. The weight on the seventh and final day was taken as the 'dry weight'. Heart wet weight to dry weight ratio was calculated in order to determine if there were differences in interstitial fluid between the two groups.

2.3.4 Cardiomyocyte isolation

The isolation of cardiomyocytes is achieved by excising the heart and perfusing it with several solutions using a Langendorff preparation. This preparation allows the heart to be artificially perfused and digested, therefore allowing individual cardiomyocytes to be analysed.

Male DelI and C57BL/6 control mice, aged 12 weeks, were injected intraperitoneally with 200 µl heparin solution (100 units/ml in sterile 0.9 % saline). After 5 min the mice were culled by cervical dislocation and the heart was dissected out just below the thymus, ensuring approximately 5 mm of aorta remained attached to the heart. The heart was massaged in ice cold Krebs solution to remove any residual blood and then transferred to a beaker of fresh, room temperature Krebs solution. A 22 gauge

cannula (AD Instruments) was inserted into the aorta and the aorta was tied onto the cannula using 5-0 mersilk suture (Ethicon). The heart was then perfused, at a flow rate of 4 ml/min, with Krebs solution (40 ^{o}C for 2 min) before being perfused with collagenase solution (25 mg collagenase type 1 (Worthington Biochemical) and 2.5 mg protease type XIV (Sigma) in 50 ml Krebs solution at 40 ^{o}C for 12 min). External Ca^{2+} concentration was zero. Visual cues were used to determine when a satisfactory digestion had been achieved; the heart feeling soft when squeezed gently with forceps, the heart appearing translucent, and the vessels being clearly visible on the surface of the heart.

Once successful digestion had been achieved the heart was perfused with bovine serum albumin (BSA) Fraction V solution (467 mg BSA in 100 ml Krebs solution at 40 ^{o}C for 5 min) before it was removed from the cannula. The aorta, atria and right ventricle were carefully removed using a surgical scalpel and forceps, and the remaining heart tissue was cut up into small pieces using surgical scissors. These pieces of tissue were then transferred to a 15 ml Falcon tube containing 5 ml BSA solution. This solution was then agitated using a sterile pastette until the solution became cloudy, and one drop of this solution was added to a glass slide. Isolated, intact cardiomyocytes were identified and their diastolic length was measured using Image Pro 6.2 and a Stereologer Analyser 6 (MediaCybernetics). Only cell length was measured due to equipment limitations.

2.4 Histology

Immunohistochemical analysis is performed by excising the tissue in question, then dehydrating and fixing it, before microtoming it into sections and allowing it to adhere to a microscope slide. The purpose of this is allow a specific antibody to bind to its target protein in order to analyse the abundance of this protein. This is done by amplifying the signal from the antibody either by using fluorescent secondary and tertiary antibodies, or by subjecting a secondary antibody to a reactive dye. Providing the antibodies used are specific to the protein in question, the protein can be identified and quantified. Histological analysis is performed by subjecting these tissue sections to various solutions which will bind and/or react when they bind to a particular protein.

2.4.1 Picrosirius Red staining

Picrosirius Red staining was performed to calculate myocardial collagen content (McSweeney, *et al*., 2010). 4 μm thick sections of paraffin wax-embedded heart were cut using a microtome and transferred to glass slides. These sections were allowed to adhere to the slide overnight before being deparaffinised and rehydrated using xylene (2 x 5 min), 100 % EtOH (2 x 5 min), 90 % EtOH (3 min), 70 % EtOH (3 min) and finally dH_2O (30 s). The slides were submerged in Weigert's haematoxylin (8 min), rinsed under running tap water (10 min) and incubated in Picrosirius Red solution (0.5 g Direct Red in 500 ml saturated picric acid) for 1 h. Slides were then washed twice in acidified water and dehydrated using 70 % EtOH (1 min), 80 % EtOH (1 min), 95 % EtOH (1 min), 100 % EtOH (2 x 1 min) and xylene (2 x 1 min) before

being mounted in DPX and coverslipped. The staining was performed by the Histology Department (Queen's Medical Research Institute, University of Edinburgh).

Quantification was performed using Image Pro 6.2 and a Stereologer Analyser 6 (MediaCybernetics). The entire heart section was tiled at 40 x magnification and the area of the left ventricle was measured. A colour threshold was set manually so as to only select positive pink staining (see Figure 3.18) for collagen. This was done by eye to ensure only appropriate, specific, positive staining was included for analysis. The area of this positive staining within the left ventricle was calculated automatically. Myocardial collagen content was then expressed as percentage of positive staining in the left ventricle.

2.4.2 Masson's Trichrome staining

4 μm thick sections of paraffin wax-embedded heart were cut using a microtome and transferred to glass slides. These sections were taken at the level of the papillary muscles to ensure reproducibility, and they were allowed to adhere to the slide overnight before being deparaffinised and rehydrated using xylene (2 x 5 min), 100 % EtOH (2 x 5 min), 90 % EtOH (3 min), 70% EtOH (3 min) and finally dH_2O (30 s). The slides were submerged in Weigert's haematoxylin (10 min) and rinsed under warm running tap water (10 min). Slides were incubated in phosphomolybdic-phosphotungstic acid solution until the collagen no longer appeared red (approximately 15 min). Slides were then incubated with aniline blue solution (10 min), washed in distilled water and incubated with 1 % acetic acid (3 – 5 min).

Following further washing in distilled water the slides were dehydrated using 70 % EtOH (1 min), 80 % EtOH (1 min), 95 % EtOH (1 min), 100 % EtOH (2 x 1 min) and xylene (2 x 1 min) before being mounted in DPX and coverslipped. This staining was performed by the Histology Department (Queen's Medical Research Institute, University of Edinburgh).

Quantification was performed using Image Pro 6.2 and a Stereologer Analyser 6 (MediaCybernetics). The entire heart section was tiled at 40 x magnification and the area of the left ventricle was measured. Collagen and scar tissue were stained blue, muscle and cytoplasm were stained pink and nuclei were stained black thus providing clear delineation of infarcted and non-infarcted tissue (Harada, *et al*., 2005). The infarcted area (blue, see Figure 4.5) was drawn around manually and expressed as a percentage of the total area of the left ventricle. Infarct thickness was determined by averaging scar thickness from five equally-spaced points along the length of the infarct. Eight slices per heart were used for each mouse.

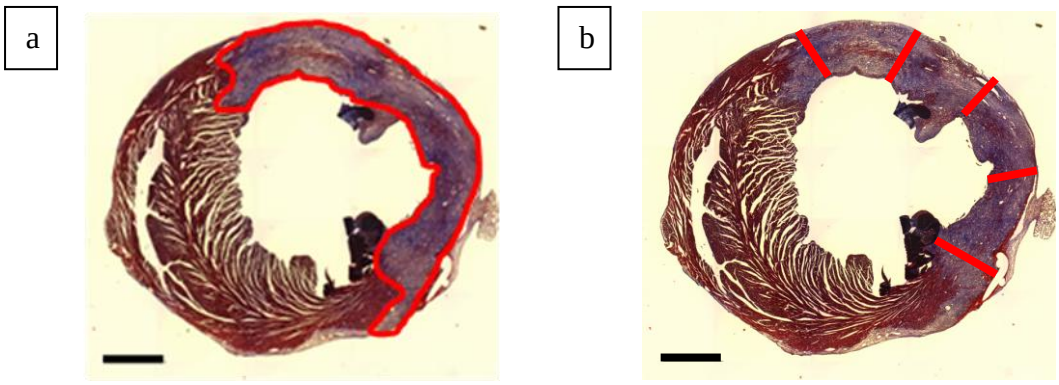

Figure 2.5 Infarct size and thickness analysis
Infarct size (a) was calculated by manually drawing round the infarcted area (red line) and expressing this as a percentage of the total area of the left ventricle. Infarct thickness (b) was calculated by averaging scar thickness (red lines) from five equally-spaced points along the length of the infarct. This was performed on eight heart sections at the mid-point of the papillary muscle.

2.5 Immunohistochemistry

2.5.1 Vessel density

Vessel density was assessed using the method described by Meloni *et al* (2010). Isolectin B4 detects endothelial cells and α-SMA detects smooth muscle cells. 4 μm thick sections of paraffin wax-embedded heart were cut in the short axis using a microtome and transferred to glass slides. These sections were taken at the level of the papillary muscles in all hearts to ensure reproducibility. The sections were allowed to adhere to the slide overnight before being deparaffinised and rehydrated using xylene (2 x 5 min), 100 % EtOH (2 x 5 min), 90 % EtOH (3 min), 70 % EtOH (3 min) and finally dH_2O (30 s). Antigen retrieval was performed by submerging slides in 10 mM sodium citrate buffer, pH 6 and boiling in a microwave (3 x 4 min). After allowing the slides to cool to room temperature, they were washed in dH_2O (3 min) and PBS (3 min). A blocking step was performed using 10 % goat serum in PBS (1 h at room temperature). Slides were incubated overnight in a dark, humidified chamber at 4 ^{o}C with primary antibodies for isolectin B4 (1:100 biotinylated isolectin B4 (Invitrogen)) and α-smooth muscle actin α-SMA (1:400 α-SMA-Cy3 (Sigma)) diluted in 1 % goat serum in PBS. Slides were then washed in PBS (2 x 3 min) and incubated in a dark, humidified chamber with the secondary antibody for isolectin B4 (1:100 streptavidin-Alexa 488 diluted in PBS (Invitrogen)) for 1 h at room temperature. Slides were washed again in PBS (2 x 3 min) and counterstained with DAPI (1 min (Sigma)) diluted 1:1000 in PBS. After washing with PBS (4 x 3 min), slides were mounted using Fluoromount G (Southern Biotech) and coverslipped.

Five randomly selected regions of interest were visualised in the left ventricular free wall using a 40 x objective on a Nikon E800 Microscope. Adobe Photoshop CS5 Extended (Adobe) was then used to manually count the number of individual isolectinB4^{+}α-SMA^{-} capillaries (<4 μm diameter), isolectinB4^{+}α-SMA^{+} small arterioles (4 – 200 μm diameter) and large arterioles (>200 μm diameter) present per mm^{2} in the left ventricular wall (see Figure. 3.11).

2.5.1.1 Post-MI angiogenesis

CD31, also known as PECAM-1, is a marker of endothelial cells and can be detected by immunohistochemistry to quantify peri-infarct angiogenesis in the heart after MI (Ismail, *et al*., 2003; McSweeney, *et al*., 2010).

4 μm sections of paraffin wax-embedded heart were cut using a microtome and transferred to glass slides. These sections were allowed to adhere to the glass slides overnight before being deparaffinised and rehydrated using xylene (2 x 5 min), 100 % EtOH (2 x 5 min), 90 % EtOH (3 min), 70 % EtOH (3 min) and finally dH_2O (30 s). Antigen retrieval was performed by submerging slides in 10 mM sodium citrate buffer, pH 6 and boiling in a microwave (3 x 4 min). After allowing the slides to cool to room temperature, they were washed in dH_2O (3 min) and PBS (3 min). Endogenous peroxidase activity was quenched by submerging the slides in 3 % H_2O_2 for 10 min at room temperature. The slides were then washed in PBS (2 x 5 min) and a blocking step was performed using 10 % goat serum in 5 % BSA in PBS (30 min at room temperature). Two drops of Avidin Block (Vector) were added to each section and incubated for 15 min at room temperature, then the slides were washed in PBS (3

x 5 min). Two drops of Biotin Block (Vector) were added to each section and incubated for 15 min at room temperature, then the slides were again washed in PBS (3 x 5 min). Slides were incubated overnight in a humidified chamber at 4 ^{o}C with the primary antibody for CD31 (1:50 rabbit anti-mouse CD31 (Abcam) in PBS).

Slides were then washed in PBS (2 x 3 min) and incubated in a dark, humidified chamber for 90 min at room temperature with the secondary antibody (1:200 biotinylated goat anti-rabbit (Vector) in PBS). Two drops of RTU ABC Reagent (Vector) were added to each section and incubated for 30 min at room temperature before being washing in PBS (2 x 3 min). DAB solution (Vector) was made up immediately prior to using it. 80 µl of DAB solution was added to each section and the slides were observed for the development of brown staining.

Once established, the reaction was stopped by washing the slides in PBS (3 x 3 min). Slides were then counterstained using tap water (10 s), Mayer's haematoxylin (30 s), tap water (10 s), acid alcohol (5 s), tap water (10 s) and finally Scott's tap water (20 s). Slides were then dehydrated using 70 % EtOH (1 min), 90 % EtOH (1 min), 100 % EtOH (2 x 1 min) and finally xylene (2 x 1 min) before being mounted in DPX (Sigma) and coverslipped.

Quantification of peri-infarct angiogenesis was performed using Image Pro 6.2 and a Stereologer Analyser 6 (MediaCybernetics). Using a 40 x objective, 20 randomly assigned fields of view, which consisted of 50 % to 75 % infarct, were analysed. The number of $CD31^{+}$ vessels were measured and categorised according to size; capillaries (<4 µm diameter), small arterioles (4 – 200 µm diameter) and large arterioles (>200 µm diameter). Each category was then expressed as number of peri-infarct vessels per 16000 μm^2.

2.5.2 Cardiomyocyte cross-sectional area

Cardiomyocyte cross-sectional area can be calculated by immunohistochemical staining of heart sections with wheat germ agglutinin (Schultz, *et al*., 2002). 4 μm thick sections of paraffin wax-embedded heart were cut using a microtome and transferred to glass slides. These sections were taken at the level of the papillary muscles in all hearts to ensure reproducibility, and were allowed to adhere to the slide overnight before being deparaffinised and rehydrated using xylene (2 x 5 min), 100 % EtOH (2 x 5 min), 90 % EtOH (3 min), 70 % EtOH (3 min) and finally dH_2O (30 s). Antigen retrieval was performed by submerging slides in 10 mM sodium citrate buffer, pH 6 and boiling in a microwave (3 x 4 min). After allowing the slides to cool to room temperature, they were washed in dH_2O (3 min) and PBS (3 min). A blocking step was performed using 10 % goat serum in PBS (1 h at room temperature). Slides were incubated overnight in a humidified chamber at 4 ^{o}C with the primary antibody for isolectin B4 (1:100 biotinylated isolectin B4 (Invitrogen)) diluted in 1 % goat serum in PBS. Slides were then washed in PBS (2 x 3 min) and incubated in a dark, humidified chamber for 90 min at room temperature with the antibody for wheat germ agglutinin (1:75 wheat germ agglutinin-rhodamine (Vector)) and the secondary antibody for isolectin B4 (1:100 streptavidin-Alexa 488 (Invitrogen)) diluted in PBS. Slides were washed again in PBS (2x3min) and counterstained with DAPI (1min (Sigma)) diluted 1:1000 in PBS. After washing with PBS (4 x 3 min), slides were mounted using Floromount G (Southern Biotech) and coverslipped.

Five randomly selected regions of interest were visualised in the left ventricular free wall using a 40 x objective on a Nikon E800 Microscope. Adobe Photoshop CS5

Extended (Adobe) was used to calculate cardiomyocyte cross-sectional area in cardiomyocytes which a) appeared to be cut in the short axis, b) had a nucleus in the middle of the cell and, c) were surrounded by capillaries which were also cut in the short axis (see Figure 3.10).

2.5.3 Macrophage quantification

Mac2 (galectin-3) is expressed and secreted by activated macrophages and can be detected by immunohistochemistry to quantify macrophage infiltration into the heart after MI (MacKinnon, *et al*., 2008; McSweeney, *et al*., 2010).

4 μm sections of paraffin wax-embedded heart were cut using a microtome and transferred to glass slides. These sections were allowed to adhere to the glass slides overnight before being deparaffinised and rehydrated using xylene (2 x 5 min), 100 % EtOH (2 x 5 min), 90 % EtOH (3 min), 70 % EtOH (3 min) and finally dH_2O (30 s). Antigen retrieval was performed by submerging slides in 10 mM sodium citrate buffer, pH 6 and boiling in a microwave (3 x 4 min). After allowing the slides to cool to room temperature, they were washed in dH_2O (3 min) and PBS (3 min). Endogenous peroxidase activity was quenched by submerging the slides in 3 % H_2O_2 for 10 min at room temperature. The slides were then washed in PBS (2 x 5 min) and a blocking step was performed using 10 % goat serum in 5 % BSA in PBS (30 min at room temperature). Two drops of Avidin Block (Vector) were added to each section and incubated for 15 min at room temperature, then the slides were washed in PBS (3 x 5 min). Two drops of Biotin Block (Vector) were added to each section and incubated for 15 min at room temperature, then the slides were again washed in PBS

(3 x 5 min). Slides were incubated overnight in a humidified chamber at 4 ^{o}C with the primary antibody for mac2 (1:200 anti-mac2 FITC (Cedarlane) in PBS).

Slides were then washed in PBS (2 x 3 min) and incubated in a dark, humidified chamber for 90 min at room temperature with the secondary antibody (1:4,000 rabbit anti-FITC (Vector) in PBS). Slides were washed again in PBS (2 x 3 min) and incubated with the biotinylated tertiary antibody (1:200 biotinylated goat anti-rabbit (Vector) in PBS) for 40 min at room temperature. Two drops of RTU ABC Reagent (Vector) were added to each section and incubated for 30 min at room temperature before being washed in PBS (2 x 3 min). DAB solution (Vector) was made up immediately prior to using it. 80 µl of DAB solution was added to each section and the slides were observed for the development of brown staining.

Once established, the reaction was stopped by washing the slides in PBS (3 x 3 min). Slides were then counterstained using tap water (10 s), Mayer's haematoxylin (30 s), tap water (10 s), acid alcohol (5 s), tap water (10 s) and finally Scott's tap water (20 s). Slides were then dehydrated using 70 % EtOH (1 min), 90 % EtOH (1 min), 100 % EtOH (2 x 1 min) and finally xylene (2 x 1 min) before being mounted in DPX (Sigma) and coverslipped. Antibody concentrations were optimised by performing titration experiments.

Quantification was performed using Image Pro 6.2 and a Stereologer Analyser 6 (MediaCybernetics). The entire heart section was tiled at 40 x magnification and the area of the infarct was measured. A colour threshold was set manually so as to only select positive brown staining for Mac2 and the area of this positive staining within the infarct was calculated automatically. Total macrophage infiltration was then expressed as the percentage area of positive brown DAB staining within the infarct.

2.5.4 Alternatively-activated macrophage identification

Ym1 is a marker of alternatively activated macrophages and can be detected by immunohistochemistry to quantify these macrophages in the heart after MI (Loke, *et al*., 2002; McSweeney, *et al*., 2010).

4 μm sections of paraffin wax-embedded heart were cut using a microtome and transferred to glass slides. These sections were allowed to adhere to the glass slides overnight before being deparaffinised and rehydrated using xylene (2 x 5 min), 100 % EtOH (2 x 5 min), 90 % EtOH (3 min), 70 % EtOH (3 min) and finally dH_2O (30 s). Antigen retrieval was performed by submerging slides in 10 mM sodium citrate buffer, pH 6 and boiling in a microwave (3 x 4 min). After allowing the slides to cool to room temperature, they were washed in dH_2O (3 min) and PBS (3 min). Endogenous peroxidase activity was quenched by submerging the slides in 3 % H_2O_2 for 10 min at room temperature. The slides were then washed in PBS (2 x 5 min) and a blocking step was performed using 10 % goat serum in 5 % BSA in PBS (30 min at room temperature). Two drops of Avidin Block (Vector) were added to each section and incubated for 15 min at room temperature, then the slides were washed in PBS (3 x 5 min). Two drops of Biotin Block (Vector) were added to each section and incubated for 15 min at room temperature, then the slides were again washed in PBS (3 x 5 min). Slides were incubated overnight in a humidified chamber at 4 ^{o}C with the primary antibody for Ym1 (1:500 anti-Ym1 FITC (Stem Cell Technologies) in PBS).

Slides were then washed in PBS (2 x 3 min) and incubated in a dark, humidified chamber for 90 min at room temperature with the secondary antibody (1:4,000 rabbit anti-FITC (Vector) in PBS). Slides were washed again in PBS (2 x 3 min) and

incubated with the biotinylated tertiary antibody (1:200 biotinylated goat anti-rabbit (Vector) in PBS) for 40 min at room temperature. Two drops of RTU ABC Reagent (Vector) were added to each section and incubated for 30 min at room temperature before being washed in PBS (2 x 3 min). DAB solution (Vector) was made up immediately prior to using it. 80 µl of DAB solution was added to each section and the slides were observed for the development of brown staining.

Once established, the reaction was stopped by washing the slides in PBS (3 x 3 min). Slides were then counterstained using tap water (10 s), Mayer's haematoxylin (30 s), tap water (10 s), acid alcohol (5 s), tap water (10 s) and finally Scott's tap water (20 s). Slides were then dehydrated using 70 % EtOH (1 min), 90 % EtOH (1 min), 100 % EtOH (2 x 1 min) and finally xylene (2 x 1 min) before being mounted in DPX (Sigma) and coverslipped.

Quantification was performed using Image Pro 6.2 and a Stereologer Analyser 6 (MediaCybernetics). The entire heart section was tiled at 40 x magnification and the area of the infarct was measured. A colour threshold was set manually so as to only select positive brown staining for Ym1 and the area of this positive staining within the infarct was calculated automatically. Alternatively-activated macrophage infiltration was then expressed as the percentage area of positive brown DAB staining within the infarct.

2.6 Molecular techniques

qRT-PCR is a technique used to amplify and determine the relative concentration of one target gene mRNA in one tissue compared to another. Essentially, mRNA is extracted from a tissue, reverse transcribed to complimentary DNA (cDNA) before primers specific to one gene amplify the gene of interest. The rate of amplification then allows the relative abundance of this gene to be determined, meaning differences in gene expression between mice of different genotypes/treatments can be investigated.

2.6.1 RNA extraction

Mice were killed by cervical dislocation and tissues were harvested, rinsed in ice cold sterile PBS, rapidly frozen on dry ice and stored at -80 ^{o}C until required for RNA extraction. RNA extraction and isolation was performed using a Trizol Plus RNA Purification Kit (Invitrogen).

Approximately 30 – 40 mg of each left ventricular tissue sample and 400 µl Trizol (Invitrogen) were added to a 2 ml RNase-free tube and homogenised using a homogeniser. Another 100 µl of Trizol was added to give a final volume of 500 µl and the samples were left to incubate at room temperature for 5 min. The homogeniser was cleaned between samples using dH_2O and 10 % H_2O_2. 200 µl chloroform was added to each tube and the samples were shaken vigorously by hand for 15 s before being incubated at room temperature for 2 min. They were then centrifuged at 12,000 G for 15 min at 4 ^{o}C. After centrifugation the mixture had 3

distinct layers; a colourless upper phase containing the RNA, an interphase containing protein, and a lower red-phenol phase. The colourless upper phase was transferred to a fresh RNase-free tube and an equal volume of 70 % EtOH was added before the tubes were vortexed.

500 µl of this mixture was added to an RNA spin cartridge, which was centrifuged at 12,000 G for 15 min. The flow-through was discarded and 700 µl Wash Buffer I was added before the spin cartridge was centrifuged at 12,000 G for 15 s. The collection tube was discarded and replaced then 500 µl Wash Buffer II was added before the spin cartridge was again centrifuged at 12,000 G for 15 s. The flow-through was discarded and the spin cartridge centrifuged at 12,000 G for 1 min to remove any remaining buffer. The RNA spin cartridge was then placed in a clean RNA recovery tube. 30 µl RNase-free water was added to the spin cartridge and incubated for 1 min at room temperature before being centrifuged at 12,000 G for 2 min to elute the RNA.

RNA concentration and the A_{260}/A_{280} ratio was determined for each sample using a Nanodrop 1000 Version 3.3 (Thermo Scientific). In order to remove genomic DNA, each sample was DNase I treated with a Deoxyribonuclease I Amplification Kit (Invitrogen). The sample volume which corresponded to 1 µg RNA was added to a 0.2 µl RNase-free PCR tube along with 1 µl 10 x DNase I Reaction Buffer, 1 µl DNase I, and made up to a total volume of 10 µl with RNase-free H_2O. The samples were incubated for 15 min at room temperature before 1 µl 25 mM EDTA was added to activate the DNase I. The samples were then heated to 65 ^{o}C for 10 min before being reverse transcribed to cDNA.

2.6.2 cDNA synthesis

To reverse transcribe the RNA to cDNA, two mastermixes were prepared using a High Capacity cDNA Reverse Transcription Kit (Applied Biosystems); one for an internal control gene, and one for the gene of interest. Each reaction consisted of 2 µl 10 X RT Buffer, 0.8 µl 25 X dNTP Mix (100 mM), 2 µl 10 X Random Primers, 1 µl Multiscribe RT, 1 µl RNase Inhibitor and 3.2 µl RNase free water and was scaled up as appropriate, depending on the number of samples being analysed. One sample was chosen at random to serve as the RT- control; this reaction consisted of 2 µl 10 X RT Buffer, 0.8 µl 25 X dNTP Mix (100 mM), 2 µl 10 X Random Primers, 1 µl RNase Inhibitor and 4.2 µl RNase free water. 10 µl of the mastermix was added to each sample RNA from above to give a final volume of 20 µl. cDNA synthesis was performed in a thermal cycler using the following conditions; 25 ^{o}C for 10 min, 48 ^{o}C for 40 min, 95 ^{o}C for 5 min, then cooled to 4 ^{o}C. Once cooled, the cDNA was stored at -20 ^{o}C until required for qRT-PCR.

2.6.3 qRT-PCR

11β-HSD1 mRNA levels were investigated using Taqman Gene Expression Assays. Taqman mastermixes (Applied Biosystems) were made for 11β-HSD1 and an internal control gene (β-actin or TBP) and consisted of 5 µl Taqman Fast Advanced MM, 0.5 µl Taqman Gene Expression Assay and 3.5 µl RNase-free water. This was scaled up as appropriate depending on the number of samples analysed. 9 µl of the mastermix was transferred to each well on a 384 well plate. Standards were made by pooling 2 µl from each cDNA sample and making serial dilutions of 1/5, 1/10, 1/20,

1/40, 1/80, 1/160 and 1/320 in RNase-free water. 1 µl of each standard was added to the plate in triplicate and 1 µl water was added to the end of the standard curve as a blank control. An aliquot of sample cDNA (at a dilution of 1/10 for liver samples, 1/5 for heart and skeletal muscle samples and 1/2 for aorta samples) was made, and 1 µl was added to the plate in triplicate. The plate was sealed using a plastic cover, turned upside down to mix the contents then centrifuged at 1,500 G for 2 min to ensure all the mixture was at the bottom of the wells.

All other genes were investigated using the Universal Probe Library System (Roche). Roche Probe Mastermixes (Roche) were made for each gene and consisted of 2.7 µl Lightcycler H_2O, 5 µl Roche Probe Mastermix, 0.1 µl forward primer (Invitrogen), 0.1 µl reverse primer (Invitrogen) and 0.1 µl UPL Probe. This was scaled up as appropriate depending on the number of samples analysed. 8 µl of the mastermix was transferred to each well on a 384 well plate. Standards were made by pooling 2 µl from each cDNA sample and making serial dilutions of 1/5, 1/10, 1/20, 1/40, 1/80, 1/160 and 1/320 in RNase-free water. 2 µl of each standard was added to the plate in triplicate and 2 µl water was added to the end of the standard curve as a blank control. An aliquot of sample cDNA (at a dilution of 1/5 for heart samples) was made, and 1 µl was added to the plate in triplicate. The plate was sealed using a plastic cover, turned upside down to mix the contents then centrifuged at 1,500 G for 2 min to ensure all the mixture was at the bottom of the wells.

qRT-PCR to assess mRNA levels of target genes and housekeeping genes was performed using a Lightcycler 480 System (Roche) and the Taqman Fast Advanced template or the Roche Fam Hydrolysis (Roche) template as appropriate. Standard curves were used to determine mRNA levels of the housekeeping genes and the

target genes. Target gene mRNA levels were normalised to housekeeping gene mRNA levels, which was similar in all samples. Triplicate values for qRT-PCR were averages and accepted providing the standard deviation of the crossing point (Cp) values were <0.5 cycles. Table 2.2 shows the Taqman Gene Expression Assays (Applied Biosystems) and Table 2.3 shows the custom primers (Invitrogen) used for the genes analysed.

Gene (Protein)	Taqman Gene Expression Assay	Amplicon Length
Hsd11b1 (11β-HSD1)	Mm00476182_m1	67
Actb (β-actin)	Mm00525061_m1	118
Tbp (TBP)	Mm00446971_m1	93

Table 2.2 Taqman Gene Expression Assay codes for qRT-PCR

	Primer Sequence 5'-3'		
Gene (Protein)	**Forward**	**Reverse**	**Design**
Nr3c1 (GR)	caaagattgcaggtatcctatgaa	cttggctcttcagaccttcc	E R-Z
Nr3c2 (MR)	ccctaccatgtcctagaaaagc	agaacgctccaaggtctgag	E R-Z
Fkbp5 (FKBP5)	aaacgaaggagcaacggtaa	tcaaatgtccttccaccaca	E R-Z
Tsc22d3 (GILZ)	tccgttaaactggataacagtgc	tggttcttcacgaggtccat	E R-Z
Ppargc1 (PGC1α)	gaaagggccaaacagagaga	gtaaatcacacggcgctctt	E R-Z
Sgk1 (SGK)	tttccaaaaggggatgct	tgttggcatgattacattgttct	E R-Z
Tgfb1 (TGFβ)	tggagcaacatgtggaactc	cagcagccggttaccaag	R R
Col1α2 (Col1α2)	gcaggttcacctactctgtcct	cttgccccattcatttgtct	R R
Col3α1 (Col3α1)	tcccctggaatctgtgaatc	tgagtcgaattggggagaat	R R
Atp2a2 (SERCA)	tcgaccagtcaattcttacagg	cagggacagggtcagtatgc	E R-Z
Slc8a1 (NCX)	gtcagccttcagagctggtc	gacttccaactgctccaacc	E R-Z
Ryr2 (RyR)	ttcaacacgctcacggagta	tgccaggctctgctgatt	E R-Z
Cacna1c ($CaV_{1.2}$)	cctgcacaagggctctttc	agatgagggacacgctaacc	R R
Myh6 (αMHC)	cgcatcaaggagctcacc	cctgcagccgcattaagt	E R-Z
Myh7 (βMHC)	gcatctggaaattccgttagg	ggctcgtcatccttattagacc	E R-Z
Nppa (ANP)	cacagatctgatggatttcaaga	cctcatcttctaccggcatc	E R-Z
Actb (β-actin)	ctaaggccaaccgtgaaaag	accagaggcatacagggaca	E R-Z

Table 2.3 Primer sequences for qRT-PCR

Primer sequences for qRT-PCR. 'E R-Z' denotes primers designed by Eva Rog-Zielinska and 'R R' denotes primers designed by Rachel Richardson.

2.6.4 Western blotting

Western blotting involves the extraction of proteins from a tissue sample and further separation on an agarose gel via gel electrophoresis before transferring these separated proteins onto a membrane. This membrane is then subjected to a primary antibody specific to a particular protein and, once further subjected to a fluorescent secondary antibody which amplifies the signal of the primary antibody, it is then developed onto x-ray film. Determination of protein density from each sample allows for differences in protein levels to be elucidated.

11β-HSD1 protein expression was examined by Western blot in the heart and liver to check for appropriate deletion of the enzyme. 50 mg of tissue and 300 µl lysis buffer (5 ml stock solution consisting of 500 µl 10 X radio-immunoprecipitation assay (RIPA) buffer (Sigma), 50 µl Protease Inhibitor Cocktail (Sigma), 50 µl Phosphatase Inhibitor Cocktail P1 (Sigma), 50 µl Phosphatase Inhibitor Cocktail P2 (Sigma) and 4350 µl water) were placed in a 1.5 ml Eppendorf and homogenised using a homogeniser. This was then centrifuged at 12,000 G for 15 min at 4 ^{o}C and the supernatant, containing the protein, was transferred to a fresh 1.5 ml tube. Protein concentration was determined using a Pierce BCA Protein Assay Kit (Thermo Scientific). Albumin (BSA) standards at concentrations of 25, 125, 250, 500, 750, 1,000, 1,500 and 2,000 µg/ml were prepared and 20 µl of each was added to a 96 well plate in replicate. Aliquots of protein lysate were diluted 1/10 with RIPA buffer and 20 µl of each were also added to the 96 well plate in replicate. The bicinchoninic acid (BCA) working reagent was prepared by mixing Reagent A with Reagent B at a ratio of 50:1. 200 µl was then added to each well of the 96 well plate. The plate was

incubated for 30 min in the dark at 37 ^{o}C, allowed to cool to room temperature and the optical density was read at 562 nm to determine protein concentration.

Sodium dodecyl sulphate polyacrylamide gel electrophoresis (SDS-PAGE) was used to separate the proteins in the lysate. The top 2 cm of the gel consisted of a 5 % SDS stacking gel (1.7 ml 30 % acrylamide, 2.5 ml 0.5 M Tris, 100 µl 10 % SDS, 100 µl 10 % ammonium persulfate (APS), 30 µl tetramethylethylenediamine (TEMED) and 5.6 ml water) and the remaining 8 cm consisted of an SDS running gel (12.7 % for 11β-HSD1 (12.7 ml 30 % acrylamide, 7.5 ml 1.5 M Tris, 300 µl 10 % SDS, 300 µl 10 % APS, 30 µl TEMED and 9.2 ml water), 9.2 % for SERCA (9.2 ml 30 % acrylamide, 7.5 ml 1.5 M Tris, 300 µl 10 % SDS, 300 µl 10 % APS, 30 µl TEMED and 12.7 ml water) and 13.1 % for phospholamban (PLN) (13.1 ml 30 % acrylamide, 7.5 ml 1.5 M Tris, 300 µl 10 % SDS, 300 µl 10 % APS, 30 µl TEMED and 8.8 ml water)). TEMED was added last as this causes the gel to set. The protein lysates were aliquoted at a concentration of 2 µg/µl using RIPA buffer; 10 µl of this (20 µg protein) was added to a 1.5 ml Eppendorf, along with 1.67 µl 6 x sample buffer. 20 µl ColorPlus Prestained Protein Marker Broad Range (7-175kDa) (New England Biolabs) was also added to a 1.5 ml Eppendorf and this, and the protein samples, were incubated at 95 ^{o}C for 5 min before being centrifuged at 12,000 G for 1 min. 10 µl of the protein samples and 20 µl of the marker were loaded onto the gel and 10 µl RIPA buffer was added at the end as a blank control. The gel was run at 80 V for 15 min then 120 V for 1 h in running buffer (12.11 g Tris, 57.65 g glycine and 2 g SDS in 2 L dH_2O, stored at 4 ^{o}C).

The gel was then placed in transfer buffer (2.93 g glycine, 5.81 g Tris, 0.375 g SDS, 200 ml methanol and 800 ml water) and the stacking gel was carefully removed.

Amersham Hybond ECL nitrocellulose membrane (GE Healthcare) and extra thick blot paper (Bio-Rad) were trimmed to the same size as the gel and also placed in transfer buffer. These were then placed on a Trans-Blot Semi Dry Transfer Cell (Bio-Rad) in the following order: blot paper, then nitrocellulose membrane, then the gel, and finally another sheet of blot paper. Bubbles between the layers were removed by gently pressing the top sheet of blot paper. The appropriate mA for transferring the proteins from the gel to the nitrocellulose membrane was calculated using the following equation:

$$mA = Gel\ surface\ area\ (cm^2) x\ 0.8$$

As all the gels were 40 cm^2, they were all transferred using 32 mA for 90 min. The nitrocellulose membrane was removed and placed in 0.1 % Tris-buffered saline/Tween 20 (TBST) (100 ml TBS 10 X, 900 ml water and 1 ml Tween 20) for 10 min. The gel was then transferred to a 50 ml Falcon tube and 10 ml 5 % blocking buffer (100 ml TBST and 5 g powdered milk (Marvel)) was added. The tube was placed on a roller for 1 h at room temperature before the gel was washed in TBST for 5 min. The primary antibody, diluted in 5 % BSA in water, was added to the tube and incubated on a roller overnight at 4 ^{o}C.

The membrane was then washed with TBST (3 x 15 min) and the secondary antibody, diluted in 5 % BSA in water, was added. The tube was placed on the roller for 1 h at room temperature and again washed (3 x 15 min) with TBST. The membrane was blocked using blocking buffer and the primary internal control antibody, diluted in 5 % BSA in water, was added to the tube and incubated on the roller for 45 min at room temperature. The membrane was then washed with TBST (3 x 15 min) and the secondary internal control antibody, diluted in 5 % BSA in

water, was added. The tube was again placed on the roller and incubated for 45 min at room temperature, before being developed using an ECL Prime Western Blotting Detection Reagent (GE Healthcare). The membrane was wrapped in cling film and placed in a cassette. 1 ml of Reagent A was mixed with 1 ml of Reagent B in a 2 ml Eppendorf tube. This solution was then added to the membrane and incubated for 1 min at room temperature. The membrane was the exposed to X-ray film before being developed. Target protein levels were then calculated by normalising the density of this band to that of the housekeeping protein. Table 2.4 lists all the primary and secondary antibodies used for western blotting in this project.

Protein	Primary antibody	Secondary antibody
11β-HSD1	Anti- 11β-HSD1 (in-house (De Sousa Peixoto, *et al*., 2008)) Raised in sheep 1/10,000	Anti-sheep-HRP (Abcam) Raised in donkey 1/5,000
SERCA	Anti-SERCA2A (Thermo Scientific) Raised in rabbit 1/5,000	Anti-rabbit-HRP (Abcam) Raised in goat 1/5,000
PLN	Anti-PLN (Badrilla) Raised in mouse 1/5,000	Anti-mouse-HRP (Abcam) Raised in goat 1/5,000
PLN Ser^{16}	Anti-PLN-Ser^{16} (Badrilla) Raised in rabbit 1/5,000	Anti-rabbit-HRP (Abcam) Raised in goat 1/5,000
PLN Thr^{17}	Anti-PLN-Thr^{17} (Badrilla) Raised in rabbit 1/5,000	Anti-rabbit-HRP (Abcam) Raised in goat 1/5,000
β-actin	Anti-β-actin (Sigma) Raised in mouse 1/10,000	Anti-mouse-HRP (Abcam) Raised in rabbit 1/5,000
α-tubulin	Anti-α-tubulin (Sigma) Raised in mouse 1/10,000	Anti-mouse-HRP (Abcam) Raised in rabbit 1/5,000

Table 2.4 List of Western blot antibodies and dilutions

2.6.5 Cardiac troponin-I assay

Cardiac Troponin-I (cTnI) is released by cardiomyocytes in response to injury and is used as a clinical tool for diagnosing acute MI (Gassenmaier, *et al*., 2012). Plasma levels of cardiac troponin-I were measured using a High Sensitivity Mouse Cardiac Troponin-I ELISA Kit (Life Diagnostics). Troponin standards were prepared at concentrations of 10, 5, 2.5, 1.25, 0.625, 0.312, 0.156 and 0 ng/ml. Sample plasma was diluted four fold with plasma diluent. 100 µl of cTnI HRP Conjugate and 100 µl of diluted plasma were added in replicate to the anti-cTnI coated wells on the 96 well plate. The plate was incubated on an orbital shaker at 100 G for 60 min at room temperature then the wells were emptied and washed six times with 1 X wash solution. The wells were again emptied ensuring no residual mixture remained before 100 µl TMB Reagent was added to each well and incubated on an orbital shaker at 100 G for 20 min at room temperature. 100 µl Stop Solution was added to each well and the plate was gently agitated ensuring all the blue colour in the wells changed to yellow. Absorbance was read at 450 nm to determine troponin-I concentration using the linear line standard curve constructed using the troponin standards detailed above. This assay was performed by Kieran McGregor.

2.7 Statistical Analysis

Statistical analysis was performed using GraphPad Prism 5.00 (GraphPad Software) with data presented as the mean ± standard error of the mean. Statistical significance was reached with a *p* value of less than 0.05.

Mortality data was compared using Fisher's exact test and chi square test, and cardiomyocyte cross-sectional area distribution data was compared using a Kolmogorov-Smirnov test.

Other statistical comparisons were performed using one way ANOVAs and two way ANOVAs, both with Bonferroni's post-hoc test, and two-tailed unpaired Student's *t* tests. Full details are given in Section 2 of Chapters 3, 4 and 5.

2.8 Materials

Abcam

Rabbit anti-mouse-CD31 primary antibody, anti-sheep-HRP secondary antibody, anti-rabbit-HRP secondary antibody, anti-mouse-HRP secondary antibody

AD Instruments

22 gauge cannulae

Adobe

Adobe Photoshop CS5 Extended

Agilent Technologies

7T MRI Scanner

Allergan

Lacri-lube eye ointment

Applied Biosystems

High Capacity cDNA Reverse Transcription Kit, Taqman Mastermix, Taqman Gene Expression Assays (Mm00476182_m1, Mm00525061_m1, Mm00446971_m1)

Badrilla

Anti-PLN primary antibody, anti-PLN-serine16 primary antibody, anti-PLN-threonine17 primary antibody

Bio-Rad

Extra thick blot paper, Trans-blot Semi Dry Transfer Cell

Biotium

GelRed

Capillary Tube Supplies

Capillary tubes

Cedarlane

Anti-Mac2-FITC primary antibody

Dako

Phosphomolybdic-phosphotungstic acid

Drug Discovery Core, QMRI, University of Edinburgh

Anti-11β-HSD1 primary antibody

Ethicon

6-0 prolene suture, 5-0 mersilk suture

Fine Science Tools

Mini-Goldstein retractors

Fisher Scientific

15ml Falcon tubes, 50ml Falcon tubes

GE Healthcare

Amersham Hybond ECL, ECL Prime Western Blot Detection Reagent

GraphPad Software

GraphPad Prism 5.00

Harvard Apparatus

HSE-Harvard MiniVent ventilator, 9mm autoclips

Invitrogen

PCR primers (DelI and SMAC), qRT-PCR primers (GR, MR, FKBP5, SGK, GILZ, PGC1α, TGFβ, Col1α2, Col3α1, SERCA, NCX, RyR, $CaV_{1.2}$, αMHC, βMHC, ANP and β-actin) Taq DNA Polymerase, biotinylated anti-isolectin B4 primary antibody, streptavidin-Alexa 488 secondary antibody, DAPI, Trizol Plus RNA Purification Kit, Trizol, Deoxyribonuclease I Amplification Kit

Life Diagnostics

High Sensitivity Mouse Cardiac Troponin I ELISA Kit

Marvel

Powdered milk

MediaCybernetics

Image Pro 6.2

National Institutes of Health

ImageJ Software

New England Biolabs

1kb DNA ladder, ColorPlus Prestained Protein Marker Broad Range (7-175kDa)

Promega

dNTPs

Qiagen

DNeasy Blood and Tissue Kit

Rathburn Chemicals

Chloroform

Roche

Lightcycler 480, Universal Probe Library System

Sigma-Aldrich

Sodium citrate tribasic dihydrate, hydrochloric acid, magnesium chloride, agarose, PBS tablets, formalin, ethanol, Krebs solution, protease type XIV, bovine serum albumin, anti-αSMA-Cy3 primary antibody, hydrogen peroxide, DPX mounting media, RIPA buffer, protease inhibitor cocktail, phosphatise inhibitor cocktail, Tris base, acrylamide, SDS, APS, TEMED, clear 96 well plates, glycine, TBS, Tween 20, anti-β-actin primary antibody, anti-α-tubulin primary antibody, aniline blue solution, acetic acid

Small Animal Instruments

Needle electrodes

Southern Biotech

Floromount G

Stem Cell Technologies

Anti-Ym1-FITC primary antibody

Thermo Scientific

Nanodrop 1000 Version 3.3, Pierce BCA Protein Assay Kit, anti-SERCA2A primary antibody

Vector

Goat serum, donkey serum, rabbit serum, WGA-Rhodamine primary antibody, avidin block, biotin block, rabbit anti-FITC secondary antibody, DAB solution, biotinylated goat anti-rabbit secondary antibody, RTU ABC Reagent

Visulasonics

Vevo 770 High Resolution Ultrasound Scanner, Vevo Image Analysis Software

Worthington Biochemical

Collagenase type 1

2.9 Solutions

Krebs solution

Dissolve 6.95 g NaCl, 0.19 g KCl, 0.14 g NaH_2PO_4 (monobasic), 0.37 g $CaCl_2.2H_2O$, 0.26 g $MgCl_2.6H_2O$, 4.77 g HEPES and 1.98 g D-glucose in 1 L dH_2O.

PBS solution

Dissolve 5 tablets in 1 L of dH_2O.

Sodium citrate buffer (10mM)

Add 2.94 g sodium citrate tribasic dehydrate to 1 L dH_2O and adjust to pH 6 using concentrated hydrochloric acid.

TE buffer

Make a 1 M Tris solution by dissolving 60.57 g Tris in 500 ml dH_2O. Make a 0.5 M ethylenediamine tetraacetic acid (EDTA) solution by dissolving 18.6 g EDTA in 100 ml dH_2O and adjust to pH 8 using concentrated sodium hydroxide (NaOH). To make a 1 X TE buffer solution, dilute 5 ml 1 M Tris solution and 1 ml 0.5 M EDTA solution in 494 ml dH_2O.

TBE solution

Make a 0.5 M EDTA solution by dissolving 93.05 g EDTA in 500 ml dH_2O and adjust to pH 8 using concentrated NaOH. Make a TBE 5 X stock solution by adding 54 g Tris base and 27.5 g boric acid in 980 ml dH_2O and then add 20 ml of 0.5 M EDTA solution. To make a 0.5 X TBE solution, dilute 100 ml of 5 X TBE solution in 900 ml dH_2O.

TBST solution

Make a TBS 10 X stock solution by dissolving 24.2 g Tris base and 80 g NaCL in 1 L dH_2O. Add 100 ml of TBS 10 X to 900 ml dH_2O and add 1 ml Tween 20.

Chapter 3

Basal Characterisation of Global and Cardiovascular-specific 11β-HSD1 Knock-out Mice

3.1 Introduction

Intracellular pre-receptor metabolism by the two isozymes of the enzyme 11β-HSD controls the local bioavailability of glucocorticoids for binding to GR and MR (Zhang, *et al*., 2005). 11β-HSD type 1 regenerates glucocorticoids, converting inactive cortisone (11-dehydrocorticosterone in rodents) to its active form cortisol (corticosterone in rodents). 11β-HSD type 2 catalyses the reverse reaction, essentially inactivating glucocorticoids in the cytosol and preventing them from binding to GR or MR (Zhang, *et al*., 2005).

In the cardiovascular system, glucocorticoids are involved in maintaining blood pressure and vascular tone (see Section 1.1.4.1) (Ullian, 1999; Hadoke, *et al*., 2006; Goodwin, *et al*., 2011). Glucocorticoids have been implicated in vascular remodelling using the 11β-HSD1 deficient mouse, which is unable to regenerate glucocorticoids intracellularly. 11β-HSD1 deficient mice show increased angiogenesis *in vivo* in response to implantation of subcutaneous sponges and in aortic ring preparations *in vitro* (Small, *et al*., 2005). Furthermore, 11β-HSD1 deficiency results in increased angiogenesis *in vivo* in the peri-infarct region of the heart 7d after MI (Small, *et al*., 2005; McSweeney, *et al*., 2010). There is some debate as to whether 11β-HSD2 is present in the vasculature, however 11β-HSD2 KO mice exhibit altered vascular function suggesting a functional role for 11β-HSD2 in this tissue (Hadoke, *et al*., 2001). There is no evidence for 11β-HSD2 in cardiomyocytes. Approximately 50% of 11β-HSD2 KO mice die within 48h of birth, with survivors displaying renal hypertrophy, hypokalaemia and hypertension, in addition to the impaired vascular function mentioned above (Kotelevtsev, *et al*.,

1999). Human mutations in the 11β-HSD2 gene can lead to the Syndrome of Apparent Mineralocorticoid Excess (SAME), characterised by high blood pressure (Draper & Stewart, 2005).

11β-HSD1 deficient mice have reduced heart size and weight but the mechanism for this remains unknown (McSweeney, *et al*., 2010). Systolic function appears to be maintained but diastolic function and calcium regulation have not been studied. Moreover, a single nucleotide polymorphism in the *Hsd11b1* gene, which encodes the 11β-HSD1 protein, has been associated with reduced left ventricular mass in a human population study (Rahman, *et al*., 2011). Further work using the GR knock-out (KO) mouse has shown a crucial role for glucocorticoids in heart maturation. GR KO mice die at birth due to underdeveloped lungs (Cole, *et al*., 1995), however a number of these mice die prenatally prior to lung function being required. It is suggested that this is due to diastolic dysfunction, disorganised myofibrils within cardiomyocytes, and impaired calcium-induced calcium release (Rog-Zielinska, *et al*., 2013). GR overexpression studies have also shown the importance of glucocorticoids in maintaining cardiac homeostasis with tissue-specific myocardial overexpression of GR contributing to bradycardia, atrio-ventricular block, and altered calcium cycling (Sainte-Marie, *et al*., 2007).

The importance of 11β-HSD1 in regulating cardiovascular function has led to the generation of a cardiovascular-specific 11β-HSD1 KO mouse in order to differentiate between global and local 11β-HSD1 regulation of the cardiovascular system. These *Hsd11b1*$^{fl/fl}$*Sm22α-Cre*$^{+}$ (SMAC) mice have 'floxed' 11β-HSD1 alleles and a Cre recombinase transgene inserted into the *Sm22α* gene. *Sm22α* is a cytoskeletal protein expressed exclusively in cardiomyocytes during development and in smooth muscle

cells post-natally (Lees-Miller, *et al*., 1987; Li, *et al*., 1996). In tissues where *Sm22α* is expressed, Cre recombinase will also be expressed and will cut at the loxP sites flanking exon 3 on the 'floxed' 11β-HSD1 alleles. This excision removes exon three which contains the binding site for the co-factor NADPH, and thus renders the enzyme non-functional in these cells. However, to date there has been no characterisation of 'cardiovascular' 11β-HSD1 deletion in these mouse strains.

Comparison of SMAC mice and their Cre^- controls with global 11β-HSD1 KO (DelI) mice and their controls (C57BL/6 mice) will allow the role of cardiovascular 11β-HSD1 to be investigated. The aims of this chapter were to a) determine the distribution of 11β-HSD1 in the heart and vasculature, b) confirm global deletion in DelI mice and cardiovascular-specific deletion in SMAC mice, c) investigate the cardiovascular phenotype of mice with global and cardiovascular-specific 11β-HSD1 deletion, and d) determine whether any phenotype could be reproduced by chronic pharmacological inhibition of 11β-HSD1. It was hypothesised that SMAC mice will show tissue specific deletion of 11β-HSD1 only in the heart and vasculature and that their basal cardiac phenotype will mimic that of the DelI mice; they will have reduced heart size and weight and their systolic function will be preserved. Considering the previous literature showing the importance of GR-mediated glucocorticoid action on subcellular cardiomyocyte structure and function, it is also hypothesised that these mice will have altered calcium regulation and impaired diastolic function. Furthermore, it was hypothesised that chronic pharmacological inhibition of 11β-HSD1 would also result in reduced heart size and weight, and mild diastolic dysfunction.

3.2 Methods

3.2.1 Mice

Three groups of male experimental mice, aged 6w-78w, were used; global 11β-HSD1 KO mice (DelI), cardiovascular-specific 11β-HSD1 KO mice (*Hsd11b1*$^{fl/fl}$*Sm22α-Cre*$^{+}$ mice*;* SMAC) and C57BL/6SJL mice which had UE2316, a selective 11β-HSD1 inhibitor, introduced in to their diet at 9 months of age, and delivered for a further 9 months. Each mouse received approximately 20mg of drug per kg of bodyweight. In livers collected, 11β-HSD1 activity was reduced to 44.2 ± 13.7 % of control, as measured by thin layer chromatography (Liu, *et al*., 2008). These mice were part of an aging study being conducted by another group in the laboratory, whereby the end point was 78 weeks (18months). The opportunity arose to investigate their heart function, and thus they were included in this thesis. Treatment and 11β-HSD1 activity assay were performed by Karen Sooy. Controls for the DelI mice were in-house C57BL/6 mice, controls for the SMAC mice were *Hsd11b1*$^{fl/fl}$*Sm22α-Cre*$^{-}$ (Cre^{-}) littermate mice and controls for the UE2316-treated mice were vehicle-treated C57BL/6SJL mice.

Echocardiography (Section 2.2.2) was performed at time points detailed in Section 3.2.6, and blood pressure was measured by tail plethysmography in DelI and SMAC mice, and their respective controls, at 10 weeks of age (Section 2.2.1). Mice were culled either by cervical dislocation or perfusion fixation (Section 2.3.1). Cervical dislocation was performed in order to harvest tissue for qRT-PCR and western blotting, for tissue gravimetrics, for myocardial interstitial fluid volume assessment (Section 2.2.3), for cardiomyocyte length measurement (Section 2.3.4) or after blood

volume measurement (Section 2.3.2). Perfusion fixation was performed in order to harvest tissue for immunohistochemistry and histology.

3.2.2 Genotyping

DNA was extracted from ear notches obtained at weaning, and PCR was performed to identify DelI mice and SMAC mice and their Cre^- controls, as described in Section 2.1.2.

3.2.3 qRT-PCR

RNA was extracted from homogenised heart, aorta, liver and skeletal muscle tissue using TRIzol as described in Section 2.6.1. cDNA was synthesized as detailed in Section 2.6.2 and qRT-PCR was performed as described in Section 2.6.3 to assess mRNA levels of 11β-HSD1, GR, MR, FKBP5, GILZ, PGC1α, SGK, TGFβ, Col1α2, Col3α1, SERCA, NCX, RyR, $CaV_{1.2}$, β-actin and TBP.

3.2.4 Western blotting

Protein was extracted from homogenised heart, aorta, liver, and skeletal muscle samples, ran on a gel and transferred to a nitrocellulose membrane as described in Section 2.6.4. The membranes were exposed to antibodies for 11β-HSD1, sarcoplasmic reticulum Ca^{2+} ATPase (SERCA), phospholamban (PLN), phosphorylation of PLN at serine 16 (Ser16) or threonine 17 (Thr17), and the

internal control proteins β-actin or α-tubulin before being developed on x-ray film as detailed in Section 2.6.4.

3.2.5 Echocardiography

High frequency echocardiography was performed on DelI and C57BL/6 control mice at 6, 10 and 78 weeks (18 months) of age, on SMAC and Cre- control mice at 6, 10, 20 and 35 weeks of age and on UE2316-treated and vehicle-treated control mice at 78 weeks (18 months) of age as described in Section 2.2.2. Scanning was performed by Adrian Thomson.

3.2.6 Histology and immunohistochemistry

Heart sections, 4μm thick, were used for histology and immunohistochemistry. Picrosirius Red staining was used to determine collagen content. Immunofluorescent staining with wheat germ agglutinin, isolectin B4 and DAPI and was used to measure cardiomyocyte cross-sectional area. Vessel density was determined by immunofluorescent staining with α-SMA, isolectin B4 and DAPI. Full details are given in Sections 2.4.2, 2.5.1 and 2.5.2.

3.2.7 Statistical analysis

All values are expressed as mean ± SEM. Statistical significance was reached with a *p* value of less than 0.05. Longitudinal echocardiography data was compared using a two way ANOVA with Bonferroni's post-hoc test. Cardiomyocyte cross-sectional

area distribution data was compared using a Kolmogorov-Smirnov test. All other data were compared using two-tailed unpaired Student's *t* tests.

3.3 Results

3.3.1 Confirmation of global and cardiovascular-specific 11β-HSD1 deletion in DelI and SMAC mice, respectively

11β-HSD1 mRNA was present in heart (Figure 3.1a and b), aorta (Figure 3.1c and d), liver (Figure 3.1e and f) and skeletal muscle (SkM; Figure 3.1g and h) tissue of C57BL/6 and Cre^- mice aged 12 weeks. Twelve week old DelI mice showed a reduction of 11β-HSD1 (*Hsd11b1*) mRNA compared to control in heart ($p<0.001$), aorta ($p<0.001$), liver ($p<0.001$) and SkM ($p<0.001$). Twelve week old SMAC mice exhibited a reduction of 11β-HSD1 mRNA in heart ($p<0.01$) and aorta ($p<0.01$) only. 11β-HSD1 mRNA was normalised to internal control genes which were β-actin (*Actb*) for heart, aorta and liver tissue and TBP (*Tbp*) for SkM, which were similar in all groups (see Appendix 1).

11β-HSD1 protein (Figure 3.2 and Figure 3.3) was detected at the expected sizes of 32kDa and 34kDa, reflecting the non-glycosylated and glycosylated isoforms, respectively (Blum, *et al*., 2000; Gupta, *et al*., 2003). 11β-HSD1 protein expression was reduced in DelI heart ($p<0.001$), aorta ($p<0.001$), liver ($p<0.001$) and SkM ($p<0.001$) compared to C57BL/6 control mice. SMAC mice also displayed reduced 11β-HSD1 protein expression in heart ($p<0.001$) and aorta ($p<0.001$) compared to Cre^- control mice, but expression in liver and SkM was comparable. 11β-HSD1 protein was normalised to internal control proteins which were either β-actin for heart, aorta and liver tissue or α-tubulin for SkM, which were similar in all groups (see Appendix 2).

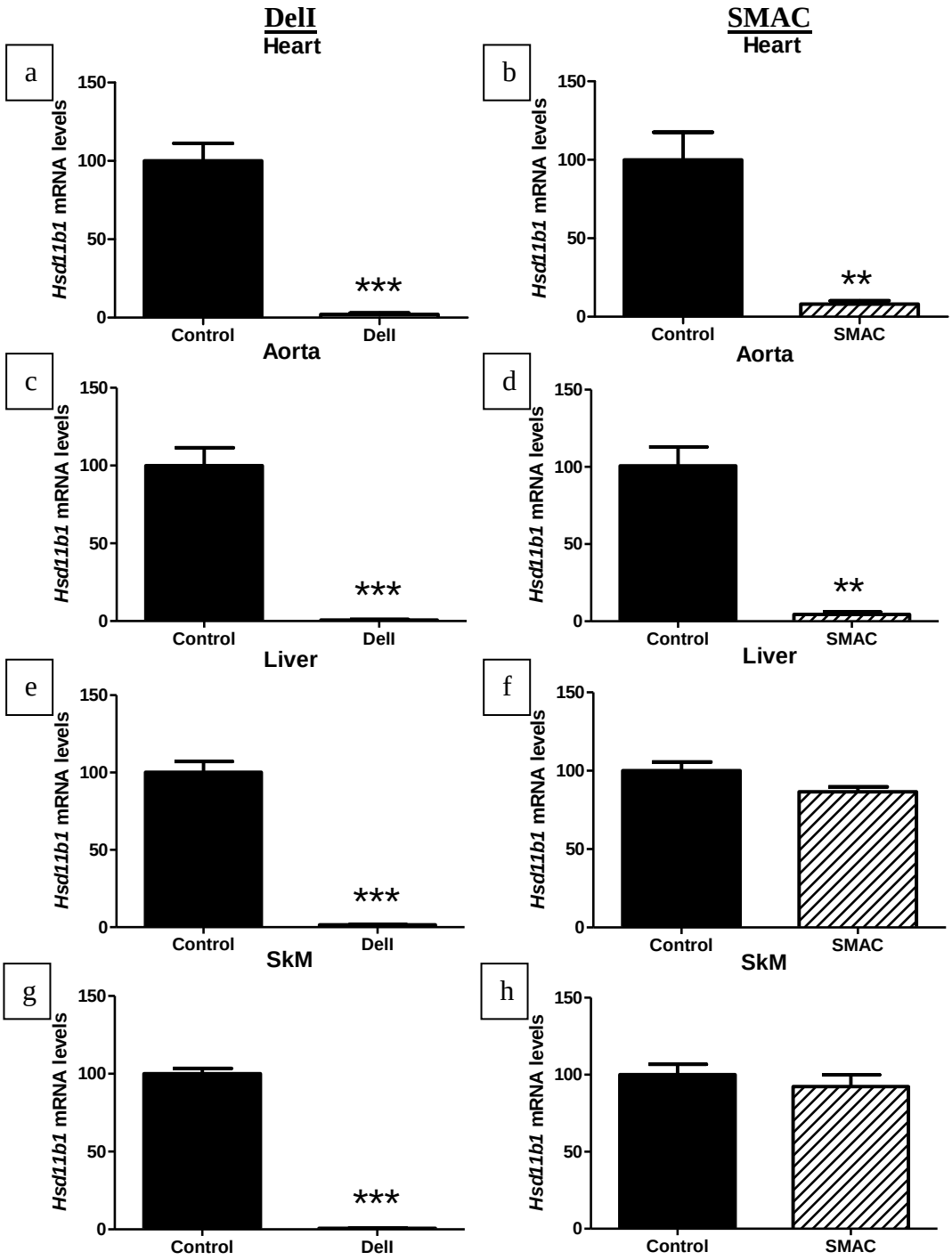

Figure 3.1 Confirmation of global 11β-HSD1 deletion in DelI mice and cardiovascular-specific 11β-HSD1 deletion in SMAC mice by qRT-PCR

mRNA levels of 11β-HSD1 were determined by qRT-PCR in DelI (left column) and SMAC (right column) mice and their respective controls at 12w of age. Heart (a & b), aorta (c & d), liver (e & f) and skeletal muscle (g & h) were investigated. 11β-HSD1 mRNA levels were normalised to β-actin, the internal control, which was similar in all groups (see Appendix 1). 11β-HSD1 mRNA levels in the control groups were set to 100% and mRNA levels in DelI and SMAC mouse hearts were expressed as a percentage of this (Student's *t* test *** = $p<0.001$, ** = $p<0.01$; n=4/group).

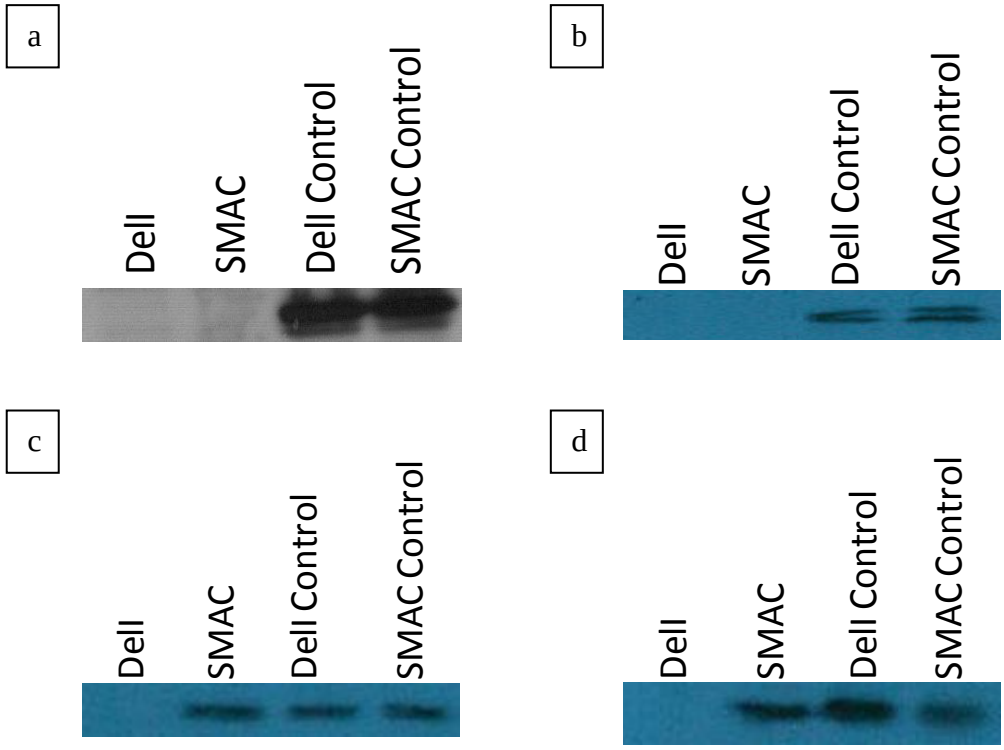

Figure 3.2 Sample 11β-HSD1 Western blots
Sample 11β-HSD1 Western blots of (a) heart, (b) aorta, (c) liver and (d) skeletal muscle tissue from DelI, SMAC, C57BL/6 and Cre^- mice at 12w of age.

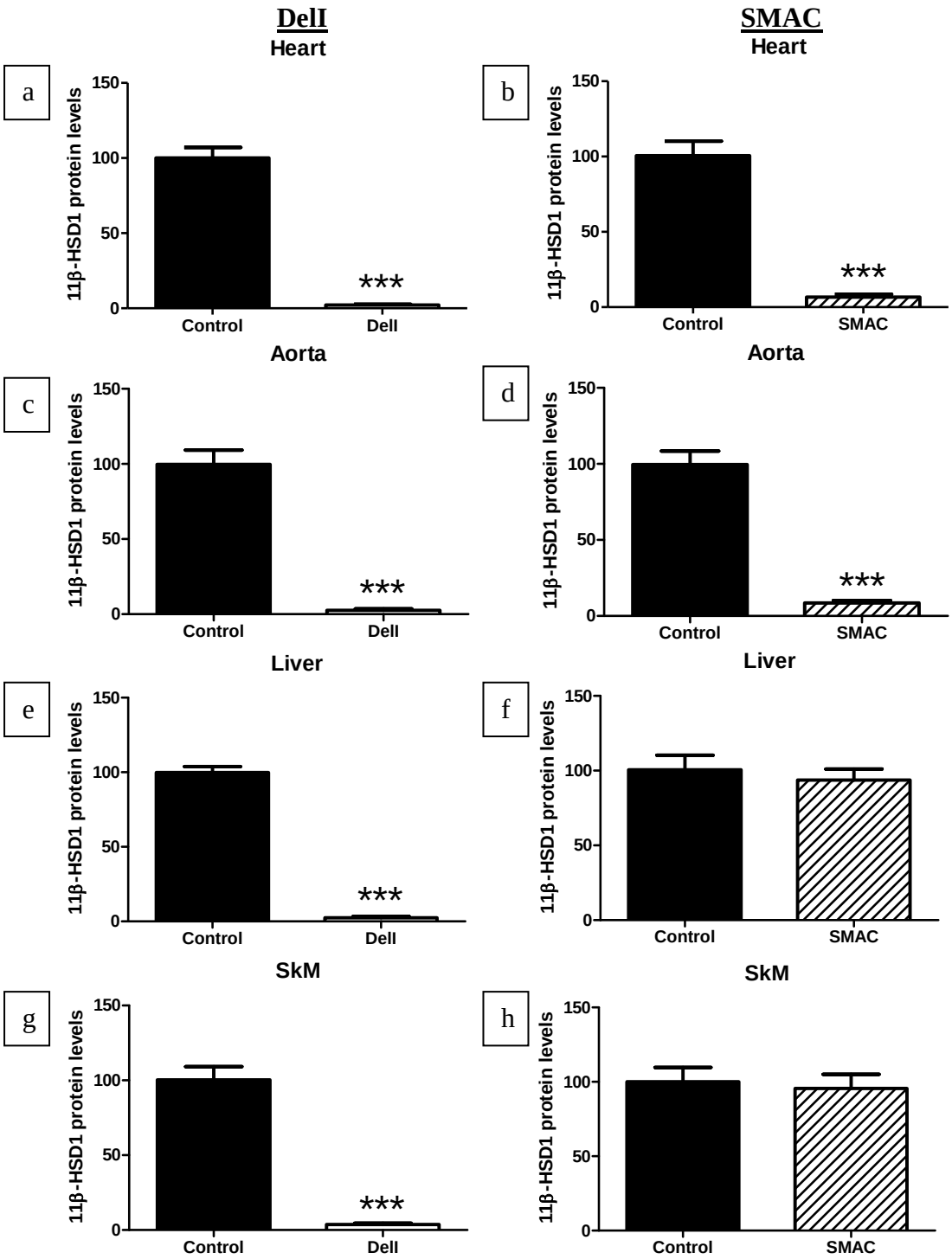

Figure 3.3 11β-HSD1 Western blotting

11β-HSD1 protein expression was assessed by Western blotting in DelI (left column) and SMAC (right column) mice and their respective controls at 12w of age. Heart (a & b), aorta (c & d), liver (e & f) and skeletal muscle (g & h) were investigated. 11β-HSD1 protein levels were normalised to the internal control (β-actin for heart, aorta and liver, or TBP for SkM) which was similar in all groups. 11β-HSD1 protein levels in the control groups were set to 100% and protein levels in DelI and SMAC tissue were expressed as a percentage of this (Student's *t* test *** = $p<0.001$; n=4/group).

3.3.2 Expression of myocardial GR, MR and their target genes does not change with 11β-HSD1 deletion

Myocardial GR (*Nr3c1*, Figure 3.4a and b), MR (*Nr3c2*, Figure 3.4c and d), FKBP5 (*Fkbp5*, Figure 3.5a and b), GILZ (*Tsc22d3*, Figure 3.5c and d), PGC1α (*Ppargc1a*, Figure 3.5e and f) and SGK (*Sgk1*, Figure 3.5g and h) mRNA levels were similar in all genotypes. Target gene mRNA was normalised to β-actin (*Actb*), an internal control gene, which was similar in all groups (see Appendix 1).

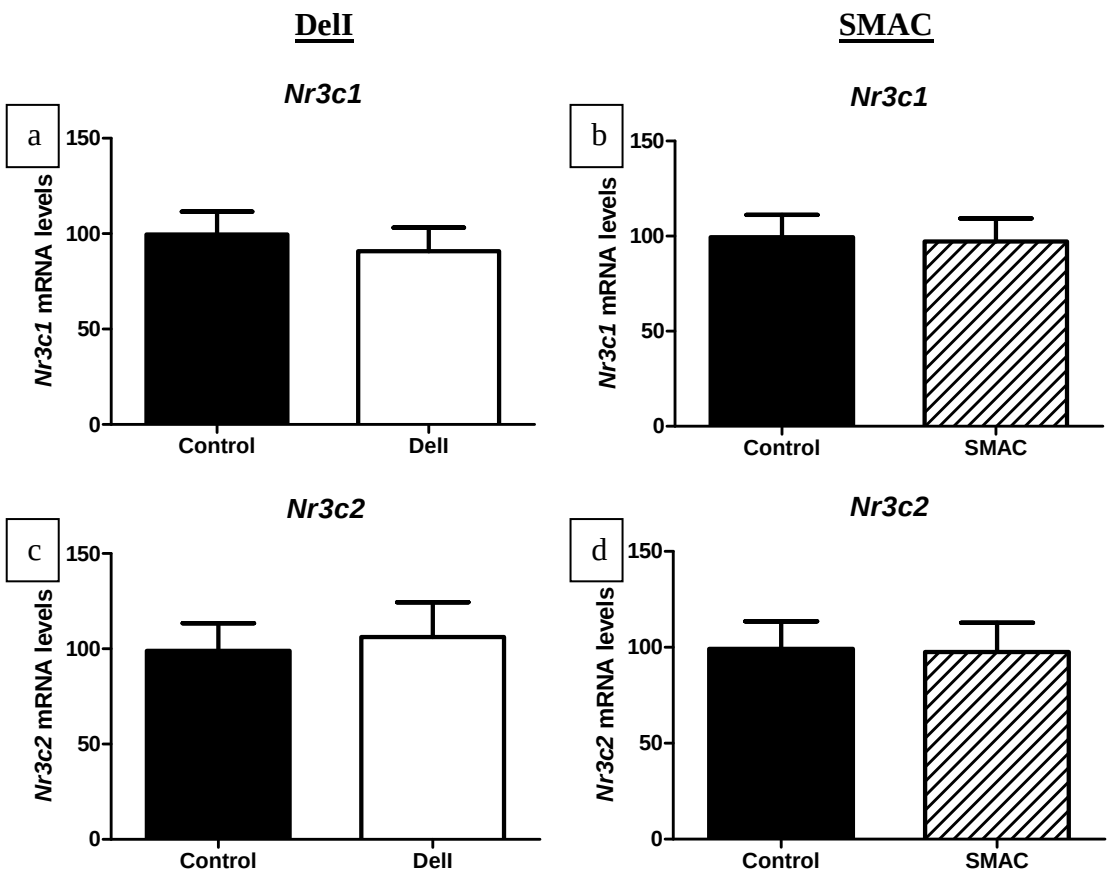

Figure 3.4 11β-HSD1 deletion does not change levels of GR or MR mRNA
mRNA levels of GR (a & b) and MR (c & d) were determined by qRT-PCR in hearts from DelI (left column) and SMAC (right column) mice and their respective controls at 12w of age. GR and MR mRNA levels were normalised to β-actin, the internal control, which was similar in all groups. GR and MR mRNA levels in the control groups were set to 100% and mRNA levels in DelI and SMAC mouse hearts were expressed as a percentage of this (Student's *t* test; n=6/group).

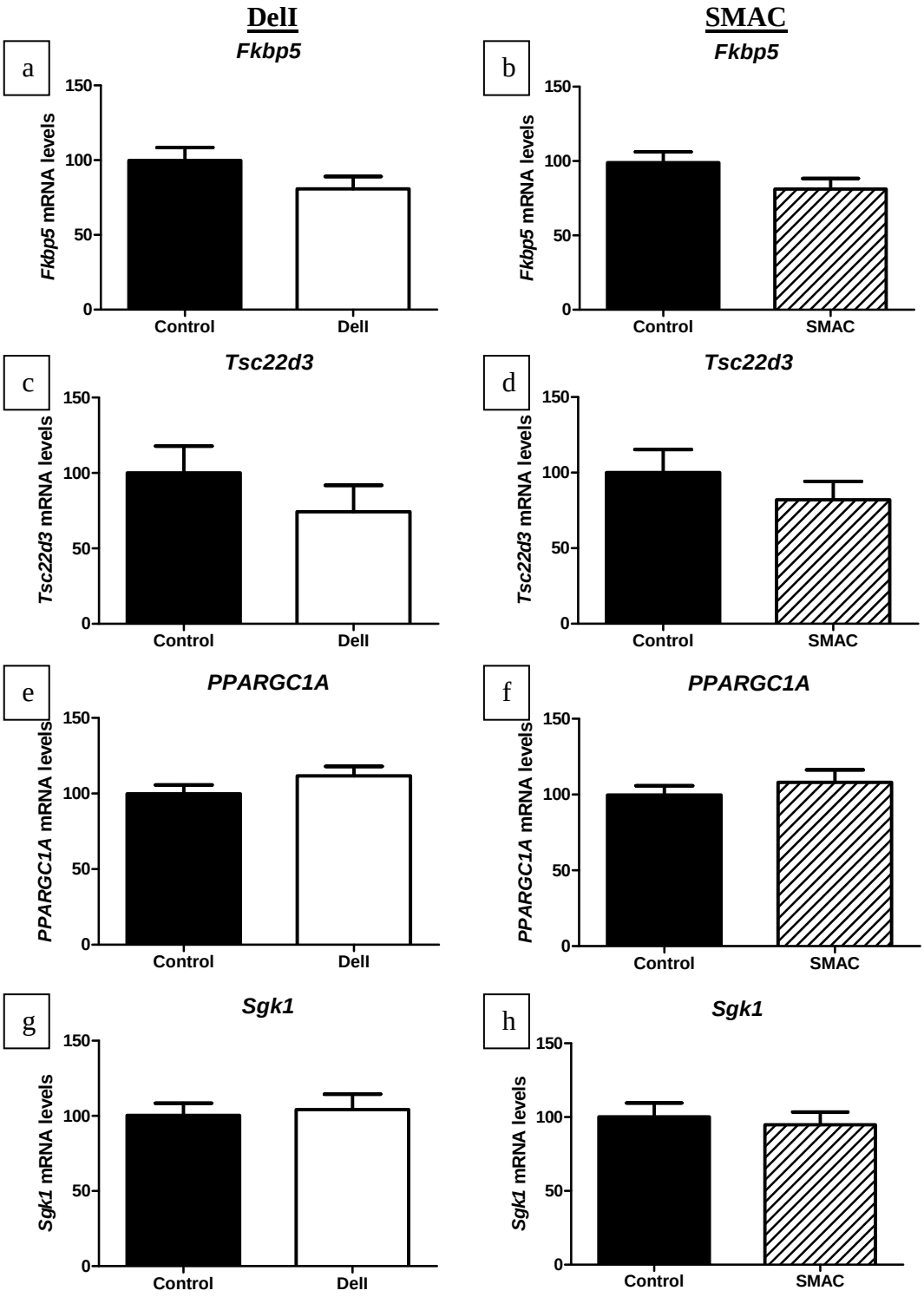

Figure 3.5 11β-HSD1 deletion does not alter levels of GR or MR target gene mRNA
mRNA levels of FKBP5 (a & b), GILZ (c & d), PGC1α (e & f) and SGK (g & h) were determined by qRT-PCR in hearts from DelI (left column) and SMAC (right column) mice and their respective controls at 12w of age. Target gene mRNA levels were normalised to β-actin, the internal control, which was similar in all groups. Target gene mRNA levels in the control groups were set to 100% and mRNA levels in DelI and SMAC mouse hearts were expressed as a percentage of this (Student's *t* test; n=6/group).

3.3.3 Systolic blood pressure is unaffected by global or cardiovascular-specific 11β-HSD1 deletion

Systolic blood pressure was similar between DelI and C57BL/6 control mice (Figure 3.6a) and between SMAC and Cre^- control mice (Figure 3.6b).

3.3.4 Ventricular growth is delayed in mice with global, but not cardiovascular-specific 11β-HSD1 deletion

3.3.4.1 Echocardiography

DelI mice had reduced left ventricular end diastolic area (LVEDA, $p<0.05$) and stroke volume (SV, $p<0.001$) compared to C57BL/6 control mice at 10 weeks of age, but not at 6 weeks or 78 weeks of age (Figure 3.7a and c). These observations were not seen in SMAC mice at any time point up to 35 weeks of age (Figure 3.7b and d). LVESA in DelI and SMAC mice was not different to their respective controls at any time point (Figure 3.7e and f).

3.3.4.2 Gravimetrics

Post-mortem data showed 12 week old DelI mice had reduced heart weights compared to C57BL/6 control mice (Figure 3.8a, $p<0.01$), despite both genotypes having similar body weights (Figure 3.8c). This resulted in a reduced heart weight to body weight ratio (Figure 3.8e, $p<0.01$). SMAC and Cre^- control mice had similar heart weights (Figure 3.8b) and body weights (Figure 3.8d) at 12 weeks of age, and therefore a similar heart weight to body weight ratio (Figure 3.8f).

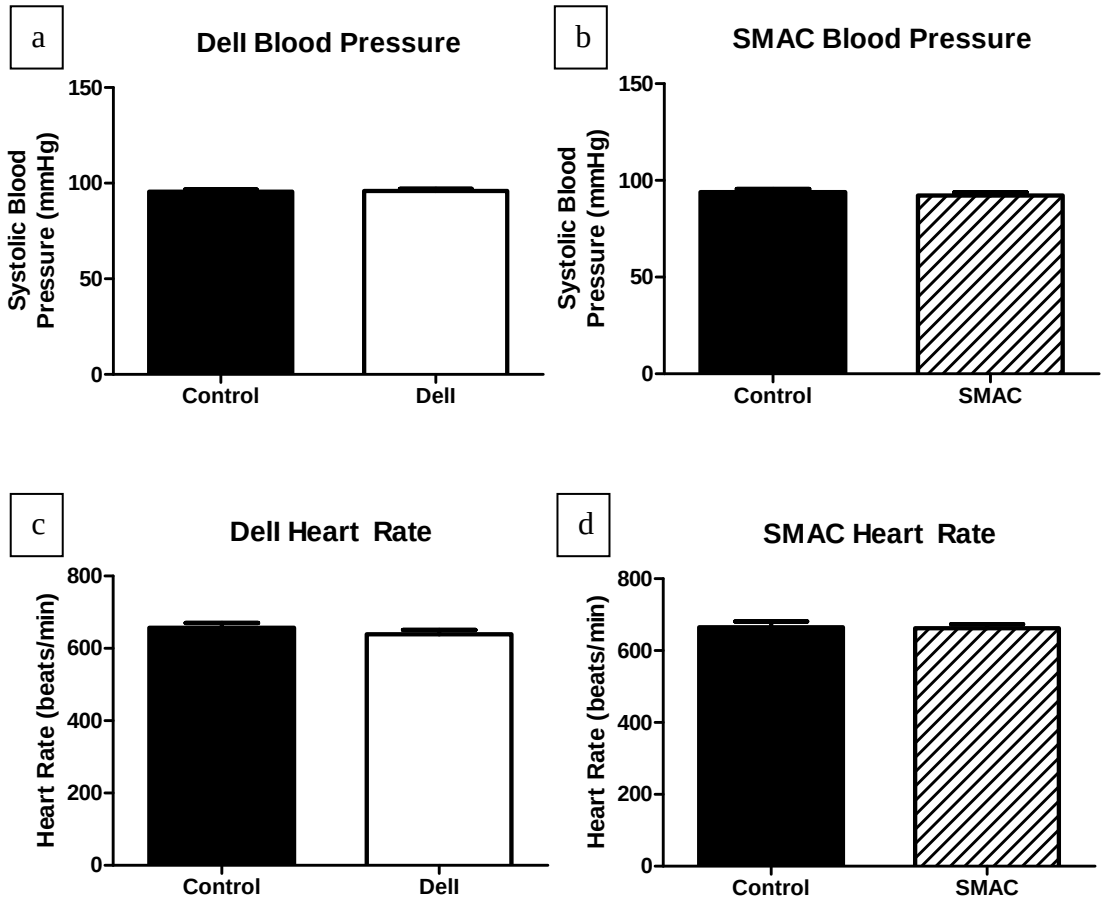

Figure 3.6 11β-HSD1 deletion does not affect systolic blood pressure
Systolic blood pressure was measured by tail plethysmography and heart rate was measured by high frequency ultrasound in DelI (a and c) and SMAC (b and d) mice and their respective controls at 12w of age (Student's *t* test; n=6/group).

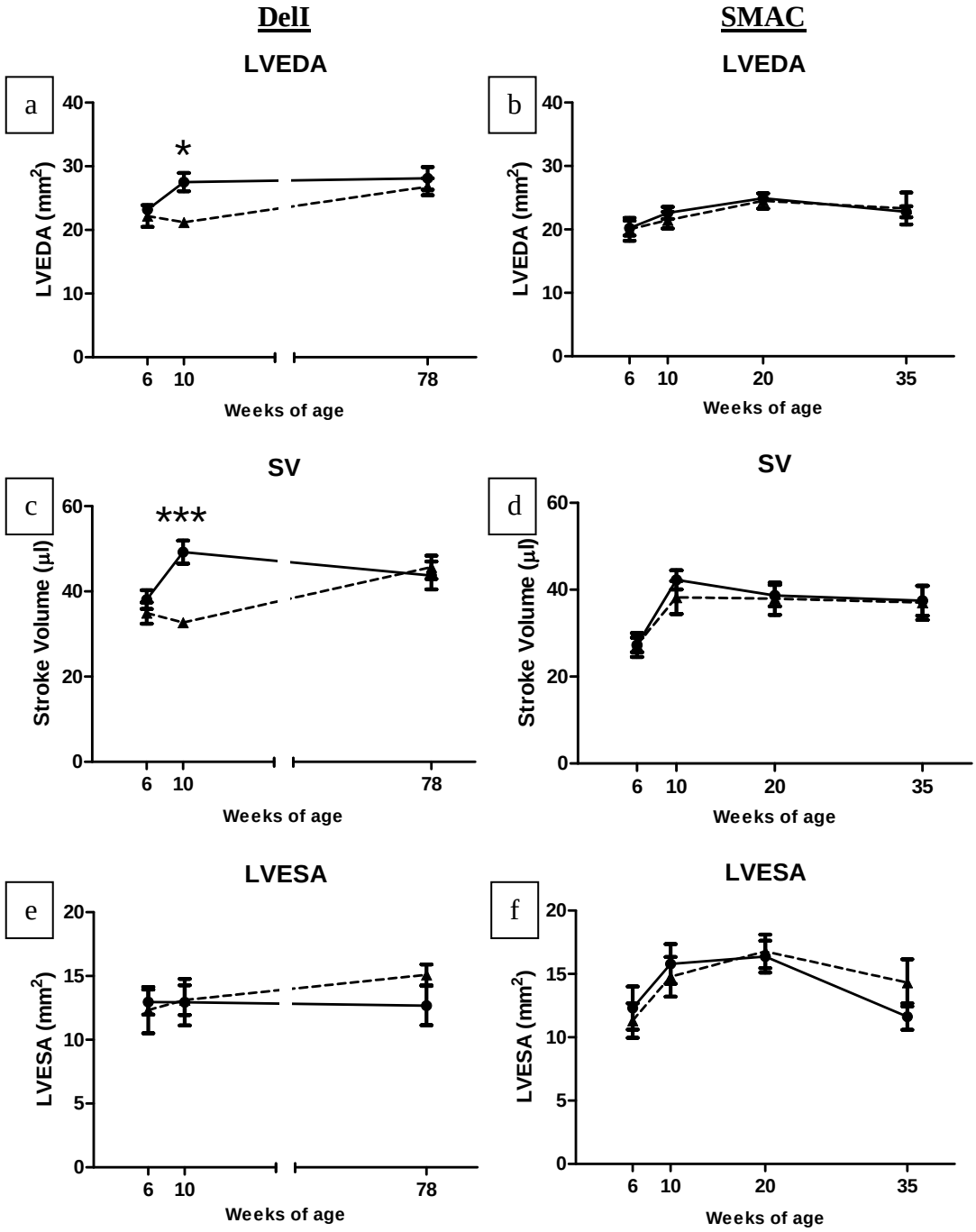

Figure 3.7 Global, but not cardiovascular-specific, 11β-HSD1 deletion delays left ventricular growth

LVEDA (a & b), SV (c & d), and LVESA (e & f) were assessed by high frequency ultrasound in DelI mice (left column, dashed lines) and C57BL/6 controls (left column, solid lines), and SMAC mice (right column, dashed lines) and Cre^- controls (right column, solid lines) at 6, 10, 20, 35 and 78w of age (two way ANOVA *** = $p<0.001$, * = $p<0.05$; n=8/group for DelI & SMAC mice, n=6/group for controls).

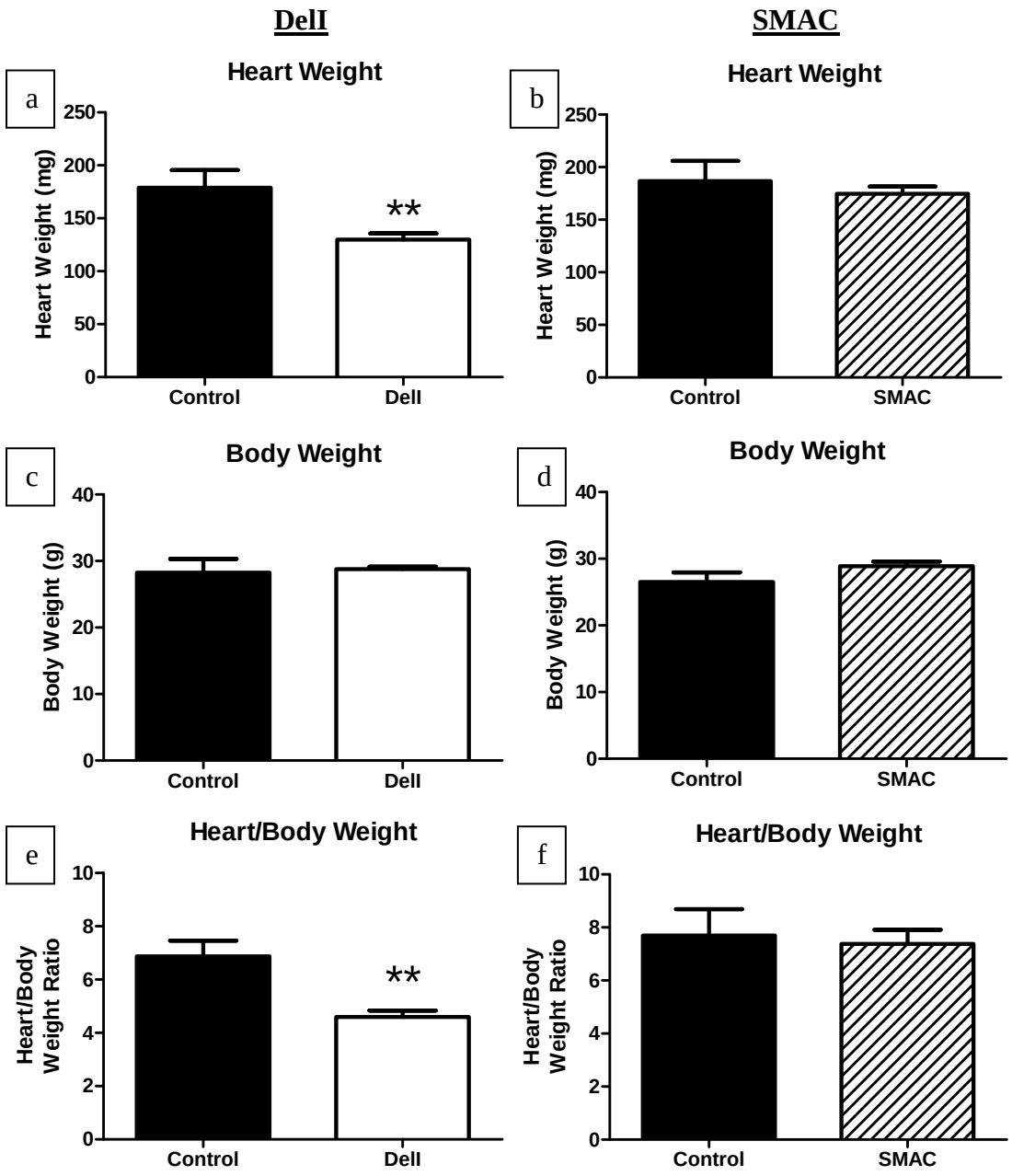

Figure 3.8 Global, but not cardiovascular-specific, 11β-HSD1 deletion reduces heart weight

Heart weight as measured by gravimetrics at post-mortem (a & b), body weight (c & d) and heart weight to body weight ratio (e & f) of DelI (left column) and SMAC (right column) mice and their respective controls at 12w of age (Student's *t* test ** = $p<0.01$; n=8/group for DelI & SMAC mice, n=6/group for controls).

3.3.4.3 Alteration in blood and interstitial fluid volume does not account for smaller, lighter left ventricles in mice with global 11β-HSD1 deletion

Blood volume was similar in DelI and C57BL/6 mice (Figure 3.9a). Heart wet weight (Figure 3.9b, $p<0.01$) and dry weight (Figure 3.9c, $p<0.01$) were both reduced in DelI mice compared to C57BL/6 controls, giving both genotypes a similar heart wet weight to dry weight ratio (Figure 3.9d).

3.3.4.4 Cardiomyocyte length, but not cross-sectional area, is reduced in hearts from mice with global 11β-HSD1 deletion

Cardiomyocyte cross-sectional area in the left ventricular wall (Figure 3.10a) was similar in DelI and C57BL/6 mice (Figure 3.10b) and in SMAC and Cre^- mice (Figure 3.10c) at 12 weeks of age. Cardiomyocyte cross-sectional area distribution demonstrated a similar distribution pattern between DelI and C57BL/6 mice (Figure 3.10d).

Cardiomyocytes, freshly isolated from the hearts of DelI mice, were significantly shorter than those from C57BL/6 mice (Figure 3.10e, $p<0.001$).

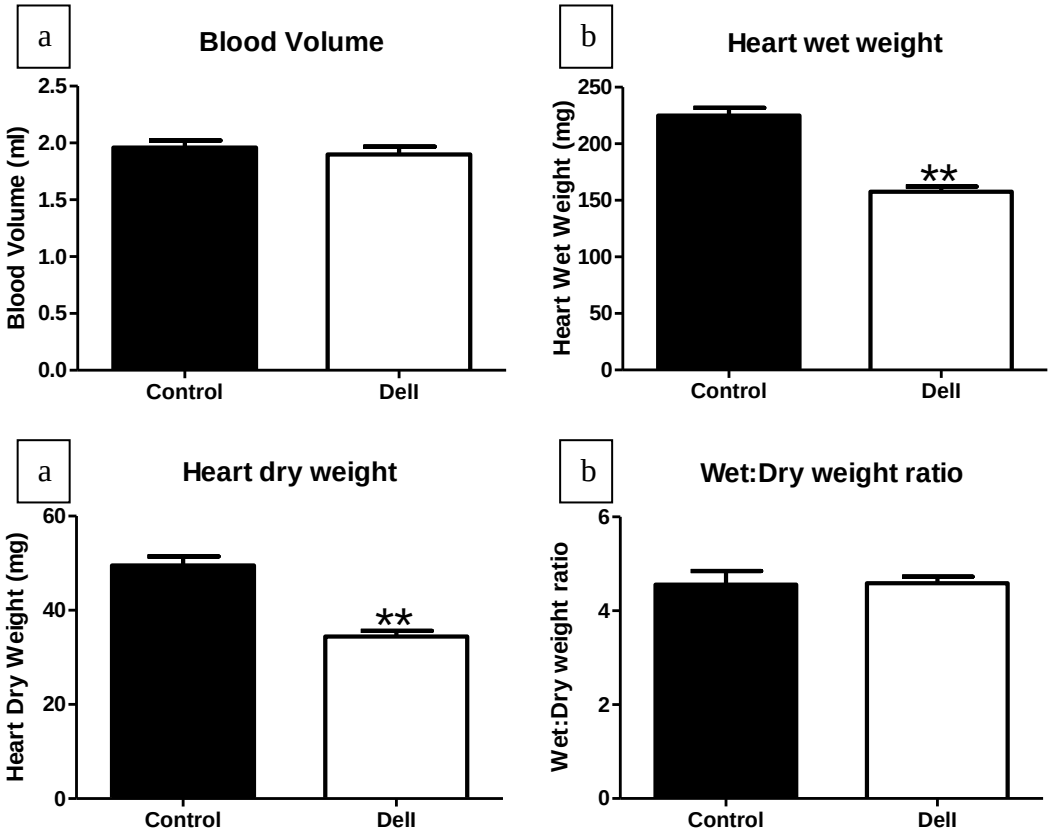

Figure 3.9 Blood volume and interstitial fluid volume are unchanged in DelI mice
Blood volume (a), heart wet weight (b), dry weight (c) and wet weight to dry weight ratio (d) in DelI mice and C57BL/6 controls at 12w of age (Student's *t* test ** = $p<0.01$; n=3/group).

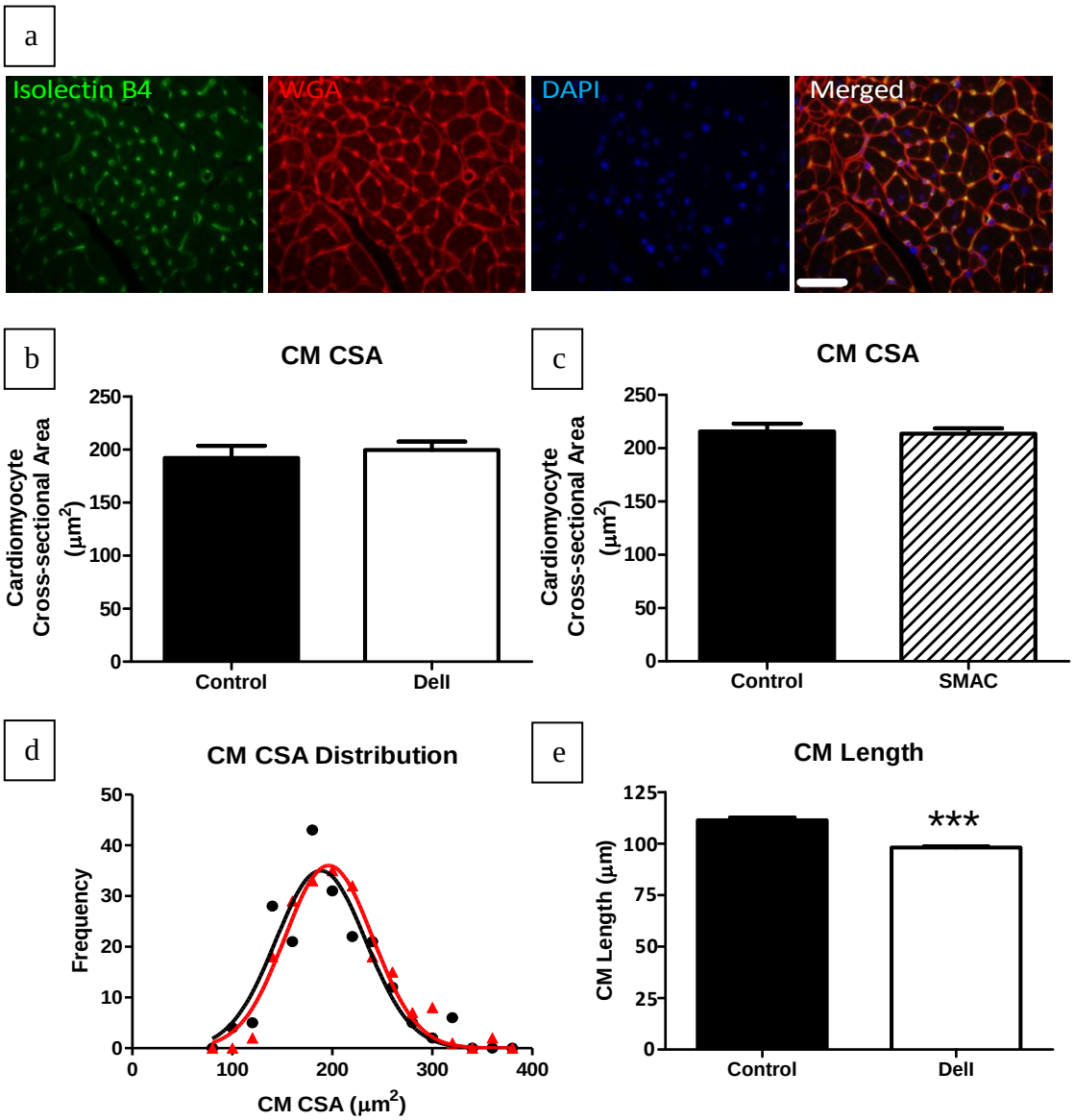

Figure 3.10 Cardiomyocyte cross-sectional area is unaltered in DelI mice, but cardiomyocyte length is reduced

Cardiomyocyte cross sectional area was assessed by staining for isolectin B4, WGA and DAPI (a) in DelI mice (b) and SMAC mice (c) and their respective controls at 12w of age (Student's *t* test; n=5/group). Isolectin B4 stains endothelial cells, WGA stains cell membranes and DAPI stains nuclei. This allowed cardiomyocyte cross-sectional area measurement by selecting cardiomyocytes which a) appeared to be cut in the short axis, b) had a nucleus in the middle of the cell and c) were surrounded by capillaries which were also cut in the short axis. The frequency of cross-sectional area distribution in DelI mice (red line) and C57BL/6 controls (black line) is shown in (d) (Kolmogorov-Smirnov test; n=5/group). The length of freshly isolated cardiomyocytes, using a Langendorff preparation, from hearts of DelI and control mice at 12w of age is shown in (e) (Student's *t* test *** = $p<0.001$; n=3/group). Scale bar is 20µm.

3.3.4.5 Myocardial vessel density is unchanged in mice with global and cardiovascular-specific 11β-HSD1 deletion

Vessel density assessment (Figure 3.11a) revealed that the number of isolectin $B4^+$α-SMA^- capillaries (<4μm diameter; Figure 3.11b and c), isolectin $B4^+$α-SMA^+ small arterioles (4-200μm diameter; Figure 3.11d and e) and large arterioles (>200μm diameter; Figure 3.11f and g) per $400\mu m^2$ in the left ventricular wall was similar in DelI and C57BL/6 mice, and in SMAC and Cre^- mice.

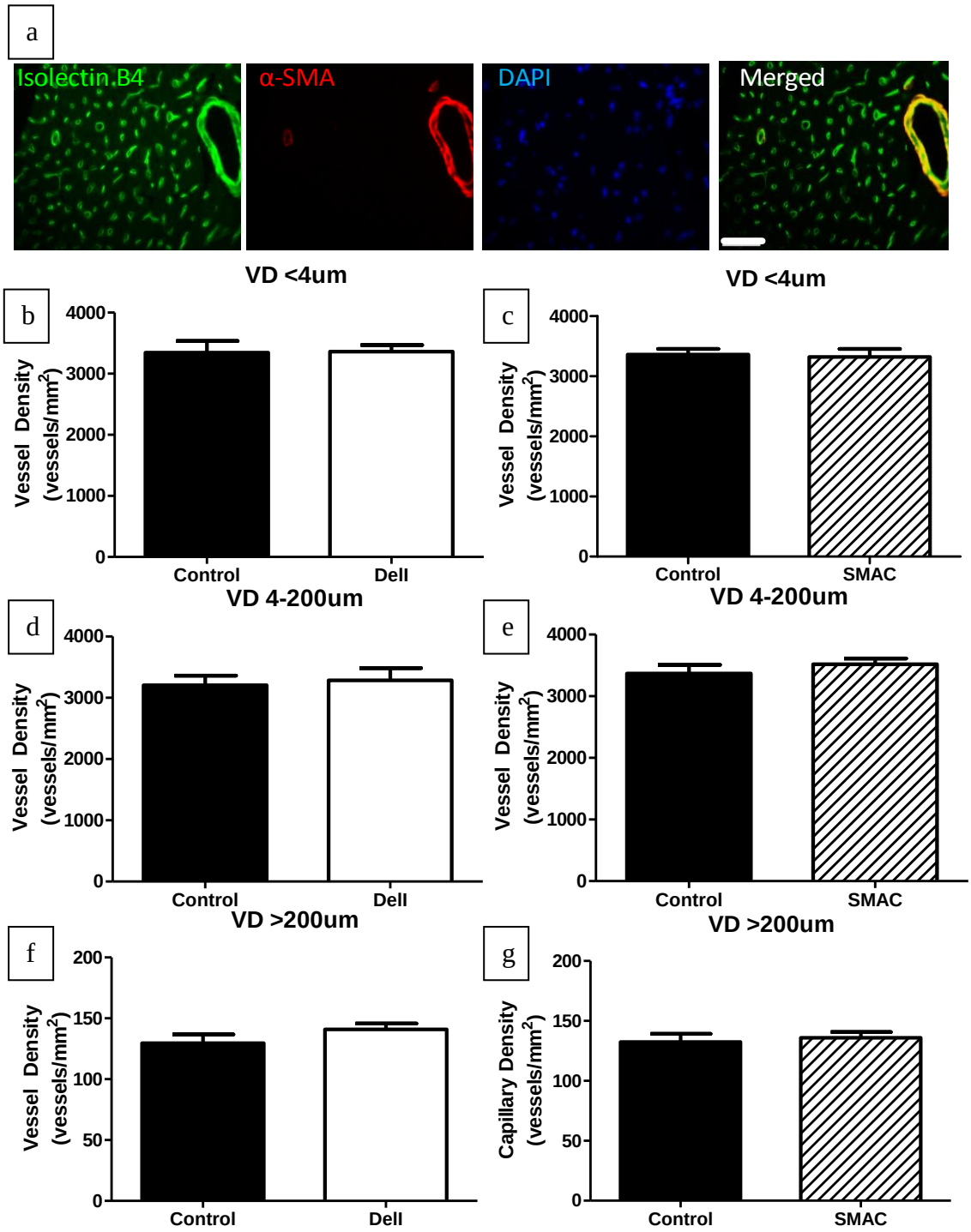

Figure 3.11 Myocardial vessel density is not influenced by 11β-HSD1 deletion
Myocardial vessel density was assessed by staining for isolectin B4, α-SMA and DAPI (a) in DelI mice (b, d & f) and SMAC mice (c, e & g) and their respective controls at 12w of age. Isolectin B4 stains endothelial cells, α-SMA stains smooth muscle cells and DAPI stains nuclei. The number of isolectinB4^{+}α-SMA^{-} capillaries (<4μm diameter), isolectinB4^{+}α-SMA^{+} small (4-200μm diameter) and large arterioles (>200μm diameter) present per mm^{2} in the left ventricular wall was calculated. (Student's *t* test; n=6/group for DelI & SMAC mice, n=4/group for controls). Scale bar is 20μm.

3.3.4.6 Chronic pharmacological inhibition of 11βHSD1 tends to increase, rather than decrease, heart dimensions and weight in aged mice

C57BL/6SJL mice which had UE2316, a selective 11β-HSD1 inhibitor, introduced into their diet for 9 months had a trend for increased left ventricular end diastolic areas (Figure 3.12a; p=0.18) and left ventricular systolic areas (Figure 3.12b; p=0.12) at 18 months of age. This was despite body weights being similar between the two groups (Figure 3.12c). Post-mortem gravimetrics revealed that mice treated with UE2316 had significantly heavier hearts (Figure 3.12d, p<0.01) and, therefore, an increased heart weight to body weight ratio (Figure 3.12e, p<0.05). Cardiomyocyte cross-sectional area was also similar between the two groups (Figure 3.13).

Measurements of food intake showed each mouse received approximately 20mg of drug per kg of bodyweight. In livers collected, 11β-HSD1 activity was reduced to 44.2 ± 13.7 % of control, as measured by thin layer chromatography. Treatment and 11β-HSD1 assay were performed by Karen Sooy.

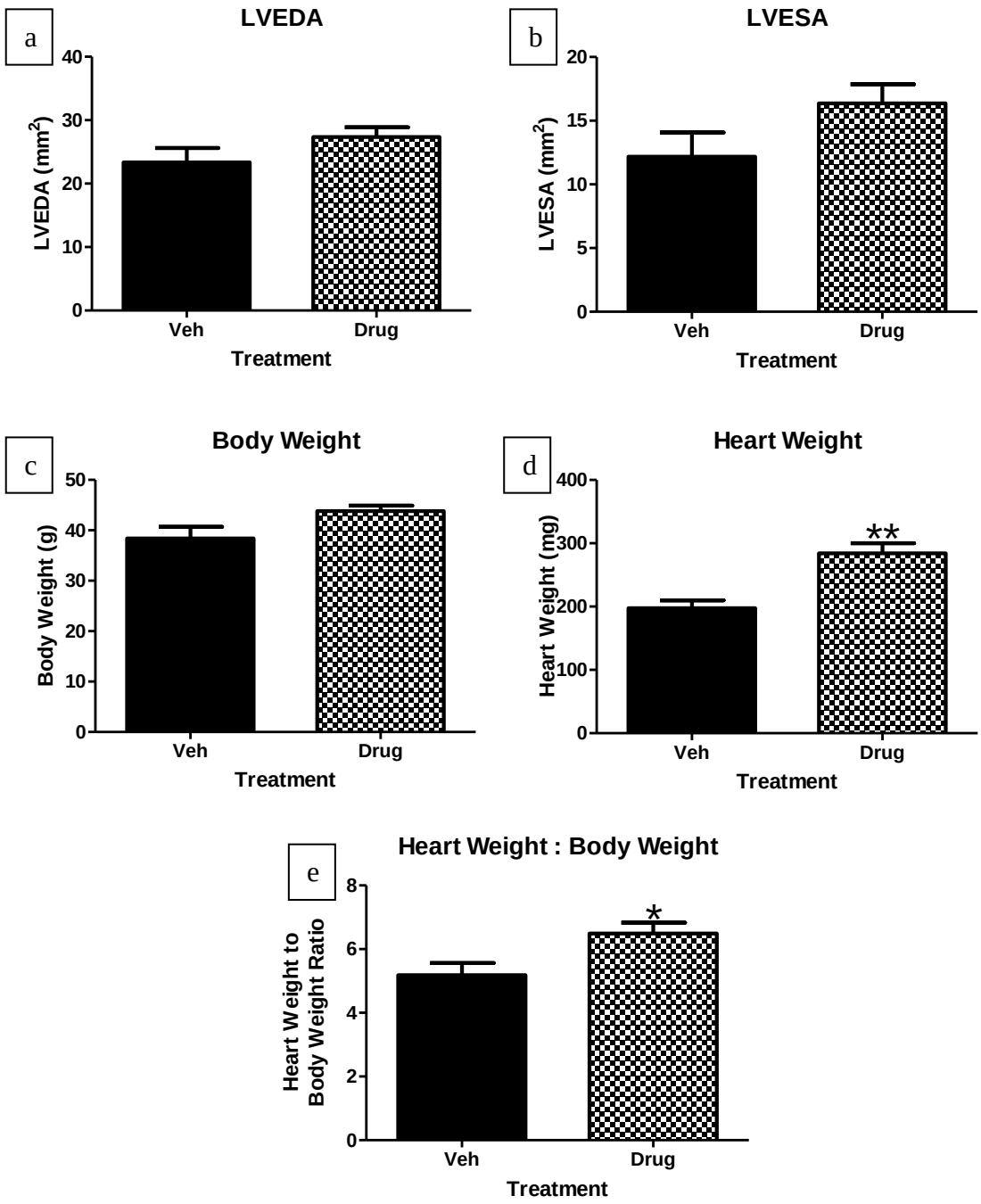

Figure 3.12 Chronic 11β-HSD1 inhibition increases heart weight

LVEDA (a) and LVESA (b) were assessed by high frequency ultrasound in 18 month old mice treated with UE2316 (20mg/kg) in their diet for 9 months (chequered bars) and vehicle treated mice (filled bars) At post-mortem, body weight (c) and heart weight (d) were measured by gravimetrics, and heart weight to body weight ratio (e) was calculated (Student's *t* test ** = $p<0.01$, * = $p<0.05$; n=5/group).

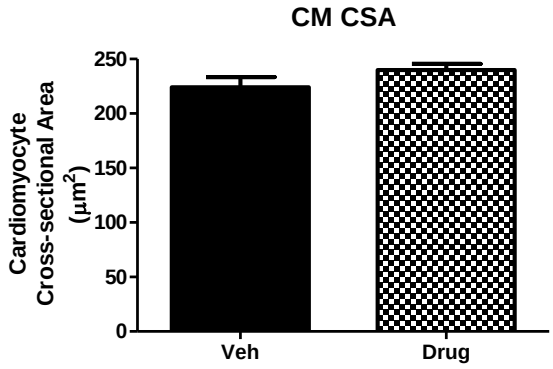

Figure 3.13 Chronic 11β-HSD1 inhibition does not alter cardiomyocyte cross-sectional area

Cardiomyocyte cross sectional area was assessed by staining for isolectin B4, WGA and DAPI in 18 month old mice treated with UE2316 (20mg/kg) in their diet for 9 months (chequered bars) and vehicle treated mice (filled bars). Isolectin B4 stains endothelial cells, WGA stains cell membranes and DAPI stains nuclei. This allowed cardiomyocyte cross-sectional area measurement by selecting cardiomyocytes which a) appeared to be cut in the short axis, b) had a nucleus in the middle of the cell and c) were surrounded by capillaries which were also cut in the short axis (Student's *t* test; n=5/group).

3.3.5 11β-HSD1 deletion and chronic inhibition influences diastolic, but not systolic, function

3.3.5.1 Systolic function is unaffected by 11β-HSD1 deletion or inhibition

Ejection fraction (Figure 3.14a and b) and fractional shortening (Figure 3.14c and d) were similar in DelI and C57BL/6 control mice and in SMAC and Cre^- control mice at all time points investigated. Reduced heart size and weight observed in DelI mice had a direct impact on stroke volume and therefore cardiac output, which was significantly reduced compared to C57BL/6 mice (Figure 3.14e, $p<0.001$). Cardiac output was similar in SMAC and Cre^- controls (Figure 3.14f). Heart rate was similar between all groups.

UE2316-treated mice showed similar systolic function compared to vehicle-treated mice (Figure 3.15a-c).

3.3.5.2 Mild diastolic dysfunction is evident in mice with global 11β-HSD1 deletion and is reproduced in mice with cardiovascular-specific 11β-HSD1 deletion, and following chronic 11β-HSD1 inhibition

There was no change in E wave to A wave ratio in DelI mice or SMAC mice compared to their respective controls (Figure 3.16a and b). However, reduced E wave deceleration was seen in DelI mice (Figure 3.16c, $p<0.05$) and SMAC mice (Figure 3.16d, $p<0.05$, $p<0.01$ and $p<0.001$), and a corresponding increase in mitral valve deceleration time (MV DT) was observed in both DelI mice (Figure 3.16e, $p<0.01$ and $p<0.001$) and SMAC mice (Figure 3.16f, $p<0.05$, $p<0.01$ and $p<0.001$) compared to their respective controls.

A similar phenotype was observed in UE2316-treated mice, with these mice also displaying a similar E wave to A wave ratio to vehicle-treated control mice (Figure 3.17a) but a reduced E wave deceleration (Figure 3.17b, $p<0.05$) and increased MV DT (Figure 3.17c, $p<0.05$).

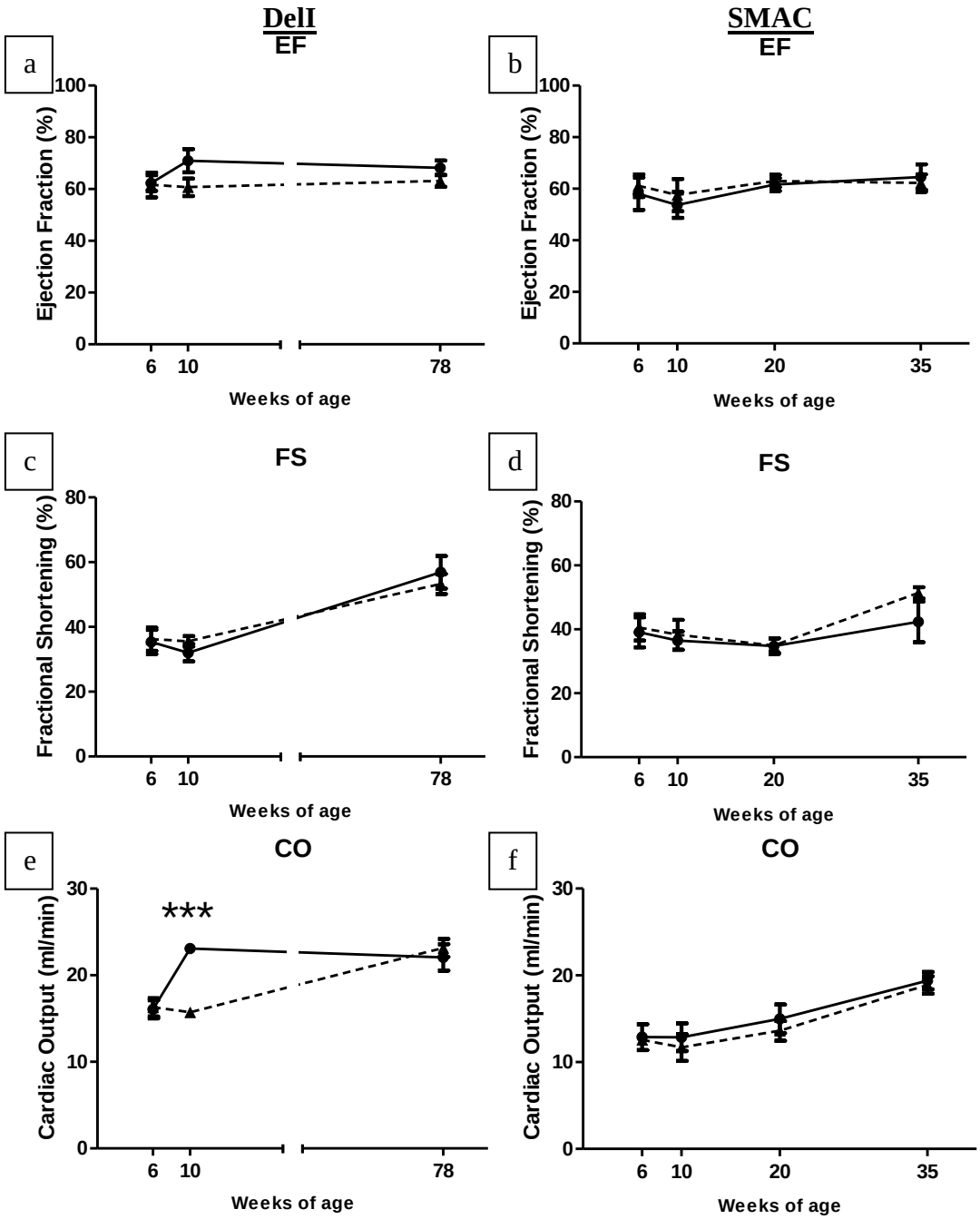

Figure 3.14 Systolic function is unaltered after 11β-HSD1 deletion

EF (a and b), FS (c and d) and CO (e and f) were assessed by high frequency ultrasound in DelI mice (left column, dashed lines) and SMAC mice (right column, dashed lines) and their respective controls (solid lines) at 6, 10, 20, 35 and 78 weeks of age (two way ANOVA, *** = $p<0.001$; n=8/group for DelI & SMAC mice, n=6/group for controls).

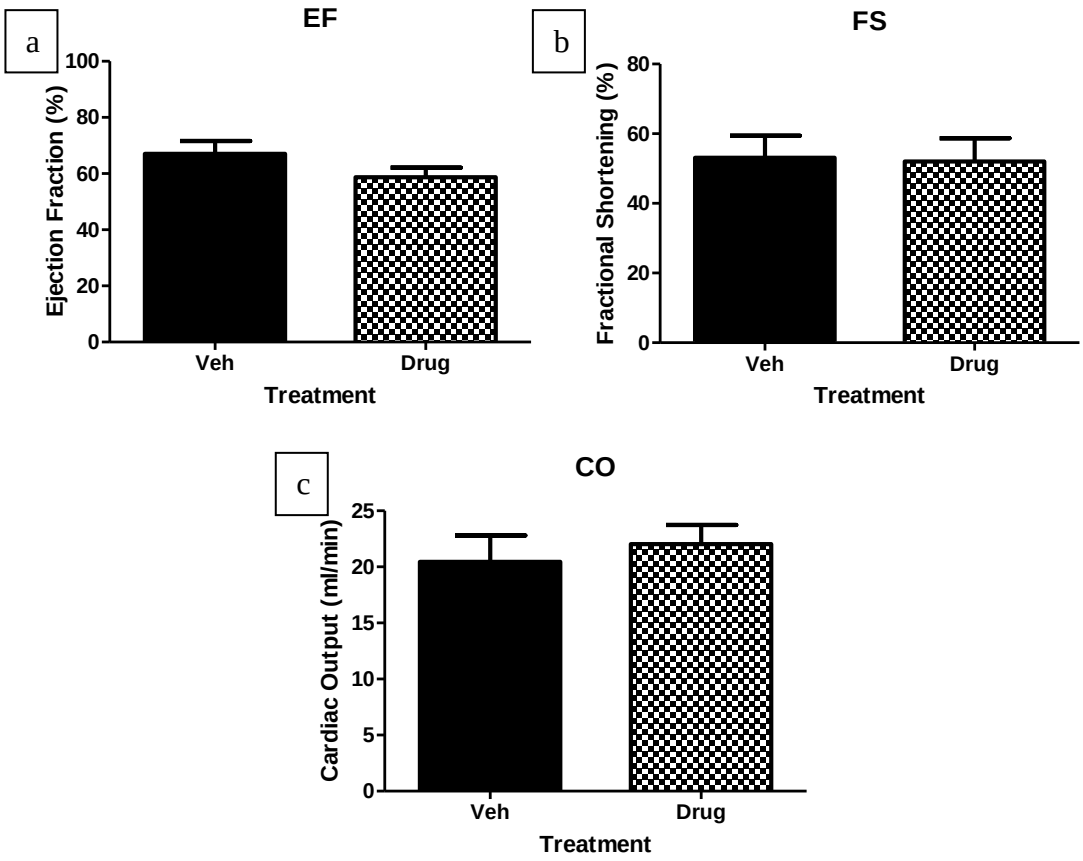

Figure 3.15 Chronic 11β-HSD1 inhibition does not influence systolic function
EF (a), FS (b) and CO (c) were assessed by high frequency ultrasound in 18 month old mice treated with UE2316 (20mg/kg) in their diet for 9 months (chequered bars) and vehicle-treated controls (filled bars) (Student's *t* test; n=5/group).

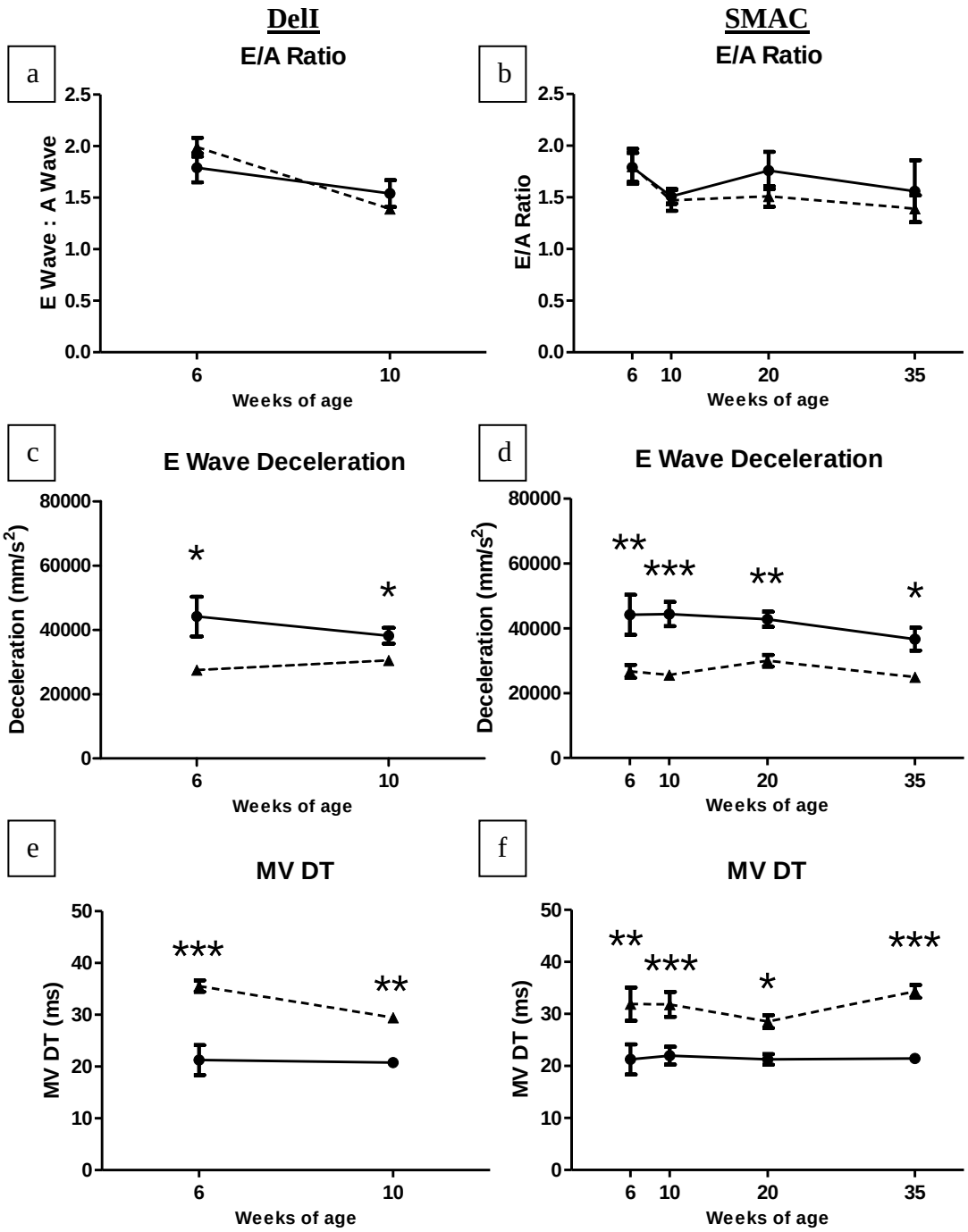

Figure 3.16 Global and cardiovascular-specific 11β-HSD1 deletion leads to mild diastolic dysfunction

E to A wave ratio (a and b), E wave deceleration (c and d) and MV DT (e and f) were assessed by Doppler ultrasound across the mitral valve in DelI (left column, dashed lines) and SMAC mice (right column, dashed lines) and their respective controls (solid lines) at 6, 10, 20 and 35 weeks of age (two way ANOVA *** = $p<0.001$, ** = $p<0.01$, * = $p<0.05$; n=8/group for DelI & SMAC mice, n=6/group for controls).

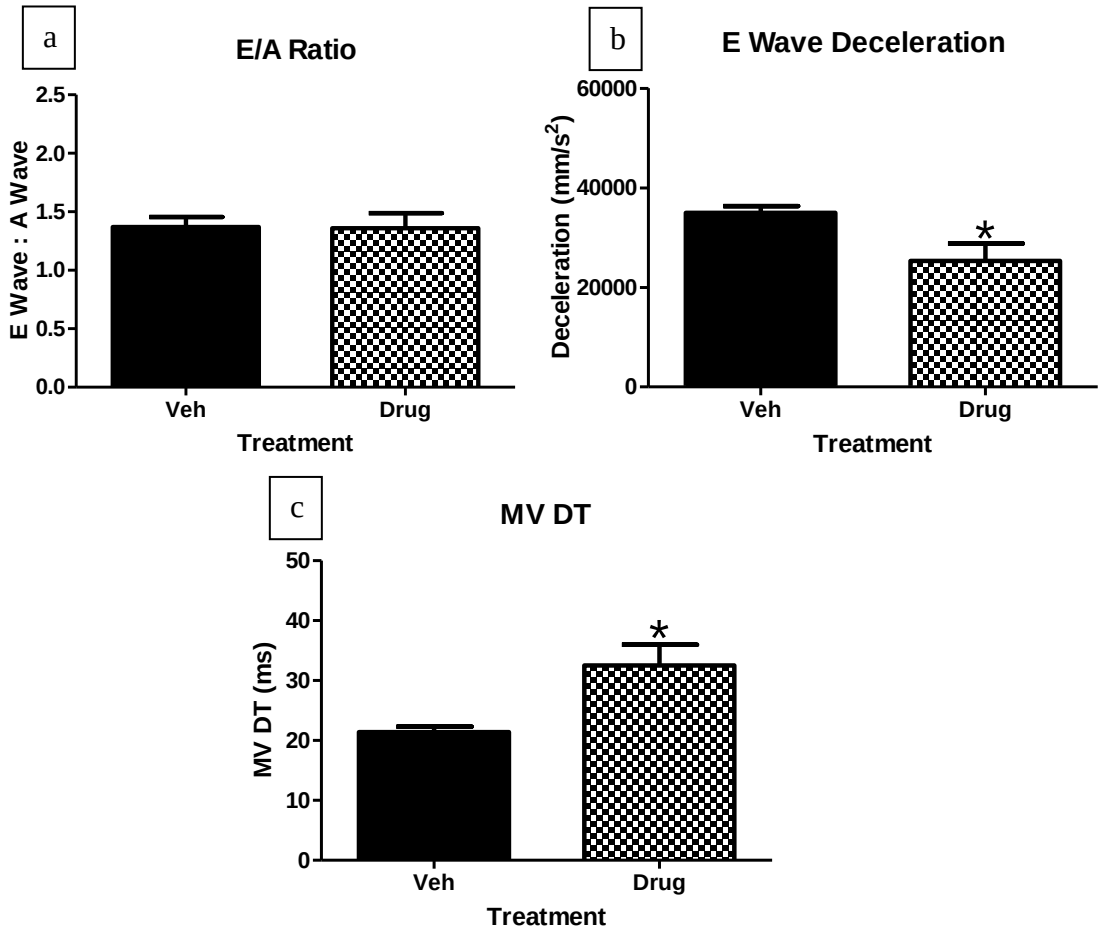

Figure 3.17 Chronic 11β-HSD1 inhibition leads to mild diastolic dysfunction
E to A wave ratio (a), E wave deceleration (b) and MV DT (c) were assessed by Doppler ultrasound across the mitral valve in 18 month old mice treated with UE2316 (20mg/kg) in their diet for 9 months (chequered bars) and vehicle-treated controls (filled bars) (Student's *t* test, * = $p<0.05$; n=5/group).

3.3.5.3 Alteration in myocardial collagen content does not account for diastolic dysfunction in mice with 11β-HSD1 deletion or inhibition

Collagen content (Figure 3.18a) was similar in DelI, SMAC and UE2316-treated mice compared to their respective controls (Figure 3.18b-d).

Furthermore, myocardial mRNA levels of the alpha 2 subunit of type 1 collagen (*Col1α2*, Figure 3.19a and b), the alpha 1 subunit of type 3 collagen (*Col3α1*, Figure 3.19c and d) and transforming growth factor β (*Tgfb1*, Figure 3.19e and f) were similar in 12w old DelI and C57BL/6 hearts, and in 12w old SMAC and Cre^- hearts. β-actin, the internal control, was similar in all groups (see Appendix 1).

mRNA levels of *Tgfb1*, *Col1α2* and *Col3α1* in 18 month old UE2316-treated and vehicle-treated hearts were also similar (Figure 3.20a-c).

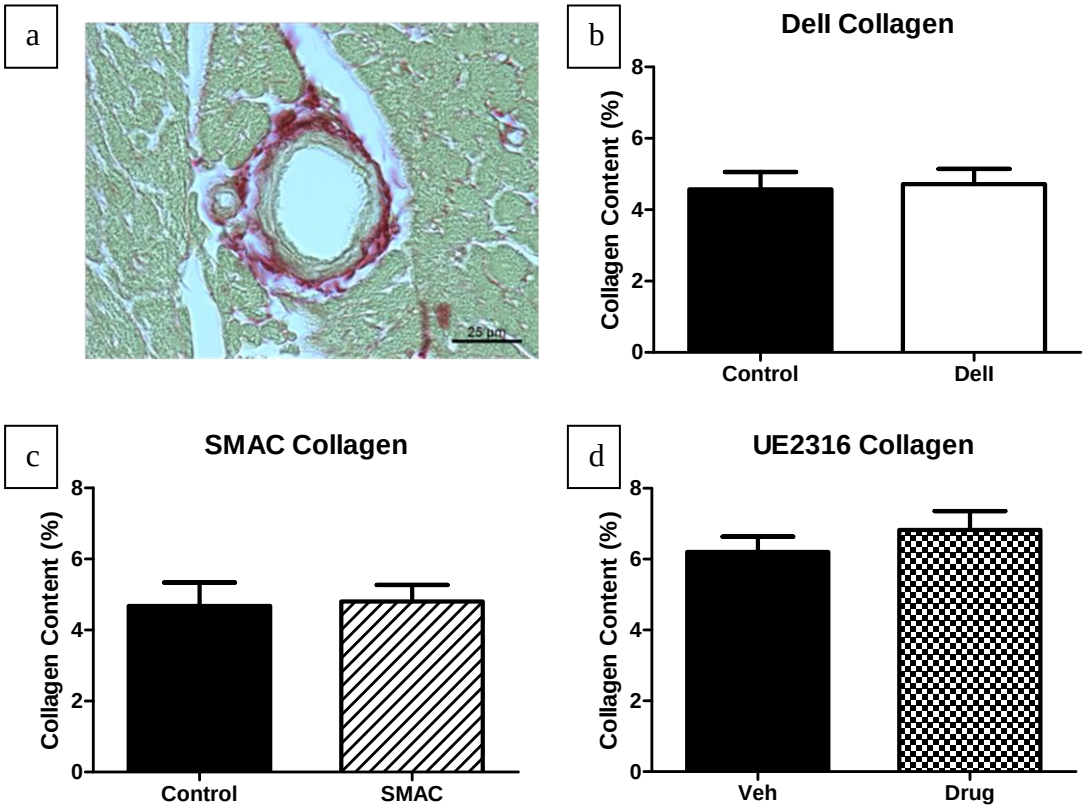

Figure 3.18 Myocardial collagen content is unaltered by 11β-HSD1 deletion or chronic 11β-HSD1 inhibition

Myocardial collagen content was assessed by Picrosirius Red staining (a) of DelI (b), SMAC (c) and UE2316-treated heart sections (d) and their respective controls at 12w of age (Student's *t* test; n=5/group). Scale bar is 25µm.

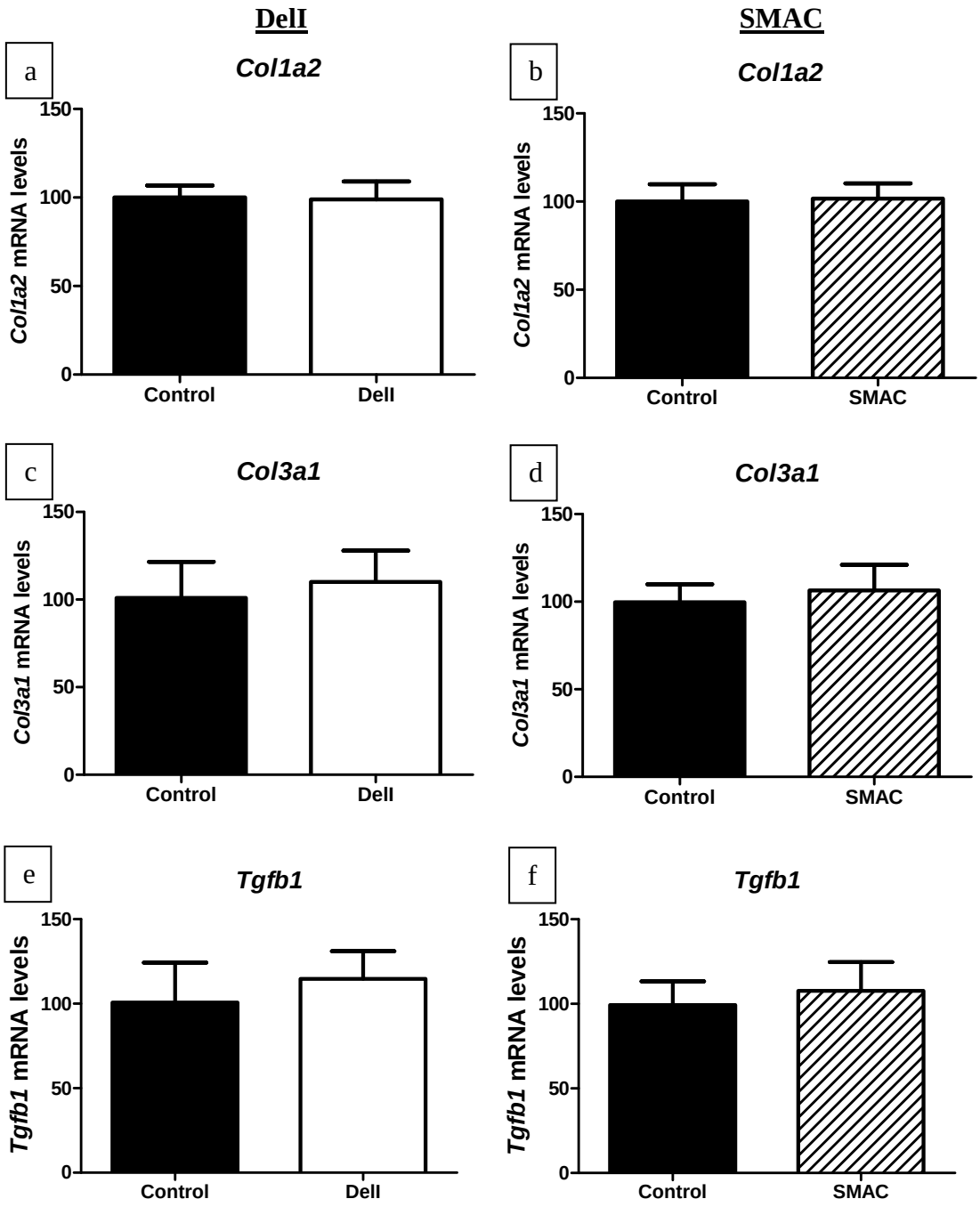

Figure 3.19 Fibrotic gene mRNA levels are unaltered by 11β-HSD1 deletion
mRNA levels of Col1α2 (a & b), Col3α1(c & d) and TGFβ (e & f) were determined by qRT-PCR in hearts from DelI (left column) and SMAC (right column) mice and their respective controls at 12w of age. Target gene mRNA levels were normalised to β-actin, the internal control, which was similar in all groups. Target gene mRNA levels in the control groups were set to 100% and mRNA levels in DelI and SMAC mouse hearts were expressed as a percentage of this (Student's *t* test; n=6/group for DelI & SMAC mice, n=4/group for controls).

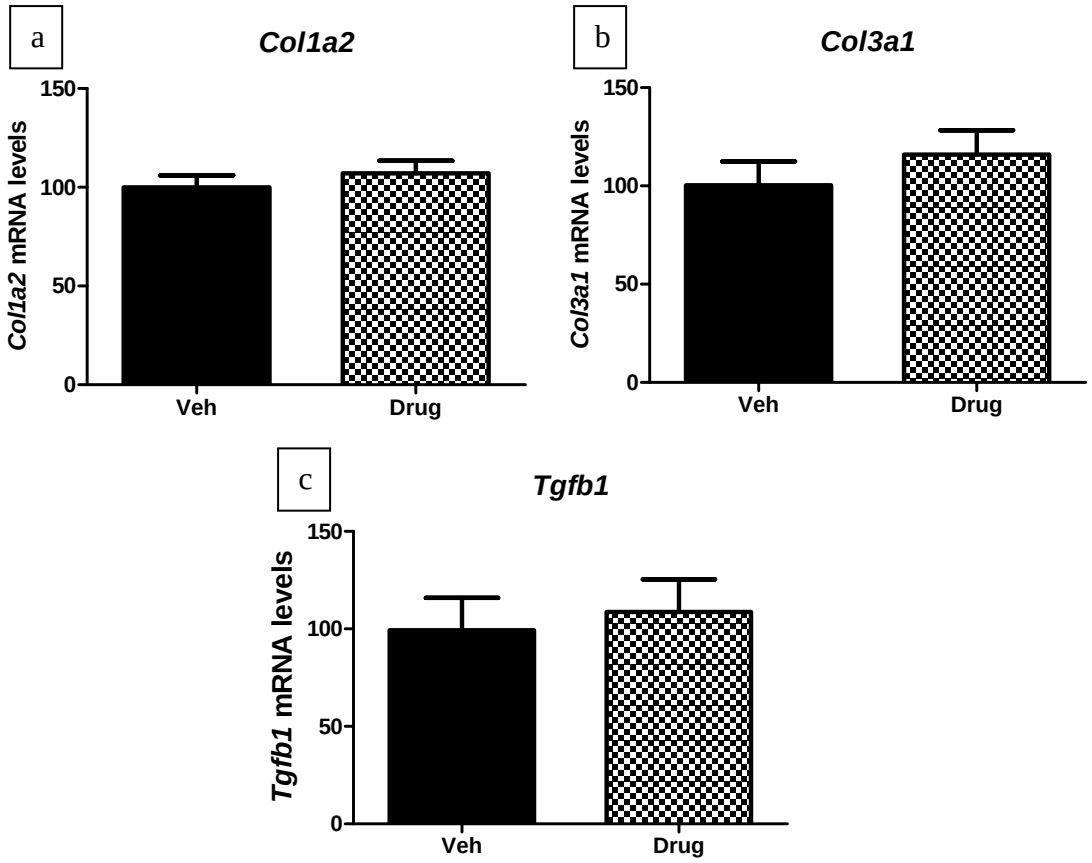

Figure 3.20 Fibrotic gene mRNA levels are unaltered after 11β-HSD1 inhibition
mRNA levels of Col1α2 (a), Col3α1(b) and TGFβ (c) were determined by qRT-PCR in hearts from 18 month old mice treated with UE2316 (20mg/kg) in their diet for 9 months (chequered bars) and vehicle-treated controls (filled bars). Target gene mRNA levels were normalised to β-actin, the internal control, which was similar in all groups. Target gene mRNA levels in the vehicle-treated groups were set to 100% and mRNA levels in UE2316-treated mouse hearts were expressed as a percentage of this (Student's *t* test; n=5/group).

3.3.5.4 Alteration in expression of calcium handling genes is evident in mice with global 11β-HSD1 deletion, and is reproduced in mice with cardiovascular-specific 11β-HSD1 deletion and following chronic 11β-HSD1 inhibition

NCX (*Slc8a1*, Figure 3.21c and d), RyR (*Ryr2*, Figure 3.21e and f) and $CaV_{1.2}$ (*Cacna1c*, Figure 3.21g and h) mRNA were similar in all groups at 12w of age, however SERCA mRNA levels (*Atp2a2*, Figure 3.21a and b) were reduced in DelI mice ($p<0.01$) and SMAC mice ($p<0.001$). This was also seen in 18 month old UE2316-treated mice ($p<0.001$) compared to their respective controls (Figure 3.22a-d).

SERCA protein expression was also reduced in 12w old DelI mice (Figure 3.23a, $p<0.001$), SMAC mice (Figure 3.23b, $p<0.001$) and 18 month old UE2316-treated mice (Figure 3.23c, $p<0.001$) compared to their respective controls. Sample blots are shown in Figure 3.23d.

Further investigation into regulation of SERCA revealed no change in phospholamban (PLN) protein expression (Figure 3.24a-d), nor any changes in phospholamban phosphorylation at two key phosphorylation sites; serine 16 (Figure 3.25a, c, e and g) and threonine 17 (Figure 3.25b, d, f and h).

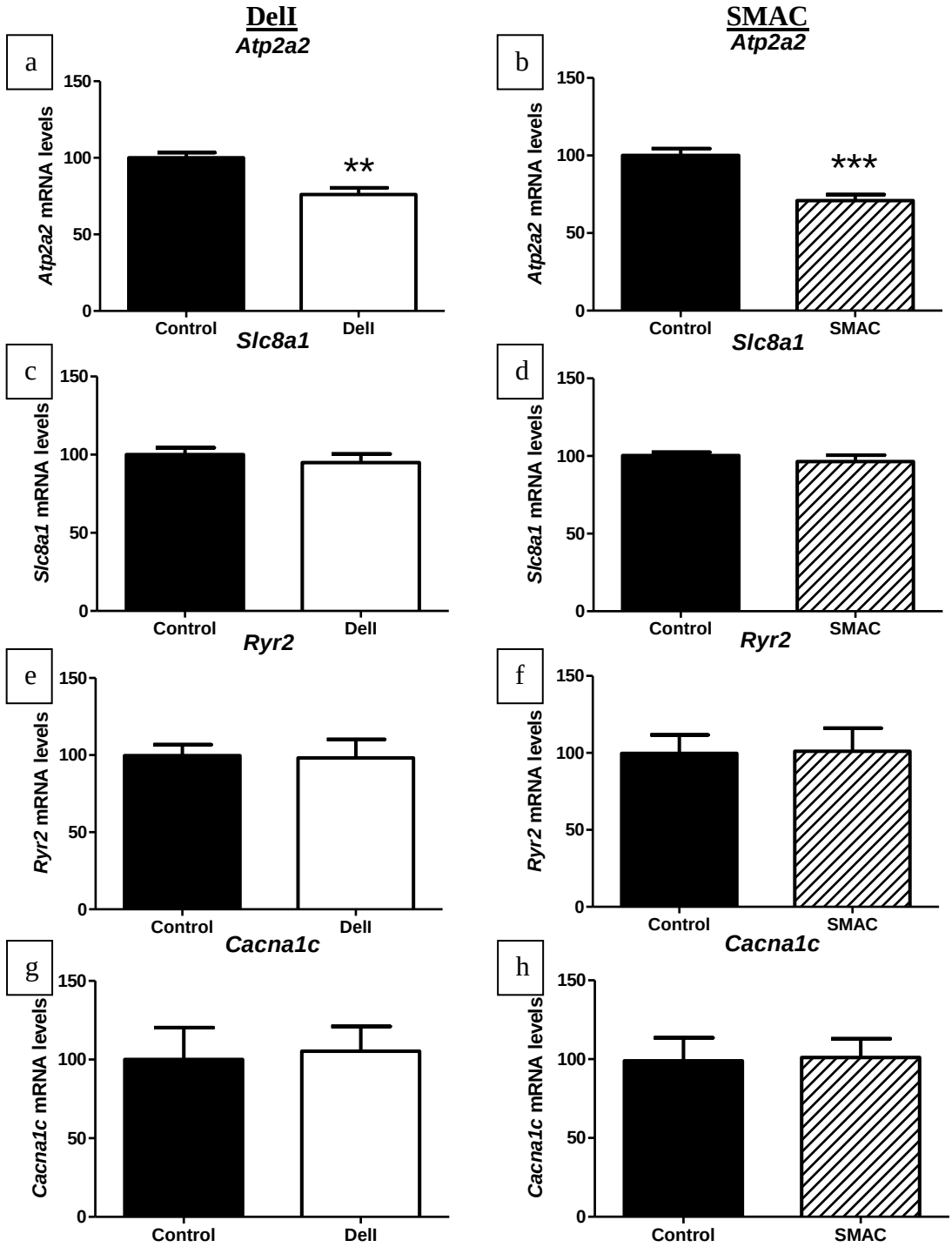

Figure 3.21 11β-HSD1 deletion results in reduced SERCA mRNA levels in the heart
mRNA levels of SERCA (a & b), NCX (c & d), RyR (e & f) and $CaV_{1.2}$ (g & h) were determined by qRT-PCR in hearts from DelI (left column) and SMAC (right column) mice and their respective controls at 12w of age. Target gene mRNA levels were normalised to β-actin, the internal control, which was similar in all groups. Target gene mRNA levels in the control groups were set to 100% and mRNA levels in DelI and SMAC mouse hearts were expressed as a percentage of this (Student's *t* test; *** = $p<0.001$, ** = $p<0.01$; n=6/group for DelI & SMAC mice, n=4/group for controls).

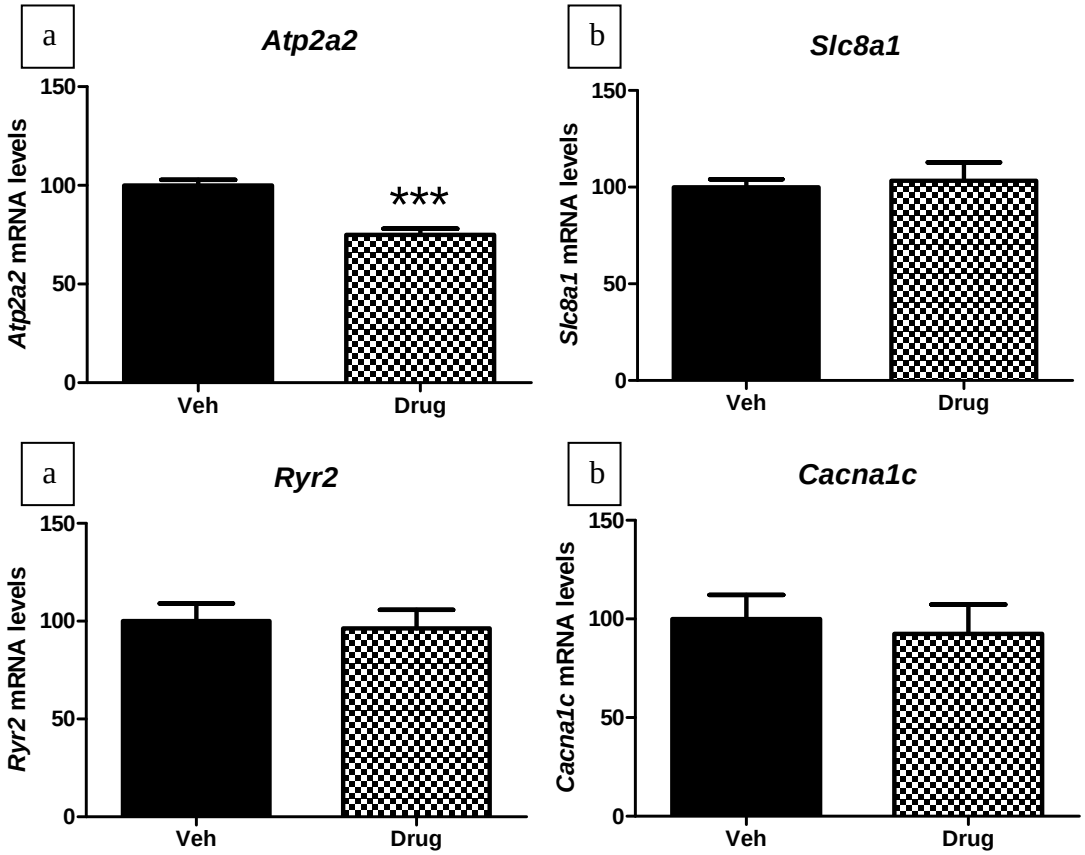

Figure 3.22 Chronic 11β-HSD1 inhibition reduces SERCA mRNA levels in the heart
mRNA levels of SERCA (a), NCX (b), RyR (c) and $CaV_{1.2}$ (d) were determined by qRT-PCR in hearts from from 18 month old mice treated with UE2316 (20mg/kg) in their diet for 9 months (chequered bars) and vehicle-treated controls (filled bars). Target gene mRNA levels were normalised to β-actin, the internal control, which was similar in all groups. Target gene mRNA levels in the vehicle-treated groups were set to 100% and mRNA levels in UE2316-treated mouse hearts were expressed as a percentage of this (Student's *t* test; *** = $p<0.001$, ** = $p<0.01$; n=5/group).

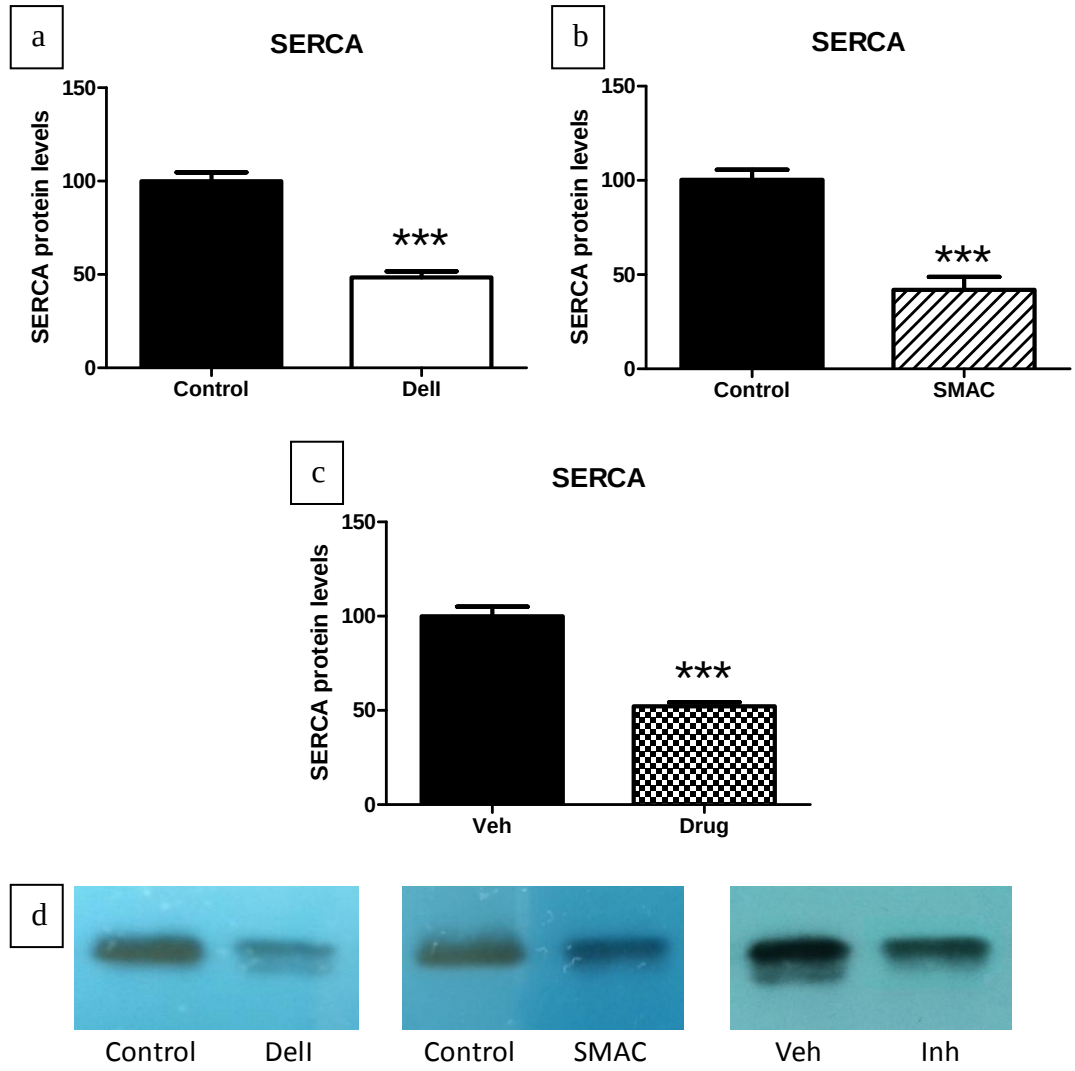

Figure 3.23 11β-HSD1 deletion or chronic inhibition results in reduced SERCA protein levels in the heart

SERCA protein levels were assessed by Western blotting in ventricular tissue from 12w old DelI (a) and SMAC mice (b), and 18 month old mice treated with UE2316 (20mg/kg) in their diet for 9 months (c) and their respective controls. SERCA protein levels were normalised to the internal control, β-actin, which was similar in all groups. SERCA protein levels in the control groups were set to 100% and protein levels in DelI, SMAC and UE2316-treated tissue were expressed as a percentage of this. Sample Western blots are shown in (d). (Student's *t* test *** = $p<0.001$; n=6/group for DelI & SMAC mice, n=4/group for controls).

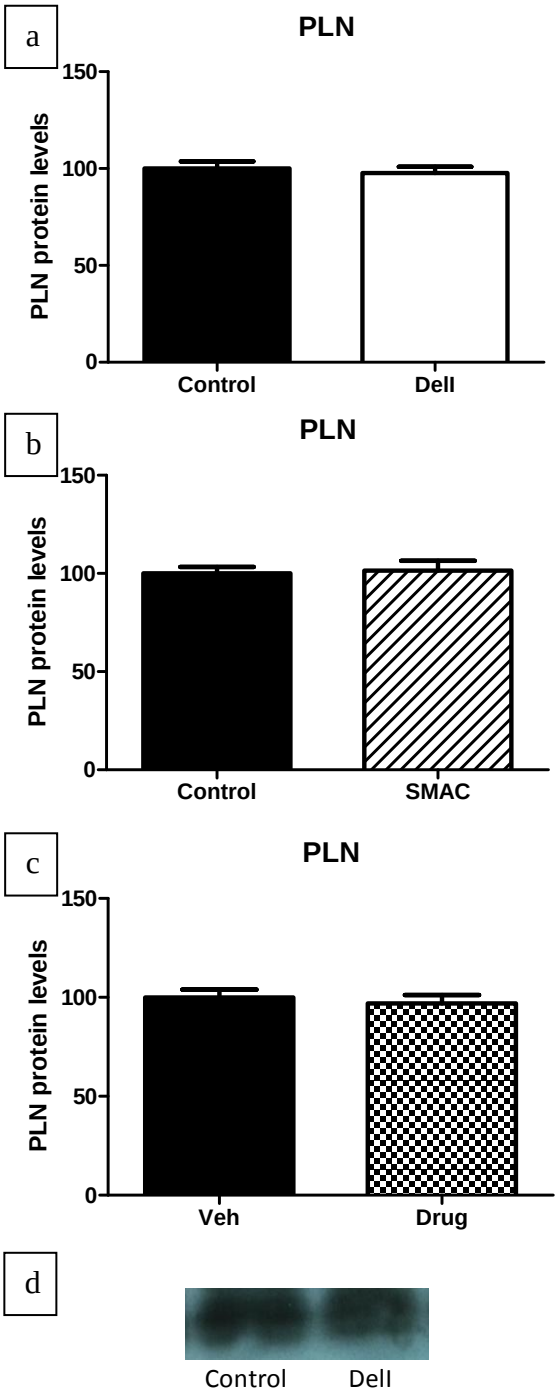

Figure 3.24 11β-HSD1 deletion or chronic inhibition does not affect phospholamban protein levels in the heart

Phospholamban (PLN) protein levels were assessed by Western blotting in ventricular tissue from 12w old DelI (a) and SMAC mice (b), and 18 month old mice treated with UE2316 (20mg/kg) in their diet for 9 months (c) and their respective controls. PLN protein levels were normalised to the internal control, β-actin, which was similar in all groups. PLN protein levels in the control groups were set to 100% and protein levels in DelI, SMAC and UE2316-treated tissue were expressed as a percentage of this. A sample Western blot is shown in (d). (Student's *t* test; n=4/group).

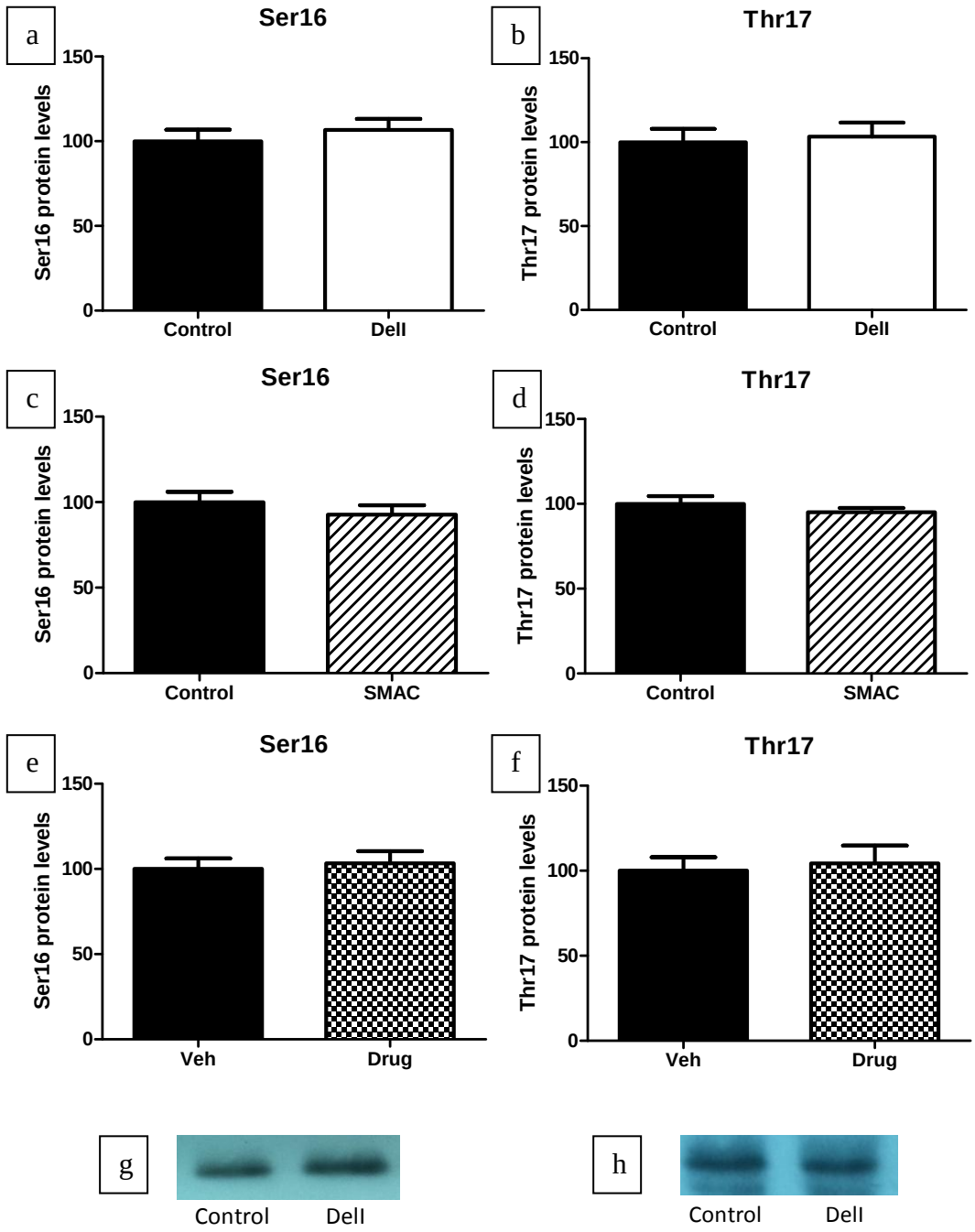

Figure 3.25 Phospholamban phosphorylation is not influenced by 11β-HSD1 deletion or chronic inhibition

Phosphorylation of phospholamban (PLN) at serine 16 (Ser16, a, c & e) and threonine 17 (Thr17, b, d & f) was assessed by Western blotting in ventricular tissue from 12w old DelI, SMAC and UE2316-treated mice and their respective controls. Example DelI Western blots are shown for Ser16 (g) and Thr7 (h) (Student's *t* test; n=4/group). Phosphorylated PLN protein levels were normalised to the internal control, β-actin, which was similar in all groups. Phosphorylated PLN protein levels in the control groups were set to 100% and protein levels in DelI, SMAC and UE2316-treated tissue were expressed as a percentage of this.(Student's *t* test; n=4/group).

3.4 Discussion

GR-mediated action of glucocorticoids has previously been shown to regulate heart maturation (Rog-Zielinska, *et al*., 2013), vascular tone (Ullian, 1999; Hadoke, *et al*., 2006; Goodwin, *et al*., 2011) and calcium handling within cardiomyocytes (Sainte-Marie, *et al*., 2007). Furthermore, local glucocorticoid regeneration by the enzyme 11β-HSD1 has been shown to be involved in regulating both heart size (McSweeney, *et al*., 2010; Rahman, *et al*., 2011) and angiogenesis (Small, *et al*., 2005). However, expression of 11β-HSD1 in the heart and its specific roles in regulating heart growth and function are incompletely understood. The aim of this study was to investigate the impact of global and cardiovascular-specific 11β-HSD1 deletion on heart size and function, and determine whether this could be reproduced by chronic pharmacological inhibition of 11β-HSD1.

The data presented in this chapter shows that global 11β-HSD1 deletion (DelI mice) results in smaller, lighter hearts at 12 weeks of age which may be due to shorter cardiomyocytes. However, this phenotype appears to be transient because by 18 months of age, heart size in DelI and C67BL/6 mice is similar. This does not seem to be a result of 11β-HSD1 deficiency in cardiomyocytes or VSMCs themselves, because this phenotype is not reproduced in mice with cardiovascular-specific deletion (SMAC mice). There is a clear role for 11β-HSD1 in cardiomyocytes and VSMCs, however, in regulating genes associated with calcium cycling and maintaining normal diastolic function, as deletion of the enzyme in these cells leads to mild diastolic dysfunction and reduced SERCA expression; a phenotype also seen in the global KO. Moreover, this diastolic phenotype occurred following

pharmacological inhibition of 11β-HSD1, by administration of UE2316, a selective 11β-HSD1 inhibitor.

This data therefore suggests that 11β-HSD1 in cardiomyocytes and VSMCs influences physiological cardiac function, possibly by regulating calcium handling within cardiomyocytes. However, 11β-HSD1 in another cell type influences cardiomyocyte length, resulting in smaller hearts in its absence.

3.4.1 Expression of 11β-HSD1 and corticosteroid-related genes

Myocardial 11β-HSD1 is present in cardiomyocytes, vascular smooth muscle cells and cardiac fibroblasts (Christy, *et al*., 2003; Klusonova, *et al*., 2009; McSweeney, 2010) as well as in the vascular wall (Hadoke, *et al*., 2001). Outside the cardiovascular system, 11β-HSD1 expression is highest in liver (Tannin, *et al*., 1991) with lower levels present in skeletal muscle (Morgan, *et al*., 2009). GR are expressed almost ubiquitously in all cell types (Hadoke, *et al*., 2009) whereas MR are restricted to aldosterone target organs such as the kidneys, the colon and the salivary glands, but are also present in cardiomyocytes and the vascular endothelium (Walker, 2007a; Fraccarollo, *et al*., 2011).

Consistent with these findings, 11β-HSD1 mRNA and protein was found in heart, aorta, liver and skeletal muscle tissue of C57BL/6 and Cre^- control mice. DelI mice showed deletion of 11β-HSD1 in each of these tissues whereas SMAC mice only showed deletion in heart and aortic tissue. Expression in liver and skeletal muscle was unaffected, demonstrating the strategy of selectively targeting 11β-HSD1 expression in the cardiovascular system using SM22α-Cre^+ was a successful one.

However, 11β-HSD1 activity in these tissues was not investigated and should be performed in future studies. The low levels of 11β-HSD1 mRNA and protein detected in hearts and aortas from SMAC mice may be due to cardiac and adventitial fibroblasts, which known to express 11β-HSD1 (Brereton, *et al*., 2001; McSweeney, 2010). These cells may therefore account for this expression. Furthermore, although the connective and adipose tissue surrounding the aorta was removed as extensively as possible, some cells may have remained. Adipose cells also express 11β-HSD1 and may therefore have contributed to the small levels of 11β-HSD1 mRNA and protein detected in SMAC mice (Walker & Seckl, 2003; Tomlinson & Stewart, 2005).

Levels of GR and MR mRNA in heart tissue were unaffected, as were myocardial mRNA levels of genes affected by glucocorticoid signalling; FKBP5, GILZ, PGC1α and SGK. FKBP5 is an immunophilin which binds to GR, along with HSP90, and regulates GR affinity for glucocorticoids (Wochnik, *et al*., 2005). GILZ is a leucine zipper which regulates several GR-mediated processes including apoptosis, cell proliferation and the immune response where it elicits and anti-inflammatory action (Ayroldi & Riccardi, 2009). PGC1α is a nuclear receptor co-activator which co-activates HNF-4α and GR (Herzig, *et al*., 2001). SGK is induced by glucocorticoids and aldosterone via both GR and MR and can be phosphorylated by the phosphoinositide 3-kinase, a kinase which is involved in cardiomyocyte hypertrophy (Sheppard & Autelitano, 2002). The data presented here suggest that basal GR- and MR-mediated signalling in the heart was unaffected despite DelI and SMAC mice being unable to locally regenerate glucocorticoids globally or in cardiomyocytes and

VSMCs, respectively. Therefore, systemic glucocorticoid release from the adrenal glands must be sufficient to overcome this deficiency, at least in the healthy mouse.

Although 11β-HSD1 mRNA levels and protein expression was measured in the current study, 11β-HSD1 activity was not and this should be investigated in future studies. Furthermore, since tissue homogenate was used to assess expression, localisation of 11β-HSD1 was not examined, and so it remains unclear as to whether 11β-HSD1 is absent in cardiac fibroblasts of SMAC mice. It has been shown that Sm22α is not present in isolated fibroblasts from chronic obstructive pulmonary disease (COPD) patients, and is only present in myofibroblasts and VSMCs, not fibroblasts in rabbit bladder (Chiavegato, *et al*., 1999; Hallgren, *et al*., 2010). However, investigation of this by immunohistochemistry and in isolated fibroblasts warrants further study.

3.4.2 Heart dimensions

11β-HSD1 deficient mice have previously been observed to have smaller hearts at 10-12w of age (McSweeney, *et al*., 2010), although the reason for this was not completely understood. In the present study, global deletion of 11β-HSD1 resulted in the same phenotype with smaller, lighter hearts in 12 week old DelI mice compared to C57BL/6 control mice, but without changes in blood pressure, cardiomyocyte cross sectional-area, blood volume and myocardial interstitial volume.

Preload is a term used to describe the pressure exerted on the left ventricle at the end of diastole and can be affected by several physiological parameters, primarily blood pressure and blood volume. A reduced blood volume decreases the end diastolic

filling pressure and results in a smaller left ventricular end diastolic volume (De Simone, 2003). This is because the pressure experienced by the cardiomyocytes in the left ventricular wall is reduced and so cardiomyocyte diastolic length is reduced (Hanft, *et al*., 2008). The effect of glucocorticoids on elevating blood pressure are well established (Connell, *et al*., 1987; Fraser, *et al*., 1999; Masuzaki, *et al*., 2003; Van Raalte, *et al*., 2013), however lack of 11β-HSD1 in DelI mice did not lower blood pressure or modify blood volume, suggesting these parameters are not responsible for reducing heart size and weight in these mice.

Further investigation of DelI hearts revealed these mice had shorter cardiomyocytes which may account for them having smaller hearts. Having said that, cardiomyocyte length was only reduced approximately 10% whereas heart weight was reduced by approximately 30% suggesting further changes take place in DelI mice which contribute to the reduction in heart size and this needs further investigation. Deletion of 11β-HSD1 in cardiomyocytes and VSMCs did not reproduce this 'small heart' phenotype suggesting lack of 11β-HSD1 in another cell type is responsible. This phenotype was not seen in adult mice treated with UE2316, suggesting that it may be due to the developmental or early post-natal action of 11β-HSD1. Furthermore, this phenotype appeared to be transient, as a similar heart size was observed in DelI and C57BL/6 control mice at 78w (18 months) of age.

Cardiac fibroblasts secrete a number of factors crucial for cardiomyocytes growth, and loss of 11β-HSD1 in these cells may alter growth factor secretion. For example, fibroblasts express fibroblast growth factor-2 (FGF-2) (Jiang, *et al*., 2007), and deletion of this has been shown to attenuate eccentric hypertrophy after pressure overload, whereby cardiomyocyte length increases, but cross-sectional area does not

(Schultz, *et al*., 1999). Furthermore, leukaemia inhibitory factor (LIF) and cardiotrophin-1 (CT-1) are members of the IL-6 family which are both secreted by fibroblasts and involved in cardiomyocytes growth (Matsui, *et al*., 1996; Wollert, *et al*., 1996; Wang, *et al*., 2002). IL-33 is a fibroblast-derived cytokine which exerts an antihypertrophic effect after phenylephrine or angiotensin II stimulation (Sanada, *et al*., 2007). Indeed, administration of IL-33 *in vivo* has been shown to attenuate hypertrophy after pressure overload (Sanada, *et al*., 2007). Fibroblast-cardiomyocyte cell-cell interactions appear to be mediated by connexin 43 and connexin 45 (Oyamada, *et al*., 1994; Zhang, *et al*., 2008), and may also contribute to cardiomyocytes entering a 'hibernation state' which is characterised, among other things, by a loss of sarcomeres, and thus cell shortening (Dispersyn, *et al*., 2001). Investigation into the secretion of growth factors by fibroblasts in DelI mice, including those described above, may provide further insight into why these mice have shorter cardiomyocytes.

A direct effect of glucocorticoids on cardiomyocyte structure and maturation has recently been elucidated. GR-mediated glucocorticoid action is necessary for lung development i*n utero*, and GR KO mice die at birth due to underdeveloped lungs (Cole, *et al*., 1995). However, a proportion of these mice die prenatally and it is suggested that this is due to diastolic dysfunction, disorganised cardiomyocyte myofibrils, and impaired calcium-induced calcium release (Rog-Zielinska, *et al*., 2013). Furthermore, administration of the synthetic GR-specific glucocorticoid cortivasol to neonatal rat cardiomyocytes has been shown to upregulate hypertrophic gene expression (Yoshikawa, *et al*., 2009). Hypercortisolaemia in patients with Cushing's syndrome and chronic administration of glucocorticoids in animal models

has been shown to result in left ventricular hypertrophy (Walker, 2007a; De, *et al*., 2011), possibly in an angiotensin II-dependent manner (Ghose Roy, *et al*., 2009). It may therefore be hypothesised that DelI mice have reduced expression of pro-hypertrophic genes, such as B-type natriuretic peptide (BNP), skeletal muscle α-actin (SKA), atrial natriuretic peptide (ANP) and β-myosin heavy chain (β-MHC) (Ren, *et al*., 2012; Katoh, *et al*., 2014) because they are unable to regenerate glucocorticoids intracellularly, which results in them having shorter cardiomyocytes and smaller, lighter hearts. Cardiomyocyte length increases rapidly in the first 4 weeks after birth, with the rate of growth decreasing from 4 weeks onwards (Leu, *et al*., 2001). Heart growth in DelI mice at early postnatal time points should therefore be investigated.

11β-HSD1 deletion in cardiac fibroblasts or resident macrophages may be key to modifying growth factor secretion or hypertrophic gene induction and thus warrants further study. In addition to the growth factors secreted by fibroblasts, above, macrophages also secrete factors involved in cardiomyocytes growth. For example, insulin-like growth factor-1 (IGF-1) is expressed by macrophages (Gow, *et al*., 2010) and transgenic cardiac overexpression of IGF-1 or its receptor (IGF-1R) results in increased cardiomyocytes growth and cell hypertrophy (McMullen, *et al*., 2004; Torella, *et al*., 2004).

One further interesting observation was that, at 18 months of age and after 9 months of pharmacological 11β-HSD1 inhibition, relative to vehicle-treated age-matched mice, UE2316-treated mice showed a trend for larger hearts as measured by echocardiography, and significantly heavier hearts as weighed at post-mortem. However, the level of 11β-HSD1 inhibition in the heart was not measured, and should be performed.

Blood pressure and circulating cortisol are both known to increase with age, and both have been shown to enhance the development of cardiac hypertrophy (Landahl, *et al*., 1986; Van Cauter, *et al*., 1996; Walker, 2007a; De, *et al*., 2011; Drazner, 2011). In aged mice, such as those treated with UE2316, blood pressure and cortisol levels may be further increased as a result of impaired GR-mediated negative feedback by glucocorticoids, due to reduced intracellular glucocorticoid bioavailability. However, this must be properly investigated to determine the cause behind the heavier hearts in these mice.

It has also been shown previously that allowing aldosterone access to MR in cardiomyocytes, by overexpressing 11β-HSD2 in these cells, leads to cardiac hypertrophy (Qin, *et al*., 2003). As such, it may hypothesised that aldosterone is able to occupy MR in cardiomyocytes in mice in which 11β-HSD1 is inhibited in these cells, and therefore lead to larger hearts. Having said that, 11β-HSD2 is expressed at very low levels in the heart and so this hypothesis may be incorrect. Furthermore, this phenotype is not seen in DelI mice at 18 months of age, suggesting that this phenotype may be a result of unknown off-target effects of UE2316, or that partial 11β-HSD1 inhibition gives a different phenotype to complete KO. Further investigation into off-target drug effects, heart weight, blood pressure and corticosterone levels in 11β-HSD1 deficient mice at 18 months of age is therefore required. Moreover, further studies should attempt to elucidate the mechanism of this phenotype in UE2316-treated mice; for example, assessment of blood pressure, blood volume and myocardial interstitial fluid.

3.4.3 Cardiac function

High-resolution echocardiography showed ejection fraction and fractional shortening in DelI, SMAC and UE2316-treated mice was similar to their respective controls. This agrees with the previous finding that 11β-HSD1 deficiency does not influence cardiac function (McSweeney, *et al*., 2010). However, additional investigation by pulsed-wave Doppler ultrasound revealed that DelI, SMAC and UE2316-treated mice all exhibited mild diastolic dysfunction compared to their respective controls. In each case, E wave deceleration was reduced and mitral valve deceleration time was accordingly increased, suggesting either reduced compliance or relaxation deficit.

Collagen accumulation is associated with reduced compliance and can lead to cardiac pathology (Pauschinger, *et al*., 1999). Collagen types I and III are the most abundant in the heart with type I being significantly stiffer than the more elastic type III (Sharma, *et al*., 2004). DelI, SMAC and UE2316-treated mice have similar overall myocardial collagen content, and similar mRNA levels of Col1α2, Col3α1 and TGFβ, suggesting similar fibrosis in these mice to their respective controls.

Calcium handling in cardiomyocytes, and particularly calcium removal from the cytosol following excitation-contraction coupling, is essential to maintain normal muscle relaxation. SERCA is involved in reuptake of calcium back into the sarcoplasmic reticulum (SR) while the sodium-calcium exchanger (NCX) extrudes calcium from the cell following contraction (Reeves & Hale, 1984; Periasamy & Kalyanasundaram, 2007). Therefore these two transporters are heavily involved in regulating cardiomyocyte relaxation (see Figure 1.1) (Bers, 2001; Louch, *et al*., 2012). In the SERCA KO mouse, expression of NCX is increased to provide an

alternative means of removing calcium from the cytosol at the end of contraction (Li, *et al*., 2011). However, in the present study, reduction of SERCA was not accompanied by any change in NCX. This may indicate that a reduction in SERCA expression is already compensated for in a different way in mice with 11β-HSD1 deletion or inhibition.

Glucocorticoids have been shown to play a role in SERCA expression developmentally, in adulthood, and after an ischaemic insult. In late gestation an increase in SERCA mRNA is normally seen, however this is attenuated in GR KO mice (Rog-Zielinska, *et al*., 2013). Skeletal muscle cells from adult rat diaphragm have decreased SERCA mRNA levels after treatment with triamcinolone, a synthetic corticosteroid (Gayan-Ramirez, *et al*., 2000). In a setting of myocardial ischaemia in piglets, methylprednisolone treatment after cardio-pulmonary graft prevents loss of SERCA protein and maintains the calcium transient in cardiomyocytes (Pearl, *et al*., 2011). Furthermore, experiments using hexose-6-phosphate dehydrogenase (H6PD) KO mice have also revealed a role for glucocorticoids in regulating SERCA expression, whereby these mice have reduced SERCA protein expression in skeletal muscle (Lavery, *et al*., 2008). H6PD is responsible for converting glucose-6-phosphate to 6-phosphogluconolactonate which also results in the generation of NADPH, the cofactor required by 11β-HSD1 in order for it to function as an oxoreductase enzyme (Bujalska, *et al*., 2005; Morton, 2010). In the absence of NADPH, 11β-HSD1 functions as a dehydrogenase, inactivating glucocorticoids and converting them to their inert 11-keto metabolites (Lavery, *et al*., 2006).

The data presented in this chapter suggest a role for the local glucocorticoid regenerating enzyme 11β-HSD1 in regulating calcium homeostasis, as lack of 11β-

HSD1 in cardiomyocytes and VSMCs, or pharmacological inhibition of 11β-HSD1 in adults, results in reduced myocardial SERCA mRNA and protein expression, leading to mild diastolic dysfunction.

Regulation of SERCA by phospholamban (PLN) is also an important interaction with regard to myocardial calcium handling (MacLennan, *et al*., 2003). PLN can be thought of as a reverse inhibitor of SERCA; when it is not phosphorylated it inhibits the action of SERCA and therefore reduces the transport of calcium from the cytosol into the SR (MacLennan, *et al*., 2003). When PLN is phosphorylated this inhibition is lost and SERCA activity increases (MacLennan, *et al*., 2003). Previous studies investigating cardiomyocytes from rats which had been adrenalectomised, and rats which had been treated with dexamethasone, revealed no change in cardiomyocyte PLN protein expression or PLN phosphorylation state at two key phosphorylation sites, serine 16 and threonine 17, which are phosphorylated by PKA and CamKII, respectively (Rao, *et al*., 2001).

There was no change in PLN protein expression or PLN phosphorylation in DelI, SMAC or UE2316-treated mice compared to their respective controls, suggesting loss of 11β-HSD1 in cardiomyocytes and VSMCs directly regulates myocardial SERCA expression. Together these observations suggest PLN expression and phosphorylation is not glucocorticoid dependent. Therefore, although a reduction in SERCA protein has been demonstrated in DelI, SMAC and UE2316-treated mice, assessment of SERCA activity and intracellular calcium flux merits further investigation in order to fully understand whether cytosolic calcium availability is modified in these mice. If it is indeed reduced then contractile filament sensitivity

should also be studied as perhaps that increased sensitivity prevents the loss of contractile function in these mice.

The data presented in this chapter demonstrate that global 11β-HSD1 deletion results in shorter cardiomyocytes, and thus smaller hearts. However, this phenotype is not due to loss of 11β-HSD1 in cardiomyocytes themselves, as this phenotype is not present in SMAC mice, meaning other cell types are responsible. Loss of 11β-HSD1 in cardiomyocytes and VSMCs leads to mild diastolic dysfunction, possibly as a result of alteration in cardiomyocyte calcium handling gene expression. Furthermore, this phenotype can be induced by pharmacological inhibition of 11β-HSD1 by UE2316, a selective 11β-HSD1 inhibitor. These unexpected phenotypes should be kept in mind when analysing the acute and chronic remodelling and functional deterioration of the heart following myocardial infarction.

Chapter 4

The Acute Response of Cardiovascular-specific 11β-HSD1 Knock-out Mice to Myocardial Infarction

4.1 Introduction

In the heart, immunoreactive 11β-HSD1 is present in cardiomyocytes, vascular smooth muscle cells, cardiac fibroblasts (Christy, *et al*., 2003, Klusonova, *et al*., 2009; McSweeney, 2010) as well as in the vascular wall (Hadoke, *et al*., 2001). Global deletion of this enzyme (in DelI mice) results in smaller, lighter hearts with shorter cardiomyocytes (Chapter 3). However, cardiovascular-specific 11β-HSD1 deletion (SMAC mice) does not reproduce this finding (Chapter 3), suggesting it is the action of 11β-HSD1 out with the cardiovascular system that is responsible for this phenotype. In contrast, both DelI and SMAC mice showed diastolic abnormalities and reduced SERCA expression, although systolic function and cardiac vessel density appeared normal (Chapter 3). After infarction, mice globally deficient in 11β-HSD1 have an augmented inflammatory response, associated with increased representation of pro-reparative alternatively-activated macrophages, enhanced peri-infarct angiogenesis and improved cardiac function (McSweeney, *et al*., 2010). However, whether this is due to 'cardiovascular' 11β-HSD1 is unknown and is the focus of this chapter.

The aim of this chapter was to determine whether the beneficial acute outcomes seen previously in 11β-HSD1 deficient mice after MI could be reproduced by selective cardiovascular deletion of the enzyme. Considering previous work from our laboratory describing the anti-angiogenic role of 11β-HSD1 in the vessel wall (Small, *et al*., 2005), it was hypothesised that SMAC mice would reproduce the beneficial phenotype previously seen in mice globally deficient in 11β-HSD1. It was hypothesised that, following MI, SMAC mice would exhibit enhanced angiogenesis,

a modified inflammatory response, reduced scar size, attenuated left ventricular dilatation and maintained cardiac function.

4.2 Methods

Male cardiovascular-specific 11β-HSD1 KO (SMAC) mice, and Cre^- control mice, aged 10-12 weeks underwent coronary artery ligation or sham surgery (Section 2.2.3). Tail blood was collected 24h after surgery (Section 2.2.4) to determine the extent of initial cardiac injury, by measurement of cardiac troponin-I (Section 2.6.5). High frequency echocardiography was performed 7d after surgery to assess cardiac size and function (Section 2.2.2). Mice were killed by perfusion fixation (Section 2.3.1) immediately following echocardiography and hearts were harvested, processed, embedded in paraffin wax and microtomed into 4μm thick sections. Histology and immunohistochemical analysis allowed determination of infarct size, peri-infarct angiogenesis, total macrophage recruitment and alternatively-activated macrophage recruitment.

4.2.1 Histology and immunohistochemistry

Masson's Trichrome staining was used to determine infarct size as detailed in Section 2.4.3. CD31 staining was used to measure peri-infarct angiogenesis, Mac2 staining was used to quantify macrophage infiltration into the heart, and Ym1 staining was used to identify alternatively-activated macrophages. Full details are given in Sections 2.5.3, 2.5.4 and 2.5.5.

4.2.2 Statistical analysis

All values are expressed as mean ± SEM. Statistical significance was reached with a *p* value of less than 0.05. Mortality data was compared using Fisher's exact test and chi square test. Echocardiography and cardiac troponin-I data were compared using two way ANOVA with Bonferroni's post-hoc test. Masson's Trichrome staining, peri-infarct angiogenesis, total macrophage and alternatively activated macrophage data were compared using two-tailed unpaired Student's *t* tests.

4.3 Results

4.3.1 Cardiovascular 11β-HSD1 deletion does not influence mortality after MI

Mortality was similar in SMAC and Cre^- control mice after surgery, with 65% of SMAC mice and 76% of control mice surviving until 7d post-MI (Figure 4.1). Post mortem investigation of deaths revealed they were all a result of cardiac rupture, as determined by the presence of blood in the chest cavity and a rupture of the left ventricular wall. All sham-operated mice (100%, n=6/group) survived until 7 days post surgery.

4.3.2 Cardiovascular 11β-HSD1 deletion does not influence initial ischaemic injury

24h after ligation surgery, plasma levels of cardiac troponin-I were elevated to a similar extent in SMAC and Cre^- control mice (Con), compared to sham-operated mice (Figure 4.2), suggesting a similar extent of initial cardiac injury in both genotypes following surgery.

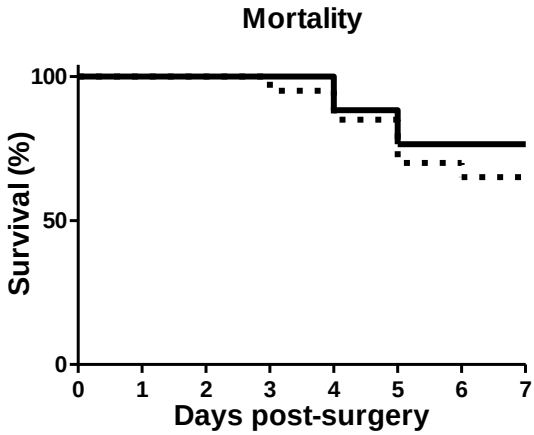

Figure 4.1 Cardiovascular 11β-HSD1 deletion does not affect mortality after coronary artery ligation

Mortality after coronary artery ligation surgery in Cre^- control mice (solid line, n=20 at day 0 and n=13 at day 7) and SMAC mice (dashed line, n=17 at day 0 and n=13 at day 7) (no significant difference; Fisher's exact test, chi square p=0.49).

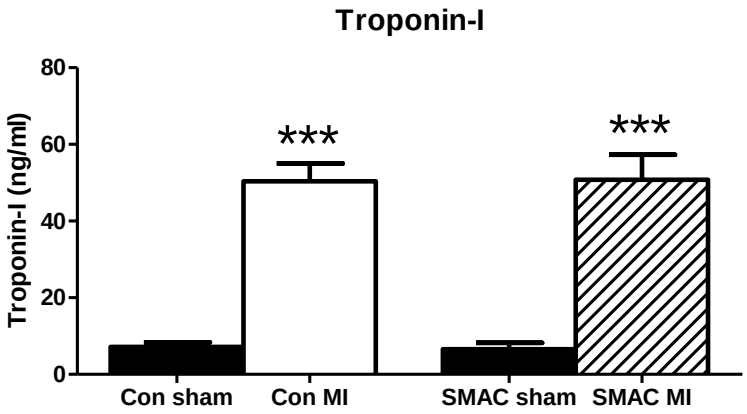

Figure 4.2 Cardiovascular 11β-HSD1 deletion does not affect the extent of initial injury after coronary artery ligation

Plasma cardiac troponin-I levels, measured by ELISA, in 10-12w old SMAC and Cre^- control mice, and sham-operated mice 24hr after surgery (two way ANOVA *** = $p<0.001$; n=8/group for SMAC & Cre^- mice, n=6/group for shams).

4.3.3 Ventricular dilatation and systolic function 7d after MI are not changed in mice with cardiovascular 11β-HSD1 deletion

4.3.3.1 Heart size

SMAC mice and their Cre$^-$ controls (Con) had increased left ventricular end diastolic areas (LVEDA, Figure 4.3a) and left ventricular end systolic areas (LVESA, Figure 4.3b) following MI compared to sham-operated mice, indicating similar levels of left ventricular dilatation in both genotypes.

4.3.3.2 Systolic function

Ejection fraction (EF, Figure 4.4a) and fractional shortening (FS, Figure 4.4b), were similar in sham-operated SMAC and Cre$^-$ control mice, and similarly reduced in both genotypes following MI.

4.3.4 Infarct size 7d after MI is not influenced by cardiovascular 11β-HSD1 deletion

Quantification of scar tissue showed SMAC (Figure 4.5a) and control mice (Figure 4.5b) had similar sized infarcts (Figure 4.5c).

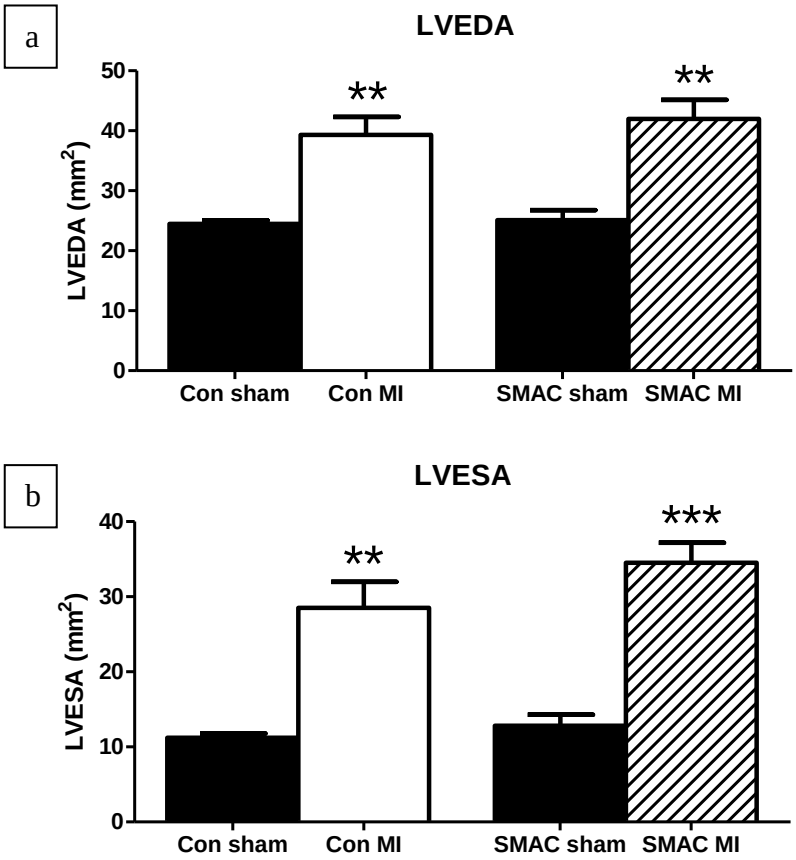

Figure 4.3 Heart size 7d post-MI is not influenced by cardiovascular 11β-HSD1 deletion Left ventricular end diastolic area (LVEDA, a) and left ventricular end systolic area (LVESA, b) of SMAC and Cre$^-$ mice 7d post-MI, and sham-operated control mice 7d after sham surgery, was assessed using high frequency ultrasound (two way ANOVA *** = $p<0.001$, ** = $p<0.01$; n=8/group for SMAC & Cre$^-$ mice, n=6/group for shams).

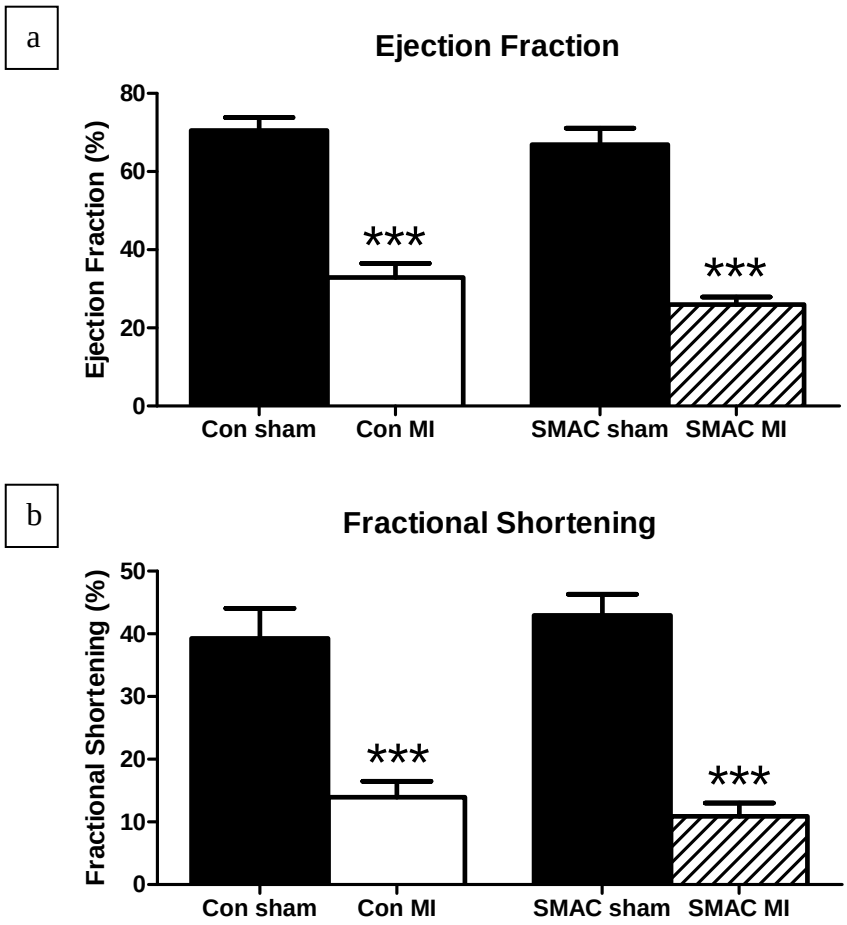

Figure 4.4 Systolic function 7d post-MI is not influenced by cardiovascular 11β-HSD1 deletion

Ejection fraction (a) and fractional shortening (b) of 10-12w old SMAC and Cre^- mice 7d post-MI, and sham-operated control mice 7d after sham surgery, was assessed using high frequency ultrasound (two way ANOVA *** = $p<0.001$; n=8/group for SMAC & Cre^- mice, n=6/group for shams).

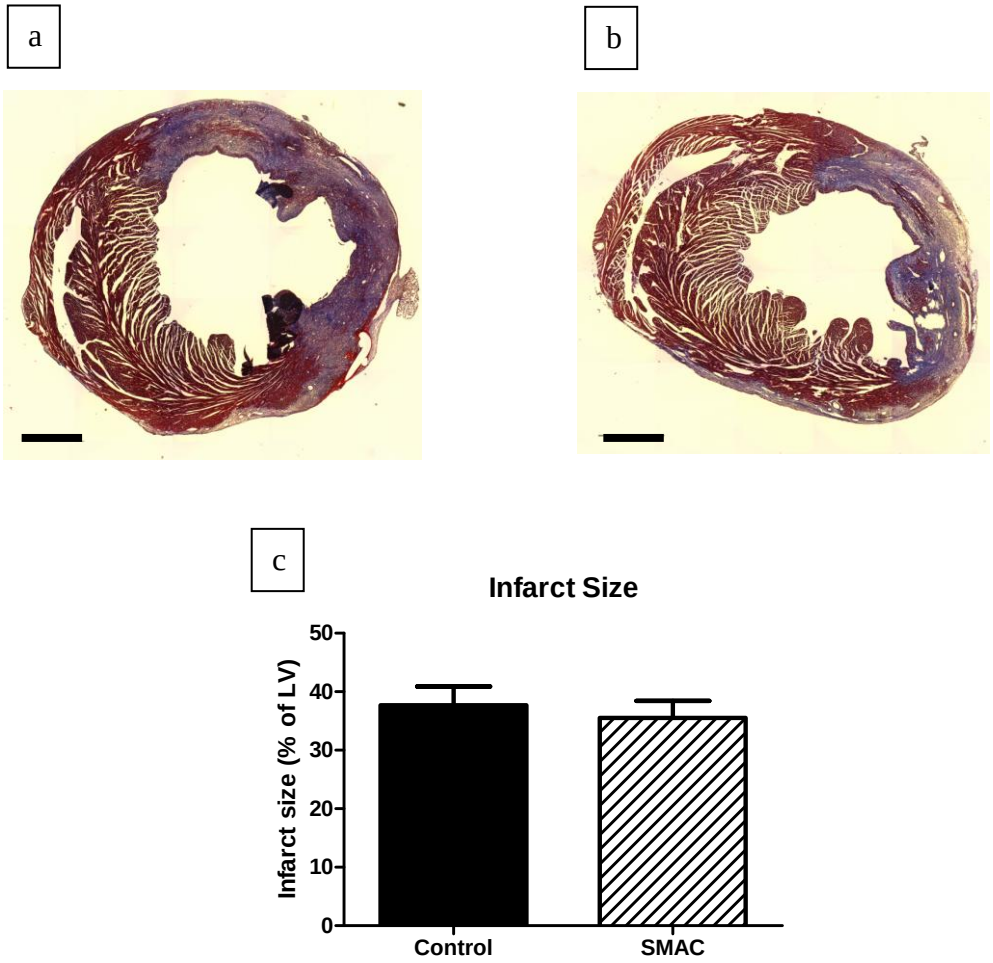

Figure 4.5 Cardiovascular 11β-HSD1 deletion does not affect infarct size 7d post-MI
Representative Masson's Trichrome stained heart sections from 10-12w old (a) SMAC and (b) Cre^- mice 7d post-MI. Quantification of infarct size is shown in (c) (Student's *t* test; n=8/group). Scale bar is 25μm.

4.3.5 Macrophage recruitment 7d after MI is unaffected by cardiovascular 11β-HSD1 deletion

Mac2 staining of macrophages amounted to approximately 1.2% of the left ventricle in sham-operated SMAC and Cre^- control mice (Con). Macrophage content (Mac2 staining, Figure 4.6 a and b) of the left ventricle 7d post-MI was elevated to a similar extent in both SMAC and Cre^- mice (Figure 4.6c) compared to their sham-operated controls.

Recruitment of alternatively-activated macrophages, identified by Ym1 staining, to the left ventricle was elevated to a similar extent in SMAC and Cre^- mice 7d after MI, compared to their sham-operated controls (Con) (Figure 4.7).

4.3.6 Peri-infarct angiogenesis 7d after MI is not influenced by cardiovascular 11β-HSD1 deletion

The number of $CD31^+$ vessels per $400\mu m^2$ in the peri-infarct region was similar for each of the three vessel diameter categories (<4μm, 4-200μm, and >200μm) in SMAC and Cre^- mice 7d post-MI (Figure 4.8).

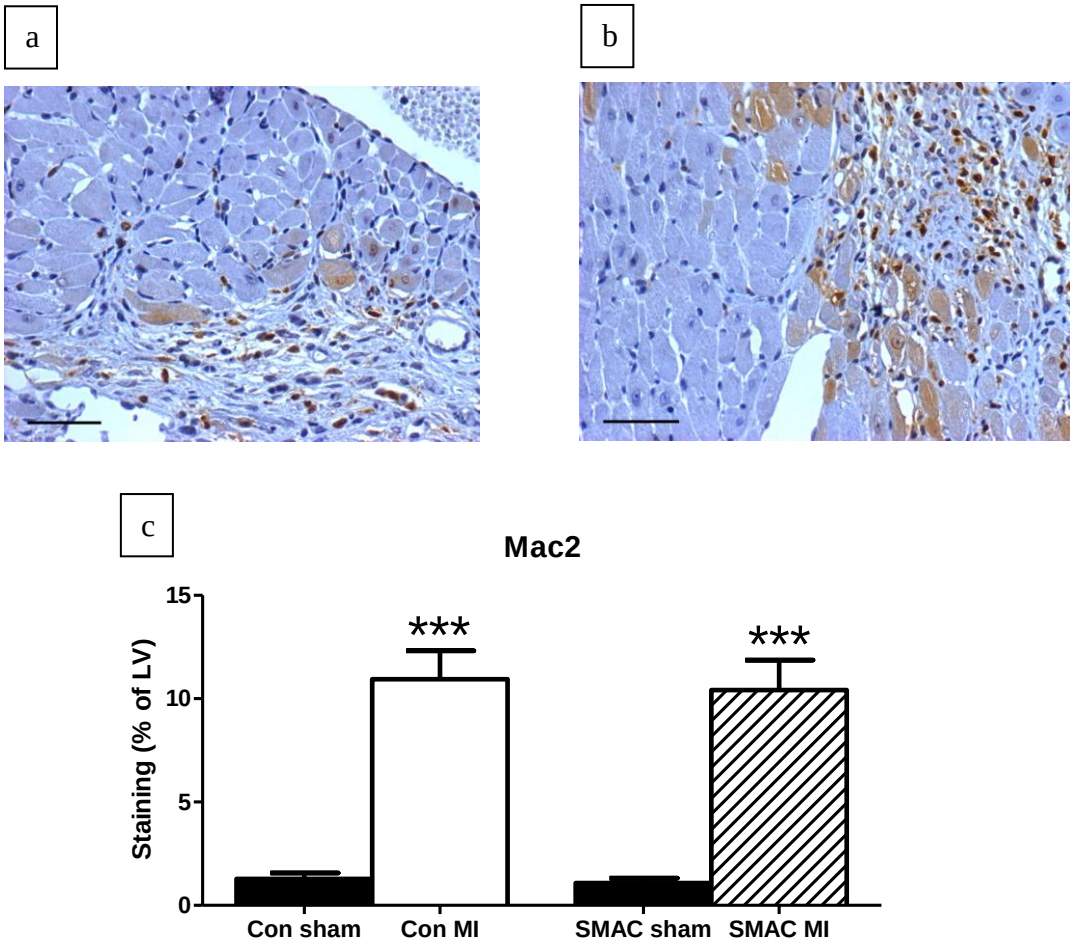

Figure 4.6 Macrophage recruitment to the heart 7d post-MI is unaffected by cardiovascular 11β-HSD1 deletion

Representative Mac2 stained heart sections from 10-12w old (a) SMAC and (b) Cre$^-$ mice 7d post-MI. Some cardiomyocytes in hearts from both SMAC and Cre$^-$ mice show very light staining, which appears to be non-specific staining. Quantification of Mac2 staining in hearts from SMAC and Cre$^-$ mice 7d post-MI and sham-operated controls 7d after sham surgery is shown in (c) (two way ANOVA *** = $p<0.001$; n=8/group for SMAC & Cre$^-$ mice, n=6/group for shams). Scale bar is 20μm.

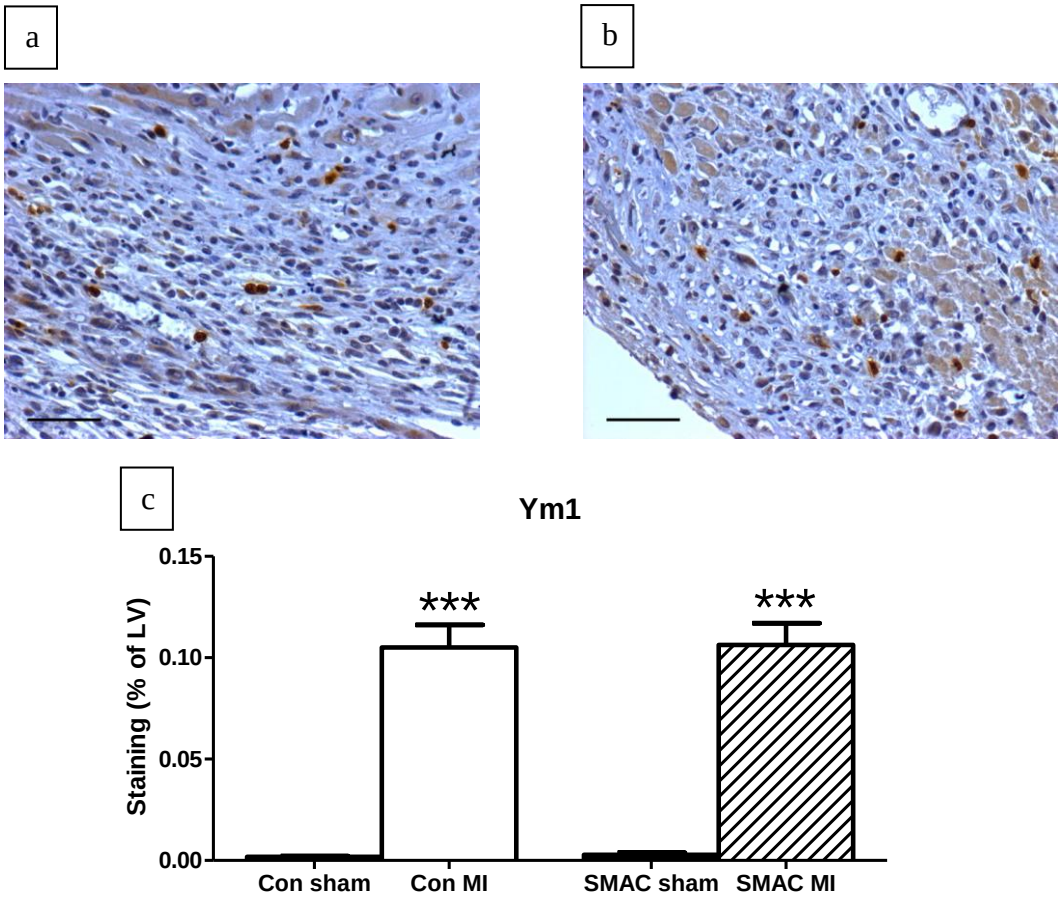

Figure 4.7 Alternatively-activated macrophage recruitment to the heart 7d post-MI is unaffected by cardiovascular 11β-HSD1 deletion

Representative Ym1 stained heart sections from 10-12w old (a) SMAC and (b) Cre^- mice 7d post-MI. Quantification of Ym1 staining in hearts from SMAC mice and Cre^- mice 7d post-MI and sham-operated controls 7d after sham surgery is shown in (c) (two way ANOVA *** = $p<0.001$; n=8/group for SMAC & Cre^- mice, n=6/group for shams). Scale bar is 25μm.

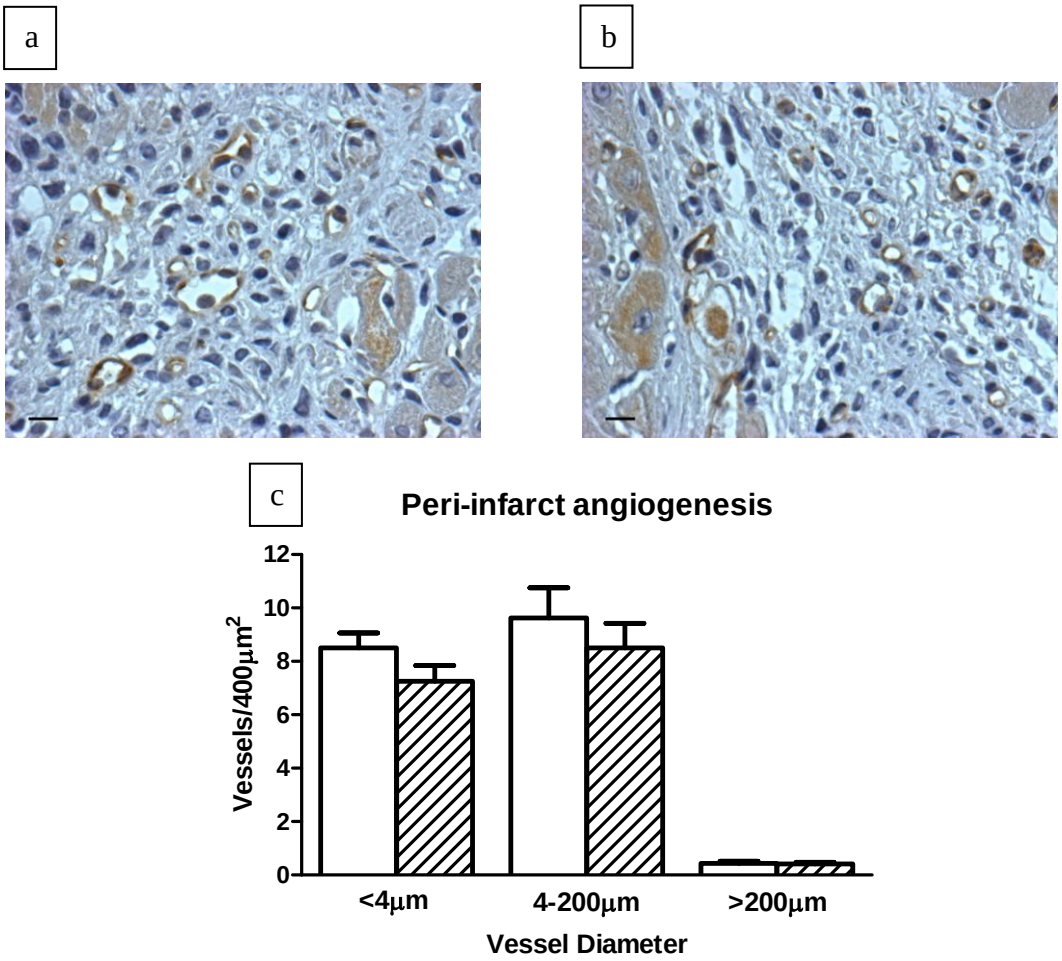

Figure 4.8 Cardiovascular 11β-HSD1 deletion does not alter peri-infarct angiogenesis 7d post-MI

Representative CD31 stained heart sections from 10-12w old (a) SMAC and (b) Cre^- mice 7d post-MI. Quantification of peri-infarct angiogenesis in hearts from SMAC and Cre^- mice 7d post-MI is shown in (c) (Student's *t* test; n=8/group). Scale bar is 10μm.

4.4 Discussion

11β-HSD1 deletion has previously been shown to result in increased angiogenesis in subcutaneous sponge implants (Small, *et al*., 2005). Moreover, mice globally deficient in 11β-HSD1 have an augmented inflammatory response 7d post-MI, with increased representation of pro-reparative alternatively-activated macrophages, enhanced peri-infarct angiogenesis and improved cardiac function (McSweeney, *et al*., 2010). The data presented in this chapter shows that selective 'cardiovascular deletion' of 11β-HSD1 in cardiomyocytes and VSMCs (SMAC mice) does not reproduce this phenotype. Seven days after MI, SMAC and control mice had similar peri-infarct angiogenesis, total macrophage and alternatively-activated macrophage infiltration, infarct size, ventricular dilatation and systolic function. Thus, lack of 11β-HSD1 in one or more cell types, other than cardiomyocytes and VSMCs, must underlie this beneficial phenotype.

4.4.1 Mortality and initial ischaemic damage

Despite the inability of SMAC mice to locally regenerate glucocorticoids in cardiomyocytes and VSMCs, there was no difference in primary cause or rate of mortality, or initial ischaemic injury, in SMAC mice compared to Cre^- control. This suggests that systemic corticosterone release in these mice is sufficient to overcome any lack of intracellular glucocorticoid regeneration in cardiomyocytes, and protect these hearts from initial ischaemic damage in a similar fashion to control mice.

Several studies, going back to the 1970s, have investigated the therapeutic capacity of administering glucocorticoids after MI (Libby, *et al*., 1973; Hoffstein, *et al*.,

1976). Glucocorticoids given immediately after infarction are initially protective, by reducing ischaemic cell death, and therefore limiting infarct size (Libby, *et al*., 1973), possibly by preserving the integrity of lysosomal membranes and thus preventing the spillage of lysozymes into the cytosol (Hoffstein, *et al*., 1976). However, longer term glucocorticoid administration increases the likelihood of left ventricular rupture (Hammerman, *et al*., 1983). Nevertheless, glucocorticoids are critical to early post-MI survival (Reynolds, *et al*., 2010b).

Plasma corticosterone levels are similar in mice globally deficient in 11β-HSD1 and control mice 24h after infarction (McSweeney, *et al*., 2010). Levels were not measured in the current study, and should be investigated to confirm a similar systemic HPA axis response to infarction in SMAC mice. It is hypothesised that SMAC mice would have similar plasma corticosterone levels to control mice, given that global deletion of the enzyme had no effect.

Cardiac troponin-I is one of three subunits which comprise the actin filament found in cardiac muscle (Wu, 2006). It has been known as a highly sensitive marker of cardiac injury for over 20 years (Adams III, *et al*., 1993) as it is normally present in the bloodstream only at very low levels, and is currently used clinically to diagnose acute myocardial infarction (Gassenmaier, *et al*., 2012). The degree of elevation of plasma cardiac troponin-I correlates with the extent of myocardial injury, and can thus be used to determine initial ischaemic damage (Selvanayagam, *et al*., 2005). As such, it was crucial to investigate the initial response of SMAC mice to coronary artery ligation surgery by measuring plasma cardiac troponin-I levels 24hr after infarction. A differential release of cardiac troponin-I immediately following

occlusion may modify the inflammatory response and thus modify longer term infarct healing.

The data presented in this study show that SMAC mice had similar plasma levels of cardiac troponin-I compared to control, and therefore had a similar extent of initial cardiac injury 24hr after coronary artery ligation surgery. This suggests that 11β-HSD1 deletion in the heart and vasculature does not impact upon initial injury.

4.4.2 Peri-infarct angiogenesis

After MI, 11β-HSD1 deficient mice have increased angiogenesis in the peri-infarct region (Small, *et al*., 2005; McSweeney, *et al*., 2010). However, SMAC mice have a similar angiogenic response to Cre^- control mice after MI, with no difference in the density of $CD31^+$ capillaries, in any size category, in the peri-infarct region. This is consistent with the finding that these mice have similar levels of macrophage infiltration, and particularly similar levels of alternatively-activated macrophage infiltration (Sections 4.3.6 and 4.3.7), as these cells play a key role in the induction of post-MI angiogenesis; they release pro-angiogenic factors such as basic FGF, IGF-1 and VEGF (Berse, *et al*., 1992; Henke, *et al*., 1993; Nahrendorf, *et al*., 2007; Dobrucki, *et al*., 2010). These data suggest that deletion of 11β-HSD1 in cardiomyocytes and VSMCs is not sufficient to alter the inflammatory response and reproduce the enhanced angiogenesis observed in globally 11β-HSD1 deficient mice after MI.

Global deficiency of 11β-HSD1 results in upregulation of myocardial expression of the pro-angiogenic cytokine IL-8 after MI, but not VEGF (McSweeney, *et al*., 2010).

The increase in IL-8 is suggested to be due to increased macrophage infiltration, as macrophages are known to secrete IL-8 and promote angiogenesis (Koch, *et al*., 1992). As such, it could contribute to the increased peri-infarct angiogenesis present in these mice (McSweeney, *et al*., 2010). Neither basic FGF, VEGF, IGF-1 nor IL-8 expression was measured in the hearts of SMAC mice and should be investigated in future studies. 11β-HSD1 in infiltrating macrophages is a possible candidate for modifying the post-MI phenotype and is therefore the most obvious focus for future studies, particularly considering the altered expression of IL-8 in globally 11β-HSD1 deficient mice compared to control mice. Additionally, cardiac fibroblasts express 11β-HSD1, and their role in regulating angiogenesis is now well recognised, with several fibroblast-derived proteins, such as collagen I, procollagen C endopeptidase enhancer, osteonectin, TGF β-induced protein ig-h3 and IGF-binding protein 7, having been shown to be critical for lumen formation (Newman, *et al*., 2011) and VEGF having been shown to play a key role in endothelial cell sprouting in tumour angiogenesis (Ito, *et al*., 2007). Inserting a Cre recombinase transgene into the *Sm22α* gene may have an effect on expression of 11β-HSD1 in myofibroblasts, as *Sm22α* has been found to be expressed in isolated myofibroblasts from rabbit bladder (Chiavegato, *et al*., 1999). However, *Sm22α* does not appear to be express in isolated human fibroblasts from COPD patients (Hallgren, *et al*., 2010). As such, 11β-HSD1 expression in cardiac fibroblasts and myofibroblasts, and its role in a post-MI setting should also be investigated further.

4.4.3 Post-infarct inflammation

Mice which are globally deficient in 11β-HSD1 have increased neutrophil infiltration into the heart after MI (McSweeney, *et al*., 2010). Recently, 11β-HSD1 deficiency in bone marrow-derived cells has been shown to be atheroprotective, pointing to a beneficial phenotype in a different inflammatory setting as a result of modified glucocorticoid regeneration in inflammatory cells (Garcia, *et al*., 2013; Kipari, *et al*., 2013). However, in the present study, neutrophil infiltration was not examined, and should be considered for further studies.

After clearing dead tissue from the infarcted myocardium, neutrophils undergo apoptosis and are recognised and subsequently phagocytosed by classically-activated macrophages (Meszaros, *et al*., 1999). Macrophage infiltration was investigated to determine if SMAC mice could reproduce the phenotype found previously in global globally 11β-HSD1 deficient mice, whereby these mice had increased $Mac2^+$ macrophage infiltration, and an increase in the proportion of alternatively-activated $Ym1^+$ macrophages (McSweeney, *et al*., 2010). However, SMAC mice had similar levels of $Mac2^+$ macrophages and $Ym1^+$ alternatively-activated macrophages in the heart, compared to control, seven days after infarction. This suggests 11β-HSD1 deletion out with cardiomyocytes and VSMCs is responsible for the phenotype observed in globally 11β-HSD1 deficient mice and points to a role for 11β-HSD1 in neutrophils or macrophages in modifying the inflammatory response after MI. Alternatively, resident fibroblasts, which also express 11β-HSD1, may underlie this phenotype and therefore warrant further investigation.

To test this hypothesis, it would necessary to generate genetically modified mice which lack 11β-HSD1 only in myeloid cells. Indeed, *Hsd11b1*$^{fl/fl}$*LysM-Cre*$^+$ have

been generated in our centre and their post-MI phenotype has been found to be similar to that of SMAC mice. Additionally, bone marrow transplant experiments have also been conducted in our laboratory whereby DelI mice received wild-type bone marrow, and wild-type mice received DelI bone marrow, prior to induction of MI. Preliminary data suggest that 11β-HSD1 deficiency in the host mouse is key to an improved post-MI outcome and so current studies are focussing on inhibiting 11β-HSD1 in fibroblasts to determine the role of 11β-HSD1 in this cell type after MI (Mylonas, *et al*., unpublished).

4.4.4 Cardiac size and function

The role of 'cardiovascular' 11β-HSD1 in maintaining systolic function was investigated in the current study. As might have been expected from the previous data (Sections 4.3.7 and 4.3.8), which showed SMAC mice have similar levels of angiogenesis and alternatively-activated macrophage recruitment to the heart after MI, cardiac function was similar to control 7d after MI. SMAC and Cre^- control mice both showed a reduction in ejection fraction and fractional shortening which is in agreement with previous studies showing a reduction in function in animal and human models of MI (Pfeffer & Braunwald, 1990; Yang, *et al*., 2002a; Numaguchi, *et al*., 2006). Moreover, 'cardiovascular deletion' of 11β-HSD1 does not impact upon infarct size, with SMAC mice having similar infarct sizes to control 7 days after MI. The similar cardiac size and function seen in SMAC mice and control mice highlights the importance of increased peri-infarct angiogenesis and the altered inflammatory response seen in globally 11β-HSD1 deficient mice; reduced scar size

and, ultimately, maintained ejection fraction would not have resulted without modification of these pathways.

The data in this chapter suggest SMAC mice do not recapitulate the beneficial post-MI phenotype previously observed in globally 11β-HSD1 deficient mice, which is in contrast to earlier research showing 11β-HSD1 deficiency in the vessel wall is key to the enhanced angiogenesis seen in sponge implants (Small, *et al*., 2005). However, it is clear that 'cardiovascular' 11β-HSD1 contributes to appropriate calcium handling gene expression and normal diastolic function (Chapter 3), parameters which are altered in the post-MI progression to heart failure. As such, the phenotype of cardiovascular-specific 11β-HSD1 KO mice, and global 11β-HSD1 deficient mice, eight weeks after infarction was investigated and is the focus of Chapter 5.

Chapter 5

The Effect of Global and Cardiovascular-specific Deletion of 11β-HSD1 on the Development of Heart Failure

5.1 Introduction

MI is a major contributor to heart failure (Jhund & McMurray, 2008). 11β-HSD1 deficient mice show enhanced angiogenesis, shorter infarcts and preserved ejection fraction 28d after MI (see Section 1.2.6) (Small, *et al*., 2005; McSweeney, *et al*., 2010), but the effects on the development of heart failure are unknown. Cardiovascular 11β-HSD1 plays a role in calcium handling gene expression, as deletion specifically in cardiomyocytes and VSMCs (SMAC mice) leads to diastolic dysfunction and reduced SERCA mRNA and protein expression (Chapter 3). Infarct healing in the short term, up to seven days post-MI, is unaffected in these mice (Chapter 4), however it is unclear how 11β-HSD1 deficient mice and SMAC mice will respond to MI in the long term. 11β-HSD1 deficient mice may be in a position to better adapt, given the they have increased angiogenesis after MI, and therefore show an improved outcome. On the other hand, they may exhibit an exaggerated detrimental phenotype compared to control, considering the ubiquitous reduction in myocardial SERCA. SMAC mice may show more severe heart failure compared to controls, since these mice do not exhibit enhanced angiogenesis, yet do have reduced myocardial SERCA.

It is therefore hypothesised that 11β-HSD1 deficient mice will still show a beneficial phenotype, and resist heart failure, eight weeks after infarction; they will have smaller infarcts, preserved cardiac function and attenuated chamber dilatation. It is hypothesised that the basal reduction in SERCA mRNA levels and protein expression limits the scope for further SERCA reduction and therefore this will not impact on the favourable outcomes previously found (McSweeney, *et al*., 2010).

However, SMAC mice do not show a beneficial response seven days post-MI (Chapter 4), and so it is hypothesised that SMAC mice will show similar left ventricular dilatation, infarct size and reduction in systolic function to controls eight weeks after MI.

5.2 Methods

Male 11β-HSD1 deficient mice and their C57BL/6 controls, and cardiovascular-specific 11β-HSD1 KO (SMAC) mice, and their Cre^- littermate controls, underwent coronary artery ligation surgery aged 10-12 weeks (Section 2.2.3). Initially, global 11β-HSD1 KO mice (DelI mice) initially underwent coronary artery ligation. However, all mice (n=16) died between d3 and d5 after surgery from cardiac rupture. This may be due to a greatly enhanced inflammatory response, which has been previously shown to result in cardiac rupture (Nian, *et al*., 2004), and this is currently being investigated. Because of the lack of survival of DelI mice beyond d5, 11β-HSD1 deficient mice, which are hypomorphic for 11β-HSD1, were used.

Tail blood was collected 24h after surgery (Section 2.2.4) to determine the extent of initial cardiac injury, by measurement of cardiac troponin-I (Section 2.6.5). CINE MRI was performed 8w after surgery (Section 2.2.5) to assess cardiac size and function. Mice were killed by cervical dislocation immediately following CINE MRI and hearts and lungs were harvested. Lungs were weighed to assess pulmonary oedema. Hearts were weighed and either frozen at -80^oC for qRT-PCR and western blotting, or processed, embedded in paraffin wax and microtomed into 4μm thick sections for histology and immunohistochemical analysis. This allowed determination of infarct size, infarct thickness, and cardiomyocyte cross-sectional area.

5.2.1 Histology and immunohistochemistry

Masson's Trichrome staining was used to determine infarct size and thickness (Section 2.4.3). Immunofluorescent staining with wheat germ agglutinin, isolectin B4 and DAPI and was used to measure cardiomyocyte cross-sectional area (Section 2.5.2).

5.2.2 qRT-PCR

RNA was extracted from homogenised heart tissue using TRIzol as described in Section 2.6.1. cDNA was synthesized as detailed in Section 2.6.2 and qRT-PCR was performed as described in Section 2.6.3 to assess mRNA levels of SERCA (*Atp2a2*), NCX (*Slc8a1*), RyR (*Ryr2*), $CaV_{1.2}$ (*Cacna1c*), ANP (*Nppa*), Col1α2 (*Col1a2*), Col3α1 (*Col3a1*), TGFβ (*Tgfb1*), α-MHC (*Myh6*), and β-MHC (*Myh7*). The internal control for all qRT-PCR experiments was β-actin (*Actb*) which was similar in all groups (See Appendix 1).

5.2.3 Western blotting

Protein was extracted from homogenised heart samples, electrophoresed on a polyacrilamide gel and transferred onto a nitrocellulose membrane as described in Section 2.6.4. The membranes were exposed to antibodies against SERCA and the internal control protein β-actin, before being exposed to x-ray film as detailed in Section 2.6.4.

5.2.4 Statistical analysis

All values are expressed as mean ± SEM. A *p* value of less than 0.05 indicated statistical significance. Mortality data were compared using Fisher's exact test and chi square test. All other data were compared using two-tailed unpaired Student's *t* tests.

5.3 Results

5.3.1 Global 11β-HSD1 deficiency and cardiovascular 11β-HSD1 deletion do not influence mortality

After coronary artery ligation, mortality was similar in 11β-HSD1 deficient mice and C57BL/6 control mice (Figure 5.1a) and in SMAC and their Cre^- control mice (Figure 5.1b), with 73%, 75%, 80% and 86% of mice, respectively, surviving until 8w post-MI. Post mortem investigation of deaths revealed they were all a result of cardiac rupture, as determined by the presence of blood in the chest cavity and a rupture of the left ventricular wall.

5.3.2 Initial ischaemic injury is unaffected by global 11β-HSD1 deficiency and cardiovascular 11β-HSD1 deletion

24hr after ligation surgery, plasma levels of cardiac troponin-I were elevated to a similar extent in 11β-HSD1 deficient mice and C57BL/6 control mice (Figure 5.2a), and in SMAC and Cre^- control mice (Figure 5.2b), suggesting a similar extent of initial cardiac injury in all genotypes.

5.3.3 Global 11β-HSD1 deficiency, but not cardiovascular 11β-HSD1 deletion, attenuates left ventricular dilatation 8w after MI

5.3.3.1 CINE MRI

11β-HSD1 deficient mice had reduced left ventricular dilatation compared to C57BL/6 control mice, with smaller left ventricular end systolic volumes (LVESV,

Figure 5.3a, $p<0.05$) and left ventricular end diastolic volumes (LVEDV, Figure 5.3c, $p<0.05$). This reduced dilatation was not seen in SMAC mice, as they had similar LVESV and LVEDV to Cre^- controls, 8w post-MI (Figure 5.3b and d). Having said that, a direct comparison between 11β-HSD1 deficient mice and SMAC mice was not made.

5.3.3.2 Gravimetrics

The difference in left ventricular volume between 11β-HSD1 deficient mice and control mice was supported by post-mortem data showing that 11β-HSD1 deficient mice had reduced heart weights compared to control (Figure 5.4a, $p<0.001$), despite both genotypes having similar body weights (Figure 5.4b). This resulted in a reduced heart weight to body weight ratio (Figure 5.4c, $p<0.001$). In contrast, heart weight to body weight ratio was similar between SMAC and Cre^- control mice.

5.3.3.3 Cardiomyocyte cross-sectional area

Cardiomyocyte cross-sectional area was similar in all genotypes (Figure 5.5a–c).

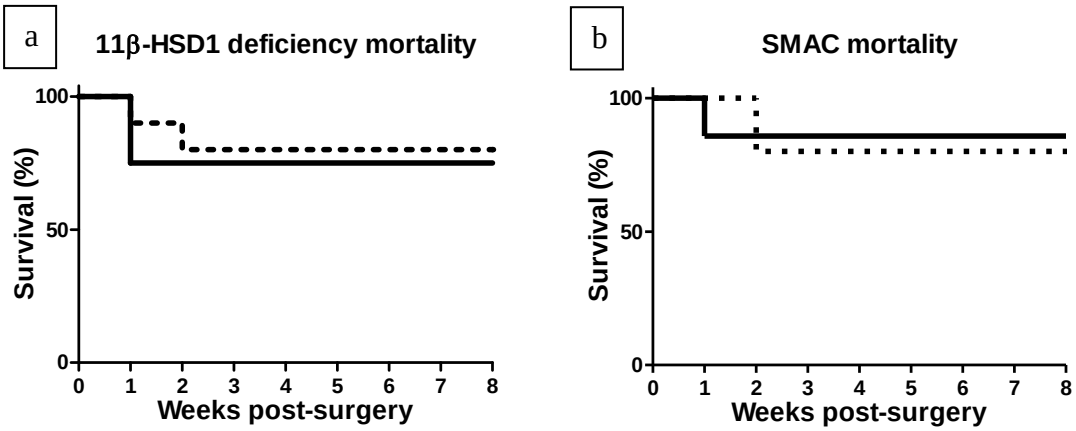

Figure 5.1 Global 11β-HSD1 deficiency, or cardiovascular 11β-HSD1 deletion does not affect mortality after coronary artery ligation

Mortality after coronary artery ligation surgery in 10-12w old (a) 11β-HSD1 deficient mice (dashed line, n=10) and C57BL/6 mice (solid line, n=8) (no significant difference; Fisher's exact test, chi square p=0.71) and in (b) SMAC mice (dashed line, n=10) and Cre^- control mice (solid line, n=8) (no significant difference; Fisher's exact test, chi square p=0.88).

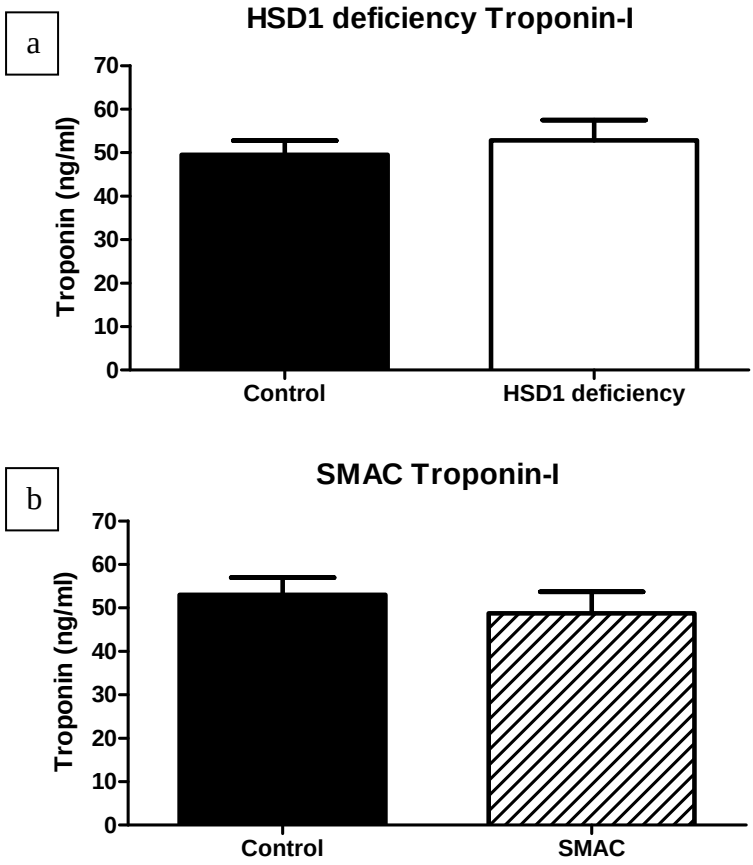

Figure 5.2 Global 11β-HSD1 deficiency, or cardiovascular 11β-HSD1 deletion, does not affect the extent of initial injury after coronary artery ligation

Plasma cardiac troponin-I levels were measured by ELISA in 10-12w old (a) 11β-HSD1 deficient mice and C57BL/6 control mice and (b) SMAC and Cre^- control mice 24h post-MI (one way ANOVA; n=8/group for SMAC & 11β-HSD1 deficient mice, n=6/group for controls).

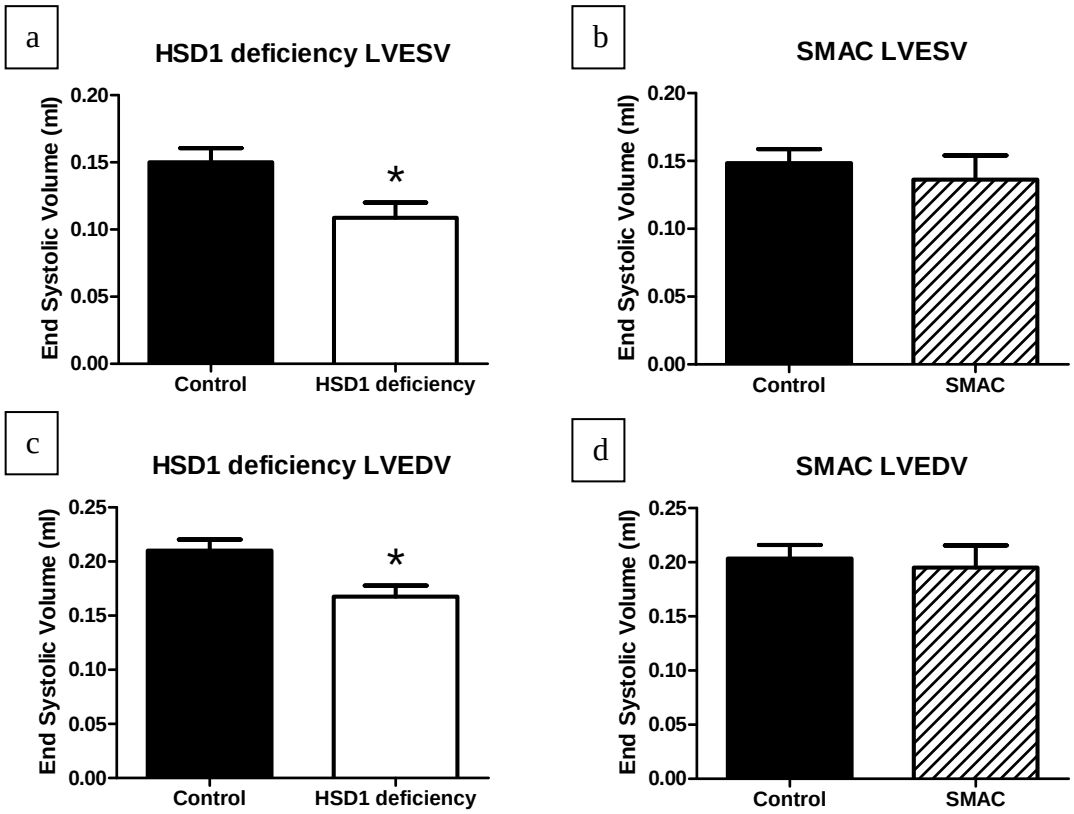

Figure 5.3 Global, but not cardiovascular, 11β-HSD1 deficiency attenuates left ventricular dilatation 8w post-MI

LVESV and LVEDV of 18-20w old 11β-HSD1 deficient mice and C57BL/6 control mice (a and c) and SMAC and Cre^- control mice (b and d) were measured by CINE MRI 8w post-MI (Student's *t* test * = $p<0.05$; n=8/group for SMAC & 11β-HSD1 deficient mice, n=6/group for controls).

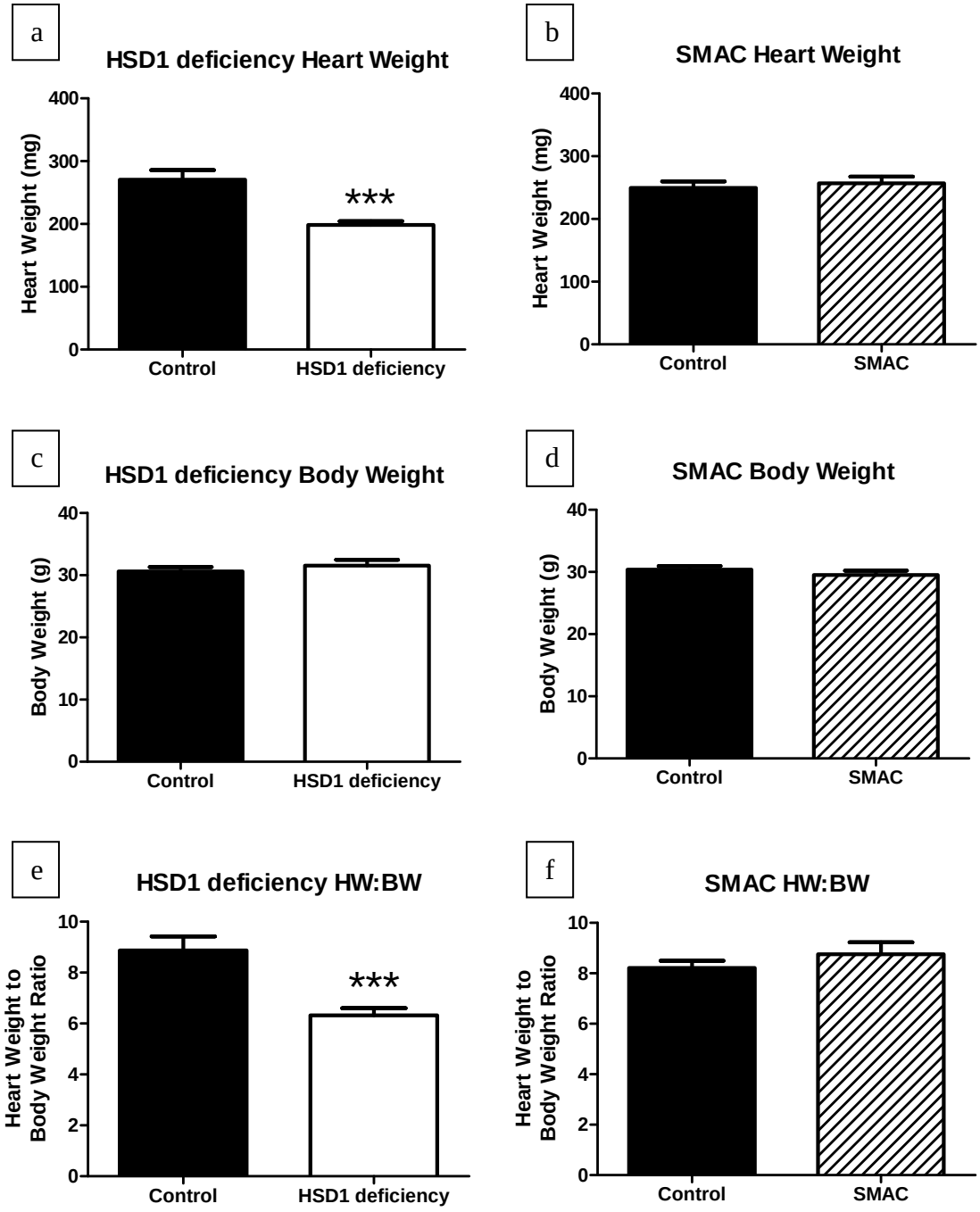

Figure 5.4 Global, but not cardiovascular, 11β-HSD1 deficiency reduces heart weight 8w post-MI

Heart weight (a and b), body weight (c and d) and heart weight to body weight ratio (e and f) in 18-20w old 11β-HSD1 deficient mice and C57BL/6 control mice, and SMAC mice and Cre^- control mice 8w post-MI (Student's *t* test *** = $p<0.001$; n=8/group for SMAC & 11β-HSD1 deficient mice, n=6/group for controls).

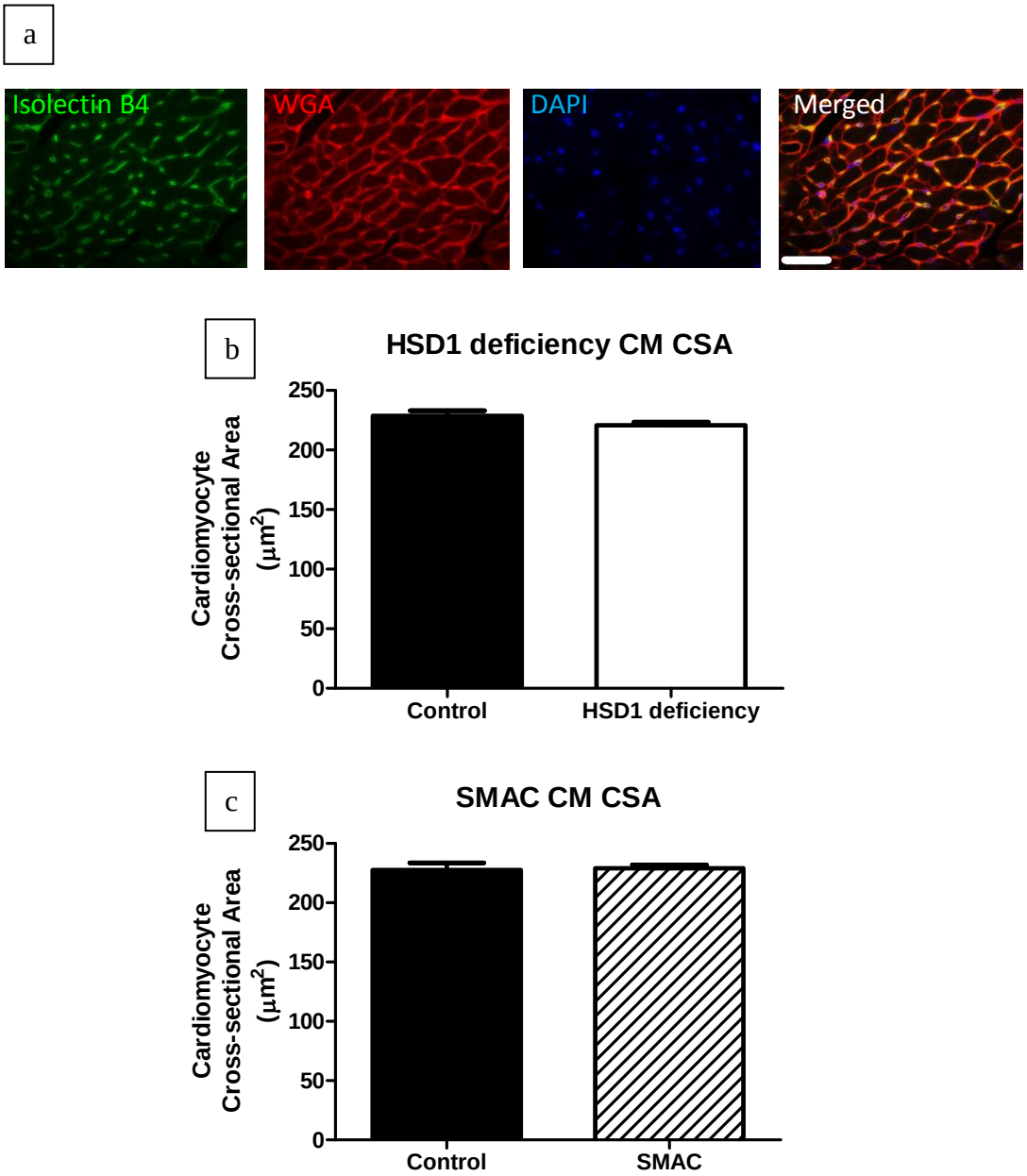

Figure 5.5 Cardiomyocyte cross-sectional area is not influenced by 11β-HSD1 deficiency 8w post-MI

Cardiomyocyte cross sectional area (a) in 18-20w old 11β-HSD1 deficient mice and C57BL/6 control mice (b), and SMAC and Cre^- control mice (c) 8w post-MI (Student's *t* test; n=8/group for SMAC & 11β-HSD1 deficient mice, n=6/group for controls). Scale bar is 20μm.

5.3.4 Global 11β-HSD1 deficiency, but not cardiovascular 11β-HSD1 deletion, reduces foetal gene expression and pulmonary oedema 8w after MI

5.3.4.1 ANP and β-MHC expression

ANP mRNA levels were significantly reduced in 11β-HSD1 deficient mice 8w post-MI compared to C57BL/6 control mice (Figure 5.6a, $p<0.01$). 11β-HSD1 deficient mice also exhibited an increased α-MHC to β-MHC mRNA ratio compared to control mice (Figure 5.6c, $p<0.05$). ANP mRNA levels and α-MHC to β-MHC ratio were similar in SMAC mice and Cre^- control mice (Figure 5.6b and d).

5.3.4.2 Pulmonary Oedema

Lung wet weight was measured immediately following cull by cervical dislocation. 11β-HSD1 deficient mice had significantly lighter lungs compared to their C57BL/6 control mice (Figure 5.7a, $p<0.05$), whereas SMAC and their respective control mice had similar lung weights (Figure 5.7b).

5.3.5 Systolic function is preserved in mice with global 11β-HSD1 deficiency, but not in mice with cardiovascular 11β-HSD1 deletion 8w after MI

Ejection fraction (EF), assessed by CINE MRI, was increased in 11β-HSD1 deficient mice compared to their C57BL/6 control mice (Figure 5.8a, $p<0.05$). SMAC and their Cre^- control mice had similar ejection fractions (Figure 5.8b).

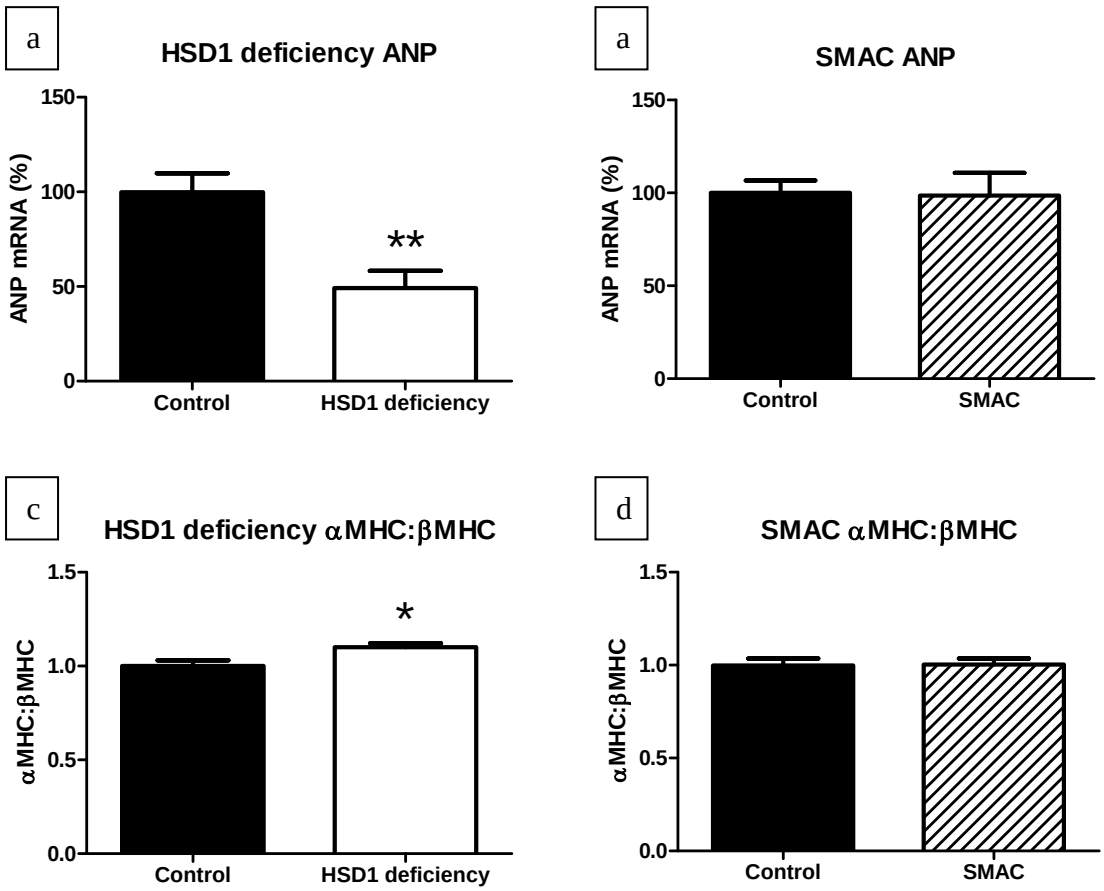

Figure 5.6 Global, but not cardiovascular, 11β-HSD1 deficiency reduces ANP and β-MHC mRNA levels in the heart 8w post-MI

ANP mRNA levels and α-MHC:β-MHC ratio, as measured by qRT-PCR, in 18-20w old 11β-HSD1 deficient mice and C57BL/6 control mice (a and c) and SMAC and Cre^- control mice (b and d) 8w post-MI (Student's *t* test ** = $p<0.01$, * = $p<0.05$; n=8/group for SMAC & 11β-HSD1 deficient mice, n=6/group for controls).

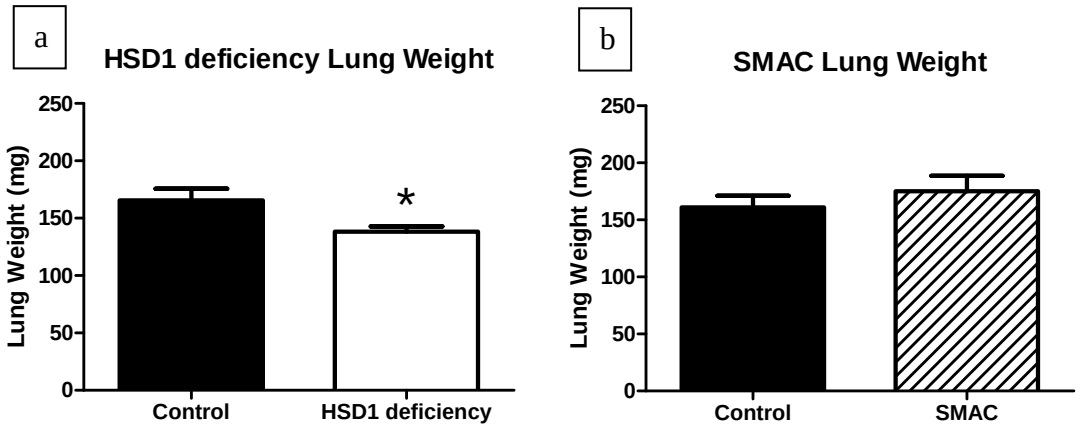

Figure 5.7 Global, but not cardiovascular, 11β-HSD1 deficiency reduces pulmonary oedema 8w post-MI

Lung weight, measured immediately following cull, in 18-20w old (a) 11β-HSD1 deficient mice and C57BL/6 control mice, and (b) SMAC and Cre^- control mice 8w post-MI (Student's *t* test * = $p<0.05$; n=8/group for SMAC & 11β-HSD1 deficient mice, n=6/group for controls).

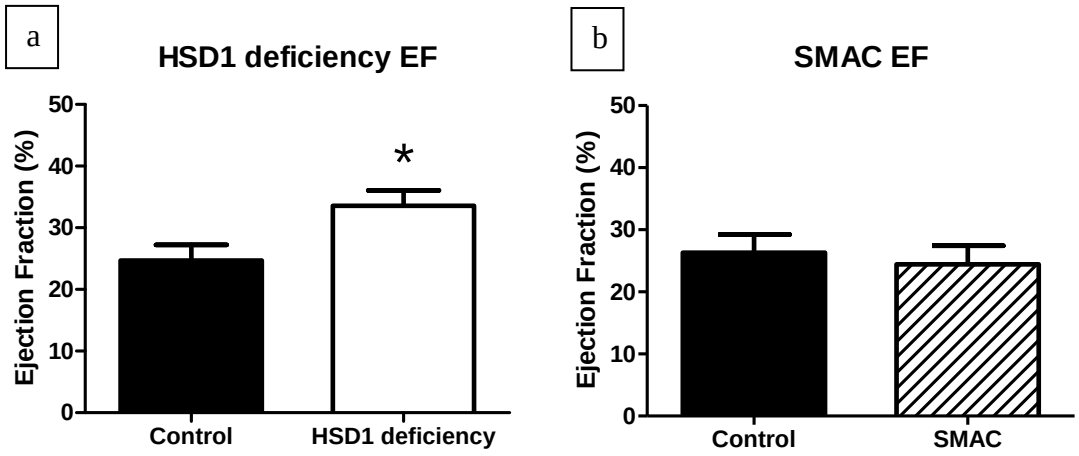

Figure 5.8 Global, but not cardiovascular, 11β-HSD1 deficiency preserves systolic function 8w post-MI

Ejection fraction of 18-20w old 11β-HSD1 deficient mice and C57BL/6 control mice (a), and SMAC and Cre^- control mice (b) was measured by CINE MRI 8w post-MI (Student's *t* test* = $p<0.05$; n=8/group for SMAC & 11β-HSD1 deficient mice, n=6/group for controls).

5.3.6 Infarct length is reduced and infarct thickness is increased in global 11β-HSD1 deficient mice, but not in mice with cardiovascular-specific 11β-HSD1 deletion, 8w after MI

5.3.6.1 Magnetic resonance imaging

Analysis of CINE MRI images revealed 11β-HSD1 deficient mice had shorter infarcts compared to their C57BL/6 controls (Figure 5.9a, $p<0.05$), whereas SMAC mice and their Cre^- controls had similar infarct lengths (Figure 5.9b).

5.3.6.2 Masson's Trichrome staining

Figure 5.10 shows example images of Masson's Trichrome staining of C57BL/6 (Figure 5.10a) and 11β-HSD1 deficient (Figure 5.10b) hearts, and Cre^- (Figure 5.10c) and SMAC (Figure 5.10d) hearts.

11β-HSD1 deficient mice had significantly shorter infarcts compared to their C57BL/6 control mice (Figure 5.10e, $p<0.01$), whereas SMAC mice and their Cre^- control mice had infarcts of similar length (Figure 5.10f).

11β-HSD1 deficient mice had significantly thicker infarcts compared to their C57BL/6 control mice (Figure 5.10g, $p<0.001$), whereas SMAC and their Cre^- control mice had infarcts of similar thickness (Figure 5.10h).

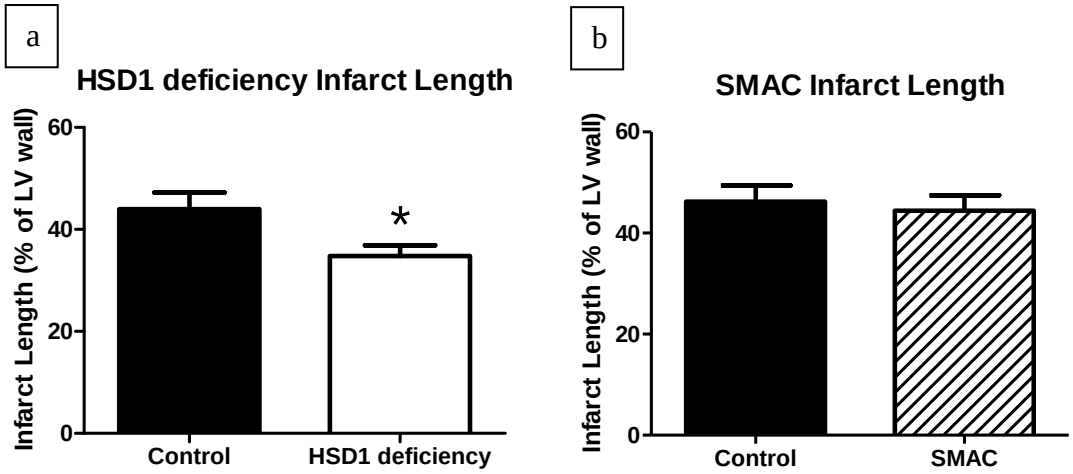

Figure 5.9 Global, but not cardiovascular, 11β-HSD1 deficiency reduces infarct length 8w post-MI

Infarct length, as measured by CINE MRI (see Section 2.2.6), of 18-20w old (a) 11β-HSD1 deficient mice and C57BL/6 control mice, and (b) SMAC mice and Cre^- control mice 8w post-MI (Student's *t* test * = $p<0.05$; n=8/group for SMAC & 11β-HSD1 deficient mice, n=6/group for controls).

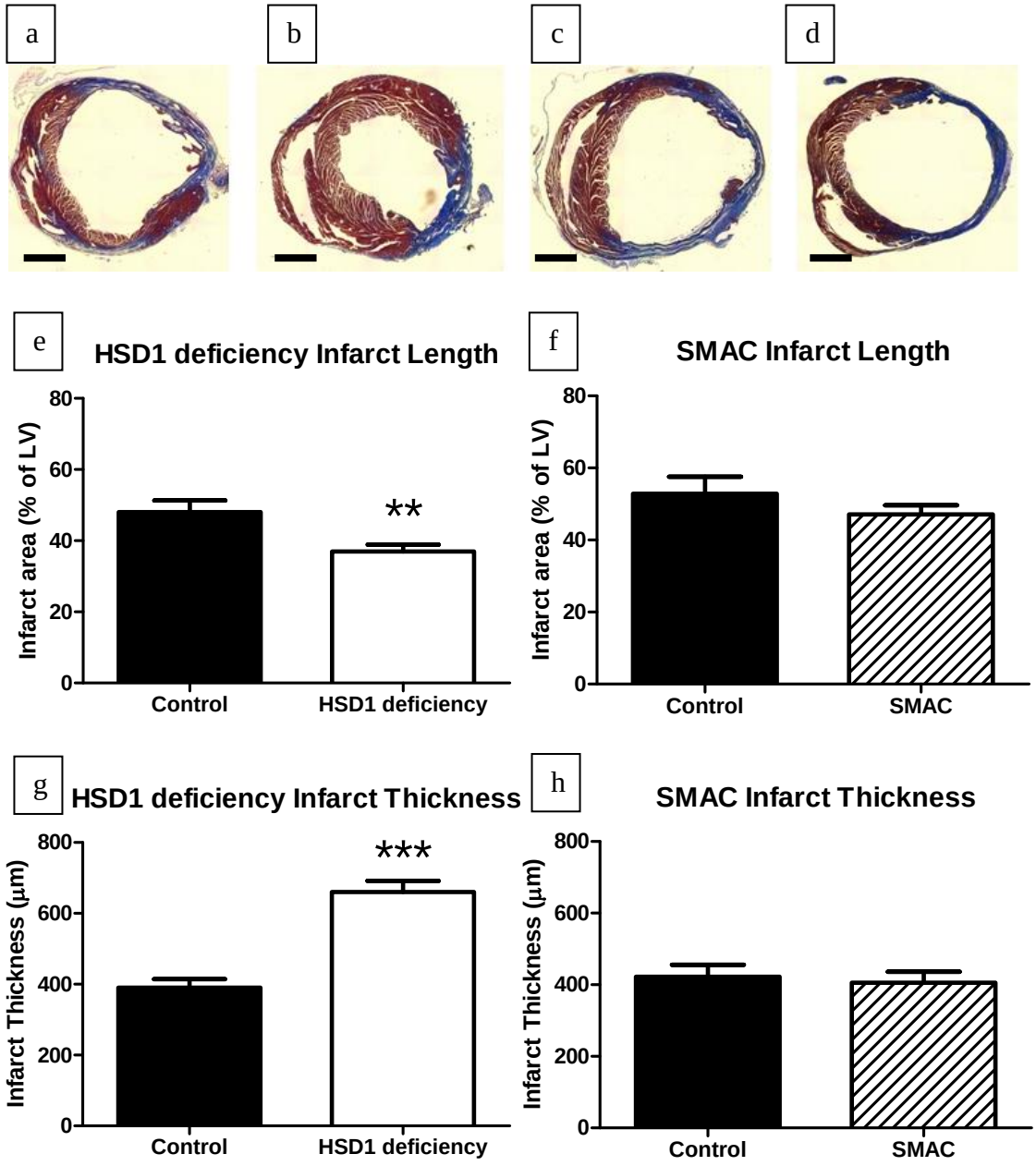

Figure 5.10 Global 11β-HSD1 deficiency reduces infarct length and increases infarct thickness 8w post-MI, but cardiovascular 11β-HSD1 deletion does not

Representative images of Masson's Trichrome stained heart sections from 18-20w old (a) C57BL/6 mice, (b) 11β-HSD1 deficient mice (c) Cre^- mice and (d) SMAC mice 8w post-MI. Infarct length and thickness in 11β-HSD1 deficient mice and C57BL/6 control mice (e and g), and SMAC mice and Cre^- control mice (f and h) were measured as detailed in Section 2.4.2 (Student's *t* test *** = $p<0.001$, ** = $p<0.01$; n=8/group for SMAC & 11β-HSD1 deficient mice, n=6/group for controls). Scale bar is 25µm.

5.3.7 Myocardial collagen gene expression, 8w after MI, is not influenced by global 11β-HSD1 deficiency or cardiovascular 11β-HSD1 deletion

mRNA levels of the alpha 2 subunit of type 1 collagen (*Col1a2*, Figure 5.11a and b), the alpha 1 subunit of type 3 collagen (*Col3a1*, Figure 5.11c and d) and TGFβ (*Tgfb1*, Figure 5.11e and f) in the heart were similar in all groups, as was β-actin (*Actb*), the internal control (see Appendix 1).

5.3.8 Calcium handling genes are not influenced by global 11β-HSD1 deficiency or cardiovascular 11β-HSD1 deletion 8w after MI

SERCA (*Atp2a2*, Figure 5.12a and b) and NCX (*Slc8a1*, Figure 5.12c and d) mRNA levels were similar in all groups. SERCA protein (Figure 5.12e) was also similar in all groups (Figure 5.12f and g).

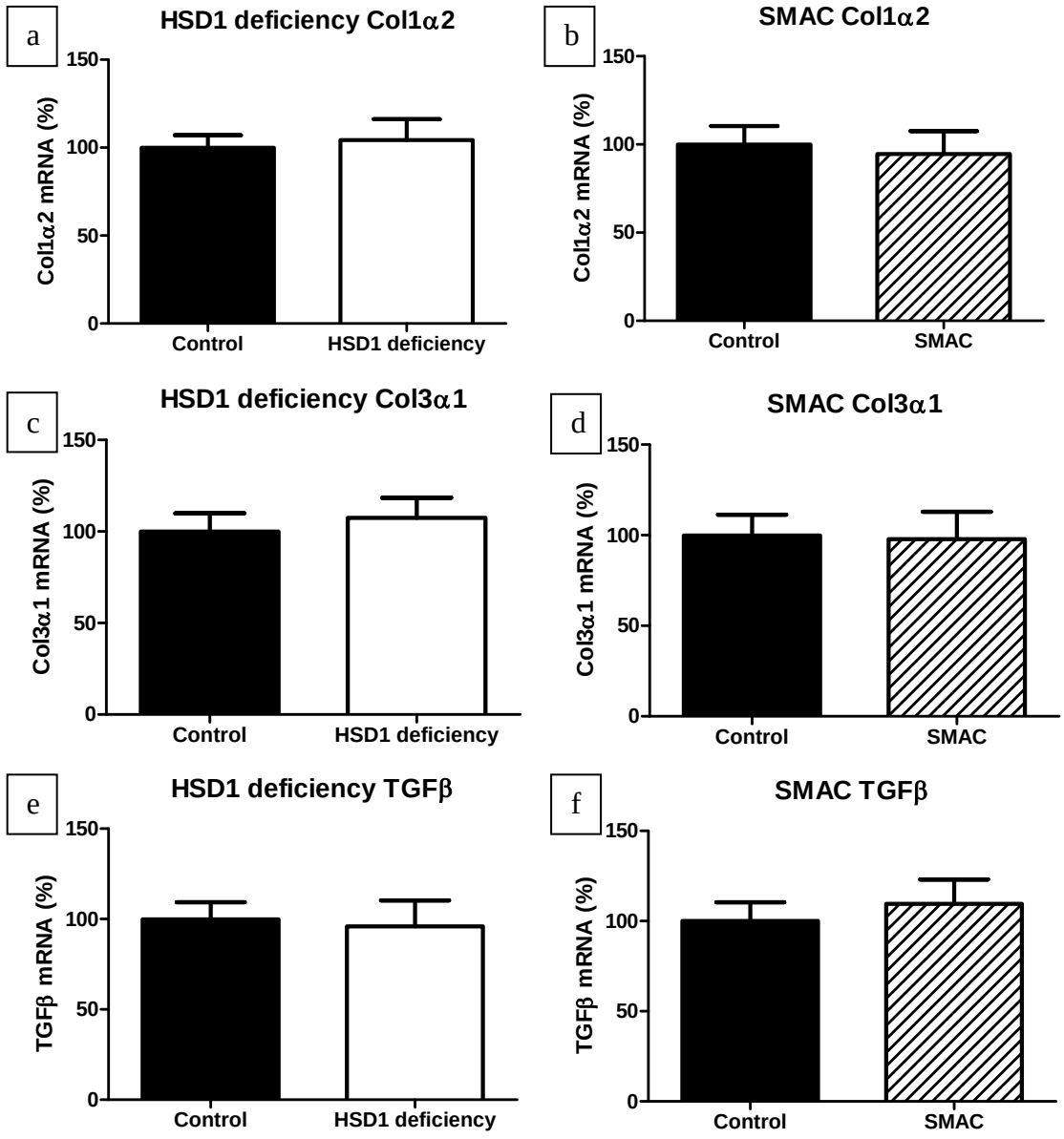

Figure 5.11 Fibrotic gene mRNA levels in the heart are not influenced by 11β-HSD1 deficiency 8w post-MI

Myocardial Col1α2 (a and b), Col3α1 (c and d) and TGFβ (e and f) mRNA levels in 18-20w old 11β-HSD1 deficient mice and C57BL/6 control mice, and SMAC and Cre^- control mice 8w post-MI (Student's *t* test; n=8/group for SMAC & 11β-HSD1 deficient mice, n=6/group for controls).

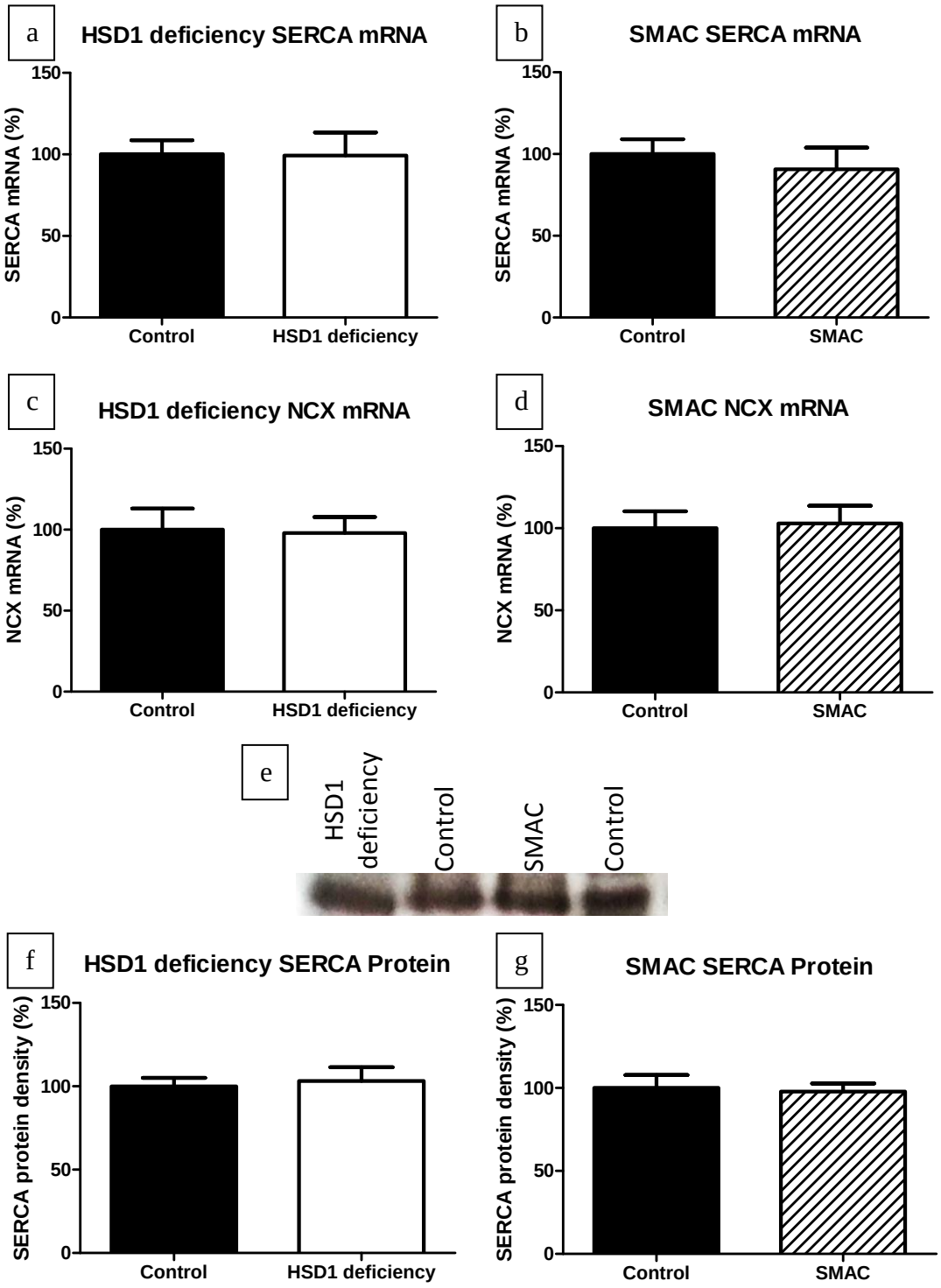

Figure 5.12 11β-HSD1 deficiency does not alter mRNA levels of calcium handling genes in the heart 8w post-MI

Myocardial SERCA (a and b) and NCX (c and d) mRNA levels, as measured by qRT-PCR, and SERCA protein expression (e – g), as measured by Western blotting, in 18-20w old 11β-HSD1 deficient mice and C57BL/6 control mice, and SMAC Cre$^-$ control mice 8w post-MI (Student's *t* test; n=8/group for SMAC & 11β-HSD1 deficient mice, n=6/group for controls).

5.4 Discussion

The data presented in this chapter shows that the beneficial phenotype seen in global 11β-HSD1 deficient mice at 28d post-MI is maintained up to 8w after MI. These mice have smaller, lighter hearts, reduced left ventricular dilatation, preserved systolic function, attenuated expression of ANP and β-MHC, attenuated pulmonary oedema and smaller infarcts than controls. SMAC mice did not recapitulate the phenotype of 11β-HSD1 deficient mice and were similar to Cre^- control mice for all parameters. Despite SMAC mice displaying mild diastolic dysfunction basally, possibly due to altered calcium handling as a result of reduced SERCA expression (Chapter 3), they did not appear to have abnormally impaired calcium handling gene expression eight weeks after infarction; SERCA mRNA levels and protein expression and NCX protein expression in these mice were similar to levels in control mice.

5.4.1 Initial ischaemic injury and mortality

The data presented in this study show that 11β-HSD1 deficient mice and SMAC mice had similar plasma cardiac troponin-I levels compared to their respective controls, and therefore had a similar extent of initial cardiac injury 24h after coronary artery ligation. This suggests that 11β-HSD1 deletion in the heart and vasculature does not impact upon initial injury and any differences in left ventricular dilatation, systolic function, infarct size, collagen deposition or gene expression 8w after MI, are not due to differences in initial injury. However, sham-operated mice were not used in this study, and so a comparison of 24h plasma cardiac troponin-I levels, or

any other parameters 8w post-MI, to sham-operated animals cannot be made. Nevertheless, previous studies have shown cardiac troponin-I is present at very low levels in sham-operated C57BL/6 mice but is significantly elevated 24h after MI (Montecucco, *et al*., 2012) to a similar level to that seen in the mice used in this study. Sham-operated Cre^- mice (Chapter 4) also show significantly reduced plasma cardiac troponin-I levels compared to Cre^- mice which had ligation surgery. As such, plasma cardiac troponin-I levels observed in 11β-HSD1 deficient mice and SMAC mice, and their respective controls, 24h after MI in this study reflect published levels. The primary cause and rate of mortality was similar in all groups, demonstrating that 11β-HSD1 deficiency, either globally or specifically in cardiovascular cells, does not result in grossly adverse cardiac remodelling.

The ability of glucocorticoids to protect ischaemic cardiomyocytes immediately following occlusion is well established (Libby, *et al*., 1973; Hoffstein, *et al*., 1976). HPA axis activation after MI leads to increased circulating corticosterone levels (McSweeney, 2010). The degree of elevation of plasma corticosterone immediately after MI can modify the extent of initial injury (Xu, *et al*., 2011), demonstrating the cardioprotective effect of corticosteroids in this setting. The extent of remodelling which occurs after MI is largely dependent on initial injury and infarct size, with infarct size negatively correlating with morbidity and mortality in the long term (Yang, *et al*., 2002a; Numaguchi, *et al*., 2006). Given that 11β-HSD1 deficient mice and SMAC mice are unable to locally regenerate glucocorticoids in cardiomyocytes, systemic corticosterone release from the adrenal glands must therefore be sufficient to protect cardiomyocytes from initial ischaemic damage, in a similar manner to control mice.

Global 11β-HSD1 deficiency on the C57BL/6 background has been shown to alter basal HPA axis function, with these mice exhibiting increased plasma corticosterone levels (Harris, *et al*., 2001; Carter, *et al*., 2009). This may impact upon the data presented in this thesis, as increased basal plasma corticosterone levels may lead to an exaggerated HPA axis response after infarction. Indeed, 11β-HSD1 deficiency has been shown to result in an augmented HPA axis response after restraint stress (Harris, *et al*., 2001). However, these mice have been shown to have similar circulating plasma corticosterone levels 24h after infarction (McSweeney, *et al*., 2010), although this was not measured in the current study. Effects of 11β-HSD1 deficiency on HPA axis regulation is strain specific as 11β-HSD1 deletion on the 129/MF1 background causes hypersecretion of glucocorticoids under basal conditions (Harris, *et al*., 2001; Carter, *et al*., 2009). It is hypothesised that 11β-HSD1 deficient mice and SMAC mice would have similar plasma corticosterone levels compared to their respective controls since all are on the C57BL/6 background. However, this should be confirmed in future studies.

5.4.2 Markers of heart failure

The inadequacy of the heart to efficiently eject blood following infarction can result in cardiogenic pulmonary oedema. This occurs because of a build up of back pressure in the pulmonary circulation which, in turn, causes fluid to extravasate from the capillary bed out into the alveoli (Vital, *et al*., 2013). This can lead to impaired gas exchange at the alveolar-capillary interface and, therefore, breathing difficulties (Vital, *et al*., 2013). Pulmonary oedema is thus a key indicator of heart failure (Lu, *et al*., 2010; Thorneloe, *et al*., 2012; Clark & Cleland, 2013) and is associated with

reduced left ventricular ejection fraction after infarction (Schiffrin & Taillefer, 1986; Jones, *et al*., 2003). Therefore, it can be used as a marker to assess the extent of heart failure. Although lung weights in mice 8w post-MI cannot be directly compared to sham-operated mice, due to an absence of sham-operated mice in this study, the lung weight in the mice which underwent ligation surgery are similar to published data (Adachi, *et al*., 2003; Lu, *et al*., 2010), suggesting these animals show signs of pulmonary oedema.

Cardiac dysfunction and hypertrophy is also characterised by an increase in atrial natriuretic peptide (ANP) levels and increased expression of β-myosin heavy chain (β-MHC) (Jones, *et al*., 1996; Harada, *et al*., 1999), which indicates a reversion of cardiomyocytes back to a foetal phenotype (Rog-Zielinska, *et al*., 2013). ANP is a hormone released from cardiomyocytes in a stretch-dependent fashion (De Bold, *et al*., 1981). Increased cytosolic calcium concentration, which is seen in a setting of hypertrophy, activates the phosphoinositide pathway leading to ANP secretion (Sonnenberg, 1986). Upon secretion, this peptide binds to its receptor, guanylyl cyclase-A (GC-A), and through a cGMP-mediated pathway it affects a number of physiological parameters (Holtwick, *et al*., 2002). It performs compensatory functions in an attempt to attenuate the progression of heart failure. It causes diuresis and natriuresis, it is hypotensive, anti-hypertrophic, anti-fibrotic and anti-proliferative, and it contributes to angiogenesis (reviewed in Saito, 2010). Indeed, ANP KO mice have salt-sensitive hypertension (John, *et al*., 1995) and GC-A KO mice have salt-insensitive hypertension (Lopez, *et al*., 1995). The mechanism of hypertension in the GC-A KO mouse is hypothesised to be due to inhibition of the

extravasation of blood from the intravascular space to the extravascular space (Holtwick, *et al*., 2002; Sabrane, *et al*., 2009).

After infarction, ANP has been shown to be vital for survival within the first seven days following occlusion, and that its action via the GC-A receptor attenuates fibrotic and hypertrophic responses (Nakanishi, *et al*., 2005). Myocardial and plasma ANP levels have been shown to increase after MI, and that increasing levels correlate with the extent of left ventricular dysfunction (Lu, *et al*., 2010; Vaz Perez, *et al*., 2010). As such, it can be used as a marker to help ascertain the degree of heart failure in an experimental model of MI. Since this study lacks sham-operated mice, myocardial ANP mRNA levels in mice 8w post-MI cannot be directly compared to levels after sham operations. However, ANP mRNA in the hearts from mice which underwent ligation surgery was detectable at a very low cDNA dilution (1/2) during qRT-PCR. This suggests ANP mRNA was abundant and, considering ANP has been shown to be present at very low levels in sham-operated hearts in other studies (Drexler, *et al*., 1989; Hama, *et al*., 1995), it can be hypothesised that the levels detected in the mice which underwent coronary artery ligation are markedly increased compared to baseline.

Another gene which is upregulated in heart failure is β-MHC (Buttrick, *et al*., 1991; Takahashi, *et al*., 1992). Cardiac muscle myosin is a hexameric protein which consists of two heavy chain subunits, two light chain subunits and two regulatory subunits. The heavy chain exists as two isoforms, α and β. In the myocardium of small mammals, such as mice, expression of the α isoform predominates (Lompre, *et al*., 1979) whereas this is reversed in humans, with the β isoform accounting for over 90% of the MHC subunits (Gorza, *et al*., 1984). The role of α-MHC in regulating

cardiac contractility has been shown by genetic manipulation in an experimental model of familial hypertrophic cardiomyopathy, with disruption of this gene resulting in cardiac dysfunction (Geisterfer-Lowrance, *et al*., 1996). A role for glucocorticoids has also been implicated, as glucocorticoids increase cardiac α-MHC expression and reduce β-MHC expression in rats (Sheer & Morkin, 1984). Transgenic mice which constitutively express β-MHC instead of α-MHC also showed a detrimental phenotype in response to chronic isoproterenol administration and in response to an MI model of heart failure (Krenz & Robbins, 2004). The ratio of α-MHC:β-MHC has been shown to directly correlate with cardiac function in both animals and humans (Miyata, *et al*., 2000; Abraham, *et al*., 2002; Herron & McDonald, 2002) and can thus be used to help determine the extent of heart failure in a model of infarction.

11β-HSD1 deficient mice showed a reduced lung weight, a reduction in myocardial ANP mRNA levels and an increased α-MHC:β-MHC ratio compared to C57BL/6 control mice. This indicates these mice have reduced remodelling 8w post-MI compared to control, and that global deficiency of 11β-HSD1 may attenuate the progression to heart failure 8w after infarction, which agrees with previous data (McSweeney, *et al*., 2010). In support of this conclusion, 11β-HSD1 deficient mice also have reduced dilatation and maintained systolic function, as well as shorter, thicker infarcts, which is discussed below.

SMAC mice, on the other hand, had no difference in any of these parameters compared to their Cre^- controls 8w post-MI. This agrees with the data in Chapter 4 which shows no change in any parameter in these mice after MI in the short term (<7d) compared to control. This suggests beneficial long term outcomes are

dependent on limiting early infarct expansion and that 11β-HSD1 in cardiomyocytes has no protective role in later remodelling. Further work to confirm this is necessary, possibly by using other models of heart failure, such as transaortic constriction or doxorubicin-induced heart failure.

5.4.3 Fibrosis and infarct size

The data presented here shows that the attenuated infarct thinning present in 11β-HSD1 deficient mice 28 days after infarction, is maintained through to eight weeks after infarction. Furthermore, 11β-HSD1 deficient mice also exhibited a reduced total infarct size as measured by both CINE MRI and Masson's Trichrome staining. This may be due to the enhanced angiogenesis previously reported in global 11β-HSD1 deficient mice (Small, *et al*., 2005; McSweeney, *et al*., 2010), which may help to limit early infarct expansion, thus maintaining function and attenuating dilatation in the longer term. This beneficial outcome is seen despite similar initial injury as measured by plasma cardiac troponin-I. The inability of SMAC mice to reproduce the favourable phenotype seen in 11β-HSD1 deficient mice after MI suggests 11β-HSD1 out with cardiomyocytes and VSMCs is responsible.

Following the inflammatory phase of infarct healing, a collagen-rich scar is formed which is necessary to maintain the structural integrity of the left ventricular wall, and to prevent cardiac rupture (Porter & Turner, 2009). Deposition of collagen type I and type III, and other molecules necessary for appropriate ECM remodelling, is primarily performed by myofibroblasts; cells which have differentiated from cardiac fibroblasts and assume phenotypic characteristics similar to smooth muscle cells

(Gabbiani, 1998). Expression of pro-inflammatory and pro-fibrotic cytokines, such as IL-1β, IL-6, TNFα and TGFβ are all increased in patients following infarction (Nian, *et al*., 2004). Fibroblast migration into tissues occurs as a result of the pro-inflammatory milieu of the infarcted heart, with TNFα and IL-1β being important chemoattractants (Nian, *et al*., 2004). IL-6, along with TNFα, has been shown to enhance fibroblast proliferation (Siwik, *et al*., 2000; Hellkvist, *et al*., 2002), with TGFβ known to stimulate fibroblast differentiation into myofibroblasts (Hao, *et al*., 2008). IL-1β and IL-6 have been shown to degrade the ECM, primarily through expression of MMPs, such as MMP-2, MMP-9, and MMP-13 (Siwik, *et al*., 2000). TGFβ also plays a crucial role in stimulating collagen, fibronectin and proteoglycan deposition from myofibroblasts (Eghbali, *et al*., 1991; Heimer, *et al*., 1995; Villarreal, *et al*., 1996). ANP, which is released from cardiomyocytes in heart failure, performs a contrasting role; it inhibits fibroblast proliferation, differentiation into myofibroblasts, and collagen synthesis (Li, *et al*., 2008). Myocardial levels of Col1α2, Col3α1 and TGFβ mRNA were similar in 11β-HSD1 deficient mice and control mice, suggesting similar myofibroblast activation. As such, it may be concluded that this is not the mechanism which results in 11β-HSD1 deficient mice having smaller infarcts.

Angiogenesis begins almost immediately after MI with endothelial cell sprouting and the formation of a primitive vessel network, which upon resolution of the inflammatory phase, is pruned and organised into an efficient network (Bergers & Song, 2005). Upon pericyte coating, these vessels mature and provide a long term blood supply to the surrounding tissue (Bergers & Song, 2005). Enhancing angiogenesis after infarction is key to salvaging affected ischaemic cardiomyocytes

in the peri-infarct region, and previous studies have shown augmenting this mechanism reduces infarct size and preserves cardiac function (Sasaki, *et al*., 2007). Moreover, maintenance of peri-infarct angiogenesis is crucial to prevent infarct expansion (Liu, *et al*., 2007). For example, in humans, capillary density in infarcted hearts correlates with reduced infarct size (Prech, *et al*., 2006).

Glucocorticoids have long been known to have anti-angiogenic effects, with 11β-HSD1 deficiency resulting in enhanced angiogenesis in subcutaneous sponge implants (Small, *et al*., 2005). Furthermore, 11β-HSD1 deficient mice fed a high fat diet have increased angiogenesis in adipose tissue which is hypothesised to protect this tissue from hypoxia, detrimental inflammation, metabolic abnormalities and fibrosis (Michailidou, *et al*., 2012). It may be hypothesised that increased peri-infarct angiogenesis in 11β-HSD1 deficient mice limits infarct expansion, leading to reduced remodelling. However, this still needs to be fully investigated. Since SMAC mice show a similar response to infarction, both acutely and in the long term, to control mice, it can be concluded that any possible change in peri-infarct angiogenesis is not a result of 11β-HSD1 deletion in cardiomyocytes or VSMCs. Key cell types involved in promoting and regulating angiogenesis include fibroblasts and alternatively-activated macrophages. As such, these cells are currently under investigation in the laboratory in a post-MI setting.

5.4.4 Cardiac size and function

Scar expansion and thinning, following resolution of the inflammatory phase, both contribute to adverse ventricular remodelling, and initial infarct size has been shown

to negatively correlate with morbidity and mortality (Pfeffer & Braunwald, 1990; Yang, *et al*., 2002a; Numaguchi, *et al*., 2006). Development of heart failure is characterised by several factors, including left ventricular dilatation and an increase in heart weight (Millar, *et al*., 2000; Gray & Sherry, 2002). Reduced cardiac function is also seen after MI, and has been reported in both human and animal studies (Pfeffer & Braunwald, 1990; Yang, *et al*., 2002a; Numaguchi, *et al*., 2006).

C57BL/6 mice and Cre^- control mice both showed similar left ventricular size to published values in other mouse models of hearts failure (Yang, *et al*., 2002b; Protti, *et al*., 2012), as well as heavier hearts compared to naïve mice (Chapter 3). Furthermore, they exhibited very low ejection fractions, in line with published data (Yang, *et al*., 2002b; Protti, *et al*., 2012), suggesting loss of systolic function. This suggests these mice did indeed show left ventricular dilatation. Coupled with the rest of the data in this chapter showing these mice had increased lung weight, increased ANP mRNA and reduced α-MHC:β-MHC ratio, it can be concluded this coronary artery ligation model does indeed lead to heart failure after eight weeks.

This study shows that global 11β-HSD1 deficiency results in attenuated left ventricular dilatation, as measured *in vivo* by MRI, as well as reduced heart weight as measured *ex vivo* by gravimetrics 8w after MI. The shorter, thicker infarcts present in 11β-HSD1 deficient mice may contribute to this phenotype, as reduced infarct thinning enhances the structural integrity of the heart. Correspondingly, ejection fraction is preserved in 11β-HSD1 deficient mice. However, this phenotype is not reproduced by 'cardiovascular' 11β-HSD1 deletion, with SMAC mice showing similar dilatation and ejection fraction to Cre^- controls. Taken together, the MRI and gravimetrics data suggests cardiovascular 11β-HSD1 deletion does not attenuate left

ventricular dilatation or maintain cardiac function 8w after MI and 11β-HSD1 out with the cardiovascular system appears to be responsible for the beneficial outcome seen in globally 11β-HSD1 deficient mice.

Recent clinical trials into blockade of MR in the Randomised Aldactone Evaluation Study (RALES) and the Eplerenone Post Acute Myocardial Infarction Heart Failure Efficacy and Survival Study (EPHESUS) have demonstrated the beneficial effects of selectively blocking these receptors in patients with heart failure, whereby these patients showed reduced remodelling and reduced myocardial fibrosis (Pitt, *et al*., 1999; Pitt, *et al*., 2003). In experimental models, eplerenone has been shown to accelerate macrophage infiltration, enhance peri-infarct angiogenesis and maintain left ventricular function in rats when administered immediately after coronary artery ligation (Fraccarollo, *et al*., 2008). Allowing aldosterone access to MR in cardiomyocytes, by overexpressing 11β-HSD2 in these cells, and thus reducing intracellular availability of glucocorticoids, leads to cardiac hypertrophy (Qin, *et al*., 2003). It may be hypothesised that a similar situation is seen with 11β-HSD1 deletion in cardiomyocytes (SMAC mice). Deletion of 11β-HSD1 specifically in these cells may also allow aldosterone access to MR, and thus result in a post-MI response similar to control, particularly since aldosterone has been shown to increase after infarction (Ceremuzynski, 1981). In globally 11β-HSD1 deficient mice, this adverse, or similar, response may be overcome by deletion of the enzyme in another cell type. For example, 11β-HSD1 deletion in fibroblasts, alternatively-activated macrophages or another cell type may be key to the differences observed in remodelling in 11β-HSD1 deficient mice versus SMAC mice, and they thus warrant further investigation. Attenuation of heart failure in a non-MI model by

administration of an 11β-HSD1 inhibitor further suggests that alterations of mechanisms over and above manipulating infarct size contribute to this beneficial outcome (Gordon, *et al*., 2014).

Electrophysiological changes also occur in heart failure, with several clinical studies in the 1990s reporting reduced SERCA mRNA levels and protein expression (Mercadier, *et al*., 1990; Takahashi, *et al*., 1992) and a subsequent increase in NCX mRNA and protein expression (Studer, *et al*., 1994; Flesch, *et al*., 1996) in this disease setting. Considering that naïve SMAC mice have lower SERCA mRNA levels and protein expression under basal conditions (Chapter 3), it was hypothesised that these mice may have had an exaggerated response to heart failure. However, mRNA levels and protein expression of SERCA and protein expression of NCX was similar across all groups suggesting this is not the case. The degree of SERCA expression relative to sham was not investigated, due to a lack of sham-operated mice in this study, and should be included in future studies, as should the regulation of SERCA by phospholamban. Phospholamban is a key regulator of SERCA activity and changes in protein expression, or its phosphorylation state, which regulates its inhibitory influence on SERCA, may provide further insights into calcium regulation during heart failure in these mice.

In conclusion, the data presented in this chapter suggests that the beneficial outcome seen 8 weeks after MI in mice globally deficient in 11β-HSD1, is not due to deletion of the enzyme in cardiomyocytes or VSMCs. As such, deletion of 11β-HSD1 out with these cell types appears to be responsible for maintaining scar thickness, attenuating infarct thinning and left ventricular dilatation and preserving systolic function through to 8w post-MI. Along with the data presented in Chapter 4, this

may suggest a key role for 11β-HSD1 deficiency in neutrophils, macrophages, or fibroblasts in modifying initial inflammatory and angiogenic pathways, leading to beneficial outcomes acutely and chronically after infarction.

This data therefore suggests that it is not lack of 11β-HSD1 in myocardial cells which maintains the beneficial phenotype seen in global 11β-HSD1 deficient mice at 28d post-MI, but rather loss of 11β-HSD1 in another cell type. Considering the data in this chapter, and the data in Chapter 4, recruited neutrophils, macrophages, or cardiac fibroblasts may be key to this beneficial outcome.

Chapter 6

General Discussion

11β-HSD1 is found in numerous cells in the heart, including cardiomyocytes, VSMCs, fibroblasts, and the vascular wall (Hadoke, *et al*., 2001; Christy, *et al*., 2003; Klusonova, *et al*., 2009; McSweeney, *et al*., 2010). This thesis aimed to determine the relative role of 11β-HSD1 in cardiomyocytes and VSMCs.

The first hypothesis investigated in this thesis was that deletion of 11β-HSD1 in cardiomyocytes and VSMCs would result in smaller, lighter hearts, but would not influence cardiac function. The second hypothesis was deletion of 11β-HSD1 in these cells would reproduce the beneficial post-MI phenotype previously seen in global 11β-HSD1 deficient mice.

6.1 11β-HSD1 in cardiomyocytes and VSMCs influences the physiological function of the heart

11β-HSD1 expression in the heart is relatively modest compared to other tissues, such as the liver, and expression is primarily found in fibroblasts (Brereton, *et al*., 2001). As such, 11β-HSD1 expression in cardiomyocytes and VSMCs contributes a small proportion to the overall 11β-HSD1 protein levels in the heart. Despite this low level, 11β-HSD1 expression in the heart is critical to normal cardiac structure and function. For example, investigation of the basal cardiac phenotype of mice globally deficient in 11β-HSD1 revealed these mice had reduced heart size and weight (McSweeney, 2010), however, the reason for this was unknown. 11β-HSD1 has also been shown to regulate heart size in a human population study, with a single nucleotide polymorphism in the *Hsd11b1* gene associating with reduced left ventricular mass in a human population study (Rahman, *et al*., 2011). The data in this

thesis (Chapter 3) show that global 11β-HSD1 deletion has no influence on cardiomyocytes cross-sectional area, but rather results in shorter cardiomyocytes in young adult males. This does not appear to be due to loss of the enzyme in cardiomyocytes (or VSMCs) themselves, as this phenotype is not reproduced in SMAC mice. As such, the mechanism behind this phenotype may lie with other cells present in the heart which express 11β-HSD1, such as cardiac fibroblasts (Brereton, *et al*., 2001) or macrophages, which are known to express 11β-HSD1 in other tissues (Gilmour, *et al*., 2006).

The work in this thesis shows that global 11β-HSD1 deletion results in mild diastolic dysfunction, a phenotype reproduced by cardiovascular-specific deletion and chronic 11β-HSD1 inhibition (Chapter 3). Further investigation into this diastolic phenotype revealed that this may be due to reduced expression of SERCA, a transporter which is crucial for reuptake of calcium back into the sarcoplasmic reticulum after cellular contraction (Periasamy & Kalyanasundaram, 2007). A reduction in SERCA, either in genetic KO animals or in a pathological setting such as heart failure, is normally compensated for by an increase in NCX, so as to sustain calcium removal from the cytosol and maintain normal cardiomyocyte relaxation (Limas, *et al*., 1987; Dash, *et al*., 2001; Li, *et al*., 2011). However, NCX mRNA levels are not increased in DelI, SMAC or UE2316-treated mice, suggesting this reduction in SERCA may be compensated for in some other way in these mice. For example, reduced SERCA has been shown to lead to increased intracellular calcium concentration during diastole, which in itself enhances SERCA activity (Stokke, *et al*., 2010; Li, *et al*., 2011).

In terms of regulation of SERCA activity, a reduction in overall SERCA protein expression was not compensated for by reduced expression of its key regulator

phospholamban, or by increased phospholamban phosphorylation at Serine 16 or Threonine 17, which would have resulted in reduced inhibition of SERCA function. The ratio of phospholamban to SERCA is a key regulator of contractility as experiments using murine atrial and ventricular tissue, which express differential levels of phospholamban, have shown (Koss, et al., 1997). Indeed, studies using phospholamban KO mice demonstrated these hearts have increased left ventricular contractility, thus reinforcing the importance of the phosopholamban:SERCA ratio (Koss, et al., 1997).

Assessment of SERCA activity and intracellular calcium flux merits further investigation in isolated cardiomyocytes, and in isolated hearts using a Langendorff preparation, in order to fully understand whether cytosolic calcium availability is modified in these mice. If this is the case, and considering systolic function is unaltered in these mice, it may be hypothesised that contractile filament sensitivity may therefore be increased to account for unaltered contractile function, although further functional studies in isolated cardiomyocytes are required to investigate this.

In a pathophysiological setting, such as heart failure, a reduction in SERCA mRNA levels and protein expression are commonly seen (Mercadier, *et al*., 1990; Takahashi, *et al*., 1992). However, 8w after MI, SERCA expression was not altered in 11β-HSD1 deficient mice or SMAC mice, and there was no compensatory increase in NCX mRNA levels, relative to their respective controls. The unaltered expression of NCX may help to prevent sodium accumulation, which is seen in the SERCA KO mouse, and contributes to diastolic dysfunction (Louch, *et al*., 2010; Li, *et al*., 2012). However, the degree of SERCA expression relative to sham was not investigated, due to a lack of sham-operated mice in this study, and should be included in future

studies, as should the regulation of SERCA by phospholamban, by determining phospholamban protein expression and phosphorylation levels.

The data presented in this thesis suggest that, despite a reduction in basal SERCA expression, loss of 11β-HSD1 is overall beneficial in terms of preventing heart failure. Therefore, it remains an area of potential therapeutic benefit.

6.2 11β-HSD1 in locations distinct from cardiomyocytes and VSMCs influences cardiac growth and the response to MI

Loss of 11β-HSD1 only in cardiomyocytes and VSMCs does not impact upon heart size, but loss elsewhere results in a reduced heart weight and shorter cardiomyocytes. Therefore, the mechanism behind this phenotype may lie with other cells present in the heart which express 11β-HSD1, such as cardiac fibroblasts (Brereton, *et al*., 2001) or macrophages (Gilmour, *et al*., 2006), or perhaps in another tissue completely. For example, male mice have high levels of 11β-HSD1 mRNA in the kidney (Rajan, e*t al*., 1995), an organ heavily involved with blood volume and blood pressure regulation; factors which directly influence cardiomyocyte length (De Simone, 2003; Hanft, *et al*., 2008). These parameters were unaltered in the present study, however other factors secreted from the kidney may play a role. Peroxisome proliferator-activator receptor-γ (PPAR-γ), which is present on cardiomyocytes (Saris, *et al*., 2001) and renin, which is secreted by the kidney, have also been shown to regulate cardiomyocyte length (Hinrichs, *et al*., 2011). Blood volume and blood pressure are unaffected by global 11β-HSD1 deletion, but levels of PPAR-γ and renin were not investigated and should be considered for further studies. This is

despite the well known effect of glucocorticoids on elevating blood pressure (Connell, *et al*., 1987; Fraser, *et al*., 1999; Masuzaki, *et al*., 2003; Van Raalte, *et al*., 2013). Therefore, 11β-HSD1 deletion in another cell type, or types, must be responsible.

Cardiac fibroblasts secrete a number of growth factors crucial for cardiomyocytes growth, such as FGF-2, IL-33, LIF and CT-1 (Matsui, *et al*., 1996; Wollert, *et al*., 1996; Wang, *et al*., 2002; Jiang, *et al*., 2007). Resident macrophages also secrete growth factors, with IGF-1 being particularly prominent with regards to stimulating cardiomyocyte growth (Gow, *et al*., 2010). Glucocorticoids are known to upregulate expression of hypertrophic genes (Yoshikawa, *et al*., 2009) and so loss of 11β-HSD1 in one or both of these cell types may alter the expression and secretion of growth factors. However, these growth factors are primarily known for regulating cardiomyocyte cross-sectional area and their influence on cardiomyocytes length has not been explored. Isolation of these cell types from DelI hearts, and investigation into their growth factor profile, may help to elucidate why global 11β-HSD1 deletion results in shorter cardiomyocytes.

The expression of 11β-HSD1 in the cardiac fibroblasts of SMAC mice should also be investigated. Previous work has shown that inserting a Cre recombinase transgene into the *Sm22α* gene may have an effect on gene expression in myofibroblasts, as *Sm22α* has been found to be expressed in isolated myofibroblasts from rabbit bladder (Chiavegato, *et al*., 1999). However, *Sm22α* does not appear to be expressed in isolated human fibroblasts from COPD patients (Hallgren, *et al*., 2010). This suggests 11β-HSD1 expression may not be altered in cardiac fibroblasts in SMAC mice but nevertheless, this should be confirmed by immunohistochemical staining.

The transient nature of this phenotype is also an area of interest. DelI mice show reduced heart size at 10 weeks of age but heart size and cardiomyocyte cross-sectional area (Appendix 3) is similar to C57BL/6 at 18 months of age, suggesting normal cardiomyocyte lengthening may be delayed rather than completely abrogated. It would be of interest to investigate cardiomyocyte length in neonate mice, or at other early post-natal stages in order to determine whether the trajectory of growth is delayed at other stages. GR-mediated glucocorticoid signalling has been shown to be critical for normal heart maturation during development (Rog-Zielinska, *et al*., 2013), showing a role for glucocorticoids in regulating cardiac size and function. It may, therefore, be hypothesised that glucocorticoid amplification by 11β-HSD1 is necessary for appropriate heart growth during early post-natal development and the progression to adulthood.

Administration of a selective 11β-HSD1 inhibitor, UE2316, for 9 months to adult C57BL/6SJL mice resulted in these mice showing a trend for larger, rather than smaller, hearts as assessed by high frequency ultrasound, and heavier, rather than lighter, hearts as weighed at post-mortem, however this was not due to a change in cardiomyocyte cross-sectional area. This suggests that inhibition of 11β-HSD1 in adults may have a separate effect to that seen in younger mice. Blood pressure and circulating cortisol are both known to increase with age, and both have been shown to enhance the development of cardiac hypertrophy (Landahl, *et al*., 1986; Van Cauter, *et al*., 1996; Walker, 2007a; De, *et al*., 2011; Drazner, 2011). As such, it may be hypothesised that global 11β-HSD1 deletion or chronic 11β-HSD1 inhibition may result in impaired GR-mediated negative feedback by glucocorticoids, due to reduced intracellular glucocorticoid bioavailability. In addition, the phenotype in UE2316-

treated mice may be a result of unknown off-target effects of UE2316, or that partial 11β-HSD1 inhibition gives a different phenotype to complete KO. Further investigation into off-target drug effects, heart weight, blood pressure and corticosterone levels in 11β-HSD1 deficient mice at 18 months of age is therefore required. Moreover, further studies should attempt to elucidate the mechanism of this phenotype in UE2316-treated mice; for example, assessment of blood pressure, blood volume and myocardial interstitial fluid.

Loss of 11β-HSD1 in cardiomyocytes and VSMCs does not reproduce the beneficial outcome seen previously with global 11β-HSD1 deficiency after MI, suggesting a key role for another cell type(s). This agrees with bone marrow experiments conducted in our laboratory using irradiated DelI mice. These mice received transplantation of wild-type bone marrow prior to coronary artery ligation surgery and demonstrated a beneficial phenotype after MI, suggesting that 11β-HSD1 deficiency in the host mouse is key to an improved post-MI outcome (Mylonas, *et al*., unpublished). As such, current studies are focussing on inhibiting 11β-HSD1 in fibroblasts to determine the role of 11β-HSD1 in this cell type in this setting. This may uncover a mechanism behind the enhanced inflammatory response seen previously in 11β-HSD1 deficient mice.

It has previously been reported that 11β-HSD1 deficient mice have enhanced peri-infarct angiogenesis 4w after MI (McSweeney, *et al*., 2010), after the pruning phase of excess vessels by endothelial cell apoptosis has passed (Patan, 2000; Conway, *et al*., 2001; Grass, *et al*., 2006), which attenuates the development of heart failure. The data in this thesis demonstrates that the beneficial phenotype observed in global 11β-HSD1 deficient mice 4w after MI is maintained through to 8w after MI when mice

have developed heart failure. It has been shown that sustained enhanced angiogenesis limits infarct expansion and thinning, and contributes to the maintenance of cardiac function (Orlic, *et al*., 2001; Kido, *et al*., 2005; Engel, *et al*., 2006; Liu, *et al*., 2007; Payne, *et al*., 2007; Sasaki, *et al*., 2007). This was not assessed in the current study and should be investigated by immunohistochemical staining, however the thicker infarcts and preserved systolic function seen in 11β-HSD1 deficient mice indicate that this enhanced angiogenesis may be sustained through to 8w after MI.

6.2.1 Why does 11β-HSD1 deletion lead to ventricular rupture, but 11β-HSD1 deficiency does not?

It has previously been shown that 11β-HSD1 deficient mice have a beneficial phenotype 7d and 4w after MI (Small, *et al*., 2005; McSweeney, *et al*., 2010). These mice, originally generated by Koteletsev *et al* (1997), have an augmented inflammatory response, with increased representation of pro-reparative alternatively-activated macrophages, enhanced peri-infarct angiogenesis, thicker infarcts and improved cardiac function (McSweeney, *et al*., 2010). However, as has been discussed above, there are profound basal effects of 11β-HSD1 deletion in cells other than cardiomyocytes and VSMCs, such as regulation of cardiomyocyte length. The beneficial outcome outlined above was not reproduced with tissue specific 11β-HSD1 deletion in cardiomyocytes and VSMCs, suggesting 11β-HSD1 deletion in other cells types may be responsible for this phenotype. Current studies in our laboratory have shown definitively that 11β-HSD1 deletion in myeloid cells does not give rise to this beneficial phenotype (Mylonas, *et al*., unpublished), however the role of 11β-HSD1 in fibroblasts after MI warrants further investigation. 11β-HSD1

has been shown to modify fibroblast inflammatory mediatory secretion (Mylonas, *et al*., unpublished), and, as such, could be the case here.

Since the creation of the original 11β-HSD1 'KO' mouse (Kotelevtsev, *et al*., 1997), it has been found to be deficient, rather than null, for 11β-HSD1, and has therefore been referred to as such throughout this thesis. This is the key difference between this mouse and the DelI mouse, which is a complete KO. After MI, all DelI mice died from cardiac rupture between d3 and d5. Recent work in our lab has started to uncover the mechanism behind the 100% rate of rupture in DelI mice after coronary artery ligation. As discussed above, 11β-HSD1 in cardiac fibroblasts may be key in regulating the improved outcome in mice deficient in 11β-HSD1, through regulation of macrophage phenotype in the proliferative phase of infarct healing. However, the differences in propensity to rupture in the earlier phase of infarct healing suggests 11β-HSD1 is also important in regulating early inflammatory cell recruitment to the infarct (Mylonas, *et al*., unpublished). Neutrophil recruitment is enhanced in 11β-HSD1 deficient mice (McSweeney, 2010; McSweeney, *et al*., 2010) but not to the extent that it is in mice with complete deletion of 11β-HSD1 (DelI mice). Expression of MCP-1 and monocyte recruitment are also both significantly increased in DelI mice (Mylonas, *et al*., unpublished) and this is associated with the increased rate of rupture, in agreement with other studies linking monocyte recruitment to rupture (Nian, *et al*., 2004). This shows, firstly, the importance of 11β-HSD1 as a regulator of the inflammatory response and, furthermore, suggests that targeting 11β-HSD1 in cardiac myofibroblasts may be key to improving outcomes post-MI.

With respect to the administration of potential drug treatments, it may by hypothesised that delaying 11β-HSD1 inhibition, so as not to detrimentally enhance

early inflammatory cell recruitment, may lead to a beneficial acute, and long term, outcome. Indeed one method of inducing heart failure is chronic isoproterenol treatment (Gordon, *et al*., 2014). After 3w of treatment, cardiac dysfunction and hypertrophy are observed, but this is completely reversed by administration of a selective 11β-HSD1 inhibitor (Gordon, *et al*., 2014). This is promising, as it shows that delayed 11β-HSD1 inhibition can still lead to a beneficial outcome. This may circumvent the fatal phenotype seen with complete global 11β-HSD1 deletion; overly-enhanced inflammatory cell recruitment. As such, pharmacological 11β-HSD1 inhibition should therefore continue to be explored as a potential area of therapeutic intervention after MI.

Chapter 7

References

Abraham, W. *et al*., 2002. Coordinate changes in myosin heavy chain gene expression are selectively associated with alterations in dilated cardiomyopathy phenotype. *Molecular Medicine,* Volume 8 (11), pp. 750-760.

Adachi, Y. *et al*., 2003. Angiotenisin II type 2 receptor deficiency exacerbates heart failure and reduces survival after acute myocardial infarction in mice. *Circulation,* Volume 107, pp. 2406-2408.

Adams III, J. *et al*., 1993. Cardiac troponin I. A marker with high specificity for cardiac injury. *Circulation,* Volume 88, pp. 101-106.

Aguilera, G., Rabadan-Diehl, C. & Nikodemova, M., 2001. Regulation of pituitary corticotropin releasing hormone receptors. *Peptides,* Volume 22 (5), pp. 769-774.

Albiston, A., Obeyesekere, V., Smith, R. & Krozowski, Z., 1994. Cloning and tissue distribution of the human 11 beta-hydroxysteroid dehydrogenase type 2 enzyme. *Molecular and Cellular Endocrinology,* Volume 105 (2), pp. R11-R17.

Arriza, J. *et al*., 1987. Cloning of human mineralocorticoid receptor complementary DNA: structural and functional kinship with the glucocorticoid receptor. *Science,* Volume 237 (4812), pp. 268-275.

Auffray, C., Sieweke, M. & Geissmann, F., 2009. Blood monocytes: development, heterogeneity, and relationship with dendritic cells. *Annual Review of Immunology,* Volume 27, pp. 669-692.

Axelrod, J. & Reisine, T., 1984. Stress hormones: their interaction and regulation. *Science,* Volume 224 (4648), pp. 452-459.

Ayroldi, E. & Riccardi, C., 2009. Glucocorticoid-induced leucine zipper (GILZ): a new important mediator of glucocorticoid action. *The Journal of the Federation of American Societies for Experimental Biology,* Volume 23, pp. 3649-3658.

Baker, D. *et al*., 1998. Targeted overexpression of the sarcoplasmic reticulum Ca^{2+}-ATPase increases cardiac contractility in transgenic mouse hearts. *Circulation Research,* Volume 83 (12), pp. 1205-1214.

Balamayooran, G. *et al*., 2011. Monocyte chemoattractant protein-1 regulates pulmonary host defense via neutrophil recruitment during Escherichia coli infection. *Infection and Immunity,* Volume 79 (7), pp. 2567-2577.

Barnes, P., 1998. Anti-inflammatory actions of glucocorticoids: molecular mechanisms. *Clinical Science (London),* Volume 94 (6), pp. 557-572.

Barzilai, D. *et al*., 1972. Use of hydrocortisone in the treatment of acute myocardial infarction. Summary of a clinical trial in 446 patients. *Chest,* Volume 61 (5), pp. 488-491.

Bassani, R., Bassani, J. & Bers, D., 1992. Mitochondrial and sarcolemmal Ca^{2+} transport reduce $[Ca^{2+}]i$ during caffeine contractures in rabbit cardiac myocytes. *Physiology,* Volume 453, pp. 591-608.

Beck, I. *et al*., 2009. Crosstalk in inflammation: the interplay of glucocorticoid receptor-based mechanisms and kinases and phosphatases. *Endocrine Reviews,* Volume 30 (7), pp. 830-882.

Beg, A., 2002. Endogenous ligands of toll-like receptors: implications for regulating inflammatory and immune responses. *Trends in Immunology,* Volume 23 (11), pp. 509-512.

Beggah, A. *et al*., 2002. Reversible cardiac fibrosis and heart failure induced by conditional expression of an antisense mRNA of the mineralocorticoid receptor in cardiomyocytes. *Proceedings of the National Academy of Sciences,* Volume 99 (10), pp. 7160-7165.

Bergers, G. & Song, S., 2005. The role of pericytes in blood-vessel formation and maintenance. *Neuro Oncology,* Volume 7 (4), pp. 452-464.

Bers, D., 2001. *Excitation-contraction coupling and cardiac contractile force.* 2nd ed. Dordrecht: Kluwer Academic Publishers.

Berse, B. *et al*., 1992. Vascular permeability factor (vascular endothelial growth factor) gene is expressed differentially in normal tissues, macrophages, and tumors. *Molecular Biology of the Cell,* Volume 3, pp. 211-220.

Bledsoe, R., Stewart, E. & Pearce, K., 2004. Structure and function of the glucocorticoid receptor ligand binding domain. *Vitamins and Hormones,* Volume 68, pp. 49-91.

Blum, A., Martin, H. & Maser, E., 2000. Human 11beta-hydroxysteroid dehydrogenase type 1 enzyme is enzymatically active in its nonglycosylated form. *Biochemical and Biophysical Research Communications,* Volume 276 (2), pp. 428-434.

Brant, E. *et al*., 2000. IL-4 production by human polymorphonuclear neutrophils. *Leukocyte Biology,* Volume 68, pp. 125-130.

Brem, A., Bina, R., King, T. & Morris, D., 1998. Localization of 2 11beta-OH steroid dehydrogenase isoforms in aortic endothelial cells. *Hypertension,* Volume 31 (1), pp. 459-462.

Brem, A., 2001. Insights into glucocorticoid-associated hypertension. *American Journal of Kidney Diseases,* Volume 37 (1), pp. 1-10.

Brereton, P. *et al*., 2001. Light and electron microscopy localization of the 11beta-hydroxysteroid dehydrogenase type 1 enzyme in the rat. *Endocrinology,* Volume 142 (4), pp. 1644-1651.

Briaud, S. *et al*., 2001. Leukocyte trafficking and myocardial reperfusion injury in ICAM-1/P-selectin-knockout mice. *American Journal of Physiology,* Volume 280, pp. H60-H67.

Brown, R. *et al*., 1996. The ontogeny of 11 beta-hydroxysteroid dehydrogenase type 2 and mineralocorticoid receptor gene expression reveal intricate control of glucocorticoid action in development. *Endocrinology,* Volume 137 (2), pp. 794-797.

Bruley, C. *et al*., 2006. A novel promoter for the 11β-hydroxysteroid dehydrogenase type 1 gene is active in lung and is C/EBPa independent. *Endocrinology,* Volume 147 (6), pp. 2879-2885.

Buckingham, J., 2006. Glucocorticoids: exemplars of multitasking. *British Journal of Pharmacology,* Volume 147, pp. S258-S268.

Bujalska, I. *et al*., 2002. A switch in dehydrogenase to reductase activity of 11 beta-hydroxysteroid dehydrogenase type 1 upon differentiation of human omental adipose stromal cells. *Clinical Endocrinology and Metabolism,* Volume 87 (3), pp. 1205-1210.

Bujalska, I. *et al*., 2005. Hexose-6-phosphate dehydrogenase confers oxo-reductase activity upon 11β-hydroxysteroid dehydrogenase type 1. *Molecular Endocrinology,* Volume 34, pp. 675-684.

Bull, D. *et al*., 2003. Effect of terplex/VEGF-165 gene therapy on left ventricular function and structure following myocardial infarction. VEGF gene therapy for myocardial infarction. *Controlled Release,* Volume 93 (2), pp. 175-181.

Burton, J., Kehrli, M., Kapil, S. & Horst, R., 1995. Regulation of L-selectin and CD18 on bovine neutrophils by glucocorticoids: effects of cortisol and dexamethasone. *Leukocyte Biology,* Volume 57 (2), pp. 317-325.

Buttrick, P. *et al*., 1991. Effects of chronic dobutamine on cardiac mechanics and biochemistry after myocardial infarction in rats. *American Journal of Physiology,* Volume 260, pp. H473-H479.

Cannell, M. & Soeller, C., 1997. Numerical analysis of ryanodine receptor activation by L-type channel activity in the cardiac muscle diad. *Biophysical Journal,* Volume 73 (1), pp. 112-122.

Carter, R. *et al*., 2009. Hypothalamic-pituitary-adrenal axis abormalities in response to deletion of 11β-HSD1 is strain-dependent. *Neuroendocrinology,* Volume 21, pp. 879-887.

Cavalcanti, D. *et al*., 2007. Endogenous glucocorticoids control neutrophil mobilization from bone marrow to blood and tissues in non-inflammatory conditions. *British Journal of Pharmacology,* Volume 152 (8), pp. 1291-1300.

Celletti, F. *et al*., 2001. Vascular endothelial growth factor enhances atherosclerotic plaque progression. *Nature Medicine,* Volume 7 (4), pp. 425-429.

Ceremuzynski, L., 1981. Hormonal and metabolic reactions evoked by acute myocardial infarction. *Circulation Research,* Volume 48 (6), pp. 767-776.

Chao, W., Shen, Y., Li, L. & Rosenzweig, A., 2002. Importance of FADD signaling in serum deprivation- and hypoxia-induced cardiomyocyte apoptosis. *Biological Chemistry,* Volume 277 (35), pp. 31639-31645.

Chapman, K. *et al*., 2009. The role and regulation of 11β-hydroxysteroid dehydrogenase type 1 in the inflammatory response. *Molecular and Cellular Endocrinology,* Volume 301, pp. 123-131.

Chapman, K., Holmes, M. & Seckl, J., 2013. 11β-hydroxysteroid dehydrogenases: intracellular gate-keepers of tissue glucocorticoid action. *Physiological Reviews,* Volume 93, pp. 1139-1206.

Cheng, H., Lederer, W. & Cannell, M., 1993. Calcium sparks: elementary events underlying excitation-contraction coupling in heart muscle. *Science,* Volume 262 (5134), pp. 740-744.

Cheung, J. *et al*., 2007. Regulation of cardiac Na^{+}/Ca^{2+} exchanger by phospholemman. *Annals of the New York Academy of Sciences,* Volume 1099, pp. 119-134.

Chiavegato, A. *et al*., 1999. Differential expression of SM22 isoforms in myofibroblasts and smooth muscle cells from rabbit bladder. *Muscle Research and Cell Motility,* Volume 20 (2), pp. 133-146.

Cho, C. *et al*., 2000. The Na^{+}-Ca^{2+} exchanger is essential for embryonic heart development in mice. *Molecules and Cells,* Volume 10 (6), pp. 712-722.

Christy, C. *et al*., 2003. 11beta-hydroxysteroid dehydrogenase type 2 in mouse aorta: localization and influence on response to glucocorticoids. *Hypertension,* Volume 42 (4), pp. 580-587.

Chrousos, G., 2004. Is 11β-hydroxysteroid dehydrogenase type 1 a good therapeutic target for blockade of glucocorticoid actions?. *Proceedings of the National Academy of Sciences,* Volume 101 (17), pp. 6329-6330.

Clark, A. & Cleland, J., 2013. Causes and treatment of oedema in patients with heart failure. *Nature Reviews Cardiology,* Volume 10, pp. 156-170.

Clark, R., Nielsen, L., Welch, M. & McPherson, J., 1995. Collagen matrices attenuate the collagen-synthetic response of cultured fibroblasts to TGF-beta. *Cell Science,* Volume 108, pp. 1251-1261.

Coelho, F. *et al*., 2008. The chemokine receptors CXCR1/CXCR2 modulate antigen-induced arthritis by regulating adhesion of neutrophils to the synovial microvasculature. *Arthritis and Rheumatism,* Volume 58 (8), pp. 2329-2337.

Cohen, B., Danon, D. & Roth, G., 1987. Wound repair in mice as influenced by age and antimacrophage serum. *Gerontology,* Volume 42 (3), pp. 295-301.

Cohn, J., Ferrari, R. & Sharpe, N., 2000. Cardiac remodeling - concepts and clinical implications: a consensus paper from an international forum on cardiac remodeling. *Journal of the American College of Cardiology,* Volume 35 (3), pp. 569-582.

Cole, T. *et al*., 1995. Targeted disruption of the glucocorticoid receptor gene blocks adrenergic chromaffin cell development and severely retards lung maturation. *Genes and Development,* Volume 9, pp. 1608-1621.

Connell, J. *et al*., 1987. Effects of ACTH and cortisol administration on blood pressure, electrolyte metabolism, atrial natriuretic peptide and renal function in normal man. *Hypertension,* Volume 5 (4), pp. 425-433.

Conway, E., Collen, D. & Carmeliet, P., 2001. Molecular mechanisms of blood vessel growth. *Cardiovascular Research,* Volume 49 (3), pp. 507-521.

Cooper, M. & Stewart, P., 2009. 11β-hydroxysteroid dehydrogenase type and its role in the hypothalamus-pituitary-adrenal axis, metabolic syndrome, and inflammation. *Clinical Endocrinology and Metabolism,* Volume 94 (12), pp. 4645-4654.

Coutinho, A., 2009. *Consequences of 11β-hydroxysteroid dehydrogenase deficiency during inflammatory responses.* Edinburgh: University of Edinburgh.

Cronstein, B. *et al*., 1992. A mechanism for the antiinflammatory effects of corticosteroids: the glucocorticoid receptor regulates leukocyte adhesion to endothelial cells and expression of endothelial-leukocyte adhesion molecule 1 and intercellular adhesion molecule 1. *Proceedings of the National Academy of Sciences,* Volume 89, pp. 9991-9995.

Cuzzocrea, S. *et al*., 1999. IL-6 knock-out mice exhibit resistance to splanchnic artery occlusion shock. *Leukocyte Biology,* Volume 66 (3), pp. 471-480.

Dai, W., Wold, L., Dow, J. & Kloner, R., 2005. Thickening of the infarcted wall by collagen injection improves left ventricular function in rats: a novel approach to preserve cardiac function after myocardial infarction. *Journal of the American College of Cardiology,* Volume 46 (4), pp. 714-719.

Dash, R. *et al*., 2001. Gender influences on sarcoplasmic reticulum Ca^{2+}-handling in failing human myocardium. *Molecular and Cellular Cardiology,* Volume 33 (7), pp. 1345-1353.

De, P., Ghose Roy, S., Kar, D. & Bandyopadhyay, A., 2011. Excess of glucocorticoid induces myocardial remodeling and alteration of calcium signaling in cardiomyocytes. *Endocrinology*, Volume 209, pp. 105-114.

De Bold, A., Borenstein, H., Veress, A. & Sonnenberg, H., 1981. A rapid and potent natriuretic response to intravenous injection of atrial myocardial extract in rats. *Life Sciences,* Volume 28 (1), pp. 89-94.

De Bosscher, K., Vanden Berghe, W. & Haegeman, G., 2003. The interplay between the glucocorticoid receptor and nuclear factor-kappaB or activator protein-1: molecular mechanisms for gene repression. *Endocrine Reviews,* Volume 24 (4), pp. 488-522.

De Haan, J., Smeets, M., Pasterkamp, G. & Arslan, F., 2013. Danger signals in the initiation of the inflammatory response after myocardial infarction. *Mediators of Inflammation,* Volume 2013, pp.1-13.

De Matteo, R. & May, C., 1997. Glucocorticoid-induced renal vasodilatation is mediated by a direct renal action involving nitric oxide. *American Journal of Physiology*, Volume 273 (6), pp. 1972-1979.

De Simone, G., 2003. Left ventricular geometry and hypotension in end-stage renal disease: a mechanical perspective. *Journal of the American Society of Nephrology,* Volume 14, pp. 2421-2427.

De Sousa Peixoto, R. *et al*., 2008. Preadipocyte 11β-hydroxysteroid dehydrogenase type 1 is a keto-reductase and contributes to diet-induced visceral obesity in vivo. *Endocrinology*, Volume 149 (4), pp. 1861-1868.

De Souza, R., 2002. Aging of myocardial collagen. *Biogerontology,* Volume 3 (6), pp. 325-335.

Dean, R. *et al*., 2005. Connective tissue growth factor and cardiac fibrosis after myocardial infarction. *Histochemistry and Cytochemistry,* Volume 53 (10), pp. 1245-1256.

DeBosch, B. *et al*., 2006. Akt1 is required for physiological cardiac growth. *Circulation,* Volume 113, pp. 2097-2104.

Dewald, O. *et al*., 2005. CCL2/monocyte chemoattractant protein-1 regulates inflammatory responses critical to healing myocardial infarcts. *Circulation Research,* Volume 96 (8), pp. 881-889.

Dhalla, A., Hill, M. & Singal, P., 1996. Role of oxidative stress in transition of hypertrophy to heart failure. *Journal of the American College of Cardiology,* Volume 28 (2), pp. 506-514.

Dispersyn, G. *et al*., 2001. Adult rabbit cardiomyocytes undergo hibernation-like dedifferentiation when co-cultured with cardiac fibroblasts. *Cardiovascular Research,* Volume 51, pp. 230-240.

Dobrucki, L. *et al*., 2010. Analysis of angiogenesis induced by local IGF-1 expression after myocardial infarction using microSPECT-CT imaging. *Molecular and Cellular Cardiology,* Volume 48 (6), pp. 1071-1079.

Draper, N. & Stewart, P., 2005. 11beta-hydroxysteroid dehydrogenase and the pre-receptor regulation of corticosteroid hormone action. *Endocrinology,* Volume 186 (2), pp. 251-271.

Drazner, M., 2011. The progression of hypertensive heart disease. *Circulation,* Volume 123, pp. 327-334.

Drexler, H. *et al*., 1989. Atrial natriuretic peptide in a rat model of cardiac failure. Atrial and ventricular mRNA, atrial content, plasma levels, and effect of volume loading. *Circulation,* Volume 79, pp. 620-633.

Dunn, J., Nisula, B. & Rodbard, D., 1981. Transport of steroid hormones: binding of 21 endogenous steroids to both testosterone-binding globulin and corticosteroid-binding globulin in human plasma. *Clinical Endocrinology and Metabolism,* Volume 53 (1), pp. 58-68.

Edwards, C. *et al*., 1988. Localisation of 11 beta-hydroxysteroid dehydrogenase - tissue specific protector of the mineralocorticoid receptor. *Lancet,* Volume 2 (8618), pp. 986-989.

Eghbali, M. *et al*., 1991. Differential effects of transforming growth factor-beta 1 and phorbol myristate acetate on cardiac fibroblasts. Regulation of fibrillar collagen mRNAs and expression of early transcription factors. *Circulation Research,* Volume 69 (2), pp. 483-490.

Ellis, S. *et al*., 2006. Granulocyte colony stimulating factor in patients with large acute myocardial infarction: results of a pilot dose-escalation randomized trial. *American Heart Journal,* Volume 152 (6), pp. e9-e14.

Engel, F., Hsieh, P., Lee, R. & Keating, M., 2006. FGF1/p38 MAP kinase inhibitor therapy induces cardiomyocyte mitosis, reduces scarring, and rescues function after myocardial infarction. *Proceedings of the National Academy of Sciences,* Volume 103 (42), pp. 15546-15551.

Esteban, N. *et al*., 1991. Daily cortisol production rate in man determined by stable isotope dilution/mass spectrometry. *Clinical Endocrinology and Metabolism,* Volume 72 (1), pp. 39-45.

Fabiato, A. & Fabiato, F., 1972. Excitation-contraction coupling of isolated cardiac fibers with disrupted or closed sarcolemmas: calcium-dependent cyclic and tonic contractions. *Circulation Research,* Volume 31, pp. 293-307.

Falahati, A. *et al*., 1999. Implementation of serum cardiac troponin I as a marker for detection of acute myocardial infarction. *American Heart Journal,* Volume 137 (2), pp. 332-337.

Falardeau, P. & Martineau, A., 1989. Prostaglandin I2 and glucocorticoid-induced rise in arterial pressure in the rat. *Hypertension,* Volume 7 (8), pp. 625-632.

Fallo, F. *et al*., 1999. Regression of cardiac abnormalities after replacement therapy in Addison's disease. *European Journal of Endocrinology,* Volume 140, pp. 425-428.

Ferrarini, M. *et al*., 2006. Adeno-associated virus-mediated transduction of VEGF165 improves cardiac tissue viability and functional recovery after permanent coronary occlusion in conscious dogs. *Circulation Research,* Volume 98 (7), pp. 954-961.

Flesch, M. *et al*., 1996. Evidence for functional relevance of an enhanced expression of the Na^{+}-Ca^{2+} exchanger in failing human myocardium. *Circulation,* Volume 94, pp. 992-1002.

Folkman, J. *et al*., 1983. Angiogenesis inhibition and tumor regression caused by heparin or a heparin fragment in the presence of cortisone. *Science,* Volume 221 (4612), pp. 719-725.

Fraccarollo, D. *et al*., 2008. Immediate mineralocorticoid receptor blockade improves myocardial infarct healing by modulation of the inflammatory response. *Hypertension,* Volume 51, pp. 905-914.

Fraccarollo, D. *et al*., 2011. Deletion of cardiomyocyte mineralocorticoid receptor ameliorates adverse remodeling after myocardial infarction. *Circulation,* Volume 123 (4), pp. 400-408.

Frangogiannis, N., Smith, C. & Entman, M., 2002. The inflammatory response in myocardial infarction. *Cardiovascular Research,* Volume 53, pp. 31-47.

Frangogiannis, N., 2008. The immune system and cardiac repair. *Pharmacology Research,* Volume 58 (2), pp. 88-111.

Frank, M., Miguel, Z., Watkins, L. & Maier, S., 2010. Prior exposure to glucocorticoids sensitizes the neuroinflammatory and peripheral inflammatory responses to E. coli lipopolysaccharide. *Brain, Behaviour and Immunity,* Volume 24 (1), pp. 19-30.

Frantz, S., Bauersachs, J. & Ertl, G., 2009. Post-infarct remodeling: contribution of wound healing and inflammation. *Cardiovascular Research,* Volume 81, pp. 474-481.

Fraser, R. *et al*., 1999. Cortisol effects on body mass, blood pressure, and cholesterol in the general population. *Hypertension,* Volume 33, pp. 1364-1368.

Fukumara, D. *et al*., 2001. Predominant role of endothelial nitric oxide synthase in vascular endothelial growth factor-induced angiogenesis and vascular permeability. *Proceedings of the National Academy of Sciences,* Volume 98 (5), pp. 2604-2609.

Funder, J., 1997. Glucocorticoid and mineralocorticoid receptors: biology and clinical relevance. *Annual Review of Medicine,* Volume 48, pp. 231-240.

Gabbiani, G., 1998. Evolution and clinical implications of the myofibroblast concept. *Cardiovascular Research,* Volume 38 (3), pp. 545-548.

Gagner, J. & Drouin, J., 1985. Opposite regulation of pro-opiomelanocortin gene transcription by glucocorticoids and CRH. *Molecular and Cellular Endocrinology,* Volume 40 (1), pp. 25-32.

Gao, E. *et al*., 2010. A novel and efficient model of coronary artery ligation and myocardial infarction in the mouse. *Circulation Research,* Volume 107, pp. 1445-1453.

Gao, H. *et al*., 1997. Hormonal regulation of oxidative and reductive activities of 11 beta-hydroxysteroid dehydrogenase in rat Leydig cells. *Endocrinology,* Volume 138 (1), pp. 156-161.

Garcia, R. *et al*., 2013. 11β-hydroxysteroid dehydrogenase type 1 gene knockout attenuates atherosclerosis and in vivo foam cell formation in hyperlipidemic apoE-/- mice. *PLoS One,* Volume 8 (2), p. e53192.

Gassenmaier, T. *et al*., 2012. High-sensitive troponin I in acute cardiac conditions: implications of baseline and sequential measurements for diagnosis of myocardial infarction. *Atherosclerosis,* Volume 222 (1), pp. 116-122.

Gayan-Ramirez, G., Vanzeir, L., Wuytack, F. & Decramer, M., 2000. Corticosteroids decrease mRNA levels of SERCA pumps, whereas they increase sarcolipin mRNA in the rat diaphragm. *Physiology,* Volume 524 (2), pp. 387-397.

Geissmann, F., Jung, S. & Littman, D., 2003. Blood monocytes consist of two principal subsets with distinct migratory properties. *Immunity,* Volume 19 (1), pp. 71-82.

Geissmann, F. *et al*., 2010. Development of monocytes, macrophages, and dendritic cells. *Science,* Volume 327 (5966), pp. 656-661.

Geisterfer-Lowrance, A. *et al*., 1996. A mouse model of familial hypertrophic cardiomyopathy. *Science,* Volume 272 (5262), pp. 731-734.

Gelati, M. *et al*., 2008. The angiogenic response of the aorta to injury and inflammatory cytokines requires macrophages. *Immunology,* Volume 181 (8), pp. 5711-5719.

Ghose Roy, S. *et al*., 2009. Excess of glucocorticoid induces cardiac dysfunction via activating angiotensin II pathway. *Cellular Physiology and Biochemistry,* Volume 24, pp. 1-10.

Gibler, W. *et al*., 1992. Acute myocardial infarction in chest pain patients with nondiagnostic ECGs: serial CK-MB sampling in the emergency department. *Annals of Emergency Medicine,* Volume 21 (5), pp. 504-512.

Gilmour, J. *et al*., 2006. Local amplification of glucocorticoids by 11 beta-hydroxysteroid dehydrogenase type 1 promotes macrophage phagocytosis of apoptotic leukocytes. *Immunology,* Volume 176 (12), pp. 7605-7611.

Giordano, F. *et al*., 1996. Intracoronary gene transfer of fibroblast growth factor-5 increases blood flow and contractile function in an ischaemic region of the heart. *Nature Medicine,* Volume 2, pp. 534-539.

Goodwin, J. *et al*., 2011. Knockout of the vascular endothelial glucocorticoid receptor abrogates dexamethasone-induced hypertension. *Hypertension,* Volume 29 (7), pp. 1347-1356.

Gordon, C. *et al*., 1994. Impaired wound healing in Cushing's syndrome: the role of heat shock proteins. *Surgery,* Volume 166 (6), pp. 1082-1087.

Gordon, O. *et al*., 2014. A transgenic platform for testing drugs intended for reversal of cardiac remodeling identifies a novel 11βHSD1 inhibitor rescuing hypertrophy independently of re-vascularization. *PLoS One,* Volume 9 (3), p. e92869.

Gordon, S., 2003. Alternative activation of macrophages. *Nature Reviews Immunology,* Volume 3 (1), pp. 23-35.

Gorza, L. *et al*., 1984. Myosin types in the human heart. An immunofluorescence study of normal and hypertrophied atrial and ventricular myocardium. *Circulation Research,* Volume 54 (6), pp. 694-702.

Goser, S. *et al*., 2006. Cardiac troponin I but not cardiac troponin T induces severe autoimmune inflammation in the myocardium. *Circulation,* Volume 114, pp. 1693-1702.

Gow, D., Sester, D. & Hume, D., 2010. CSF-1, IGF-1, and the control of postnatal growth and development. *Leukocyte Biology,* Volume 88 (3), pp. 475-481.

Grad, I. & Picard, D., 2007. The glucocorticoid responses are shaped by molecular chaperones. *Molecular and Cellular Endocrinology,* Volume 275 (1-2), pp. 2-12.

Grass, T., Lurie, D. & Coffin, J., 2006. Transitional angiogenesis and vascular remodeling during coronary angiogenesis in response to myocardial infarction. *Acta Histochemica,* Volume 108 (4), pp. 293-302.

Gray, G. & Sherry, L., 2002. Investigation of the endothelin system in experimental heart failure. *Methods in Molecular Biology,* Volume 206, pp. 217-227.

Gray, G. *et al*., 2013. Imaging the healing murine myocardial infarct in vivo: ultrasound, magnetic resonance imaging and fluorescence molecular tomography. *Journal of Experimental Physiology*, 98(3), pp. 606-613.

Greenleaf, G., Convertino, A. & Mangseth, G., 1979. Plasma volume during stress in man: osmolality and red cell volume. *Applied Physiology,* Volume 47, pp. 1031-1038.

Gupta, S. *et al*., 2003. Effects of cortisol and oestradiol on hepatic 11beta-hydroxysteroid dehydrogenase type 1 and glucocorticoid receptor proteins in late-gestation sheep fetus. *Endocrinology,* Volume 176, pp. 175-184.

Guy, J. *et al*., 2001. A mouse Mecp2-null mutation causes neurological symptoms that mimic Rett syndrome. *Nature Genetics,* Volume 27, pp. 322-326.

Hadoke, P. *et al*., 2001. Endothelial cell dysfunction in mice after transgenic knockout of type 2, but not type 1 11β-hydroxysteroid dehydrogenase. *Circulation,* Volume 104, pp. 2832-2837.

Hadoke, P. *et al*., 2006. Intra-vascular glucocorticoid metabolism as a modulator of vascular structure and function. *Cellular and Molecular Life Sciences,* Volume 63 (5), pp. 565-578.

Hadoke, P., Iqbal, J. & Walker, B., 2009. Therapeutic manipulation of glucocorticoid metabolism in cardiovascular disease. *British Journal of Pharmacology,* Volume 156 (5), pp. 689-712.

Haghighi, K. *et al*., 2003. Human phospholamban null results in lethal dilated cardiomyopathy revealing a critical difference between mouse and human. *Journal of Clinical Investigation*, Volume 111 (6), pp. 869-876.

Haikala, H. *et al*., 1995. Cardiac troponin C as a target protein for a novel calcium sensitizing drug, levosimendan. *Molecular and Cellular Cardiology,* Volume 27 (9), pp. 1859-1866.

Haleagrahara, N., Chakravarthi, S. & Mathews, L., 2011. Insulin like growth factor-1 (IGF-1) causes overproduction of IL-8, an angiogenic cytokine and stimulates neovascularisation in isoproterenol-induced myocardial infarction in rats. *International Journal of Molecular Sciences,* Volume 12, pp. 8562-8574.

Hallgren, O. *et al*., 2010. Altered fibroblast proteoglycan production in COPD. *Respiratory Research,* Volume 11 (55), pp. 1-11.

Hama, N. *et al*., 1995. Rapid ventricular induction of brain natriuretic peptide gene expression in experimental acute myocardial infarction. *Circulation,* Volume 92, pp. 1558-1564.

Hammerman, H. *et al*., 1983. Dose dependent effects of short-term methylprednisolone on myocardial infarct extent, scar formation, and ventricular function. *Circulation,* Volume 68, pp. 446-452.

Hanft, L., Korte, F. & McDonald, K., 2008. Cardiac function and modulation of sarcomeric function by length. *Cardiovascular Research,* Volume 77, pp. 627-636.

Hao, G. *et al*., 2008. Agonists at PPAR-γ suppress angiotensin II-induced production of plasminogen activator inhibitor-1 and extracellular matrix in rat cardiac fibroblasts. *British Journal of Pharmacology,* Volume 153, pp. 1409-1419.

Hao, X. *et al*., 2007. Myocardial angiogenesis after plasmid or adenoviral VEGF-A(165) gene transfer in rat myocardial infarction model. *Cardiovascular Research,* Volume 73 (3), pp. 481-487.

Harada, K. *et al*., 1999. Angiotensin II type 1A receptor knockout mice display less left ventricular remodeling and improved survival after mycoardial infarction. *Circulation,* Volume 100, pp. 2093-2099.

Harada, M. *et al*., 2005. G-CSF prevents cardiac remodeling after myocardial infarction by activating the Jak-Stat pathway in cardiomyocytes. *Nature Medicine,* Volume 11 (3), pp. 305-311.

Harris, H. *et al*., 2001. Intracellular regeneration of glucocorticoids by 11β-hydroxysteroid dehydrogenase (11β-HSD)-1 plays a key role in regulation of the hypothalamic-pituitary-adrenal axis: analysis of 11β-HSD-1-deficient mice. *Endocrinology,* Volume 142 (1), pp. 114-120.

He, Y. *et al*., 2011. A physiological concentration of glucocorticoid inhibits the pro-inflammatory cytokine-induced proliferation of adult rat cardiac fibroblasts: roles of extracellular signal-regulated kinase 1/2 and nuclear factor-κB. *Clinical and Experimental Pharmacology and Physiology,* Volume 38 (11), pp. 739-746.

Heidemann, J. *et al*., 2003. Angiogenic effects of interleukin 8 (CXCL8) in human intestinal microvascular endothelial cells are mediated by CXCR2. *Biological Chemistry,* Volume 278, pp. 8508-8515.

Heimer, R., Bashey, R., Kyle, J. & Jimenez, S., 1995. TGF-beta modulates the synthesis of proteoglycans by myocardial fibroblasts in culture. *Molecular and Cellular Cardiology,* Volume 27 (10), pp. 2191-2198.

Hellkvist, J., Tufveson, G., Gerdin, B. & Johnsson, C., 2002. Characterization of fibroblasts from rejecting tissue: the hyaluronan production is increased. *Transplantation,* Volume 74 (12), pp. 1672-1677.

Hench, P. & Slocumb, C., 1949. The effects of the adrenal cortical hormone 17-hydroxy-11-dehydrocorticosterone (Compound E) on the acute phase of rheumatic fever; preliminary report. *Proceedings of the Staff Meetings. Mayo Clinic,* Volume 24 (11), pp. 277-297.

Henderson, S. *et al*., 2004. Functional adult myocardium in the absence of Na^{+}-Ca^{2+} exchange: cardiac-specific knockout of NCX1. *Circulation Research,* Volume 95, pp. 604-611.

Henkart, P., 1996. ICE family proteases: mediators of all apoptotic cell death?. *Immunity,* Volume 4 (3), pp. 195-201.

Henke, C. *et al*., 1993. Macrophage production of basic fibroblast growth factor in the fibroproliferative disorder of alveolar fibrosis after lung injury. *American Journal of Pathology,* Volume 143, pp. 1189-1199.

Hermanowski-Vosatka, A. *et al*., 2005. 11beta-HSD1 inhibition ameliorates metabolic syndrome and prevents progression of atherosclerosis in mice. *Experimental Medicine,* 202(4), pp. 517-527.

Herron, T. & McDonald, K., 2002. Small amounts of α-myosin heavy chain isoform expression significantly increase power output of rat cardiac myocyte fragments. *Circulation Research,* Volume 90, pp. 1150-1152.

Herzig, S. *et al*., 2001. CREB regulates hepatic gluconeogenesis through the coactivator PGC-1. *Nature,* Volume 413 (6852), pp. 179-183.

Hey, T., Dahl, J., Brix, T. & Sondergaard, E., 2013. Biventricular hypertrophy and heart failure as initial presentation of Cushing's disease. *British Medical Journal Case Reports,* Volume 2013, pp. 1-7.

Hinrichs, S. *et al*., 2011. Controlling cardiomyocyte length: the role of renin and PPAR-γ. *Cardiovascular Research,* Volume 89, pp. 344-352.

Hoffstein, S., Weissmann, G. & Fox, A., 1976. Lysosomes in myocardial infarction: studies by means of cytochemistry and subcellular fractionation, with observations on the effects of methylprednisolone. *Circulation,* Volume 53, pp. I34-I40.

Hollenberg, S. *et al*., 1985. Primary structure and expression of a functional human glucocorticoid receptor cDNA. *Nature,* Volume 318, pp. 635-641.

Holtwick, R. *et al*., 2002. Smooth muscle-selective deletion of guanylyl cyclase-A prevents the acute but not chronic effects of ANP on blood pressure. *Proceedings of the National Academy of Sciences,* Volume 99 (10), pp. 7142-7147.

Hosogai, N. *et al*., 2007. Adipose tissue hypoxia in obesity and its impact on adipocytokine dysregulation. *Diabetes,* Volume 56 (4), pp. 901-911.

Huynh, M., Fadok, V. & Henson, P., 2002. Phosphatidylserine-dependent ingestion of apoptotic cells promotes TGF-beta1 secretion and the resolution of inflammation. *Journal of Clinical Investigation,* Volume 109 (1), pp. 41-50.

Ishii, T. *et al*., 2007. Augmentation of 11β-hydroxysteroid dehydrogenase type 1 in LPS-activated J774.1 macrophages - role of 11β-HSD1 in pro-inflammatory properties in macrophages. *Federation of European Biochemical Societies Letters,* Volume 581, pp. 349-354.

Ismail, J. *et al*., 2003. Immunohistologic labeling of murine endothelium. *Cardiovascular Pathology,* Volume 12, pp. 82-90.

Ito, T., Ishii, G., Chiba, H. & Ochiai, A., 2007. The VEGF angiogenic switch of fibroblasts is regulated by MMP-7 from cancer cells. *Oncogene,* Volume 26 (51), pp. 7194-7203.

Iwai, A. *et al*., 2004. Down-regulation of vascular endothelial growth factor in renal cell carcinoma cells by glucocorticoids. *Molecular and Cellular Endocrinology,* Volume 226, pp. 11-17.

Jacobson, L., 2005. Hypothalamic-pituitary-adrenocortical axis regulation. *Endocrinology and Metabolism Clinics of North America,* Volume 34 (2), pp. 271-292.

Jessup, M. & Brozena, S., 2003. Heart Failure. *New England Journal of Medicine,* Volume 348, pp. 2007-2018.

Jhund, P. & McMurray, J., 2008. Heart failure after acute myocardial infarction. *Circulation,* Volume 118, pp. 2019-2021.

Ji, Y. *et al*., 2000. Disruption of a single copy of the SERCA2 gene results in altered Ca^{2+} homeostasis and cardiomyocyte function. Journal *of Biological Chemistry*, Volume 275 (48), pp. 38073-38080.

Jiang, Z. *et al*., 2007. High- but not low-molecular weight FGF-2 causes cardiac hypertrophy in vivo; possible involvement of cardiotrophin-1. *Molecular and Cellular Cardiology,* Volume 42 (1), pp. 222-233.

Jilma, B. *et al*., 1997. Dexamethasone down-regulates the expression of L-selectin on the surface of neutrophils and lymphocytes in humans. *Clinical Pharmacology and Therapeutics,* Volume 62 (5), pp. 562-568.

John, S. *et al*., 1995. Genetic decreases in atrial natriuretic peptide and salt-sensitive hypertension. *Science,* Volume 267 (5198), pp. 679-681.

Jones, S. *et al*., 2003. Endothelial nitric oxide synthase overexpression attenuates congestive heart failure in mice. *Proceedings of the National Academy of Sciences,* Volume 100 (8), pp. 4891-4896.

Jones, W. *et al*., 1996. Ablation of the murine α myosin heavy chain gene leads to dosage effects and functional deficits in the heart. *Volume* 98 (8), pp. 1906-1917.

Jung, K. *et al*., 2013. Endoscopic time-lapse imaging of immune cells in infarcted mouse hearts. *Circulation Research,* Volume 112 (6), pp. 891-899.

Kakio, T. *et al*., 2000. Roles and relationship of macrophages and monocyte chemotactic and activating factor/monocyte chemoattractant protein-1 in the ischemic and reperfused rat heart. *Laboratory Investigation,* Volume 80 (7), pp. 1127-1136.

Kardon, T. *et al*., 2008. Maintenance of luminal NADPH in the endoplasmic reticulum promotes the survival of human neutrophil granulocytes. *Federation of European Biochemical Societies Letters,* Volume 582 (13), pp. 1809-1815.

Kass, DA., Bronzwaer, JGF. & Paulus, WJ., 2004. What mechanisms underlie diastolic dysfunction in heart failure? *Circulation Research,* Volume 94, pp. 1533-1542.

Kastrup, J. *et al*., 2005. Direct intramyocardial plasmid vascular endothelial growth factor-A165 gene therapy in patients with stable severe angina pectoris. A randomized double-blind placebo-controlled study: the Euroinject One trial. *Journal of the American College of Cardiology,* Volume 45 (7), pp. 982-988.

Katoh, D. *et al*., 2014. Corticosteroids increase intracellular free sodium ion concentration via glucocorticoid receptor pathway in cultured neonatal rat cardiomyocytes. *International Journal of Cardiology Heart and Vessels,* Volume 3, pp. 49-56.

Ke, Q. & Costa, M., 2006. Hypoxia-inducible factor-1 (HIF-1). *Molecular Pharmacology,* Volume 70 (5), pp. 1469-1480.

Kelly, B. *et al*., 2003. Cell type-specific regulation of angiogenic growth factor gene expression and induction of angiogenesis in nonischaemic tissue by a constitutively active form of hypoxia-inducible factor-1. *Circulation Research,* Volume 93, pp. 1074-1081.

Kido, M. *et al*., 2005. Hypoxia-inducible factor 1-alpha reduces infarction and attenuates progression of cardiac dysfunction after myocardial infarction in the mouse. *Journal of the American College of Cardiology,* Volume 46 (11), pp. 2116-2124.

Kim, J., Kim, S. & Park, J., 2014. Dilated cardiomyopathy with left ventricular thrombi as a presenting feature of Cushing's disease. *Canadian Journal of Cardiology*,Volume 30 (11), pp. e11-e13.

Kin, H. *et al*., 2006. Neutrophil depletion induces myocardial apoptosis and attenuates NFκB activation/TGFβ release after ischaemia and reperfusion. *Surgical Research,* Volume 135, pp. 170-178.

Kipari, T. *et al*., 2013. 11β-hydroxysteroid dehydrogenase type 1 deficiency in bone marrow-derived cells reduces atherosclerosis. *The Journal of the Federation of American Societies for Experimental Biology*, Volume 27, pp. 1519-1531.

Klusonova, P. *et al*., 2009. Chronic intermittent hypoxia induces 11β-hydroxysteroid dehydrogenase in rat heart. *Endocrinology,* Volume 150 (9), pp. 4270-4277.

Koch, A. *et al*., 1992. Enhanced production of monocyte chemoattractant protein-1 in rheumatoid arthritis. *Journal of Clinical Investigation,* Volume 90 (3), pp. 772-779.

Koch, A. *et al*., 1992. Interleukin-8 as a macrophage-derived mediator of angiogenesis. *Science,* Volume 258 (5089), pp. 1798-1801.

Kolovou, G., Anagnostopoulou, K., Mikhailidis, D. & Cokkinos, D., 2008. Apolipoprotein e knockout models. *Current Pharmaceutical Design,* Volume 14 (4), pp. 338-351.

Korpisalo, P. *et al*., 2008. Vascular endothelial growth factor-A and platelet-derived growth factor-B combination gene therapy prolongs angiogenic effects via recruitment of interstitial mononuclear cells & paracrine effects rather than improved pericyte coverage of angiogenic vessels. *Circulation Research,* Volume 103 (10), pp. 1092-1099.

Koss, KL., Grupp, IL. & Kranias, EG., 1997. The relative phospholamban and SERCA2 ratio: a critical determinant of myocardial contractility. *Basic Research in Cardiology,* Volume 92 (S1), pp. 17-24.

Kotelevtsev, Y. *et al*., 1997. 11beta-hydroxysteroid dehydrogenase type 1 knockout mice show attenuated glucocorticoid-inducible responses and resist hyperglycaemia in obesity or stress. *Proceedings of the National Academy of Sciences,* Volume 94 (26), pp. 14924-14929.

Kotelevtsev, Y. *et al*., 1999. Hypertension in mice lacking 11beta-hydroxysteroid dehydrogenase type 2. *Journal of Clinical Investigation,* Volume 103 (5), pp. 683-689.

Krenz, M. & Robbins, J., 2004. Impact of beta-myosin heavy chain expression on cardiac function during stress. *Journal of the American College of Cardiology,* Volume 44 (12), pp. 2390-2397.

Kroll, J. & Waltenberger, J., 1998. VEGF-A induces expression of eNOS and iNOS in endothelial cells via VEGF receptor-2 (KDR). *Biochemical and Biophysical Research Communications,* Volume 252 (3), pp. 743-746.

Kroop, I. & Shackman, N., 1957. The C-reactive protein determination as an index of myocardial necrosis in coronary artery disease. *American Journal of Medicine,* Volume 22 (1), pp. 90-98.

Krozowski, Z. & Funder, J., 1983. Renal mineralocorticoid receptors and hippocampal corticosterone-binding species have identical intrinsic steroid specificity. *Proceedings of the National Academy of Sciences,* Volume 80 (19), pp. 6056-6060.

Kukielka, G. *et al*., 1995. Interleukin-8 gene induction in the myocardium after ischaemia and reperfusion in vivo. *Journal of Clinical Investigation,* Volume 95 (1), pp. 89-103.

Kumarswamy, R. *et al*., 2012. SERCA2a gene therapy restores microRNA-1 expression in heart failure via an Akt/FoxO3A-dependent pathway. *European Heart Journal,* Volume 33, pp. 1067-1075.

Labugger, R. *et al*., 2000. Extensive troponin I and T modification detected in serum from patients with acute myocardial infarction. *Circulation,* Volume 102, pp. 1221-1226.

Lambert, J., Lopez, E. & Lindsey, M., 2008. Macrophage roles following myocardial infarction. *International Journal of Cardiology,* Volume 130 (2), pp. 147-158.

Landahl, S. *et al*., 1986. Age-related changes in blood pressure. *Hypertension,* Volume 8, pp. 1044-1049.

Lavery, G. *et al*., 2006. Hexose-6-phosphate dehydrogenase knock-out mice lack 11 beta-hydroxysteroid dehydrogenase type 1-mediated glucocorticoid regeneration. *Biological Chemistry,* Volume 281 (10), pp. 6546-6551.

Lavery, G. *et al*., 2008. Deletion of hexose-6-phosphate dehydrogenase activates the unfolded protein response pathway and induces skeletal myopathy. *Biological Chemistry,* Volume 283, pp. 8453-8461.

Lawson, A. *et al*., 2011. Cortisone-reductase deficiency associated with heterozygous mutations in 11beta-hydroxysteroid dehydrogenase type 1. *Proceedings of the National Academy of Sciences,* Volume 108 (10), pp. 4111-4116.

Lee, R. *et al*., 2000. VEGF gene delivery to myocardium. *Circulation,* Volume 102, pp. 898-901.

Lee, S. *et al*., 2000. Early expression of angiogenesis factors in acute myocardial ischaemia and infarction. *New England Journal of Medicine,* Volume 342, pp. 626-633.

Lees-Miller, J., Heeley, D. & Smillie, L., 1987. An abundant and novel protein of 22kDa (SM22) is widely distributed in smooth muscles. *Biochemistry,* Volume 244, pp. 705-709.

Lefer, A., 1968. Influence of corticosteroids on mechanical performance of isolated rat papillary muscles. *American Journal of Physiology,* Volume 214 (3), pp. 518-524.

Leor, J. *et al*., 2006. Ex vivo activated human macrophages improve healing, remodeling, and function of the infarcted heart. *Circulation,* Volume 114 (1S), pp. I94-I100.

Leu, M., Ehler, E. & Perriard, J., 2001. Characterisation of postnatal growth of the murine heart. *Anatomy and Embryology,* Volume 204 (3), pp. 217-224.

Levinger, E., Levy, H. & Elster, S., 1957. Study of C-reactive protein in the sera of patients with acute myocardial infarction. *Annals of Internal Medicine,* Volume 46 (1), pp. 68-78.

Lewis, J. *et al*., 2005. Plasma free cortisol fraction reflects levels of functioning corticosteroid-binding globulin. *Clinica Chimica Acta,* Volume 359 (1-2), pp. 189-194.

Li, A. *et al*., 2003. IL-8 directly enhanced endothelial cell survival, proliferation, and matric metalloproteinases production and regulated angiogenesis. *Immunology,* Volume 170, pp. 3369-3376.

Li, L., Miano, J., Cserjesi, P. & Olson, E., 1996. SM22 alpha, a marker of adult smooth muscle, in expressed in multiple myogenic lineages during embryogenesis. *Circulation Research,* Volume 78, pp. 188-195.

Li, L. *et al*., 2011. Calcium dynamics in the ventricular myocytes of SERCA2 knockout mice: a modeling study. *Biophysical Journal,* Volume 100 (2), pp. 322-331.

Li, L. *et al*., 2012. Sodium accumulation in SERCA knockout-induced heart failure. *Biophysical Journal,* Volume 102 (9), pp. 2039-2048.

Li, M. *et al*., 2001. An essential role of the NF-κB/toll-like receptor pathway in induction of inflammation and tissue repair gene expression by necrotic cells. *Immunology,* Volume 166, pp. 7128-7135.

Li, P. *et al*., 2008. Atrial natriuretic peptide inhibits transforming growth factor beta-induced smad signaling and myofibroblast transformation in mouse cardiac fibroblasts. *Circulation Research,* Volume 102 (2), pp. 185-192.

Libby, P. *et al*., 1973. Reduction of experimental myocardial infarct size by corticosteroid administration. *Journal of Clinical Investigation,* Volume 52, pp. 599-607.

Liberman, A., Druker, J., Perone, M. & Arzt, E., 2007. Glucocorticoids in the regulation of transcription factors that control cytokine synthesis. *Cytokine & Growth Factor Reviews,* Volume 18 (1-2), pp. 45-56.

Liles, W. *et al*., 1997. A comparative trial of granulocyte-colony-stimulating factor and dexamethasone, separately and in combination, for the mobilization of neutrophils in the peripheral blood of normal volunteers. *Transfusion,* Volume 37 (2), pp. 182-187.

Limas, C. *et al*., 1987. Calcium uptake by cardiac sarcoplasmic reticulum in human dilated cardiomyopathy. *Cardiovascular Research,* Volume 21 (8), pp. 601-605.

Lin, L. & Achermann, J., 2004. The adrenal. *Hormone Research,* Volume 62, pp. 22-29.

Liu, L. *et al*., 2005. Rapid non-genomic inhibitory effects of glucocorticoids on human neutrophil degranulation. *Inflammation Research,* Volume 54 (1), pp. 37-41.

Liu, X. *et al*., 2007. Nitric oxide inhalation improves microvascular flow and decreases infarction size after myocardial ischaemia and reperfusion. *Journal of the American College of Cardiology,* Volume 50 (8), pp. 808-817.

Liu, Y. *et al*., 2008. Reduction of hepatic glucocorticoid receptor and hexose-6-phosphate dehydrogenase expression ameliorates diet-induced obesity and insulin resistance in mice. *Molecular Endocrinology,* Volume 41 (2), pp. 53-64.

Livingstone, D. *et al*., 2000. Understanding the role of glucocorticoids in obesity: tissue-specific alterations of corticosterone metabolism in obese Zucker rats. *Endocrinology,* Volume 141 (2), pp. 560-563.

Logie, J. *et al*., 2010. Glucocorticoid-mediated inhibition of angiogenic changes in human endothelial cells is not caused by reductions in cell proliferation or migration. *PLoS One,* Volume 5 (12), pp. e14476.

Loke, P. *et al*., 2002. IL-4 dependent alternatively-activated macrophages have a distinctive in vivo gene expression phenotype. *BMC Immunology,* Volume 3 (7), pp. 1-11.

Lompre, A. *et al*., 1979. Myosin isoenzyme redistribution in chronic heart overload. *Nature,* Volume 282 (5734), pp. 105-107.

Longenecker, J., Kilty, L. & Johnson, L., 1982. Glucocorticoid influence on growth of vascular wall cells in culture. *Cellular Physiology,* Volume 113 (2), pp. 197-202.

Longenecker, J., Kilty, L. & Johnson, L., 1984. Glucocorticoid inhibition of vascular smooth muscle cell proliferation: influence of homologous extracellular matrix and serum mitogens. *Cell Biology,* Volume 98 (2), pp. 534-540.

Long, F. *et al*., 2005. Rapid nongenomic inhibitory effects of glucocorticoids on phagocytosis and superoxide anion production by macrophages. *Steroids,* Volume 70 (1), pp. 55-61.

Lopez, M. *et al*., 1995. Salt-resistant hypertension in mice lacking the guanylyl cyclase-A receptor for atrial natriuretic peptide. *Nature,* Volume 378 (6552), pp. 65-68.

Lopez-Lopez, J., Shacklock, P., Balke, C. & Wier, W., 1995. Local calcium transients triggered by single L-type calcium channel currents in cardiac cells. *Science,* Volume 268 (5213), pp. 1042-1045.

Losordo, D. *et al*., 1998. Gene therapy for myocardial angiogenesis: initial clinical results with direct myocardial injection of phVEGF165 as sole therapy for myocardial ischemia. *Circulation,* Volume 98 (25), pp. 2800-2804.

Lother, A. *et al*., 2011. Ablation of mineralocorticoid receptors in myocytes but not in fibroblasts preserves cardiac function. *Hypertension,* Volume 57, pp. 746-754.

Louch, W. *et al*., 2010. Sodium accumulation promotes diastolic dysfunction in end-stage heart failure following SERCA2 knockout. *Physiology,* Volume 588, pp. 465-478.

Louch, W. *et al*., 2012. No rest for the weary: diastolic calcium homeostasis in the normal and failing myocardium. *Physiology,* Volume 27, pp. 308-323.

Lu, Z. *et al*., 2010. Oxidative stress regulates left ventricular PDE5 expression in the failing heart. *Circulation,* Volume 121 (13), pp. 1474-1483.

Lucas, T. *et al*., 2010. Differential roles of macrophages in diverse phases of skin repair. *Immunology,* Volume 184 (7), pp. 3964-3977.

Lupien, S. *et al*., 1998. Cortisol levels during human aging predict hippocampal atrophy and memory deficits. *Nature Neuroscience,* Volume 1, pp. 69-73.

Lyon, A. *et al*., 2011. SERCA2a gene transfer decreases sarcoplasmic reticulum calcium leak and reduces ventricular arrhythmias in a model of chronic heart failure. *Circulation Arrhythmia and Electrophysiology,* Volume 4, pp. 362-372.

Ma, X., Camacho, C. & Aguilera, G., 2001. Regulation of corticotropin-releasing hormone (CRH) transcription and CRH mRNA stability by glucocorticoids. *Cellular and Molecular Neurobiology,* Volume 21 (5), pp. 465-475.

MacKinnon, A. *et al*., 2008. Regulation of alternative macrophage activation by galectin-3. *Immunology,* Volume 180, pp. 2650-2658.

MacLennan, D., Asahi, M. & Tupling, A., 2003. The regulation of SERCA-type pumps by phospholamban and sarcolipin. *Annals of the New York Academy of Sciences,* Volume 986, pp. 472-480.

Mani, K., 2008. Programmed cell death in cardiomyocytes: strategies to maximize post-ischemic salvage. *Heart Failure Reviews,* Volume 13 (2), pp. 193-209.

Marshall, I. *et al*., 2013. Application of kt-BLAST acceleration to reduce cardiac MR imaging time in healthy and infarcted mice. *Magnetic Resonance Materials in Physics, Biology and Medicine,* Volume 27, pp, 201-210.

Marwick, J. *et al*., 2013. Oxygen levels determine the ability of glucocorticoids to influence neutrophil survival in inflammatory environments. *Leukocyte Biology,* Volume 94, pp. 1285-1292.

Masuzaki, H. *et al*., 2001. A transgenic model of visceral obesity and the metabolic syndrome. *Science,* Volume 294 (5549), pp. 2166-2170.

Masuzaki, H. *et al*., 2003. Transgenic amplification of glucocorticoid action in adipose tissue causes high blood pressure in mice. *Journal of Clinical Investigation,* Volume 112 (1), pp. 83-90.

Matsui, H. *et al*., 1996. Leukemia inhibitory factor induces a hypertrophic response mediated by gp130 in murine cardiac myocytes. *Research Communications in Molecular Pathology and Pharmacology,* Volume 93 (2), pp. 149-162.

Matsukawa, A. *et al*., 1999. Endogenous monocyte chemoattractant protein-1 (MCP-1) protects mice in a model of acute septic peritonitis: cross-talk between MCP-1 and leukotriene B4. *Immunology,* Volume 163 (11), pp. 6148-6154.

Matsunaga, T. *et al*., 2000. Ischaemia-induced coronary artery collateral growth is dependent on vascular endothelial growth factor and nitric oxide. *Circulation,* Volume 102, pp. 3098-3103.

McIvor, M., Orchard, C. & Lakatta, E., 1988. Dissociation of changes in apparent myofibrillar Ca^{2+} sensitivity and twitch relaxation induced by adrenergic and cholinergic stimulation in isolated ferret cardiac muscle. *General Physiology,* Volume 92 (4), pp. 509-529.

McKay, L. & Cidlowski, J., 1999. Molecular control of immune/inflammatory responses: interactions between nuclear factor-kappa B and steroid receptor-signaling pathways. *Endocrine Reviews,* Volume 20 (4), pp. 435-459.

McMullen, J. *et al*., 2004. The insulin-like growth factor 1 receptor induces physiological heart growth via the phosphoinositide 3-1kinase (p110alpha) pathway. *Biological Chemistry,* Volume 279 (6), pp. 4782-4793.

McSweeney, S., 2010. *11β-hydroxysteroid dehydrogenase type 1: a new therapeutic target post-myocardial infarction?.* Edinburgh: University of Edinburgh.

McSweeney, S. *et al*., 2010. Improved heart function follows enhanced inflammatory cell recruitment and angiogenesis in 11β-HSD1 deficient mice post-MI. *Cardiovascular Research,* Volume 88 (1), pp. 159-167.

Meir, S. & Leitersdorf, E., 2004. Atherosclerosis in the apolipoprotein e-deficient mouse. *Arteriosclerosis, Thrombosis, and Vascular Biology,* Volume 24, pp. 1006-1014.

Meloni, M. *et al*., 2010. Nerve growth factor promotes cardiac repair following myocardial infarction. *Circulation Research,* Volume 106 (7), pp. 1275-1284.

Mercadier, J. *et al*., 1990. Altered sarcoplasmic reticulum Ca^{2+}-ATPase gene expression in the human ventricle during end-stage heart failure. *Journal of Clinical Investigation,* Volume 85 (1), pp. 305-309.

Meszaros, A., Rechner, J. & Albina, J., 1999. Macrophage phagocytosis of wound neutrophils. *Leukocyte Biology,* Volume 65, pp. 35-42.

Michailidou, Z. *et al*., 2012. Increased angiogenesis protects against adipose hypoxia and fibrosis in metabolic disease-resistant 11β-hydroxysteroid dehydrogenase type 1 (HSD1)-deficient mice. *Biological Chemistry,* Volume 287, pp. 4188-4197.

Milik, E., Szczepanska-Sadowska, E., Maslinski, W. & Cudnoch-Jedrzejewska, A., 2007. Enhanced expression of mineralocorticoid receptors in the heart after myocardial infarct in rats. *Physiology and Pharmacology,* Volume 58 (4), pp. 745-755.

Millar, A., Megson, I. & Gray, G., 2000. Inducible nitric oxide synthase-derived superoxide contributes to hyperactivity in small mesenteric arteries from a rat model of chronic heart failure. *British Journal of Pharmacology,* Volume 131, pp. 29-36.

Mills, N. *et al*., 2011. Implementation of a sensitive troponin I assay and risk of recurrent myocardial infarction and death in patients with suspected acute coronary syndrome. *Journal of the American Medical Association,* Volume 305 (12), pp. 1210-1216.

Mirza, R., DiPietro, L. & Koh, T., 2009. Selective and specific macrophage ablation is detrimental to wound healing in mice. *American Journal of Pathology,* Volume 175 (6), pp. 2454-2462.

Mitchell, B. & Webb, R., 2002. Impaired vasodilation and nitric oxide synthase activity in glucocorticoid-induced hypertension. *Biological Research for Nursing,* Volume 4 (1), pp. 16-21.

Miyata, S., Minobe, W., Bristow, M. & Leinwand, L., 2000. Myosin heavy chain isoform expression in the failing and nonfailing human heart. *Circulation Research,* Volume 86, pp. 386-390.

Moisan, M., Seckl, J. & Edwards, C., 1990. 11 beta-hydroxysteroid dehydrogenase bioactivity and messenger RNA expression in rat forebrain: localization in hypothalamus, hippocampus, and cortex. *Endocrinology,* Volume 127 (3), pp. 1450-1455.

Montecucco, F. *et al*., 2012. CC chemokine CCL5 plays a central role impacting infarct size and post-infarction heart failure in mice. *European Heart Journal,* Volume 33, pp. 1964-1974.

Moreo, A. *et al*., 2009. Influence of myocardial fibrosis on left ventricular diastolic function. *Circulation Cardiovascular Imaging,* Volume 2, pp. 437-443.

Morgan, S. *et al*., 2009. 11β-hydroxysteroid dehydrogenase type 1 regulates glucocorticoid-induced insulin resistance in skeletal muscle. *Diabetes,* Volume 58, pp. 2506-2515.

Morimoto, H. *et al*., 2006. Cardiac overexpression of monocyte chemoattractant protein-1 in transgenic mice prevents cardiac dysfunction and remodeling after myocardial infarction. *Circulation Research,* Volume 99 (8), pp. 891-899.

Mork, H., Sjaastad, I., Sejersted, O. & Louch, W., 2009. Slowing of cardiomyocyte Ca^{2+} release and contraction during heart failure progression in postinfarction mice. *American Journal of Physiology,* Volume 296, pp. H1069-H1079.

Morrison, J. *et al*., 1976. Modification of myocardial injury in man by corticosteroid administration. *Circulation,* Volume 53 (3), pp. 200-204.

Morton, N. *et al*., 2001. Improved lipid and lipoprotein profile, hepatic insulin sensitivity, and glucose tolerance in 11beta-hydroxysteroid dehydrogenase type 1 null mice. *Biological Chemistry,* Volume 276 (44), pp. 41293-41300.

Morton, N. *et al*., 2004. Novel adipose tissue-mediated resistance to diet-induced visceral obesity in 11 beta-hydroxysteroid dehydrogenase type 1-deficient mice. *Diabetes,* Volume 53 (4), pp. 931-938.

Morton, N. & Seckl, J., 2008. 11beta-hydroxysteroid dehydrogenase. *Frontiers of Hormone Research,* Volume 36, pp. 146-164.

Morton, N., 2010. Obesity and corticosteroids: 11beta-hydroxysteroid type 1 as a cause and therapeutic target in metabolic disease. *Molecular and Cellular Endocrinology,* Volume 316 (2), pp. 154-164.

Nahrendorf, M. *et al*., 2000. In vivo assessment of cardiac remodeling after myocardial infarction in rats by cine-magnetic resonance imaging. *Cardiovascular Magnetic Resonance,* Volume 2 (3), pp. 171-180.

Nahrendorf, M. *et al*., 2007. The healing myocardium sequentially mobilizes two monocyte subsets with divergent and complementary functions. *Experimental Medicine,* Volume 204, pp. 3037-3047.

Nakanishi, M. *et al*., 2005. Role of natriuretic peptide receptor guanylyl cyclase-A in myocardial infarction evaluated using genetically engineered mice. *Hypertension,* Volume 46 (2), pp. 441-447.

Nelken, N., Coughlin, S., Gordon, D. & Wilcox, J., 1991. Monocyte chemoattractant protein-1 in human atheromatous plaques. *Journal of Clinical Investigation,* Volume 88 (4), pp. 1121-1127.

Newman, A. *et al*., 2011. The requirement for fibroblasts in angiogenesis: fibroblast-derived matrix proteins are essential for endothelial cell lumen formation. *Molecular Biology of the Cell,* Volume 22 (20), pp. 3791-3800.

Newton, R. & Holden, N., 2007. Separating transrepression and activation: a distressing divorce for the glucocorticoid receptor?. *Molecular Pharmacology,* Volume 72 (4), pp. 799-809.

Nian, M., Lee, P., Khaper, N. & Liu, P., 2004. Inflammatory cytokines and postmyocardial infarction remodeling. *Circulation Research,* Volume 94 (12), pp. 1543-1553.

Niehaus Jr, W., 1978. A proposed role of superoxide anion as a biological nucleophile in the deesterification of phospholipids. *Bioorganic Chemistry,* Volume 7 (1), pp. 77-84.

Nishi, M. & Kawata, M., 2007. Dynamics of glucocorticoid receptor and mineralocorticoid receptor: implications from live cell imaging studies. *Neuroendocrinology,* Volume 85 (3), pp. 186-192.

Nito, I., Waspasji, S., Harun, S. & Markum, H., 2004. Correlation between cortisol levels and myocardial infarction mortality among intensive coronary care unit patients during first seven days in hospital. *Acta Medica Indonesiana,* Volume 36 (1), pp. 8-14.

Numaguchi, Y. *et al*., 2006. The impact of the capability of circulating progenitor cells to differentiate on myocardial salvage in patients with primary acute myocardial infarction. *Circulation,* Volume 114, pp. I114-I119.

Oakley, R. *et al*., 2013. Essential role of stress hormone signaling in cardiomyocytes for the prevention of heart disease. *Proceedings of the National Academy of Sciences,* Volume 110 (42), pp. 17035-17040.

Odermatt, A. *et al*., 1999. The N-terminal anchor sequences of 11beta-hydroxysteroid dehydrogenases determine their orientation in the endoplasmic reticulum membrane. *Biochemistry,* Volume 274 (40), pp. 28762-28770.

Orlic, D. *et al*., 2001. Mobilized bone marrow cells repair the infarcted heart, improving function and survival. *Proceedings of the National Academy of Sciences,* Volume 98 (18), pp. 10344-10349.

Ouvrard-Pascaud, A. *et al*., 2005. Conditional mineralocorticoid receptor expression in the heart leads to life-threatening arrhythmias. *Circulation,* Volume 111 (23), pp. 3025-3033.

Oyamada, M. *et al*., 1994. The expression, phosphorylation, and localization of connexin 43 gap-junctional intercellular communication during the establishment of a synchronized contraction of cultured neonatal rat cardiac myocytes. *Experimental Cell Research,* Volume 212 (2), pp. 351-358.

Ozols, J., 1998. Determination of lumenal orientation of microsomal 50-kDa esterase/N-deacetylase. *Biochemistry,* Volume 37 (28), pp. 10336-10344.

Palmer, R., Ashton, D. & Moncada, S., 1988. Vascular endothelial cells synthesize nitric oxide from L-arginine. *Nature,* Volume 333, pp. 664-666.

Papapetropoulos, A., Garcia-Cardena, G., Madri, J. & Sessa, W., 1997. Nitric oxide production contributes to the angiogenic properties of vascular endothelial growth factor in human endothelial cells. *Journal of Clinical Investigation,* Volume 100 (12), pp. 3131-3139.

Patan, S., 2000. Vasculogenesis and angiogenesis as mechanisms of vascular network formation, growth and remodeling. *Neuro Oncology,* Volume 50 (1-2), pp. 1-15.

Paterson, J., Seckl, J. & Mullins, J., 2005. Genetic manipulation of 11beta-hydroxysteroid dehydrogenases in mice. *American Journal of Physiology,* Volume 289 (3), pp. R642-R652.

Paterson, J. *et al*., 2007. Liver-selective transgene rescue of hypothalamic-pituitary-adrenal axis dysfunction in 11β-hydroxysteroid dehydrogenase type 1-deficient mice. *Endocrinology,* Volume 148 (3), pp. 961-966.

Pauschinger, M. *et al*., 1999. Dilated cardiomyopathy is associated with significant changes in collagen type I/III ratio. *Circulation,* Volume 99 (21), pp. 2750-2756.

Payne, T. *et al*., 2007. A relationship between vascular endothelial growth factor, angiogenesis, and cardiac repair after muscle stem cell transplantation into ischaemic hearts. *Journal of the American College of Cardiology,* Volume 50 (17), pp. 1677-1684.

Pearl, J. *et al*., 2011. Glucocorticoids inprove calcium cycling in cardiac myocytes after cardiopulmonary bypass. *Surgical Research,* Volume 167 (2), pp. 279-286.

Pearlman, J. *et al*., 1995. Magnetic resonance mapping demonstrates benefits of VEGF-induced myocardial angiogenesis. *Nature Medicine,* Volume 1 (10), pp. 1085-1089.

Periasamy, M. & Kalyanasundaram, A., 2007. SERCA pump isoforms: their role in calcium transport and disease. *Muscle & Nerve,* Volume 35 (4), pp. 430-442.

Petramala, L. *et al*., 2007. Cushing's Syndrome patient who exhibited congestive heart failure. *Endocrinological Investigation,* Volume 30 (6), pp. 525-528.

Pfeffer, M. & Braunwald, E., 1990. Ventricular remodeling after myocardial infarction. Experimental observations and clinical implications. *Circulation,* Volume 81, pp. 1161-1172.

Phillips, DIW. *et al*., 1998. Elevated plasma cortisol concentrations: a link between low birth weight and the insulin resistance syndrome?. *Clinical Endocrinology and Metabolism,* Volume 83 (3), pp. 757-760.

Picht, E. *et al*., 2007. CaMKII inhibition targeted to the sarcoplasmic reticulum inhibits frequency-dependent acceleration of relaxation and Ca^{2+} current facilitation. *Molecular and Cellular Cardiology,* Volume 42 (1), pp. 196-205.

Pitt, B. *et al*., 1999. The effect of spironolactone on morbidity and mortality in patients with severe heart failure. *New England Journal of Medicine,* Volume 341, pp. 709-717.

Pitt, B. *et al*., 2003. Eplerenone, a selective aldosterone blocker, in patients with left ventricular dysfunction after myocardial infarction. *New England Journal of Medicine,* Volume 348, pp. 1309-1321.

Porter, K. & Turner, N., 2009. Cardiac fibroblasts: at the heart of myocardial remodeling. *Pharmacology and Therapeutics,* Volume 123, pp. 255-278.

Pratt, W., Galigniana, M., Harrell, J. & De Franco, D., 2004. Role of hsp90 and the hsp90-binding immunophilins in signalling protein movement. *Cellular Signalling,* Volume 16 (8), pp. 857-872.

Prech, M. *et al*., 2006. Chronic infarct-related artery occlusion is associated with a reduction in capillary density. Effects on infarct healing. *European Journal of Heart Failure,* Volume 8, pp. 373-380.

Protti, A. *et al*., 2012. MRI-based prediction of adverse cardiac remodeling after murine myocardial infarction. *American Journal of Physiology,* Volume 303, pp. H309-H314.

Qin, W. *et al*., 2003. Transgenic model of aldosterone-driven cardiac hypertrophy and heart failure. *Circulation Research,* Volume 93, pp. 69-76.

Rahman, T. *et al*., 2011. Common variation at the 11β-hydroxysteroid dehydrogenase type 1 gene is associated with left ventricular mass. *Circulation Cardiovascular Genetics,* Volume 4, pp. 156-162.

Rajan, V. *et al*., 1995. Cloning, sequencing and tissue-distribution of mouse 11β-hydroxysteroid dehydrogenase-1 cDNA. *Steroid Biochemistry and Molecular Biology,* Volume 52 (2), pp. 141-147.

Rao, M., Xu, A. & Narayanan, N., 2001. Glucocorticoid modulation of protein phosphorylation and sarcoplasmic reticulum function in rat myocardium. *American Journal of Physiology,* Volume 281, pp. H325-H333.

Reeves, J. & Hale, C., 1984. The stoichiometry of the cardiac sodium-calcium exchange system. *Biological Chemistry,* Volume 259 (12), pp. 7733-7739.

Reichardt, H. *et al*., 1998. DNA binding of the glucocorticoid receptor is not essential for survival. *Cell,* Volume 93 (4), pp. 531-541.

Ren, G., Michael, L., Entman, M. & Frangogiannis, N., 2002. Morphological characteristics of the microvasculature in healing myocardial infarcts. *Histochemistry and Cytochemistry,* Volume 50 (1), pp. 71-79.

Ren, R., Oakley, R., Cruz-Topete, D. & Cidlowski, J., 2012. Dual role for glucocorticoids in cardiomyocyte hypertrophy and apoptosis. *Endocrinology,* Volume 153 (11), pp. 5346-5360.

Reynolds, R. *et al*., 2010a. Elevated fasting plasma cortisol is associated with ischaemic heart disease and its risk factors in people with type 2 diabetes: the Edinburgh Type 2 Diabetes Study. *Journal of Clinical Endocrinology and Metabolism,* 95(4), pp. 1602-1608.

Reynolds, R. *et al*., 2010b. Low serum cortisol predicts early death after acute myocardial infarction. *Critical Care Medicine,* 38(3), pp. 973-975.

Rissanen, T. & Yla-Herttuala, S., 2007. Current status of cardiovascular gene therapy. *Molecular Therapy,* Volume 15 (7), pp. 1233-1247.

Roberts, R., DeMello, V. & Sobel, B., 1976. Deleterious effects of methyprednisolone in patients with myocardial infarction. *Circulation,* Volume 53 (3), pp. 204-206.

Rog-Zielinska, E. *et al*., 2013. Glucocorticoid receptor is required for foetal heart maturation. *Human Molecular Genetics,* Volume 22 (16), pp. 3269-3282.

Rossen, R. *et al*., 1994. Cardiolipin-protein complexes and initiation of complement activation after coronary artery occlusion. *Circulation Research,* Volume 75 (3), pp. 546-555.

Roth, J., Kaeberle, M. & Hsu, W., 1982. Effects of ACTH administration on bovine polymorphonuclear leukocyte function and lymphocyte blastogenesis. *American Journal of Veterinary Research,* Volume 43 (3), pp. 412-416.

Ruiz, L. *et al*., 2002. Dexamethasone inhibits apoptosis of human neutrophils induced by reactive oxygen species. *Inflammation,* Volume 26 (5), pp. 215-222.

Rupprecht, H. *et al*., 2000. Cardioprotective effects of the Na^+/H^+ exchanger inhibitor cariporide in patients with acute anterior myocardial infarction undergoing direct PTCA. *Circulation,* Volume 101, pp. 2902-2908.

Sabbah, H. & Goldstein, S., 1993. Ventricular remodeling: consequences and therapy. *European Heart Journal,* Volume 14, pp. 24-29.

Sabrane, K., Kruse, M., Gazinski, A. & Kuhn, M., 2009. Chronic endothelium-dependent regulation of arterial blood pressure by atrial natriuretic peptide: role of nitric oxide and endothelin-1. *Endocrinology,* Volume 150 (5), pp. 2382-2387.

Sainte-Marie, Y. *et al*., 2007. Conditional glucocorticoid receptor expression in the heart induces atrio-ventricular block. *Journal of the Federation of American Societies for Experimental Biology,* Volume 21, pp. 3133-3141.

Saito, Y., 2010. Roles of atrial natriuretic peptide and its therapeutic use. *Cardiology,* Volume 56, pp. 262-270.

Sakahira, H., Enari, M. & Nagata, S., 1998. Cleavage of CAD inhibitor in CAD activation and DNA degradation during apoptosis. *Nature,* Volume 391 (6662), pp. 96-99.

Sanada, S. *et al*., 2007. IL-33 and ST2 comprise a critical biochemically induced and cardioprotective signaling system. *Journal of Clinical Investigation,* Volume 117 (6), pp. 1538-1549.

Sapolsky, R., Romero, L. & Munck, A., 2000. How do glucocorticoids influence stress responses? Integrating permissive, suppressive, stimulatory and preparative actions. *Endocrine Reviews,* Volume 21 (1), pp. 55-89.

Saris, J. *et al*., 2001. High-affinity prorenin binding to cardiac man-6-P/IGF-II receptors preceeds proteolytic activation to renin. *American Journal of Physiology,* Volume 280 (4), pp. H1706-H1715.

Sasaki, T. *et al*., 2007. Stromal cell-derived factor-1α improves infarcted heart function through angiogenesis in mice. *Paediatrics International,* Volume 49, pp. 966-971.

Sato, A. *et al*., 1994. Glucocorticoid increases angiotensin II type 1 receptor and its gene expression. *Hypertension,* Volume 23 (1), pp. 25-30.

Scarborough, P. *et al*., 2010. Coronary heart disease statistics. *British Heart Foundation Promotion Research Group, Department of Public Health, University of Oxford.*

Scheuer, D. & Mifflin, S., 1997. Chronic corticosterone treatment increases myocardial infarct size in rats with ischemia-reperfusion injury. *American Journal of Physiology,* Volume 272 (6), pp. 2017-2024.

Schiffrin, E. & Taillefer, R., 1986. Correlation of left ventricular ejection fraction and plasma atrial natriuretic peptide in congestive heart failure. *New England Journal of Medicine,* Volume 315 (12), pp. 765-766.

Schmidt, R. *et al*., 2006. Extracellular matrix metalloproteinase inducer regulates matrix metalloproteinase activity in cardiovascular cells: implications in acute myocardial infarction. *Circulation,* Volume 113, pp. 834-841.

Schultz, J. *et al*., 1999. Fibroblast growth factor-2 mediates pressure-induced hypertrophic response. *Journal of Clinical Investigation,* Volume 104, pp. 709-719.

Schultz, J. *et al*., 2002. TGF-β1 mediates the hypertrophic cardiomyocyte growth induced by angiotensin II. *Journal of Clinical Investigation,* Volume 109 (6), pp. 787-796.

Schultz, J. *et al*., 2004. Accelerated onset of heart failure in mice during pressure overload with chronically decreased SERCA2 calcium pump activity. *American Journal of Physiology,* Volume 286 (3), pp. H1146-H1153.

Schwarz, E. *et al*., 2000. Evaluation of the effects of intramyocardial injection of DNA expressing vascular endothelial growth factor (VEGF) in a myocardial infarction model in the rat - angiogenesis and angioma formation. *Journal of the American College of Cardiology,* Volume 35 (5), pp. 1323-1330.

Seckl, J., 2004. 11beta-hydroxysteroid dehydrogenases: changing glucocorticoid action. *Current Opinion in Pharmacology,* Volume 4 (6), pp. 597-602.

Selvanayagam, J. *et al*., 2005. Troponin elevation after percutaneous coronary intervention directly represents the extent of irreversible myocardial injury: insights from cardiovascular magnetic resonance imaging. *Circulation,* Volume 111, pp. 1027-1032.

Sham, J., Cleemann, L. & Morad, M., 1995. Functional coupling of calcium channels and ryanodine receptors in cardiac myocytes. *Proceedings of the National Academy of Sciences,* Volume 92, pp. 121-125.

Sharma, U. *et al*., 2004. Galectin-3 marks activated macrophages in failure-prone hypertrophied hearts and contributes to cardiac dysfunction. *Circulation,* Volume 110 (19), pp. 3121-3128.

Sheer, D. & Morkin, E., 1984. Myosin isoenzyme expression in rat ventricle: effects of thyroid hormone analogs, catecholamines, glucocorticoids and high carbohydrate diet. *Pharmacology and Experimental Therapeutics,* Volume 229 (3), pp. 872-879.

Sheppard, K. & Funder, J., 1987. Mineralocorticoid specificity of renal type I receptors: in vivo binding studies. *Endocrinology and Metabolism,* Volume 252 (2), pp. E224-E229.

Sheppard, K. & Autelitano, D., 2002. 11β-hydroxysteroid dehydrogenase 1 transforms 11-dehydrocorticosterone into transcriptionally active glucocorticoid in neonatal rat heart. *Endocrinology,* Volume 143 (1), pp. 198-204.

Shesely, E. *et al*., 1996. Elevated blood pressures in mice lacking endothelial nitric oxide synthase. *Proceedings of the National Academy of Sciences,* Volume 93 (23), pp. 13176-13181.

Shih, H., Lee, B., Lee, R. & Boyle, A., 2011. The aging heart and post-infarction left ventricular remodeling. *Journal of the American College of Cardiology,* Volume 57 (1), pp. 9-17.

Shiojima, I. *et al*., 2005. Disruption of coordinated cardiac hypertrophy and angiogenesis contributes to the transition to heart failure. *Journal of Clinical Investigation,* Volume 115 (8), pp. 2108-2118.

Shishido, T. *et al*., 2003. Toll-like receptor-2 modulates ventricular remodeling after myocardial infarction. *Circulation,* Volume 108 (23), pp. 2905-2910.

Shohet, R. & Garcia, J., 2007. Keeping the engine primed: HIF factors as key regulators of cardiac metabolism and angiogenesis during ischaemia. *Molecular Medicine,* Volume 85 (12), pp. 1309-1315.

Simons, M., 2005. Angiogenesis: where do we stand now?. *Circulation,* Volume 111 (12), pp. 1556-1566.

Siwik, D., Chang, D. & Colucci, W., 2000. Interleukin-1β and tumor necrosis factor-α decrease collagen synthesis and increase matrix metalloproteinase activity in cardiac fibroblasts in vitro. *Circulation Research,* Volume 86, pp. 1259-1265.

Small, G. *et al*., 2005. Preventing local regeneration of glucocorticoids by 11β-hydroxysteroid dehydrogenase type 1 enhances angiogenesis. *Proceedings of the National Academy of Sciences,* Volume 102 (34), pp. 12165-12170.

Smoak, K. & Cidlowski, J., 2004. Mechanisms of glucocorticoid receptor signaling during inflammation. *Mechanisms of Ageing and Development,* Volume 125 (10-11), pp. 697-706.

Sonnenberg, H., 1986. Mechanisms of release and renal tubular action of atrial natriuretic factor. *Federation Proceedings,* Volume 45 (7), pp. 2106-2110.

Sooy, K. *et al*., 2010. Partial deficiency or short-term inhibition of 11β-hydroxysteroid dehydrogenase type 1 improves cognitive function in aging mice. *Neuroscience,* Volume 30, pp. 13867-13872.

Souverein, P. *et al*., 2004. Use of oral glucocorticoids and risk of cardiovascular and cerebrovascular disease in a population based case-control study. *Heart,* Volume 90 (8), pp. 859-865.

Speirs, H., Seckl, J. & Brown, R., 2004. Ontogeny of glucocorticoid receptor and 11beta-hydroxysteroid dehydrogenase type-1 gene expression identifies potential critical periods of glucocorticoid susceptibility during development. *Endocrinology,* Volume 181 (1), pp. 105-116.

Spyracopoulos, L. *et al*., 1997. Calcium-induced structural transition in the regulatory domain of human cardiac troponin C. *Biochemistry,* Volume 36 (40), pp. 12138-12146.

Stanley, A., Athanasuleas, C. & Buckberg, G., 2004. Heart failure following anterior myocardial infarction: an indication for ventricular restoration, a surgical method for reverse post-infarction remodeling. *Heart Failure Reviews,* Volume 9 (4), pp. 241-254.

Stewart, D. *et al*., 2009. VEGF gene therapy fails to improve perfusion of ischemic myocardium in patients with advanced coronary disease: results of the NORTHERN trial. *Molecular Therapy,* Volume 17 (6), pp. 1109-1115.

Stojadinovic, O. *et al*., 2007. Novel genomic effects of glucocorticoids in epidermal keratinocytes: inhibition of apoptosis, interferon-gamma pathway, and wound healing along with promotion of terminal differentiation. *Biological Chemistry,* Volume 282 (6), pp. 4021-4034.

Stokke, M. *et al*., 2010. Reduced SERCA2 abundance decreases the propensity for Ca^{2+} wave development in ventricular cardiomyocytes. *Cardiovascular Research,* Volume 86 (1), pp. 63-71.

Studer, R. *et al*., 1994. Gene expression of the cardiac Na^{+}-Ca^{2+} exchanger in end-stage human heart failure. *Circulation Research,* Volume 75 (3), pp. 443-453.

Sunderkotter, C. *et al*., 1994. Macrophages and angiogenesis. *Leukocyte Biology,* Volume 55 (3), pp. 410-422.

Takagawa, J. *et al*., 2007. Myocardial infarct size measurement in the mouse chronic infarction model: comparison of area- and length-based approaches. *Applied Physiology*, Volume 102, pp. 2104-2111.

Takahashi, T. *et al*., 1992. Age-related differences in the expression of proto-oncogene and contractile protein genes in response to pressure overload in the rat myocardium. *Journal of Clinical Investigation,* Volume 89 (3), pp. 939-946.

Takahashi, T. *et al*., 1992. Expression of dihyrdopyridine receptor (Ca^{2+} channel) and calsequestrin genes in the myocardium of patients with end-stage heart failure. *Journal of Clinical Investigation,* Volume 90 (3), pp. 927-935.

Takeda, M. *et al*., 2007. Spironolactone modulates expressions of cardiac mineralocorticoid receptor and 11beta-hydroxysteroid dehydrogenase 2 and prevents ventricular remodeling in post-infarct rat hearts. *Hypertension Research,* Volume 30 (5), pp. 427-437.

Tannin, G. *et al*., 1991. The human gene for 11β-hydroxysteroid dehydrogenase. *Biological Chemistry,* Volume 266 (25), pp. 16653-16658.

Thannickal, V. & Fanburg, B., 2000. Reactive oxygen species in cell signaling. *American Journal of Physiology,* Volume 279 (6), pp. 1005-1028.

Thieringer, R. *et al*., 2001. 11 beta-hydroxysteroid dehydrogenase type 1 is induced in human monocytes upon differentiation to macrophages. *Immunology,* Volume 167 (1), pp. 30-35.

Thollon, C. *et al*., 1995. Nature of the cardiomyocyte injury induced by lipid hyroperoxides. *Cardiovascular Research,* Volume 30 (5), pp. 648-655.

Thompson, R. *et al*., 2001. Platelet-endothelial cell adhesion molecule-1 (PECAM-1)-deficient mice demonstrate a transient and cytokine-specific role for PECAM-1 in leukocyte migration through perivascular basement membrane. *Blood,* Volume 97 (6), pp. 1854-1860.

Thorneloe, K. *et al*., 2012. An orally active TRPV4 channel blocker prevents and resolves pulmonary edema induced by heart failure. *Science Translational Medicine,* Volume 4 (159), p. 159ra148.

Tiganescu, A. *et al*., 2013. 11β-hydroxysteroid dehydrogenase blockade prevents age-induced skin structure and function defects. *Journal of Clinical Investigation,* Volume 123 (7), pp. 3051-3060.

Tomlinson, J. & Stewart, P., 2005. Mechanisms of disease: selective inhibition of 11beta-hydroxysteroid dehydrogenase type 1 as a novel treatment for the metabolic syndrome. *Nature Clinical Practice. Endocrinology & Metabolism,* Volume 1 (2), pp. 92-99.

Torella, D. *et al*., 2004. Cardiac stem cell and myocyte aging, heart failure, and insulin-like growth factor-1 overexpression. *Circulation Research,* Volume 94, pp. 514-524.

Townsend, N. *et al*., 2012. *Coronary heart disease statistics. A compendium of health statistics.* 2012 Ed. Oxford: Department of Public Health, University of Oxford.

Tribouilloy, C. *et al*., 2008. Prognosis of heart failure with preserved ejection fraction: a 5 year prospective population-based study. *European Heart Journal,* Volume 29, pp. 339-347.

Tuckermann, J. *et al*., 2007. Macrophages and neutrophils are the targets for immune suppression by glucocorticoids in contact allergy. *Journal of Clinical Investigation,* Volume 117 (5), pp. 1381-1390.

Ullian, M., 1999. The role of corticosteroids in the regulation of vascular tone. *Cardiovascular Research,* Volume 41, pp. 55-64.

Usher, M. *et al*., 2010. Myeloid mineralocorticoid receptor controls macrophage polarization and cardiovascular hypertrophy and remodeling in mice. *Journal of Clinical Investigation,* Volume 120 (9), pp. 3350-3364.

Van Amerongen, M. *et al*., 2008. Bone marrow-derived myofibroblasts contribute functionally to scar formation after myocardial infarction. *Pathology,* Volume 214 (3), pp. 377-386.

Van Cauter, E., Leproult, R. & Kupfer, D., 1996. Effects of gender and age on the levels and circadian rhythmicity of plasma cortisol. *Clinical Endocrinology and Metabolism,* Volume 81 (7), pp. 2468-2473.

Van Furth, R. & Cohn, Z., 1968. The origin and kinetics of mononuclear phagocytes. *Experimental Medicine,* Volume 128 (3), pp. 415-435.

Van Put, D. *et al*., 1995. Dexamethasone influences intimal thickening and vascular reactivity in the rabbit collared carotid artery. *European Journal of Pharmacology,* Volume 294 (2-3), pp. 753-761.

Van Raalte, D. *et al*., 2013. Glucocorticoid treatment impairs microvascular function in healthy men in association with its adverse effects on glucose metabolism and blood pressure: a randomised controlled trial. *Diabetologia,* Volume 56 (11), pp. 2383-2391.

Vaz Perez, A. *et al*., 2010. The relationship between tumor necrosis factor-α, brain natriuretic peptide and atrial natriuretic peptide in patients with chronic heart failure. *International Journal of Cardiology,* Volume 141, pp. 39-43.

Vetter, R. *et al*., 2002. Transgenic overexpression of the sarcoplasmic reticulum Ca^{2+}-ATPase improves reticular Ca^{2+} handling in normal and diabetic rat hearts. *The Federation of American Societies for Experimental Biology Journal,* Volume 16 (12), pp. 1657-1659.

Villarreal, F., Lee, A., Dillmann, W. & Giordano, F., 1996. Adenovirus-mediated overexpression of human transforming growth factor-beta 1 in rat cardiac fibroblasts, myocytes and smooth muscle cells. *Molecular and Cellular Cardiology,* Volume 28 (4), pp. 735-742.

Vital, F., Ladiera, M. & Atallah, A., 2013. *Non-invasive positive pressure ventilation (CPAP or bilevel NPPV) for cardiogenic pulmonary oedema (Review).* The Cochrane Database of Systematic Reviews, London.

Von Harsdorf, R., Li, P. & Dietz, R., 1999. Signaling pathways in reactive oxygen species-induced cardiomyocyte apoptosis. *Circulation,* Volume 99 (22), pp. 2934-2941.

Walker, B. *et al*., 1991. 11 beta-hydroxysteroid dehydrogenase in vascular smooth muscle and heart: implications for cardiovascular responses to glucocorticoids. *Endocrinology,* Volume 129 (6), pp. 3305-3312.

Walker, B. & Williams, B., 1992. Corticosteroids and vascular tone: mapping the messenger maze. *Clinical Science (London),* Volume 82 (6), pp. 597-605.

Walker, B. & Seckl, J., 2003. 11beta-hydroxysteroid dehydrogenase type 1 as a novel therapeutic target in metabolic and neurodegenerative disease. *Expert Opinion on Therapeutic Targets,* Volume 7 (6), pp. 771-783.

Walker, B., 2007a. Glucocorticoids and cardiovascular disease. *European Journal of Endocrinology,* Volume 157, pp. 545-559.

Walker, B., 2007b. Extra-adrenal regeneration of glucocorticoids by 11β-hydroxysteroid dehydrogenase type 1: physiological regulator and pharmacological target for energy partitioning. *Proceedings of the Nutrition Society,* Volume 66, pp. 1-8.

Walker, E. & Stewart, P., 2003. 11beta-hydroxysteroid dehydrogenase: unexpected connections. *Trends in Endocrinology and Metabolism,* Volume 14 (7), pp. 334-339.

Wang, F. *et al*., 2002. Regulation of cardiac fibroblast cellular function by leukemia inhibitory factor. *Molecular and Cellular Cardiology,* Volume 34 (10), pp. 1309-1316.

Wang, J. *et al*., 2006. Cardiomyopathy associated with microcirculation dysfunction in laminin α4 chain-deficient mice. *Biological Chemistry,* Volume 281, pp. 213-220.

Weber, K. & Brilla, C., 1991. Pathological hypertrophy and cardiac interstitium. Fibrosis and renin-angiotensin-aldosterone system. *Circulation,* Volume 83, pp. 1849-1865.

Weinstein, R. *et al*., 2010. Endogenous glucocorticoids decrease skeletal angiogenesis, vascularity, hydration and strength in aged mice. *Aging Cell,* Volume 9, pp. 147-161.

Weisser-Thomas, J. *et al*., 2003. Calcium entry via Na/Ca exchange during the action potential directly contributes to contraction of failing human ventricular myocytes. *Cardiovascular Research,* Volume 57 (4), pp. 974-985.

Whitworth, J., Mangos, G. & Kelly, J., 2000. Cushing, cortisol, and cardiovascular disease. *Hypertension,* Volume 36 (5), pp. 912-916.

Windle, R. *et al*., 1998. Ultradian rhythm of basal corticosterone release in the female rat: dynamic interaction with the response to acute stress. *Endocrinology,* Volume 139 (2), pp. 443-450.

Wochnik, G. *et al*., 2005. FK506-binding proteins 51 and 52 differentially regulate dynein interaction and nuclear translocation of the glucocorticoid receptor in mammalian cells. *Biological Chemistry,* Volume 280, pp. 4609-4616.

Wollert, K. *et al*., 1996. Cardiotophin-1 activates a distinct form of cardiac muscle cell hypertrophy. Assembly of sarcomeric units in series via gp130/leukemia inhibitory factor receptor-dependent pathways. *Biological Chemistry,* Volume 271 (16), pp. 9535-9545.

Wu, A., 2006. Cardiac troponin: friend of the cardiac physician, foe to the cardiac patient?. *Circulation,* Volume 114, pp. 1673-1675.

Xu, B., Strom, J. & Chen, Q., 2011. Dexamethasone induces transcriptional activation of Bcl-xL gene and inhibits cardiac injury by myocardial ischaemia. *Cardiovascular Pharmacology,* Volume 668 (1-2), pp. 194-200.

Yang, F. *et al*., 2002b. Myocardial infarction and cardiac remodelling in mice. *Experimental Physiology,* Volume 87, pp. 547-555.

Yang, F. *et al*., 2009. 11β-hydroxysteroid dehydrogenase type 1 activity limits fibrosis following bleomycin lung injury by augmenting active glucocorticoids. *Endocrime Abstracts,* Volume 19, OC9.

Yang, S. & Zhang, L., 2004. Glucocorticoids and vascular reactivity. *Current Vascular Pharmacology,* Volume 2 (1), pp. 1-12.

Yang, Z. *et al*., 2002a. Angiotensin II type II receptor overexpression preserves left ventricular function after myocardial infarction. *Circulation,* Volume 106, pp. 106-111.

Yano, A., Fujii, Y. & Iwai, A., 2006. Glucocorticoids suppress tumor angiogenesis and in vivo growth of prostate cancer cells. *Clinical Cancer Research,* Volume 12, pp. 3003-3009.

Yau, J. *et al*., 2001. Lack of tissue glucocorticoid reactivation in 11beta-hydroxysteroid dehydrogenase type 1 knockout mice ameliorates age-related learning impairments. *Proceedings of the National Academy of Sciences,* Volume 98 (8), pp. 4716-4721.

Yau, J. *et al*., 2007. Enhanced hippocampal long-term potentiation and spatial learning in aged 11beta-hydroxysteroid dehydrogenase type 1 knock-out mice. *Neuroscience,* Volume 27 (39), pp. 10487-10496.

Yau, J., Noble, J. & Seckl, J., 2011. 11β-hydroxysteroid dehydrogenase type 1 deficiency prevents memory deficits with aging by switching from glucocorticoid receptor to mineralocorticoid receptor-mediated cognitive control. *Neuroscience,* Volume 31, pp. 4188-4193.

Yoshikawa, N. *et al*., 2009. Ligand-based gene expression profiling reveals novel roles of glucocorticoid receptor in cardiac metabolism. *American Journal of Physiology,* Volume 296, pp. E1363-E1373.

Youle, R. & Strasser, A., 2008. The BCL-2 protein family: opposing activities that mediate cell death. *Nature Reviews Molecular Cell Biology,* Volume 9 (1), pp. 47-59.

Young, M., Clyne, C., Cole, T. & Funder, J., 2001. Cardiac steroidogenesis in the normal and failing heart. *Clinical Endocrinology and Metabolism,* Volume 86, pp. 5121-5126.

Zhang, D. *et al*., 2002. Efficacy and safety of therapeutic angiogenesis from direct myocardial administration of an adenoviral vector expressing vascular endothelial growth factor 165. *Chinese Medical Journal,* Volume 115 (5), pp. 643-648.

Zhang, H. *et al*., 2005b. Collecting duct-specific deletion of peroxisome proliferator-activated receptor γ blocks thiazolidinedione-induced fluid retention. *Proceedings of the National Academy of Sciences,* Volume 102 (26), pp. 9406-9411.

Zhang, T., Ding, X. & Daynes, R., 2005a. The expression of 11β-hydroxysteroid dehydrogenase type 1 by lymphocytes provides a novel means of intracrine regulation of glucocorticoid activities. *Immunology,* Volume 174, pp. 879-889.

Zhang, Y. *et al*., 2008. Connexin 43 expression levels influence intercellular coupling and cell proliferation of native murine cardiac fibroblasts. *Cell Communication and Adhesion,* Volume 15 (3), pp. 289-303.

Zhang, Z. *et al*., 2013. Macrophage-specific 11β-hydroxysteroid dehydrogenase type 1 deficiency promotes angiogenesis but impairs resolution of K/BxN serum induced arthritis. *Endocrine Abstracts,* Volume 31, OC1.2.

Zhou, A., Scoggin, S., Gaynor, R. & Williams, N., 2003. Identification of NF-κB-regulated genes induced by TNFα utilizing expression profiling and RNA interference. *Oncogene,* Volume 22, pp. 2054-2064.

Ziche, M. *et al*., 1997. Nitric oxide synthase lies downstream from vascular endothelial growth factor-induced angiogenesis but not fibroblast growth factor-induced angiogenesis. *Journal of Clinical Investigation,* Volume 99, pp. 2625-2634.

Appendix 1

mRNA levels of β-actin, the internal control gene for heart (a), aorta (b) and liver (c) qRT-PCR was similar in all groups. mRNA levels of TBP, the internal control gene for skeletal muscle qRT-PCR, was also similar in all groups (d).

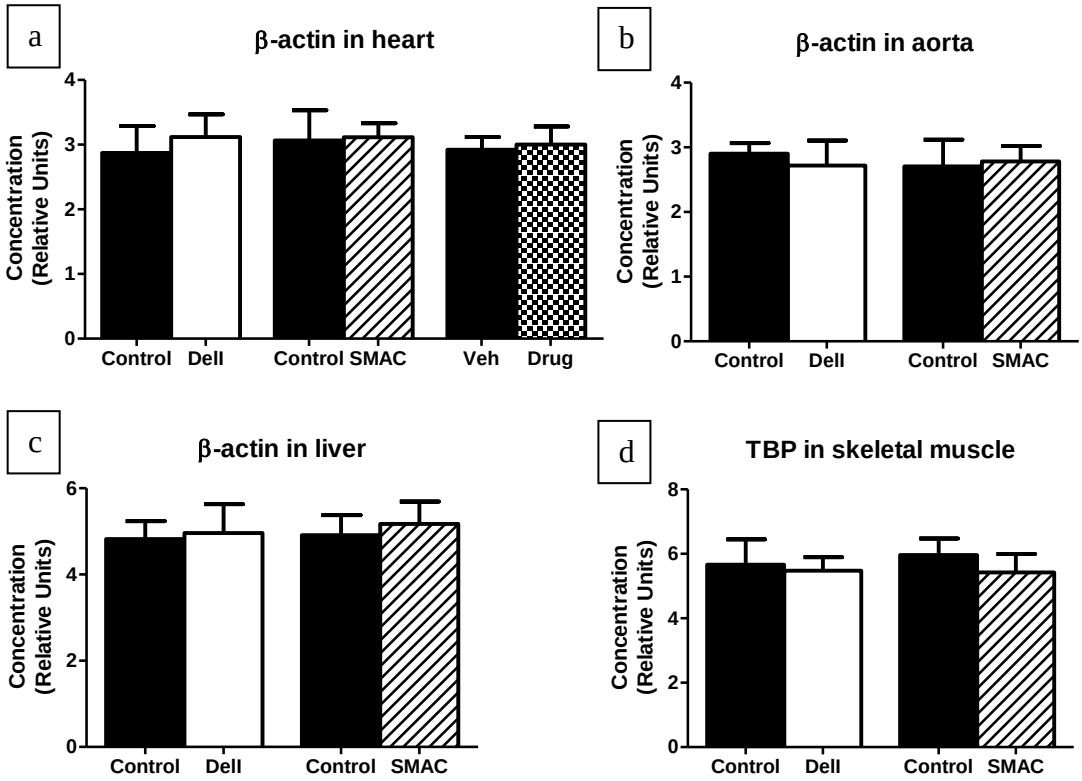

Appendix 1. qRT-PCR internal control genes
β-actin was used as the internal control for heart (a), aorta (b) and liver(c). TBP was used as the internal control for skeletal muscle (d). mRNA levels of these genes were similar in all groups in all tissues investigated (two way ANOVA).

Appendix 2

Protein expression of β-actin, the internal control gene for heart (a), aorta (b) and liver (c) western blotting was similar in all groups. Protein expression of α-tubulin, the internal control gene for skeletal muscle western blotting, was also similar in all groups (d). An example heart blot (e) shows β-actin protein at approximately 42kDa and 11β-HSD1 protein at approximately 34kDa.

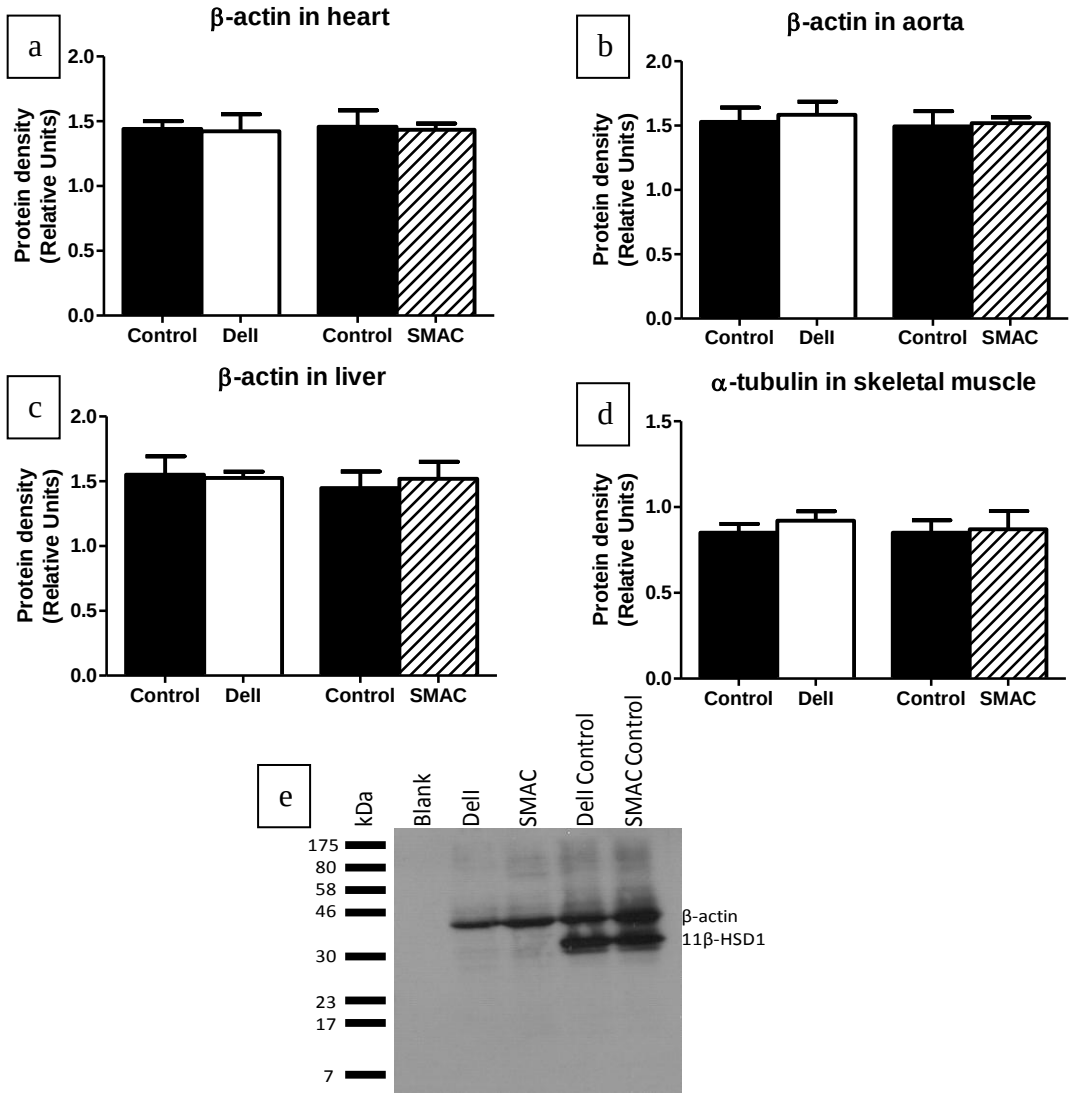

Appendix 2. Western blot internal control genes

β-actin was used as the internal control for heart (a), aorta (b) and liver (c). α-tubulin was used as the internal control for skeletal muscle (d). Protein expression was similar in all groups in all tissues investigated (two way ANOVA). An example heart western blot (e) shows β-actin at approximately 42kDa in all samples and 11β-HSD1 at approximately 34kDa only in the control mice.

Appendix 3

Cardiomyocyte cross-sectional area in the left ventricular wall was similar in DelI and C57BL/6 control mice (a) at 18 months of age.

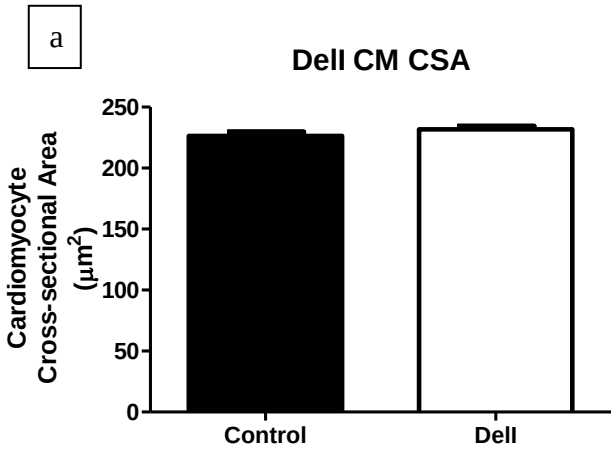

Appendix 3. Cardiomyocyte cross-sectional area is unaltered in DelI mice at 18 months of age

Cardiomyocyte cross sectional area was assessed by staining for isolectin B4, WGA and DAPI in DelI and C57BL/6 mice at 18 months of age (Student's *t* test; n=5/group). Isolectin B4 stains endothelial cells, WGA stains cell membranes and DAPI stains nuclei. This allowed cardiomyocyte cross-sectional area measurement by selecting cardiomyocytes which a) appeared to be cut in the short axis, b) had a nucleus in the middle of the cell and c) were surrounded by capillaries which were also cut in the short axis.

Appendix 4

Means plus standard error of the mean for all results in Chapter 3.

		DelI	**C57BL/6**	**SMAC**	**Cre$^-$**
11β-HSD1 mRNA (%)	Heart	1.02 ± 1.01	100 ± 6.3	8.4 ± 2.1	100 ± 17.8
	Aorta	1.05 ± 1	100 ± 11	5.3 ± 2.3	100 ± 14.8
	Liver	1.03 ± 0.5	100 ± 4	88.4 ± 3.1	100 ± 3.4
	Skeletal Muscle	0.55 ± 1.01	100 ± 2	9.2 ± 1	100 ± 4.7
11β-HSD1 protein (%)	Heart	2.05 ± 1.2	100 ± 4.3	9.04 ± 1.1	100 ± 5.3
	Aorta	2.1 ± 0.5	100 ± 5.2	10.4 ± 1.2	100 ± 5.8
	Liver	2 ± 1.1	100 ± 2.2	93 ± 4.7	100 ± 5.7
	Skeletal Muscle	3 ± 1.1	100 ± 4.5	96 ± 6.4	100 ± 4.3
Nr3c1 mRNA (%)		94 ± 10	100 ± 11.4	99 ± 11.3	100 ±10.1
Nrc32 mRNA (%)		105 ± 17.3	100 ± 11.7	99 ± 12.1	100 ± 10.2
Fkbp5 mRNA (%)		81 ± 7.8	100 ± 5.8	86 ± 4.6	100 ± 4.6
Tsc22d3 mRNA (%)		78 ± 16.4	100 ± 14.8	87 ± 10.9	100 ± 12.4
Ppargc1a mRNA (%)		113 ± 5.6	100 ± 4.3	105 ± 8.4	100 ± 6.6
Sgk1 mRNA (%)		103 ± 7.1	100 ± 5.4	93 ± 5	100 ± 5.8
Systolic BP (mmHg)		99 ± 2	97 ± 3.1	90 ± 2	92 ± 2.1
Heart Rate		644 ± 16	651 ± 14	651 ± 21.2	655 ± 19.8
LVEDA (mm^2)	6w	22 ± 1.4	23 ± 1	20 ± 1.2	20 ± 1.7
	10w	21 ± 0.5	28 ± 2.1	21 ± 1.2	22 ± 1.4
	20w			24 ± 1.6	24 ± 1.6
	35w			23 ± 4.1	23 ± 1.2
	78w	28 ± 1	28 ± 2		
SV (µl)	6w	35 ± 2.1	37 ± 2.3	28 ± 1.2	28 ± 1.6
	10w	32 ± 1	49 ± 4	39 ± 2.3	41 ± 2.8
	20w			39 ± 2	39 ± 3.8
	35w			38 ± 2.1	38 ± 2.2
	78w	42 ± 2.3	43 ± 2.6		
LVESA (mm^2)	6w	13 ± 3.5	14 ± 2.1	12 ± 2.3	12 ± 3
	10w	14 ± 2.7	14 ± 3.5	14 ± 2.1	15 ± 2
	20w			16 ± 2.2	16 ± 2.1
	35w			14 ± 3	12 ±3.5
	78w	15 ± 2	13 ± 4.8		

		DelI	C57BL/6	SMAC	Cre$^-$
Heart weight (mg)		135.4 ± 8.1	178.2 ± 18.3	173.1 ± 10	181.6 ± 20.7
Body weight (g)		29.3 ± 1.1	28.8 ± 4.3	29.7 ± 2.2	27.3 ± 3
Heart weight to body weight ratio		4.2 ± 0.2	6.8 ± 0.5	7.8 ± 0.6	7.9 ± 1.1
Blood volume (ml)		1.85 ± 0.09	1.96 ± 0.06		
Heart wet weight (mg)		158.3 ± 5.4	231.4 ± 6.8		
Heart dry weight (mg)		32 ± 1.2	49.2 ± 3.7		
Heart wet to dry weight ratio		4.4 ± 0.5	4.4 ± 0.2		
CM CSA (μm^2)		199.4 ± 9.3	190.6 ± 13.6	215.2 ± 8.3	219.4 ± 9.5
CM Length (μm)		96.7 ± 3.4	111.4 ± 3.8		
Vessel density (mm^2)	<4μm	3294 ± 83	3260 ± 121	3267 ± 58	3217 ± 101
	4-200μm	3184 ± 106	3216 ± 78	3309 ± 43	3203 ± 61
	>200μm	145 ± 4	133 ± 9	141 ± 5	135 ± 9
Ejection fraction (%)	6w	62.2 ± 4.1	64.3 ± 3.5	59.7 ± 4.2	56.6 ± 6.8
	10w	61 ± 3.5	72.4 ± 3.6	57.3 ± 5.8	54 ± 4.7
	20w			61.4 ± 3.2	61.5 ± 3.8
	35w			61.8 ± 3.1	62.9 ± 4.5
	78w	64.8 ± 3.6	66.2 ± 2.1		
Fractional shortening (%)	6w	37 ± 3.2	37.1 ± 2.8	39.6 ± 4.5	39 ± 4.2
	10w	36.3 ± 2.2	33.5 ± 2.6	38.4 ± 4.2	37.1 ± 3
	20w			36.5 ± 2.4	36.3 ± 2.7
	35w			45.8 ± 4	41.1 ± 6.3
	78w	48.2 ± 3.7	53.5 ± 5.6		
Cardiac output (ml/min)	6w	16.4 ± 2.1	16.3 ± 2.2	12.6 ± 3.8	13.4 ± 2.2
	10w	15 ± 1.1	24.6 ± 1	11.3 ± 2.6	13.4 ± 2.5
	20w			14.5 ± 2.5	16.3 ± 2
	35w			18 ± 1.3	18.3 ± 1.1
	78w	23.2 ± 2.6	22.4 ± 3.5		

		DelI	**C57BL/6**	**SMAC**	**Cre$^-$**
E/A wave ratio	6w	1.9 ± 0.2	1.75 ± 0.2	1.75 ± 0.2	1.75 ± 0.1
	10w	1.45 ± 0.05	1.5 ± 0.1	1.5 ± 0.1	1.5 ± 0.1
	20w			1.55 ± 0.1	1.7 ± 0.25
	35w			1.45 ± 0.1	1.55 ± 0.3
E wave deceleration (mm/s^2)	6w	26839 ± 1021	42367 ± 21596	27381 ± 9316	43107 ± 22096
	10w	28384 ± 837	38862 ± 7302	26322 ± 966	45063 ± 12359
	20w			29934 ± 4019	41987 ± 8219
	35w			25966 ± 473	38137 ± 13341
MV DT (ms)	6w	35.2 ± 1.1	21.5 ± 2.2	31.6 ± 3.5	21.4 ± 2.9
	10w	29.1 ± 0.5	20.5 ± 0.5	30.5 ± 2.5	21.5 ± 1
	20w			29.5 ± 1	21 ± 0.5
	35w			34.5 ± 1.5	21 ± 0.5
Collagen content (%)		4.5 ± 0.4	4.4 ± 0.3	4.7 ± 0.6	4.6 ± 0.3
Col1a2 (%)	mRNA	98.1 ± 12.4	100 ± 9.2	101.1 ± 10.3	100 ± 11.5
Col3a1 (%)	mRNA	106.4 ± 14.3	100 ± 20.6	103.3 ± 13.4	100 ± 10
Tgfb1 (%)	mRNA	113.2 ± 12.4	100 ± 24.4	104 ± 14.8	100 ± 12.1
Atp2a2 (%)	mRNA	76.4 ± 4.1	100 ± 3.3	69 ± 4.5	100 ± 6.5
Slc8a1 (%)	mRNA	94.6 ± 6.5	100 ± 5.1	96 ± 4.1	100 ± 2.2
Ryr2 (%)	mRNA	99 ± 12.1	100 ± 7.9	101 ± 13.6	100 ± 11.4
Cacna1c (%)	mRNA	102 ± 17.8	100 ± 21.4	101 ± 8	100 ± 9.9
SERCA (%)	Protein	49.2 ± 3.3	100 ± 3.6	42.8 ± 5.1	100 ± 3.8
PLN (%)	Protein	98.4 ± 3.7	100 ± 2.1	101 ± 3.2	100 ± 3.4
Ser16 (%)	Protein	107 ± 4.2	100 ± 5.2	96.3 ± 3.5	100 ± 4.7
Thr17 (%)	Protein	101.9 ± 4.9	100 ± 4	97 ± 1.1	100 ± 3.5

		UE2316	**Veh**
LVEDA (mm^2)		27.4 ± 1.1	23.5 ± 2.3
LVESA (mm^2)		16.5 ± 3.3	12.5 ± 3.2
Body weight (g)		44.1 ± 1.2	39.3 ± 2.4
Heart weight (mg)		277 ± 12.1	201.4 ± 11.6
Heart weight to body weight ratio		6.4 ± 0.4	5.1 ± 0.4
CM CSA (μm^2)		231.4 ± 5.6	224 ± 12.8
Ejection fraction (%)		58.4 ± 5.1	68.6 ± 4.2
Fractional shortening (%)		42 ± 6.3	43.2 ± 6.8
Cardiac output (ml/min)		22.4 ± 2.5	20.5 ± 3.5
E/A wave ratio		1.4 ± 0.1	1.4 ± 0.2
E wave deceleration (mm/s^2)		35362 ± 1221	23389 ± 3821
MV DT (ms)		23.5 ± 0.8	21.5 ± 2.1
Collagen content (%)		6.5 ± 0.3	6.1 ± 0.3
Col1a2 (%)	mRNA	105.1 ± 7.2	100 ± 6.3
Col3a1 (%)	mRNA	116.1 ± 9.1	100 ± 11.8
Tgfb1 (%)	mRNA	111.3 ± 14.3	100 ± 15.6
Atp2a2 (%)	mRNA	74 ± 2.2	100 ± 2.4
Slc8a1 (%)	mRNA	102.5 ± 5.1	100 ± 3.8
Ryr2 (%)	mRNA	98.2 ± 4.4	100 ± 5.7
Cacna1c (%)	mRNA	91.6 ± 6.4	100 ± 6.7
SERCA (%)	Protein	52.4 ± 2.9	100 ± 3.6
PLN (%)	Protein	98 ± 3.5	100 ± 2
Ser16 (%)	Protein	102 ± 3.4	100 ± 4.7
Thr17 (%)	Protein	102 ± 5.8	100 ± 4.6

Appendix 4. Means and standard error of the mean for all data in Chapter 3

Appendix 5

Means plus standard error of the mean for all results in Chapter 4.

		SMAC		Cre^-	
		MI	**Sham**	**MI**	**Sham**
Cardiac Troponin-I (ng/ml)		51.1 ± 7.2	8.1 ± 2.6	52.6 ± 5.1	8.2 ± 1.4
LVEDA (mm^2)		42.3 ± 5.2	25.1 ± 3.6	39.6 ± 3.4	24.7 ± 1
LVESA (mm^2)		34.9 ± 3.7	11.6 ± 2.7	28.5 ± 4	10.5 ± 1.3
Ejection fraction (%)		27.3 ± 2.2	64.5 ± 5.6	31.2 ± 4.3	70.1 ± 3
Fractional shortening		11.5 ± 2.8	43.6 ± 4.9	13.2 ± 3.3	39 ± 6.8
Infarct Size		34.2 ± 4.1		37.6 ± 5.9	
Mac2 (%)		10.5 ± 2.5	2.2 ± 0.4	11.6 ± 2.8	2 ± 0.5
Ym1 (%)		0.11 ± 0.02	0.05 ± 0.01	0.11 ± 0.02	0.05 ± 0.01
Peri-infarct angiogenesis	<4μm	7.4 ± 0.4		8.3 ± 0.5	
	4-200μm	8.2 ± 0.5		9.5 ± 0.8	
	>200μm	0.1 ± 0.01		0.1 ± 0.01	

Appendix 5. Means plus standard error of the mean for all data in Chapter 4

Appendix 6

Means plus standard error of the mean for all results in Chapter 5.

		11β-HSD1	**C57BL/6**	**SMAC**	**Cre$^-$**
Cardiac Troponin-I (ng/ml)		53.2 ± 7.1	50.5 ± 6.6	49 ± 6.3	54.1 ± 5.2
LVEDV (ml)		0.17 ± 0.01	0.22 ± 0.01	0.19 ± 0.03	0.2 ± 0.02
LVESV (ml)		0.11 ± 0.01	0.15 ± 0.1	0.13 ± 0.03	0.15 ± 0.01
Heart weight (mg)		201.3 ± 7.6	286.5 ± 19.4	256.7 ± 12	248 ± 8.9
Body weight (g)		32 ± 1.2	31.2 ± 0.5	29.5 ± 0.4	31.6 ± 0.6
Heart to body weight ratio		6.1 ± 0.2	8.8 ± 0.4	8.4 ± 0.3	8.1 ± 0.2
CM CSA (μm^2)		221.2 ± 6.3	230.5 ± 7.5	232.1 ± 4	233.5 ± 8.7
ANP (%)	mRNA	49.5 ± 9.5	100 ± 10.1	98.3 ± 12.4	100 ± 8.3
αMHC to βMHC ratio		1.15 ± 0.01	1 ± 0.03	10.5 ± 0.4	1 ± 0.05
Lung weight (mg)		136.5 ± 12.2	174 ± 15.3	178.1 ± 10.9	169 ± 8.6
Ejection fraction (%)		33.5 ± 3.5	25.6 ± 2.4	24.1 ± 2.6	26.6 ± 2
Infarct length (%)	MRI	34.3 ± 3.2	44.1 ± 3	44.5 ± 4.8	46.8 ± 3.9
Infarct length (%)	Masson's Trichrome	38.4 ± 1.8	46.9 ± 4.1	52.7 ± 4.2	49.1 ± 2.3
Infarct thickness (μm)	mRNA	642.9 ± 31.3	395.6 ± 24	401.6 ± 41.2	417.2 ± 37.4
Col1a2	mRNA	106.3 ± 18	100 ± 12.2	94.2 ± 19.3	100 ± 17.1
Col3a1	mRNA	108.9 ± 13.1	100 ± 15	98.2 ± 23.1	100 ± 18.2
Tgfb1	mRNA	94.8 ± 17.6	100 ± 13.5	113.2 ± 21.1	100 ± 18.6
Atp2a2	mRNA	99.6 ± 13.4	100 ± 7	89.7 ± 13	100 ± 6.9
Slc8a1	mRNA	99.2 ± 7.3	100 ± 11.4	103.6 ± 6.3	100 ± 9.1
SERCA	Protein	102.3 ± 8.4	100 ± 6	98.2 ± 5.3	100 ± 9.5

Appendix 6. Means plus standard error of the mean for all data in Chapter 5